Clinical Pharmacokinetics

PBPK models for prediction of complex CYP2C8 and OATP1B1 (*SLCO1B1*) drug-drug-gene interactions: a modeling network of gemfibrozil, repaglinide, pioglitazone, rifampicin, clarithromycin and itraconazole

Supplementary document

Denise Türk [1], Nina Hanke [1], Sarah Wolf [1], Sebastian Frechen [2], Thomas Eissing [2], Thomas Wendl [2], Matthias Schwab [3,4,5] and Thorsten Lehr [1]

[1] Clinical Pharmacy, Saarland University, Saarbrücken, Germany

[2] Clinical Pharmacometrics, Bayer AG, Leverkusen, Germany

[3] Dr. Margarete Fischer-Bosch-Institute of Clinical Pharmacology, Stuttgart, Germany

[4] Department of Clinical Pharmacology, University Hospital Tübingen, Tübingen, Germany

[5] Department of Pharmacy and Biochemistry, University of Tübingen, Tübingen, Germany

Corresponding Author:
Thorsten Lehr, thorsten.lehr@mx.uni-saarland.de
Clinical Pharmacy, Saarland University, Campus C2 2, 66123 Saarbrücken.
Phone: +49 681 302 70255; Fax: +49 681 302 70258

Running heading: A PBPK modeling network of CYP2C8 perpetrator and victim drugs

Funding: This project has received funding from the European Union's Horizon 2020 research and innovation programme under grant agreement No 668353. M.S. was supported by the Robert Bosch Stiftung, Stuttgart, Germany.

Table of contents

1 Mathematical implementation of drug-drug interactions (DDIs)

1.1 DDI modeling - competitive inhibition

Competitive inhibition describes the reversible binding of an inhibitor to the active site of an enzyme or transporter protein and, as a consequence, the competition of substrate and inhibitor for binding. Competitive inhibition can be overcome by high substrate concentrations (concentration-dependency). In the case of competitive inhibition, the maximum reaction velocity (v_{max}) remains unaffected, while the Michaelis-Menten constant (K_M) is apparently increased by the inhibition ($K_{M,app}$, equation 1.1). The (reduced) reaction velocity (v) during co-administration of substrate and competitive inhibitor is described by equation 1.2:

$$K_{M,app} = K_M * (1 + [I] / K_i) \quad (1.1)$$

$$v = (v_{max} * [S]) / (K_{M,app} + [S]) = (k_{cat} * [E] * [S]) / (K_{M,app} + [S]) \quad (1.2)$$

with $K_{M,app}$ = Michaelis-Menten constant in the presence of inhibitor, K_M Michaelis-Menten constant, [I] = free inhibitor concentration, K_i = dissociation constant of the inhibitor-enzyme complex, v = reaction velocity, v_{max} = maximum reaction velocity, [S] = free substrate concentration, k_{cat} = catalytic rate constant, [E] = enzyme or transporter concentration.

In the DDI models, competitive inhibition processes of cytochrome P450 (CYP) 2C8, CYP3A4, organic-anion-transporting polypeptide (OATP) 1B1 and OATP1B3 were modeled using K_i values taken from literature reports or optimized and added to the models.

1.2 DDI modeling - mechanism-based inactivation

If an enzyme is irreversibly inhibited, *de-novo* synthesis is required to restore the initial situation regarding enzyme activity (time-dependency). A special case is the mechanism-based inactivation (MBI), where an enzyme is irreversibly inhibited by a reactive species formed during the catalytic process. The change in enzyme turnover in the case of MBI can be described by equation 1.3:

$$d[E]/dt = k_{deg} * E_0 – (k_{deg} + k_{inact} * [I] / (K_I + [I]) * [E] \quad (1.3)$$

with d[E]/dt = enzyme or transporter turnover, k_{deg} = degradation rate constant, E_0 = enzyme or transporter concentration at time 0, [I] = free mechanism-based inactivator concentration, k_{inact} = maximum inactivation rate constant, K_I = concentration for half-maximal inactivation, [E] = enzyme or transporter concentration.

In the DDI models, MBI of CYP2C8 was implemented using k_{inact} and K_I values taken from literature reports.

1.3 DDI modeling - induction

DDI enzyme and transporter induction is caused by a drug-induced increase of gene expression, for example via activation of the transcription factor pregnane X receptor (PXR). The change in enzyme turnover in the case of induction can be described by equation 1.4:

$$d[E]/dt = k_{deg} * E_0 * (1 + (E_{max} * [Ind]) / (EC_{50} + [Ind])) \quad (1.4)$$

d[E]/dt = enzyme or transporter turnover, k_{deg} = degradation rate constant, E_0 = enzyme or transporter concentration at time 0, E_{max} = maximal induction effect in vivo, [Ind] = free inducer concentration, EC_{50} = concentration for half maximal induction in vivo.

In the DDI models, the induction of CYP2C8, CYP3A4, OATP1B1 and OATP1B3 was implemented using EC_{50} and E_{max} values taken from literature reports or optimized and added to the models.

2 Pharmacogenetics

2.1 Pharmacogenetics - general

Genetic polymorphisms can have an effect on drug pharmacokinetics (PK) and pharmacodynamics (PD), e.g. by leading to different phenotypes of enzymes (poor, intermediate, extensive or ultra rapid metabolizer). Single nucleotide polymorphisms (SNPs) are the main cause for genetic polymorphisms.

2.2 Pharmacogenetics - relevant *CYP2C8* polymorphisms

The *CYP2C8*3* allele is characterized by substitution of two amino acids (Arg139Lys, Lys399Arg) caused by two SNPs (G416A, A1196G) in exon 3 and exon 8 [1,2]. Carriers of the *CYP2C8*3* allele (either heterozygous or homozygous) show lower plasma concentrations and areas under the concentration-time curve (AUCs) of repaglinide and pioglitazone than *CYP2C8*1*1* (wild type) carriers [3–7], consistent with increased drug metabolism by CYP2C8. In the models, polymorphic CYP2C8 was implemented as two enzymes with halved reference concentration each (Table S3.9.1). In the repaglinide model, the catalytic rate constant (k_{cat}) was optimized for the *CYP2C8*1* and *CYP2C8*3* alleles assuming the same literature value for K_M (Table S3.4.2). For pioglitazone as CYP2C8 substrate, different K_M values for *CYP2C8*1*1* and *CYP2C8*3*3* (measured in HLM) [8] are reported in the literature and thus used in the model. As described for the repaglinide model, two different *CYP2C8* alleles were implemented into the pioglitazone model and k_{cat} values of both alleles were optimized.

2.3 Pharmacogenetics - relevant *SLCO1B1* polymorphisms

Two polymorphisms in the solute carrier organic anion transporter family member (*SLCO*) *1B1* gene (encoding OATP1B1 transporter) were considered in this project. The SNP in exon 5 of the *SLCO1B1* gene (*521T>C*), results in an amino acid change (Val174Ala) [9]. Subjects carrying this polymorphism (included in diplotypes **5*, **15* and **17*) show a decreased OATP1B1 function [10] and increased repaglinide AUC and maximum plasma concentration (C_{max}) [11]. The SNP *-11187G>A* is located in the promoter region of *SLCO1B1* (**17* and **21*) [9,10]. Heterozygous carriers also exhibit increased repaglinide AUC and C_{max} [4].

In the repaglinide model, polymorphic OATP1B1 was implemented as two transporters with halved reference concentration each (Table S3.9.1). For all genotypes, the same literature K_M value was used and the k_{cat} values of the four different alleles were optimized.

3 PBPK model development

3.1 PBPK model development – general

In this study, physiologically-based pharmacokinetic (PBPK) models of **gemfibrozil**, **gemfibrozil 1-O-β-glucuronide**, **repaglinide** and **pioglitazone** were built. For model development, plasma concentration-time profiles of published clinical studies covering the full reported dosing range were used, including data of intravenous and oral administration as single or multiple doses. If information about the amount of unchanged drug excreted to urine or feces was available, it was also utilized to inform the model optimization. All clinical studies used for single compound model development are listed in Tables S3.3.1, S3.4.1 and S3.5.1, including information about the assignment of each study to the internal (parameter optimization) or external data set (model evaluation). Parameter optimizations were performed by fitting the model simultaneously to all observed mean plasma concentration-time profiles of the internal data set, using mean individuals that were generated to match the mean age, weight, height, sex and ethnicity of each respective study population. Parameters of the final models are given in Tables S3.3.2, S3.4.2 and S3.5.2.

Previously developed PBPK models of itraconazole, rifampicin and clarithromycin [12] were extended by incorporation of CYP2C8, OATP1B1 and OATP1B3 interaction parameters and their DDI performance with victim drugs of these pathways was evaluated within the DDI network established in this study (shown in Section 4). Furthermore, the itraconazole model was adapted to describe the low plasma concentration-time profiles observed during gemfibrozil co-administration, by implementation of solubility changes for this DDI. Parameters of the itraconazole, rifampicin and clarithromycin models are given in Tables S3.6.1, S3.7.1 and S3.8.1.

Plots depicting predicted plasma concentration-time profiles of virtual populations compared to observed data are presented in Figs. S3.3.1, S3.3.3, S3.4.1, S3.4.3, S3.5.1, S3.6.1 and S3.6.2 (semilogarithmic) and Figs. S3.3.2, S3.3.4, S3.4.2, S3.4.4, S3.5.2, S3.6.1 and S3.6.2 (linear). Goodness of fit plots to compare predicted and observed plasma concentrations are shown in Figs. S3.3.5, S3.4.5 and S3.5.3. Mean relative deviation (MRD) values for all studies are given in Tables S3.3.3, S3.4.3 and S3.5.3. Figs. showing predicted compared to observed AUC values calculated from time 0 to infinity (AUC_{inf}) and C_{max} values are given in Figs. S3.3.6, S3.4.6 and S3.5.4. Tables S3.3.4, S3.4.4 and S3.5.4 list the predicted and observed AUC_{inf} and C_{max} values of all studies as well as geometric mean fold errors (GMFEs) for each model. Figs. showing

predicted compared to observed apparent oral clearance (CL/F) and half-life values are given in Figs. S3.3.7, S3.4.7 and S3.5.5. Tables S3.3.5, S3.4.5 and S3.5.5 list the predicted and observed CL/F and half-life values of all studies as well as GMFEs for each model. The results of sensitivity analyses are presented in Figs. S3.3.8, S3.3.9, S3.3.10, S3.4.8, S3.4.9, S3.5.6 and S3.5.7.

The system-dependent parameters for all models, including reference concentrations with geometric standard deviation, tissue expression as well as protein half-lives in liver and intestine of all enzymes and transporters implemented in the models are given in Table S3.9.1. In all individuals and populations, the enterohepatic circulation (EHC) was enabled (EHC continuous fraction set to 1) by assuming a continuous flow from bile to duodenum.

3.2 PBPK model development – quantitative model evaluation

As quantitative measures of the model performance, the MRDs of the predicted plasma concentrations and the GMFEs of the AUC_{inf} and C_{max} values were calculated.

The MRDs were calculated according to equation 3.1:

$$MRD = 10^{x};\ x = \sqrt{\frac{\sum\left(\log_{10}\left(c_{observed}\right) - \log_{10}\left(c_{predicted}\right)\right)^{2}}{N}} \qquad (3.1)$$

with $c_{observed}$ = observed plasma concentration, $c_{predicted}$ = corresponding predicted plasma concentration, N = number of observed values. An MRD value ≤ 2 signifies that the average of the values predicted by the model equals the observed values or deviates not more than twofold, characterizing an adequate prediction [13].

The GMFEs were calculated according to equation 3.2:

$$GMFE = 10^{x};\ x = \frac{\sum \left| \log_{10}\left(\frac{\text{predicted PK parameter}}{\text{observed PK parameter}}\right)\right|}{n} \qquad (3.2)$$

with predicted PK parameter = predicted AUC_{inf}, C_{max}, CL/F or half-life value, observed PK parameter = corresponding observed AUC_{inf}, C_{max}, CL/F or half-life value, n = number of studies. A GMFE value ≤ 2 characterizes an adequate prediction.

3.3 Gemfibrozil and gemfibrozil 1-O-β-glucuronide model development

The antihyperlipidaemic drug gemfibrozil is a strong CYP2C8 inhibitor [14], as its metabolite gemfibrozil 1-O-β-glucuronide inactivates CYP2C8 in a mechanism-based manner [15]. Gemfibrozil itself is a competitive inhibitor of CYP2C8 [16] and both, parent drug and metabolite, are competitive inhibitors of OATP1B1 [17].

A gemfibrozil-gemfibrozil 1-O-β-glucuronide parent-metabolite model was developed using 23 different clinical studies (oral administration of gemfibrozil), whereof 10 studies also show plasma concentration-time profiles of the metabolite next to the parent drug (Table S3.3.1). The dosing range of these studies is 30 – 900 mg gemfibrozil single dose and 30 – 600 mg twice daily. A hepatocyte to plasma concentration ratio of 28.5% was reported for gemfibrozil 1-O-β-glucuronide in one study [18] and used for parameter optimization.

The parent-metabolite model applies an active uptake transport of gemfibrozil into hepatocytes, metabolism by UDP-glucuronosyltransferase (UGT) 2B7 to form gemfibrozil 1-O-β-glucuronide and glomerular filtration of gemfibrozil. For gemfibrozil 1-O-β-glucuronide, the model applies hepatic uptake via OATP1B1, efflux transport into bile via multidrug resistance-associated protein (MRP) 2 and glomerular filtration. All enzyme and transporter processes are implemented with saturable Michaelis-Menten kinetics. As gemfibrozil 1-O-β-glucuronide is an OATP1B1 substrate, K_i values to describe the competitive inhibition of OATP1B1 by both gemfibrozil and its metabolite have been incorporated into the model (K_i = 25.2 µmol/l and K_i = 22.6 µmol/l for gemfibrozil and gemfibrozil 1-O-β-glucuronide, respectively [17]). As no information about fraction unbound in the incubation (fu_{inc}) of gemfibrozil and gemfibrozil 1-O-β-glucuronide in the assay used to determine these K_i values was available (uptake into OATP1B1-expressing HEK-293 cells [17]), no correction for fu_{inc} was performed. The parameters of the final parent-metabolite model are given in Table S3.3.2.

The good descriptive (internal data set) and predictive (external data set) performance of the parent-metabolite model is demonstrated in semilogarithmic (Figs. S3.3.1 and S3.3.3) as well as linear plots (Figs. S3.3.2 and S3.3.4) of population predicted compared to observed plasma concentration-time profiles of all clinical studies. Furthermore, goodness of fit plots comparing predicted versus observed plasma concentrations for gemfibrozil and gemfibrozil 1-O-β-glucuronide are presented (Fig. S3.3.5) and MRD values for each study are given in Table S3.3.3. Correlation of predicted and observed AUC, C_{max}, CL/F and half-life values is presented in Figs. S3.3.6 and S3.3.7, and the corresponding values are given in Tables S3.3.4 and S3.3.5, including calculated model GMFE values.

Sensitivity analysis of a simulation of oral 600 mg gemfibrozil twice daily with a parameter perturbation of 100% and a sensitivity threshold value of 0.5 reveals that the parent model is sensitive to the gemfibrozil lipophilicity (optimized), the UGT2B7 catalytic rate constant (optimized), the gemfibrozil fraction unbound in plasma (literature value), the UGT2B7 Michaelis-Menten constant (literature value) and the active hepatic uptake transporter catalytic rate constant (optimized) (Fig. S3.3.8). The gemfibrozil 1-O-β-glucuronide model is sensitive to the gemfibrozil 1-O-β-glucuronide lipophilicity (optimized), the MRP2 catalytic rate constant (optimized), the gemfibrozil lipophilicity (optimized), the MRP2 Michaelis-Menten constant (optimized), the gemfibrozil 1-O-β-glucuronide fraction unbound in plasma (literature value) and the OATP1B1 catalytic rate constant (optimized) (Fig. S3.3.9). Sensitivity analysis spider plots showing the change of AUC over a parameter variation range of 0.03-fold up to 30-fold are presented in Fig. S3.3.10.

Table S3.3.1. Clinical study data of gemfibrozil used for PBPK model development.

Route	Dose [mg]	*n*	Females [%]	Age [years]	Weight [kg]	Gemfibrozil 1-O-β-glucuronide measurement	Data set	References
Gemfibrozil								
po (cap, s.d.)	30	10	10	20-26 (23)	60-88 (73)	yes	i	Honkalammi 2011b [18] [a]
po (cap, b.i.d.)	30	10	40	21-30 (24)	64-88 (75)	yes	i	Honkalammi 2012 [19]
po (cap, s.d.)	100	10	10	20-26 (23)	60-88 (73)	yes	i	Honkalammi 2011b [18] [a]
po (cap, b.i.d.)	100	10	40	21-30 (24)	64-88 (75)	yes	i	Honkalammi 2012 [19]
po (cap, s.d.)	300	10	10	20-26 (23)	60-88 (73)	yes	i	Honkalammi 2011b [18] [a]
po (cap, s.d.)	300	12	-	-	-	no	e	Randinitis 1984 [20]
po (cap, s.d.)	300	12	-	-	-	no	e	Randinitis 1986 [21]
po (cap, s.d.)	300	12	-	23-35	65-80	no	e	Rouini 2006 [22]
po (-, s.d.)	450	6	0	-	-	no	e	Nakagawa 1991 [23]
po (tab, s.d.)	600	37	0	(34.8)	(77.9)	no	e	ApotexCorp. 1998 Ref [24]
po (tab, s.d.)	600	37	0	(34.8)	(77.9)	no	e	ApotexCorp. 1998 Test [24]
po (tab, s.d.)	600	15	47	(37)	(78)	no	e	Busse 2009 [25]
po (-, s.d.)	600	-	0	-	-	no	e	Gonzáles-Peñas 2001 [26]
po (tab, s.d.)	600	10	50	31-34	-	yes	e	Honkalammi 2011a [27]
po (cap, s.d.)	600	12	-	23-35	65-80	no	e	Rouini 2006 [22]
po (cap, s.d.)	600	12	-	-	-	no	e	Rouini 2008 [28]
po (tab, s.d.)	600	12	0	18-24	-	no	e	Su 2010 [29]
po (tab, b.i.d.)	600	9	22	19-25	64-87	yes	i	Backman 2009 [30]
po (cap, b.i.d.)	600	10	40	21-30 (24)	64-88 (75)	yes	e	Honkalammi 2012 [19]
po (tab, b.i.d.)	600	10	10	-	58-98 (79)	yes	e	Tornio 2008 [31]
po (cap, s.d.)	900	10	10	20-26 (23)	60-88 (73)	yes	i	Honkalammi 2011b [18] [a]
po (cap, s.d.)	900	6	50	23-33 (28)	49-85 (63)	no	e	Knauf 1990 [32]
po (cap, s.d.)	900	12	-	23-35	65-80	no	e	Rouini 2006 [22]

[a], hepatocyte to plasma concentration ratio given; values for age and weight are given as range (mean); -, not given; b.i.d., twice daily; cap, capsule; e, external data set (model evaluation); i, internal data set (model building); *n*, number of individuals studied; po, oral; s.d., single dose; tab, tablet.

Table S3.3.2. Drug-dependent parameters of the final gemfibrozil-gemfibrozil 1-O-β-glucuronide model.

Parameter	Unit	Gemfibrozil model	Gemfibrozil literature	Gemfibrozil 1-O-β-glucuronide model	Gemfibrozil 1-O-β-glucuronide literature	Description
Gemfibrozil						
MW	g/mol	250.33		426.46		Molecular weight
pKa		4.70	[33]	2.68	[34]	Acid dissociation constant
Solubility (pH)	mg/l	170 (5.9)	[35]	789 (7.0)	[36] [a]	Solubility
logP		2.8	2.8, 4.3, 4.77 [34,35,37]	1.41	1.22, 2.44 [36] [a]	Lipophilicity
fu		6.48E-03	6.48E-03, 0.021, 0.03 [34,38,39]	0.115	0.115, 0.171 [38,39]	Fraction unbound plasma
Active hepatic uptake K_M	µmol/l	2.39	n.a.	-	-	Active hepatic uptake Michaelis-Menten constant
Active hepatic uptake k_{cat}	1/min	59.42	n.a.	-	-	Active hepatic uptake catalytic rate constant
OATP1B1 K_M	µmol/l	-	-	0.43	n.a.	OATP1B1 Michaelis-Menten constant
OATP1B1 k_{cat}	1/min	-	-	15.36	n.a.	OATP1B1 catalytic rate constant
MRP2 K_M	µmol/l	-	-	21.49	n.a.	MRP2 Michaelis-Menten constant
MRP2 k_{cat}	1/min	-	-	7.13	n.a.	MRP2 catalytic rate constant
UGT2B7 K_M	µmol/l	2.20	[40]	-	-	UGT2B7 Michaelis-Menten constant
UGT2B7 k_{cat}	1/min	51.98	n.a.	-	-	UGT2B7 catalytic rate constant
GFR fraction		1		1		Fraction of GFR used for passive elimination by the kidney
K_i OATP1B1	µmol/l	25.2	[17]	22.6	[17]	Inhibitory constant
K_i CYP2C8	µmol/l	30.4	[16]	-	-	Inhibitory constant
K_I CYP2C8	µmol/l	-	-	20	[15]	Concentration for half-maximal inactivation (MBI)
k_{inact} CYP2C8	1/min	-	-	0.21	[15]	Maximum inactivation rate constant (MBI)
Formulation		Weibull [b]		-	-	Formulation used in predictions
Cell permeabilities		calculated	Charge-dependent Schmitt [41]	calculated	PK-Sim Standard [42]	Permeation across cell membranes
Partition coefficients		calculated	Berezhkovskiy [43]	calculated	PK-Sim Standard [41]	Organ-plasma partition coefficients
Specific intestinal perm.	cm/min	6.62E-03	n.a.	1.22E-04	calculated	Normalized to surface area
Specific organ perm.	cm/min	0.07	calculated	5.98E-07	calculated	Normalized to surface area

[a], DrugBank entry for gemfibrozil 1-beta-glucuronide. https://www.drugbank.ca/metabolites/DBMET01165. Accessed 21 Aug 2018; [b], weibull function with dissolution time 24.45 minutes (50% dissolved) and dissolution shape 1.56 (both optimized) (one shared dissolution profile for capsules and tablets); -, process not implemented in the model; CYP, cytochrome P450; GFR, glomerular filtration rate; MRP, multidrug resistance-associated protein; n.a., not available; OATP, organic-anion-transporting polypeptide; perm, permeability; UGT, UDP-glucuronosyltransferase.

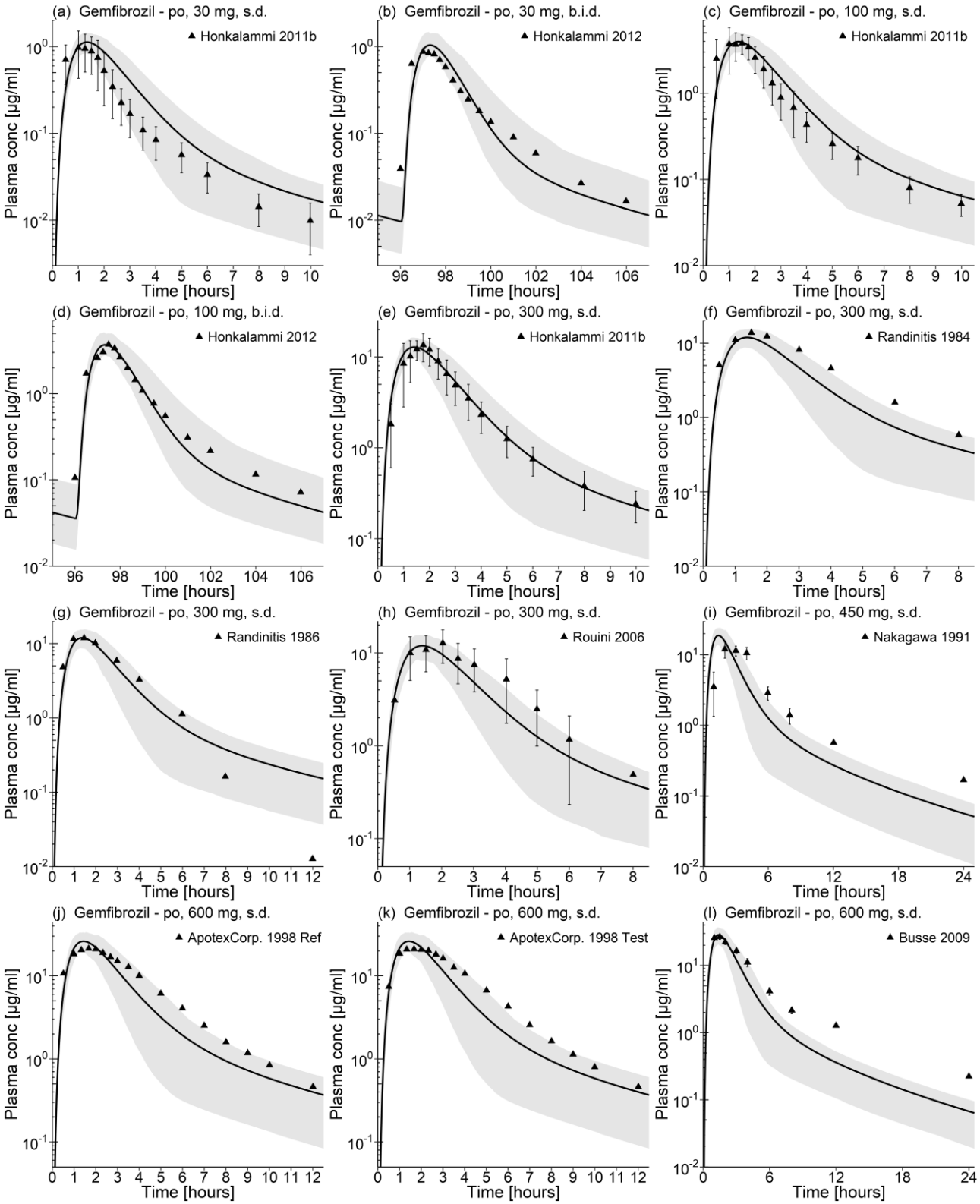
(a) Gemfibrozil - po, 30 mg, s.d.
Honkalammi 2011b
(b) Gemfibrozil - po, 30 mg, b.i.d.
Honkalammi 2012
(c) Gemfibrozil - po, 100 mg, s.d.
Honkalammi 2011b
(d) Gemfibrozil - po, 100 mg, b.i.d.
Honkalammi 2012
(e) Gemfibrozil - po, 300 mg, s.d.
Honkalammi 2011b
(f) Gemfibrozil - po, 300 mg, s.d.
Randinitis 1984
(g) Gemfibrozil - po, 300 mg, s.d.
Randinitis 1986
(h) Gemfibrozil - po, 300 mg, s.d.
Rouini 2006
(i) Gemfibrozil - po, 450 mg, s.d.
Nakagawa 1991
(j) Gemfibrozil - po, 600 mg, s.d.
ApotexCorp. 1998 Ref
(k) Gemfibrozil - po, 600 mg, s.d.
ApotexCorp. 1998 Test
(l) Gemfibrozil - po, 600 mg, s.d.
Busse 2009
Plasma conc [µg/ml]
Time [hours]

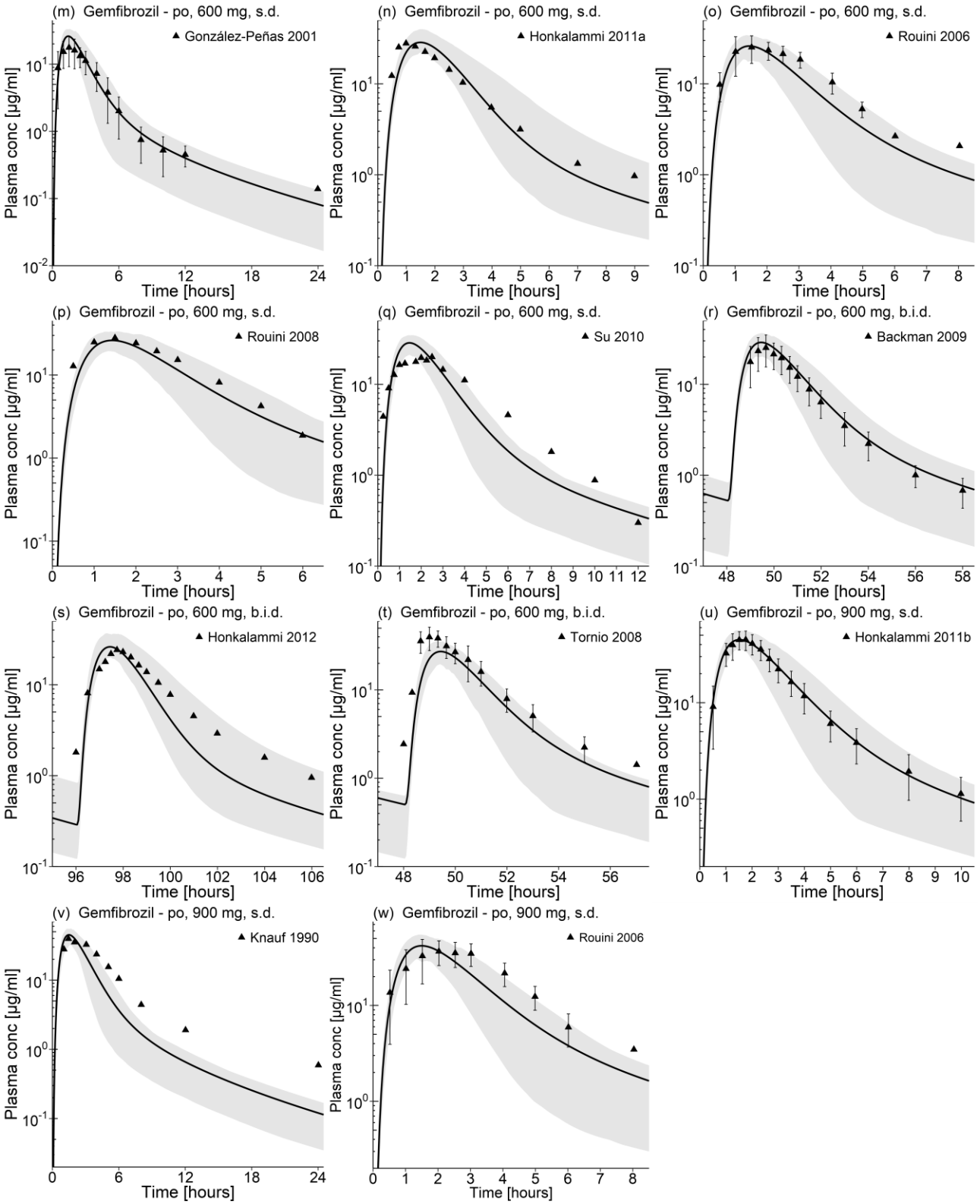

Fig. S3.3.1. Gemfibrozil plasma concentration-time profiles (semilogarithmic). Observed data are shown as triangles ± SD. Population simulation arithmetic means or geometric means (b, d, n and s) are shown as black lines; the shaded areas represent the 68% population prediction intervals. Detailed information about dosing regimens and study populations is given in Table S3.3.1. Predicted and observed AUC and C_{max} values are compared in Table S3.3.4.

b.i.d., twice daily; conc, concentration; s.d., single dose.

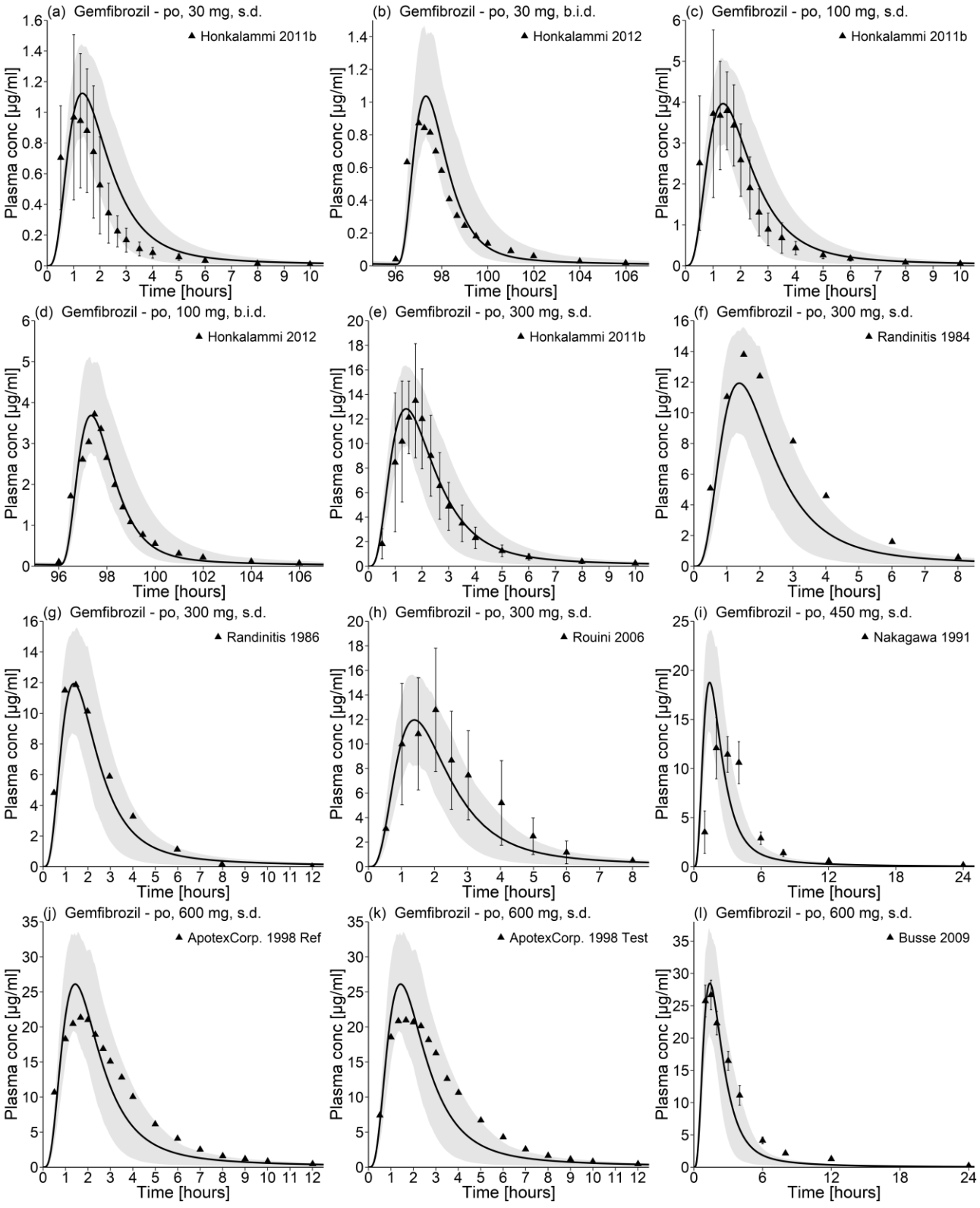
(a) Gemfibrozil - po, 30 mg, s.d.
Honkalammi 2011b
(b) Gemfibrozil - po, 30 mg, b.i.d.
Honkalammi 2012
(c) Gemfibrozil - po, 100 mg, s.d.
Honkalammi 2011b
(d) Gemfibrozil - po, 100 mg, b.i.d.
Honkalammi 2012
(e) Gemfibrozil - po, 300 mg, s.d.
Honkalammi 2011b
(f) Gemfibrozil - po, 300 mg, s.d.
Randinitis 1984
(g) Gemfibrozil - po, 300 mg, s.d.
Randinitis 1986
(h) Gemfibrozil - po, 300 mg, s.d.
Rouini 2006
(i) Gemfibrozil - po, 450 mg, s.d.
Nakagawa 1991
(j) Gemfibrozil - po, 600 mg, s.d.
ApotexCorp. 1998 Ref
(k) Gemfibrozil - po, 600 mg, s.d.
ApotexCorp. 1998 Test
(l) Gemfibrozil - po, 600 mg, s.d.
Busse 2009
Plasma conc [µg/ml]
Time [hours]

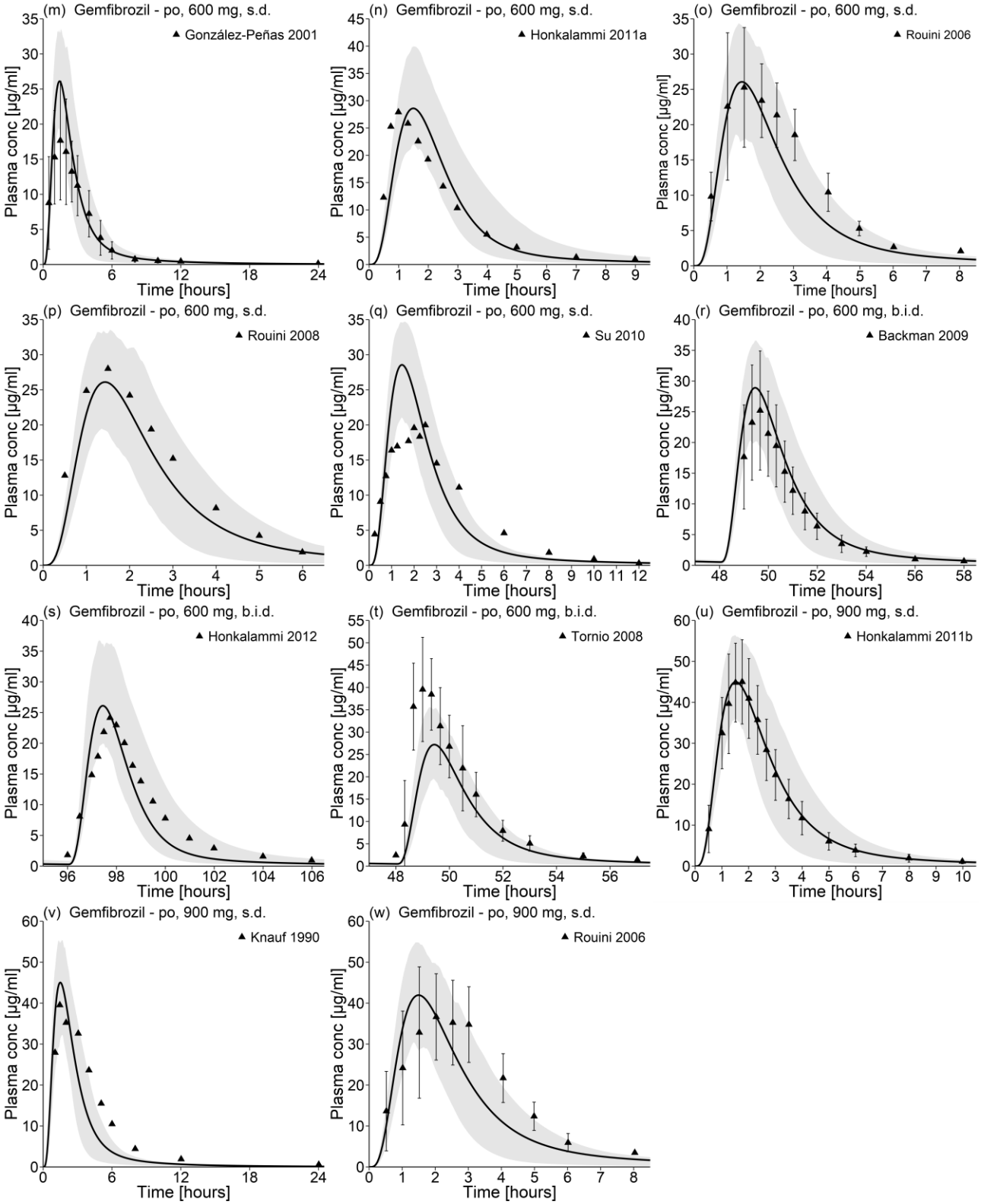

Fig. S3.3.2. Gemfibrozil plasma concentration-time profiles (linear). Observed data are shown as triangles ± SD. Population simulation arithmetic means or geometric means (b, d, n and s) are shown as black lines; the shaded areas represent the 68% population prediction intervals. Detailed information about dosing regimens and study populations is given in Table S3.3.1. Predicted and observed AUC and C_{max} values are compared in Table S3.3.4.

b.i.d., twice daily; conc, concentration; s.d., single dose.

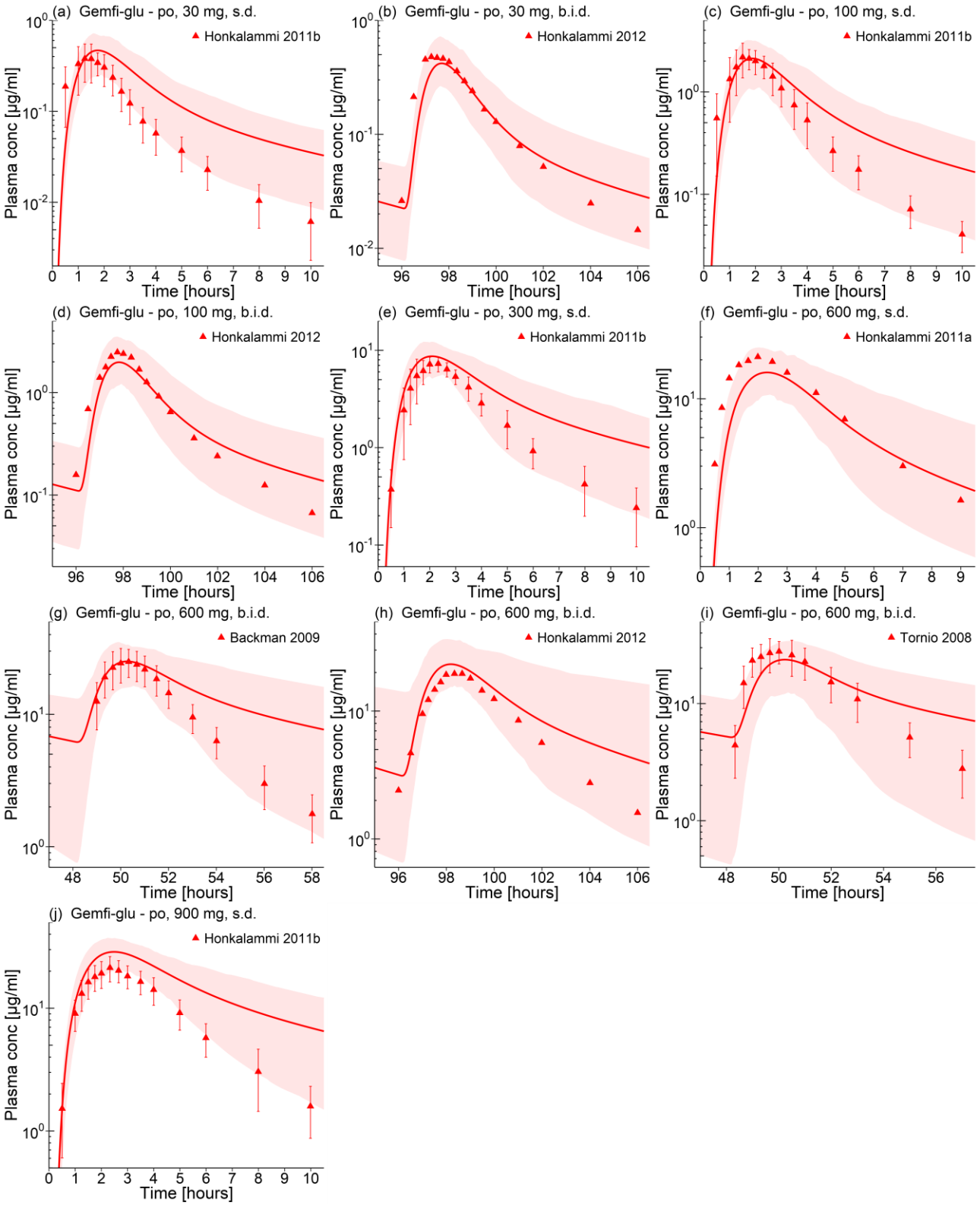

Fig. S3.3.3. Gemfibrozil 1-O-β-glucuronide (Gemfi-glu) concentration-time profiles (semilogarithmic) following administration of gemfibrozil. Observed data are shown as triangles ± SD. Population simulation arithmetic means or geometric means (b, d, f and h) are shown as red lines; the shaded areas represent the 68% population prediction intervals. Detailed information about dosing regimens and study populations is given in Table S3.3.1 Predicted and observed AUC and C_{max} values are compared in Table S3.3.4.

b.i.d., twice daily; conc, concentration; s.d., single dose.

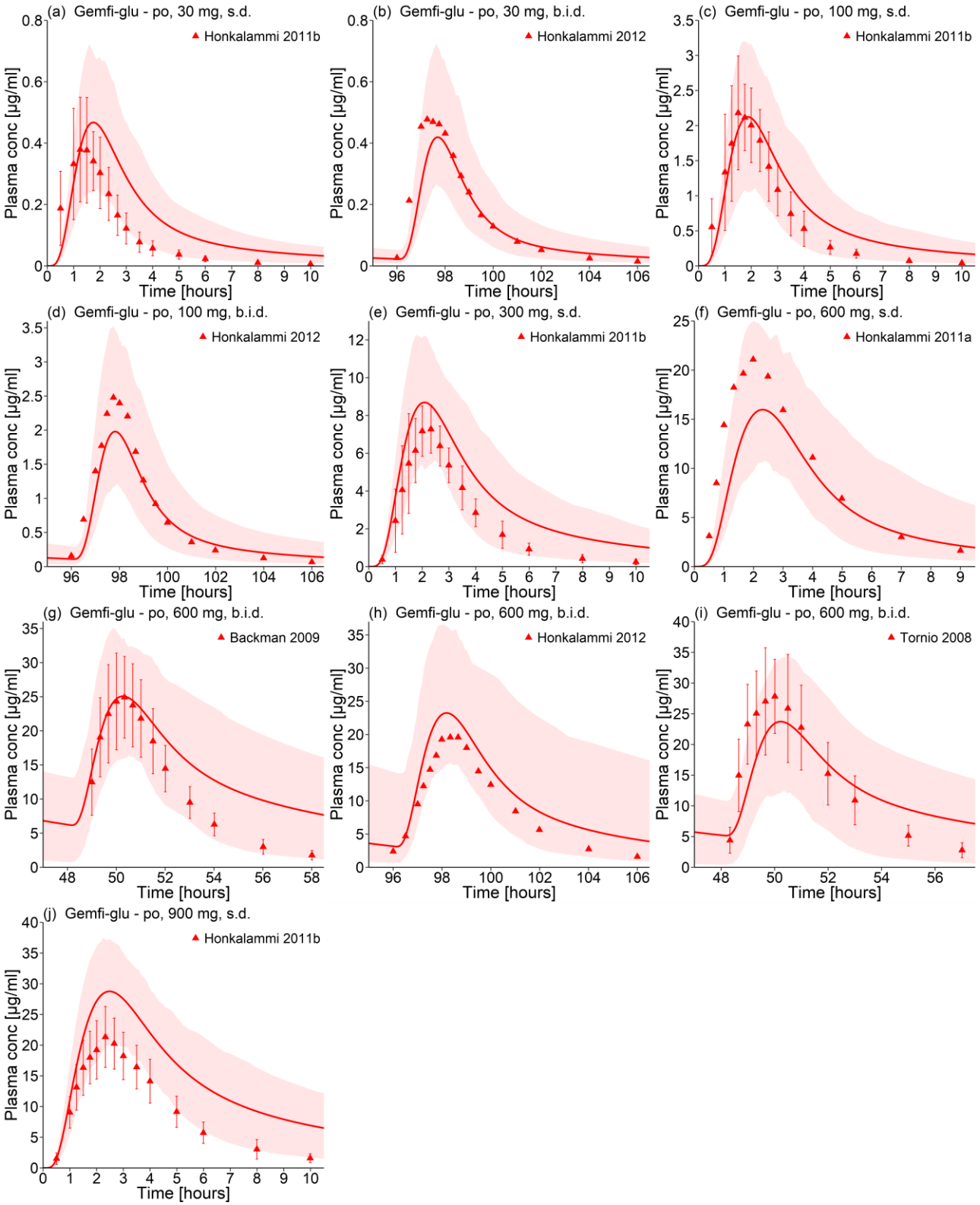

Fig. S3.3.4. Gemfibrozil 1-O-β-glucuronide (Gemfi-glu) plasma concentration-time profiles (linear) following administration of gemfibrozil. Observed data are shown as triangles ± SD. Population simulation arithmetic means or geometric means (b, d, f and h) are shown as red lines; the shaded areas represent the 68% population prediction intervals. Detailed information about dosing regimens and study populations is given in Table S3.3.1. Predicted and observed AUC and C_{max} values are compared in Table S3.3.4.

b.i.d., twice daily; conc, concentration; s.d., single dose.

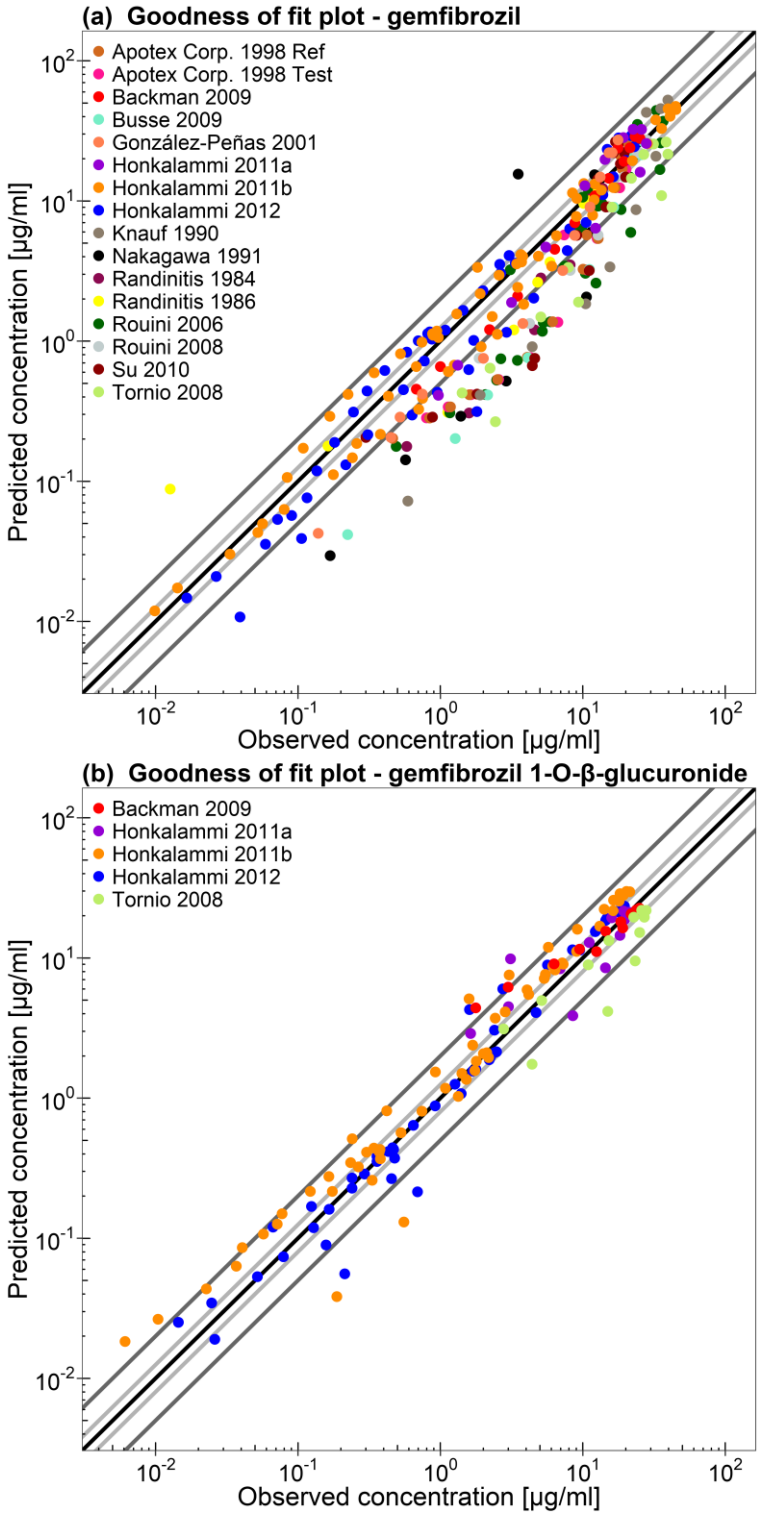

Fig. S3.3.5. Goodness of fit plots. Comparison of predicted versus observed gemfibrozil (a) and gemfibrozil 1-O-β-glucuronide (b) plasma concentration values of all studies. The black line marks the line of identity. Light grey lines indicate 0.8- to 1.25-fold; dark grey lines indicate 0.5- to 2-fold prediction acceptance limits. Detailed information about dosing regimens and study populations is given in Table S3.3.1.

Table S3.3.3. Mean relative deviation values of gemfibrozil and gemfibrozil 1-O-β-glucuronide plasma concentration predictions.

Route	Dose [mg]	Gemfibrozil MRD	Gemfibrozil 1-O-β-glucuronide MRD	References
Gemfibrozil				
po (cap, s.d.)	30	1.48	1.99	Honkalammi 2011b [18]
po (cap, b.i.d.)	30	1.62	1.51	Honkalammi 2012 [19]
po (cap, s.d.)	100	1.33	1.58	Honkalammi 2011b [18]
po (cap, b.i.d.)	100	1.45	1.46	Honkalammi 2012 [19]
po (cap, s.d.)	300	1.49	1.50	Honkalammi 2011b [18]
po (cap, s.d.)	300	2.56	-	Randinitis 1984 [20]
po (cap, s.d.)	300	2.42	-	Randinitis 1986 [21]
po (cap, s.d.)	300	2.49	-	Rouini 2006 [22]
po (-, s.d.)	450	4.07	-	Nakagawa 1991 [23]
po (tab, s.d.)	600	2.60	-	ApotexCorp. 1998 Ref [24]
po (tab, s.d.)	600	2.63	-	ApotexCorp. 1998 Test [24]
po (tab, s.d.)	600	3.44	-	Busse 2009 [25]
po (-, s.d.)	600	1.98	-	Gonzáles-Peñas 2001[26]
po (tab, s.d.)	600	1.59	1.63	Honkalammi 2011a [27]
po (cap, s.d.)	600	2.51	-	Rouini 2006 [22]
po (cap, s.d.)	600	1.96	-	Rouini 2008 [28]
po (tab, s.d.)	600	2.53	-	Su 2010 [29]
po (tab, b.i.d.)	600	1.37	1.42	Backman 2009 [30]
po (cap, b.i.d.)	600	1.95	1.47	Honkalammi 2012 [19]
po (tab, b.i.d.)	600	2.95	1.76	Tornio 2008 [31]
po (cap, s.d.)	900	1.46	1.72	Honkalammi 2011b [18]
po (cap, s.d.)	900	3.56	-	Knauf 1990 [32]
po (cap, s.d.)	900	2.67	-	Rouini 2006 [22]
	MRD (mean)	**2.27**	**1.60**	
	MRD ≤ 2	**11/23**	**10/10**	

-, not given; b.i.d., twice daily; cap, capsule; MRD, mean relative deviation; po, oral; s.d., single dose; tab, tablet.

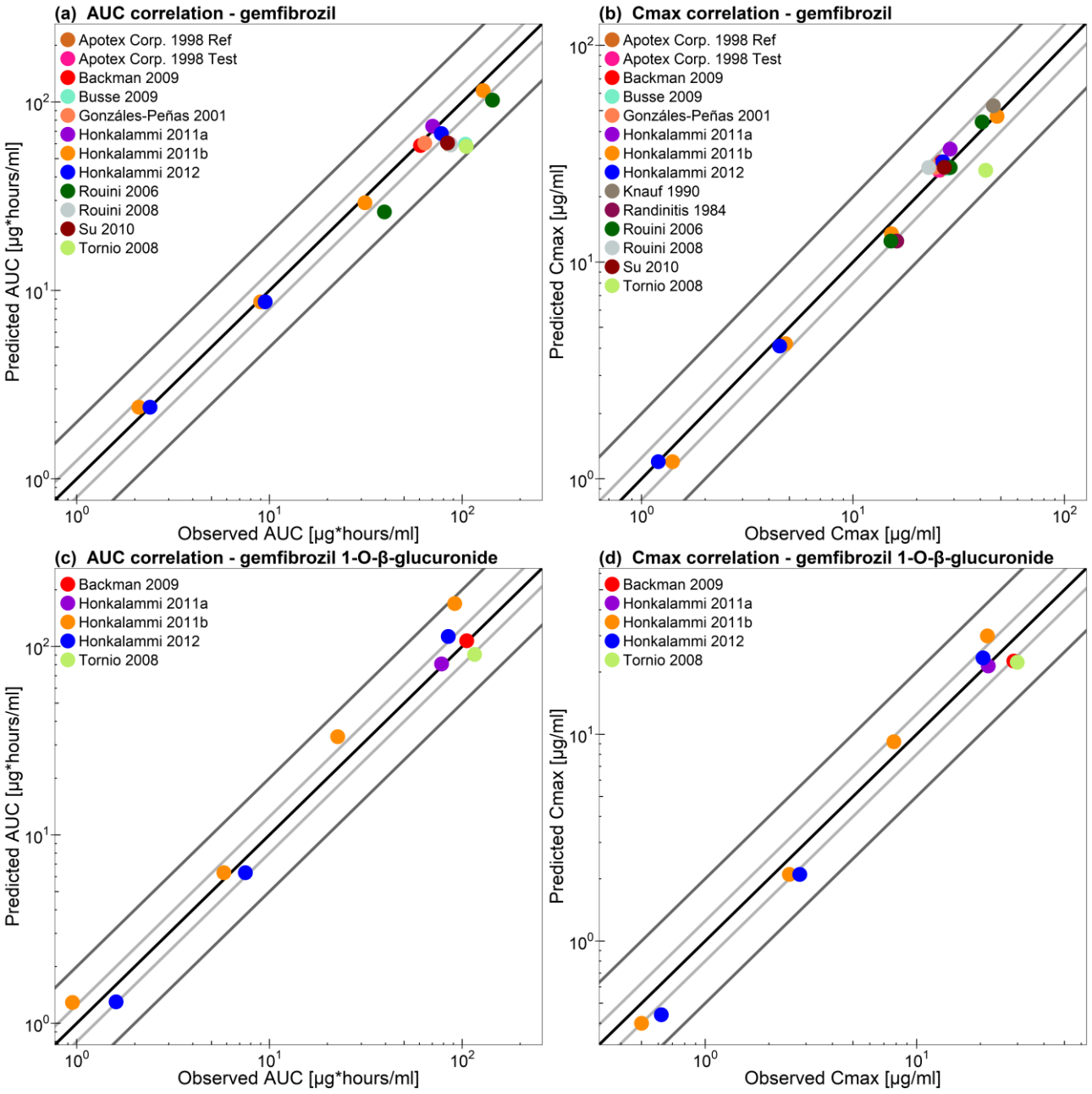

Fig. S3.3.6. Correlation of predicted and observed gemfibrozil (upper panel) and gemfibrozil 1-O-β-glucuronide (lower panel) AUC and C_{max} values of all studies. The black line marks the line of identity. Light grey lines indicate 0.8- to 1.25-fold; dark grey lines indicate 0.5- to 2-fold prediction acceptance limits. Detailed information about dosing regimens and study populations is given in Table S3.3.1. The plotted AUC and C_{max} values are listed in Table S3.3.4.

Table S3.3.4. Predicted and observed AUC and C_{max} values of gemfibrozil and gemfibrozil 1-O-β-glucuronide.

Route	Dose [mg]	AUC [µg*hours/ml]		Pred/Obs AUC	C_{max} [µg/ml]		Pred/Obs C_{max}	References
Gemfibrozil		*pred*	*obs*		*pred*	*obs*		
po (cap, s.d.)	30	2.4	2.1	1.15	1.2	1.4	0.84	Honkalammi 2011b [18]
po (cap, b.i.d.)	30	2.4	2.4 [c]	1.00	1.2	1.2	0.97	Honkalammi 2012 [19]
po (cap, s.d.)	100	8.7	9.0	0.96	4.2	4.8	0.87	Honkalammi 2011b [18]
po (cap, b.i.d.)	100	8.7	9.5 [c]	0.91	4.1	4.5	0.92	Honkalammi 2012 [19]
po (cap, s.d.)	300	29.3	31.3	0.93	13.5	15.2	0.89	Honkalammi 2011b [18]
po (cap, s.d.)	300	-	-	-	12.5	16.1	0.78	Randinitis 1984 [20]
po (cap, s.d.)	300	-	-	-	-	-	-	Randinitis 1986 [21]
po (cap, s.d.)	300	26.1	39.5	0.66	12.5	15.1	0.83	Rouini 2006 [22]
po (-, s.d.)	450	-	-	-	-	-	-	Nakagawa 1991 [23]
po (tab, s.d.)	600	59.49	85.69	0.69	26.54	25.79	1.03	ApotexCorp. 1998 Ref [24]
po (tab, s.d.)	600	59.49	86.89	0.68	26.54	25.46	1.04	ApotexCorp. 1998 Test [24]
po (tab, s.d.)	600	59.7	104	0.57	27	28	0.95	Busse 2009 [25]
po (-, s.d.)	600	60.50	63.98 [a]	0.95	27.34	24.55	1.11	Gonzáles-Peñas 2001[26]
po (tab, s.d.)	600	74.4	70.3 [b]	1.06	33.2	28.8	1.15	Honkalammi 2011a [27]
po (cap, s.d.)	600	60.1	85.2	0.70	27.3	28.8	0.95	Rouini 2006 [22]
po (cap, s.d.)	600	59.1	87.1	0.68	27.3	22.8	1.20	Rouini 2008 [28]
po (tab, s.d.)	600	60.66	83.98	0.72	27.34	27.02	1.01	Su 2010 [29]
po (tab, b.i.d.)	600	58.8	60.8 [b]	0.97	29.0	26.2	1.11	Backman 2009 [30]
po (cap, b.i.d.)	600	67.7	78.0 [c]	0.87	29.2	26.6	1.10	Honkalammi 2012 [19]
po (tab, b.i.d.)	600	58.1	105 [b]	0.55	26.5	42.4	0.63	Tornio 2008 [31]
po (cap, s.d.)	900	115.0	128.5	0.90	47.3	48.0	0.99	Honkalammi 2011b [18]
po (cap, s.d.)	900	-	-	-	52.6	46.1	1.14	Knauf 1990 [32]
po (cap, s.d.)	900	102.3	143.7	0.71	27.3	40.8	1.08	Rouini 2006 [22]
			GMFE (range)	**1.26 (1.00-1.81)**			**1.13 (1.01-1.60)**	
			Pred/Obs within 2-fold	**19/19**			**21/21**	
Gemfibrozil 1-O-β-glucuronide		*pred*	*obs*		*pred*	*obs*		
po (cap, s.d.)	30	1.29	0.95	1.35	0.4	0.5	0.88	Honkalammi 2011b [18]
po (cap, b.i.d.)	30	1.3	1.6 [c]	0.80	0.44	0.62	0.72	Honkalammi 2012 [19]
po (cap, s.d.)	100	6.3	5.8	1.08	2.1	2.5	0.85	Honkalammi 2011b [18]

continued…

continued…

Route	Dose [mg]	AUC [µg*hours/ml]		Pred/Obs AUC	C_{max} [µg/ml]		Pred/Obs C_{max}	References
po (cap, b.i.d.)	100	6.3	7.5 [c]	0.84	2.1	2.8	0.77	Honkalammi 2012 [19]
po (cap, s.d.)	300	33.2	22.6	1.47	9.2	7.8	1.18	Honkalammi 2011b [18]
po (tab, s.d.)	600	80.8	78.2 [b]	1.03	21.4	21.8	0.98	Honkalammi 2011a [27]
po (tab, b.i.d.)	600	107.2	105.6 [b]	1.02	22.6	28.8	0.79	Backman 2009 [30]
po (cap, b.i.d.)	600	113	84.7 [c]	1.34	23.4	20.6	1.14	Honkalammi 2012 [19]
po (tab, b.i.d.)	600	90.7	116 [b]	0.78	22.3	29.9	0.74	Tornio 2008 [31]
po (cap, s.d.)	900	169	91.5	1.85	29.9	21.6	1.39	Honkalammi 2011b [18]
		GMFE (range)		**1.27 (1.02-1.85)**			**1.23 (1.02-1.40)**	
		Pred/Obs within 2-fold		**10/10**			**10/10**	

[a], AUC_{0-24}; [b], AUC_{0-9}; [c], AUC_{0-10}; AUC values are AUC_{inf}, if not specified differently; -, not given; AUC, area under the concentration-time curve; b.i.d., twice daily; cap, capsule; C_{max}, maximum plasma concentration; GMFE, geometric mean fold error; obs, observed; po, oral; pred, predicted; s.d., single dose; tab, tablet.

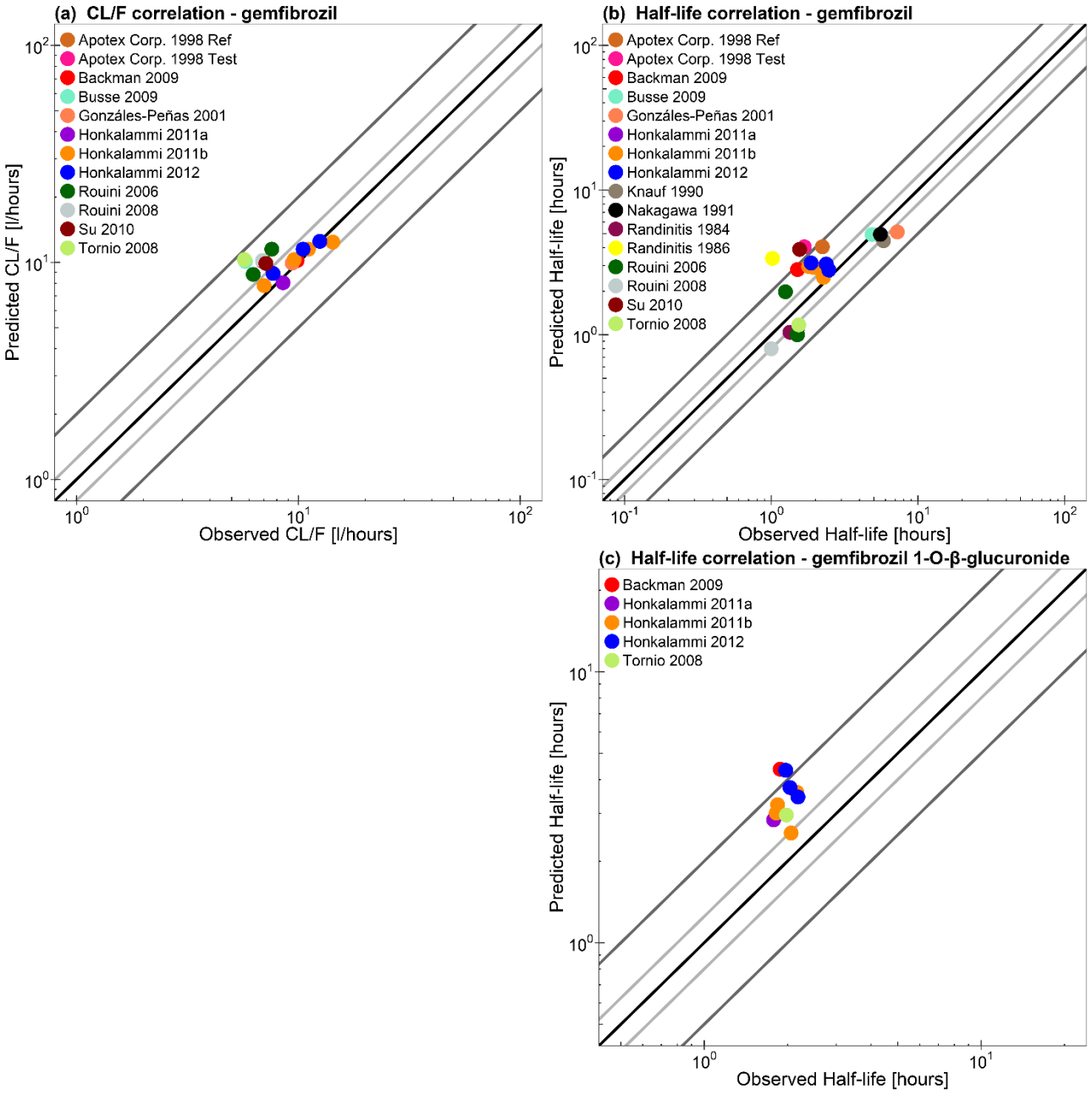

Fig. S3.3.7. Correlation of predicted and observed gemfibrozil (upper panel) and gemfibrozil 1-O-β-glucuronide (lower panel) CL/F and half-life values of all studies. The black line marks the line of identity. Light grey lines indicate 0.8- to 1.25-fold; dark grey lines indicate 0.5- to 2-fold prediction acceptance limits. Detailed information about dosing regimens and study populations is given in Table S3.3.1. The plotted CL/F and half-life values are listed in Table S3.3.5.

Table S3.3.5. Predicted and observed CL/F and half-life of gemfibrozil and gemfibrozil 1-O-β-glucuronide.

Route	Dose [mg]	CL/F [a] [l/hours]		Pred/Obs CL/F	Half-life [b] [hours]		Pred/Obs Half-life	References
Gemfibrozil		*pred*	*obs*		*pred*	*obs*		
po (cap, s.d.)	30	12.4	14.3	0.87	2.96	1.80	1.64	Honkalammi 2011b [18]
po (cap, b.i.d.)	30	12.5	12.5	1.00	3.13	1.87	1.68	Honkalammi 2012 [19]
po (cap, s.d.)	100	11.5	11.1	1.04	2.91	1.96	1.48	Honkalammi 2011b [18]
po (cap, b.i.d.)	100	11.5	10.5	1.10	3.08	2.37	1.30	Honkalammi 2012 [19]
po (cap, s.d.)	300	10.3	9.58	1.07	2.82	2.43	1.16	Honkalammi 2011b [18]
po (cap, s.d.)	300	-	-	-	1.04	1.34	0.78	Randinitis 1984 [20]
po (cap, s.d.)	300	-	-	-	3.37	1.02	3.32	Randinitis 1986 [21]
po (cap, s.d.)	300	11.5	7.59	1.52	1.98	1.25	1.58	Rouini 2006 [22]
po (-, s.d.)	450	-	-	-	4.94	5.55	0.89	Nakagawa 1991 [23]
po (tab, s.d.)	600	10.1	7.00	1.44	4.05	2.23	1.81	ApotexCorp. 1998 Ref [24]
po (tab, s.d.)	600	10.1	6.91	1.46	4.05	1.68	2.41	ApotexCorp. 1998 Test [24]
po (tab, s.d.)	600	10.1	5.77	1.74	4.93	4.87	1.01	Busse 2009 [25]
po (-, s.d.)	600	9.92	9.38	1.06	5.13	7.23	0.71	Gonzáles-Peñas 2001[26]
po (tab, s.d.)	600	8.06	8.53	0.94	1.08	1.50	0.72	Honkalammi 2011a [27]
po (cap, s.d.)	600	10.0	7.04	1.42	1.00	1.51	0.66	Rouini 2006 [22]
po (cap, s.d.)	600	10.2	6.89	1.47	0.80	1.00	0.80	Rouini 2008 [28]
po (tab, s.d.)	600	9.89	7.14	1.38	3.89	1.56	2.49	Su 2010 [29]
po (tab, b.i.d.)	600	10.2	9.87	1.03	2.82	1.51	1.87	Backman 2009 [30]
po (cap, b.i.d.)	600	8.89	7.69	1.15	2.80	2.47	1.13	Honkalammi 2012 [19]
po (tab, b.i.d.)	600	10.3	5.71	1.81	1.17	1.54	0.76	Tornio 2008 [31]
po (cap, s.d.)	900	7.82	7.00	1.12	2.49	2.27	1.10	Honkalammi 2011b [18]
po (cap, s.d.)	900	-	-	-	4.46	5.82	0.77	Knauf 1990 [32]
po (cap, s.d.)	900	8.80	6.26	1.41	1.00	1.50	0.67	Rouini 2006 [22]
			GMFE (range)	**1.26 (1.00-1.81)**			**1.50 (1.01-3.32)**	
			Pred/Obs within 2-fold	**19/19**			**20/23**	
Gemfibrozil 1-O-β-glucuronide					*pred*	*obs*		
po (cap, s.d.)	30				3.23	1.84	1.76	Honkalammi 2011b [18]
po (cap, b.i.d.)	30				3.74	2.04	1.83	Honkalammi 2012 [19]
po (cap, s.d.)	100				3.01	1.82	1.65	Honkalammi 2011b [18]

continued…

continued…

Route	Dose [mg]	Half-life [hours]		Pred/Obs Half-life	References
po (cap, b.i.d.)	100	3.45	2.18	1.59	Honkalammi 2012 [19]
po (cap, s.d.)	300	2.54	2.06	1.23	Honkalammi 2011b [18]
po (tab, s.d.)	600	2.84	1.78	1.60	Honkalammi 2011a [27]
po (tab, b.i.d.)	600	4.37	1.88	2.32	Backman 2009 [30]
po (cap, b.i.d.)	600	4.33	1.97	2.20	Honkalammi 2012 [19]
po (tab, b.i.d.)	600	2.96	1.98	1.49	Tornio 2008 [31]
po (cap, s.d.)	900	3.59	2.16	1.66	Honkalammi 2011b [18]
			GMFE (range)	**1.71 (1.23-2.32)**	
			Pred/Obs within 2-fold	**8/10**	

[a], calculated from dose/AUC; [b], calculated for observed and predicted concentration-time profiles (same time points for observed and predicted values); -, not given; AUC, area under the concentration-time curve; b.i.d., twice daily; cap, capsule; CL/F, oral clearance; GMFE, geometric mean fold error; obs, observed; po, oral; pred, predicted; s.d., single dose; tab, tablet.

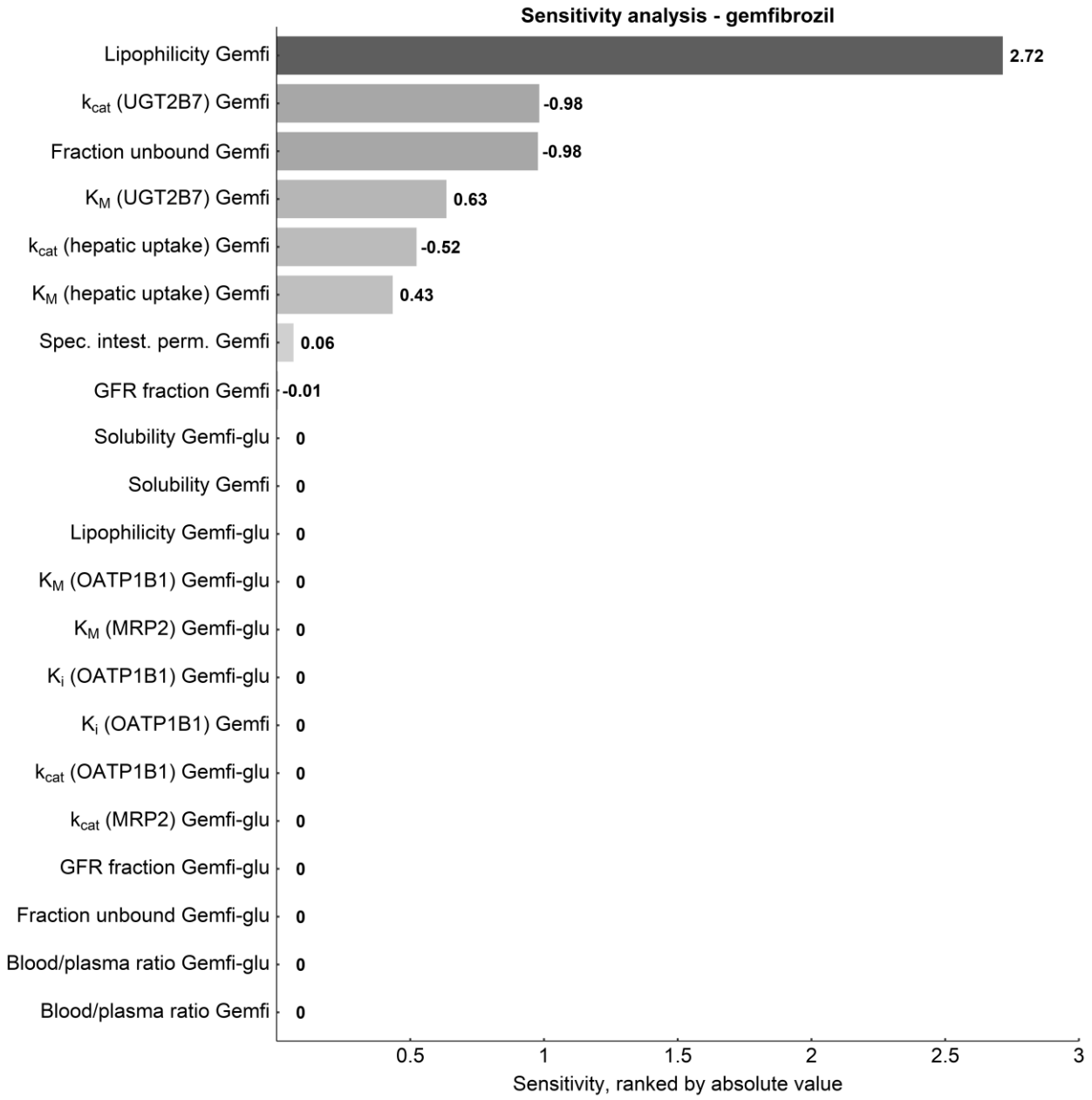

Fig. S3.3.8. Sensitivity analysis of the gemfibrozil model. Sensitivity of the model to single parameters, determined as change of the simulated AUC from time of the last dose extrapolated to infinity of an oral 600 mg twice daily administration of gemfibrozil. A sensitivity value of -0.5 indicates a 50% decrease of the simulated AUC for the examined parameter increase of 100%.
Gemfi, gemfibrozil; Gemfi-glu, gemfibrozil 1-O-β-glucuronide; GFR, glomerular filtration rate; intest., intestinal; k_{cat}, catalytic rate constant; K_i, inhibitory constant; K_M, Michaelis-Menten constant; MRP, multidrug resistance-associated protein; OATP, organic-anion-transporting polypeptide; perm., permeability; spec., specific; UGT, UDP-glucuronosyltransferase.

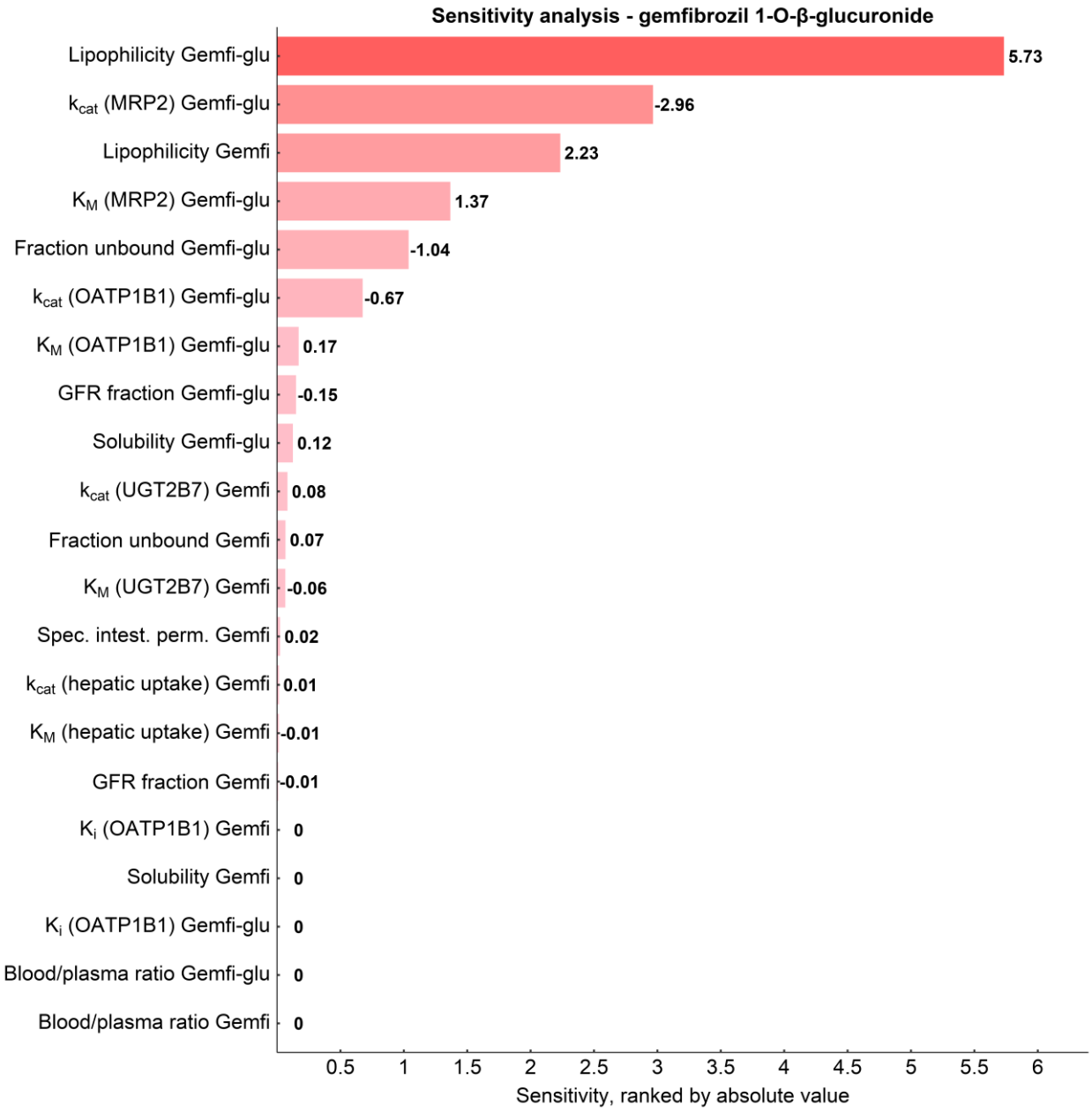

Fig. S3.3.9. Sensitivity analysis of the gemfibrozil 1-O-β-glucuronide model. Sensitivity of the model to single parameters, determined as change of the simulated AUC from time of the last dose extrapolated to infinity of an oral 600 mg twice daily administration of the parent drug gemfibrozil. A sensitivity value of -0.5 indicates a 50% decrease of the simulated AUC for the examined parameter increase of 100%.

Gemfi, gemfibrozil; Gemfi-glu, gemfibrozil 1-O-β-glucuronide; GFR, glomerular filtration rate; intest., intestinal; k_{cat}, catalytic rate constant; K_i, inhibitory constant; K_M, Michaelis-Menten constant; MRP, multidrug resistance-associated protein; OATP, organic-anion-transporting polypeptide; perm., permeability; spec., specific; UGT, UDP-glucuronosyltransferase.

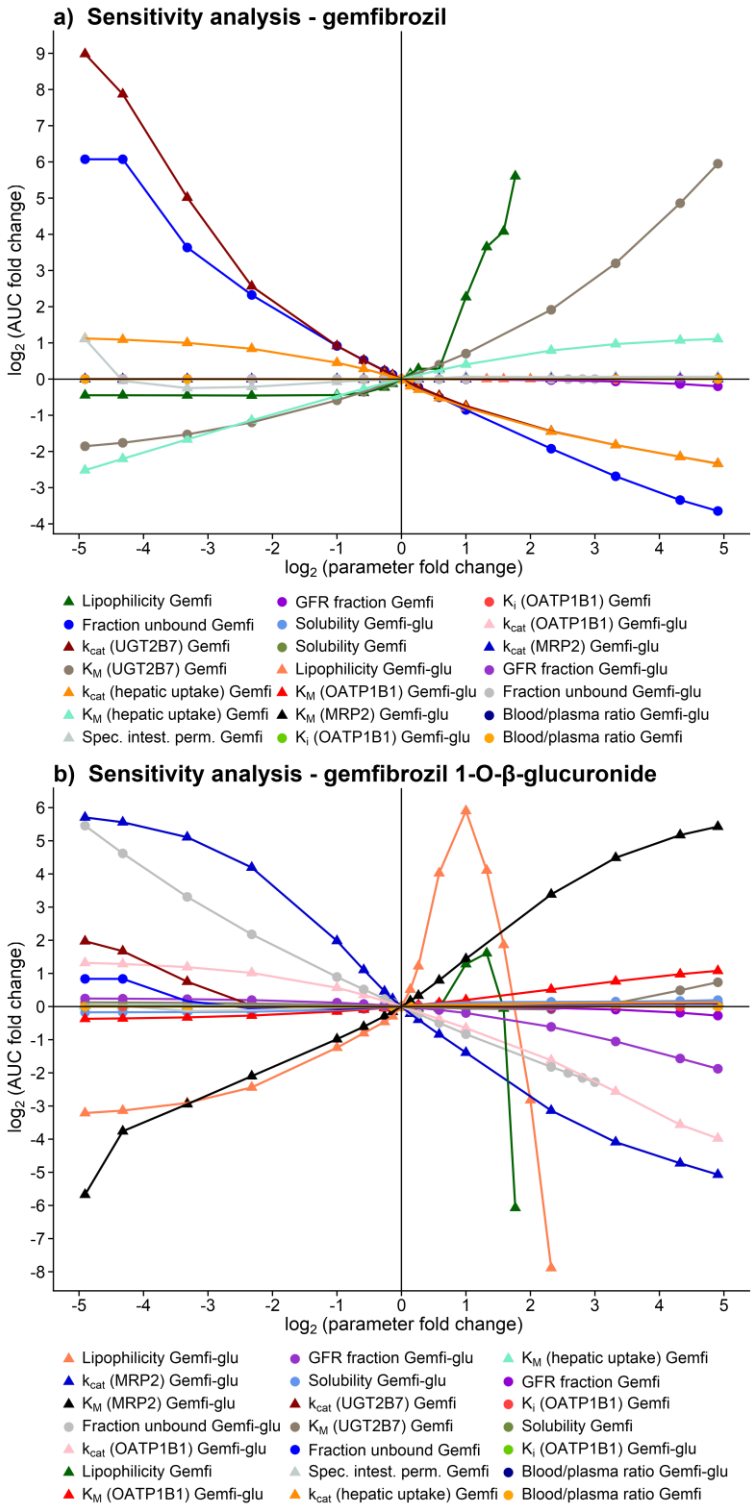

Fig. S3.3.10. Sensitivity analysis spider plots of the gemfibrozil (a) and gemfibrozil 1-O-β-glucuronide (b) parent-metabolite model. The fold change of AUC is shown as a function of the fold change of the parameter values within a 0.03-fold to 30-fold range. A $\log_2$(fold change) = 1 equals a parameter perturbation of 100% as shown in the sensitivity analysis bar plots. Literature value parameters are shown as circles, optimized parameters are shown as triangles. Lipophilicity was changed only to a maximum absolute value of 10.

3.4 Repaglinide model development

Repaglinide is applied in the treatment of type 2 diabetes mellitus and elicits a glucose-independent insulin release. It is a sensitive CYP2C8 substrate [14].

The repaglinide model was developed using 56 studies of oral single dose administration of 0.25 – 4 mg repaglinide and of oral administration of 2 mg three times daily (Table S3.4.1).

The model applies hepatic uptake of repaglinide via OATP1B1 and OATP1B3, metabolism by CYP2C8 and CYP3A4 and glomerular filtration. The fractions transported via OATP1B1 and OATP1B3 during the hepatic uptake of repaglinide (same K_M value assumed [44]) were identified with the help of plasma concentration-time profiles of subjects with the *SLCO1B1 521CC* genotype. The fraction metabolized by CYP2C8 was set to 89%, according to the findings of a gemfibrozil-repaglinide interaction study [18]. To describe the repaglinide plasma concentration-time profiles of individuals carrying the high activity *CYP2C8*3* allele, CYP2C8 was implemented as two enzymes with halved reference concentrations (Table S3.9.1), using the same literature K_M value for the **1* and **3 CYP2C8* variants and two different optimized k_{cat} values (Table S3.4.2). The same approach was used to implement the *SLCO1B1* variants for *SLCO1B1 521T>C* and *SLCO1B1 -11187G>A* allele carriers. To incorporate the polymorphic CYP2C8 and OATP1B1, the parameters of a previously developed model without polymorphisms were fixed, polymorphic enzymes / transporters were integrated and their k_{cat} values were optimized using clinical studies of repaglinide in volunteers with different respective genotypes. The parameters of the final repaglinide model are given in Table S3.4.2.

The good descriptive (internal data set) and predictive (external data set) performance of the repaglinide model is demonstrated in semilogarithmic (Figs. S3.4.1 and S3.4.3) as well as linear plots (Figs. S3.4.2 and S3.4.4) of population predicted compared to observed plasma concentration-time profiles of all clinical studies. Furthermore, goodness of fit plots comparing predicted versus observed plasma concentrations for repaglinide are presented (Fig. S3.4.5) and MRD values for each study are given in Table S3.4.3. Correlation of predicted and observed AUC, C_{max}, CL/F and half-life values is presented in Figs. S3.4.6 and S3.4.7, and the corresponding values are given in Tables S3.4.4 and S3.4.5, including calculated model GMFE values.

Sensitivity analysis of a simulation of oral 4 mg repaglinide four times daily with a parameter perturbation of 100% and a sensitivity threshold value of 0.5 reveals that the repaglinide model is sensitive to the fraction unbound in plasma (optimized), the CYP2C8 catalytic rate constant (optimized), the CYP2C8 Michaelis-Menten constant (literature value), the repaglinide lipophilicity (optimized), the specific organ permeability (optimized), the OATP1B1 catalytic rate constant (optimized) and the OATP1B1 Michaelis-Menten constant (literature value) (Fig. S3.4.8). A

sensitivity analysis spider plot showing the change of AUC over a parameter variation range of 0.03-fold up to 30-fold is presented in Fig. S3.4.9.

Table S3.4.1. Clinical study data of repaglinide used for PBPK model development.

Route	Dose [mg]	*n*	Females [%]	Age [years]	Weight [kg]	*CYP2C8* genotype	*SLCO1B1* genotype	Data set	References
Repaglinide									
iv, (15 min, s.d.)	2	12	0	18-45	-	-	-	e	Hatorp 1998 [45]
po (tab, s.d.)	0.25	9	22	19-25	64-87	-	-	e	Backman 2009 [30]
po (tab, s.d.)	0.25	10	50	31-34	-	-	-	e	Honkalammi 2011a [27]
po (tab, s.d.)	0.25	10	10	20-26 (23)	60-88 (73)	-	-	i	Honkalammi 2011b [18]
po (tab, s.d.)	0.25	10	40	21-30 (24)	64-88 (75)	-	-	e	Honkalammi 2012 [19]
po (tab, s.d.)	0.25	12	0	19-25 (23)	56-100 (75)	-	-	e	Kajosaari 2005b [46]
po (tab, s.d.)	0.25	12	33	18-24	52-85	-	-	e	Kajosaari 2006a [47]
po (tab, s.d.)	0.25	12	17	21-28 (24)	57-100 (71)	-	-	e	Kajosaari 2006b [48]
po (tab, s.d.)	0.25	12	25	(24)	(75)	-	*521TT*	e	Kalliokoski 2008b [49]
po (tab, s.d.)	0.25	6	17	(23)	(74)	-	*521TC*	e	Kalliokoski 2008b [49]
po (tab, s.d.)	0.25	6	17	(23)	(75)	-	*521CC*	e	Kalliokoski 2008b [49]
po (tab, s.d.)	0.25	12	58	(24)	(71)	-	*521TT*	i	Kalliokoski 2008c [50]
po (tab, s.d.)	0.25	8	63	(24)	(70)	-	*521CC*	i	Kalliokoski 2008c [50]
po (tab, s.d.)	0.25	9	44	22-27 (24.0)	52-83 (67.4)	-	-	e	Niemi 2001 [51]
po (tab, s.d.)	0.25	12	67	20-24	46-84	-	-	e	Niemi 2003a [52]
po (tab, s.d.)	0.25	28	43	19-27 (22)	46-97 (69)	**1/*1*: *n*=19, **1/*3*: *n*=6	-	i i	Niemi 2003b [3]
po (tab, s.d.)	0.25	9	11	19-23	62-97	-	-	e	Niemi 2004 [53]
po (tab, s.d.)	0.25	56	20	19-28 (23)	46-100 (73)	-	*521TT*: *n*=36, *521TC*: *n*=16; *521CC*: *n*=4	e, e, e	Niemi 2005 [4]
po (tab, s.d.)	0.25	56	20	19-28 (23)	46-100 (73)	-	*-11187GG*: *n*=48, *-11187GA*: *n*=8	e, e	Niemi 2005 [4]
po (tab, s.d.)	0.25	56	20	19-28 (23)	46-100 (73)	**1/*1*: *n*=41 **1/*3*: *n*=10 **1/*4*: *n*=5	-	e, e, not used	Niemi 2005 [4]
po (tab, s.d.)	0.25	10	10	-	58-98 (79)	-	-	e	Tornio 2008 [31]
po (tab, s.d.)	0.5	16	31	(22)	(73)	-	*521TT*	e	Kalliokoski 2008a [54]
po (tab, s.d.)	0.5	12	50	(22)	(68)	-	*521TC*	e	Kalliokoski 2008a [54]
po (tab, s.d.)	0.5	4	25	(22)	(78)	-	*521CC*	i	Kalliokoski 2008a [54]

continued…

continued…

Route	Dose [mg]	*n*	Females [%]	Age [years]	Weight [kg]	*CYP2C8* genotype	*SLCO1B1* genotype	Data set	References
Repaglinide									
po (tab, s.d.)	0.5	12	58	(24)	(71)	-	*521TT*	e	Kalliokoski 2008c [50]
po (tab, s.d.)	0.5	8	63	(24)	(70)	-	*521CC*	i	Kalliokoski 2008c [50]
po (tab, s.d.)	0.5	9	56	19-25	48-80	-	-	i	Niemi 2000 [55]
po (-, s.d.)	0.5	24	0	(34)	(85)	-	-	e	Skerjanec 2010 [56]
po (tab, s.d.)	1	12	58	(24)	(71)	-	*521TT*	e	Kalliokoski 2008c [50]
po (tab, s.d.)	1	8	63	(24)	(70)	-	*521CC*	i	Kalliokoski 2008c [50]
po (tab, s.d.)	2	12	58	(24)	(71)	-	*521TT*	i	Kalliokoski 2008c [50]
po (tab, s.d.)	2	8	63	(24)	(70)	-	*521CC*	i	Kalliokoski 2008c [50]
po (tab, s.d.)	2	70	0	18-55	-	-	-	i	EMA 2011 Ref [57]
po (tab, s.d.)	2	70	0	18-55	-	-	-	e	EMA 2011 Test [57]
po (sol, s.d.)	2	24	0	18-49	-	-		e	Hatorp 1998 [45]
po (tab, s.d.),	2	24	0	18-49	-	-		i	Hatorp 1998 [45]
po (-, s.d.)	2	12	50	18-40 (32.7)	63.6-102.2 (79.9)	-	-	e	Hatorp 1999 [58]
po (tab, s.d.)	2	7	0	(24.0)	(67.3)	-	*521TC*	e	He 2011 [59]
po (tab, s.d.)	2	21	0	(24.2)	(60.2)	-	*521TT*: *n*=14, *521TC*: *n*=7	e, e	Pei 2018 (1) [60]
po (tab, s.d.)	2	21 [a]	0	(24.2)	(60.2)	-	*521TT*: *n*=11, *521TC*: *n*=5	e, e	Pei 2018 (2) [60]
po (tab, s.d.)	2	29	52	24-64 (35)	-	**1/*1*: *n*=12, **1/*3*: *n*=13, **3/*3*: *n*=4	-	e, e, e	Tomalik-Sch. 2011 [5]
po (tab, s.d.)	2	22	0	20-29 (24.2)	51-74 (62.6)	-	-	i	Zhai 2013 Ref [61]
po (tab, s.d.)	2	22	0	20-29 (24.2)	51-74 (62.6)	-	-	e	Zhai 2013 Test [61]
po (tab, s.d.)	2	10	-	-	-	-	-	i	Zhang 2011 [62]
po (-, t.i.d.)	2	12	50	18-40 (32.7)	63.6-102.2 (79.9)	-	-	e	Hatorp 1999 [58]
po (-, t.i.d.)	2	6	17	(31.5)	(94.2)	-	-	e	Marbury 2000 [63]
po (tab, s.d.)	4	12	0	42-62 (53.2)	60.0-95.9 (78.5)	-	-	e	Hatorp 2000 [64]

[a], 5 subjects quit the trial - *n*=16; values for age and weight are given as range (mean); -, not given; CYP, cytochrome P450; e, external data set (model evaluation); i, internal data set (model building); iv, intravenous; *n*, number of individuals studied; po, oral; s.d., single dose; SLCO, solute carrier organic anion transporter family member; sol, solution; tab, tablet; t.i.d., three times daily.

Table S3.4.2. Drug-dependent parameters of the final repaglinide model.

Parameter	Unit	Repaglinide model	Repaglinide literature	Description
Repaglinide				
MW	g/mol	452.60		Molecular weight
pKa		4.16 (acidic), 6.01 (basic)	3.68, 3.96, 4.16, 4.19 [34,36,65] [a], 4.82, 5.78, 6.01, 6.20 [34,36,65] [a]	Acid dissociation constant
Solubility (pH)	mg/l	140.86 (7.4)	140.86, 200 (7.4) [66,67]	Solubility
logP		2.72	3.95, 3.98, 4.87, 5.05 [34,36,65] [a]	Lipophilicity
fu		0.029	0.015, 0.026, 0.036 [63,64,68]	Fraction unbound plasma
CYP2C8 K_M [b]	µmol/l	2.8	[16]	CYP2C8 Michaelis-Menten constant
CYP2C8 k_{cat}	1/min	4.56	n.a.	CYP2C8 catalytic rate constant
CYP2C8 (*CYP2C8*1*) k_{cat}	1/min	2.91	n.a	CYP2C8 catalytic rate constant
CYP2C8 (*CYP2C8*3*) k_{cat}	1/min	9.03	n.a.	CYP2C8 catalytic rate constant
CYP3A4 K_M	µmol/l	15.6	[16]	CYP3A4 Michaelis-Menten constant
CYP3A4 k_{cat}	1/min	0.86	n.a.	CYP3A4 catalytic rate constant
OATP1B1 K_M [c]	µmol/l	12.8	[44] [d]	OATP1B1 Michaelis-Menten constant
OATP1B1 k_{cat}	1/min	1600.24	n.a.	OATP1B1 catalytic rate constant
OATP1B1 (*SLCO1B1 521T*) k_{cat}	1/min	2161.15	n.a.	OATP1B1 catalytic rate constant
OATP1B1 (*SLCO1B1 521C*) k_{cat}	1/min	620.47	n.a.	OATP1B1 catalytic rate constant
OATP1B1 (*SLCO1B1 -11187G*) k_{cat}	1/min	1535.86	n.a.	OATP1B1 catalytic rate constant
OATP1B1 (*SLCO1B1 -11187A*) k_{cat}	1/min	19.23	n.a.	OATP1B1 catalytic rate constant
OATP1B3 K_M	µmol/l	12.8	[44] [d]	OATP1B3 Michaelis-Menten constant
OATP1B3 k_{cat}	1/min	551.24	n.a.	OATP1B3 catalytic rate constant
GFR fraction		1		Fraction of GFR used for passive elimination by the kidney
Formulation		tab/weibull [e]	[69]	Formulation used in predictions
Cell permeabilities		calculated	Charge-dependent Schmitt [41]	Permeation across cell membranes
Partition coefficients		calculated	Schmitt [70]	Organ-plasma partition coefficients
Specific intestinal perm.	cm/min	0.04	n.a.	Normalized to surface area
Specific organ perm.	cm/min	2.02E-05	n.a.	Normalized to surface area

[a], DrugBank entry for repaglinide. https //www.drugbank.ca/drugs/DB00912. Accessed 26 Jul 2018; [b], CYP2C8 Michaelis Menten constant assumed for CYP2C8 genotype unknown, *CYP2C8*1* and *CYP2C8*3* alleles; [c], OATP1B1 Michaelis-Menten constant assumed for OATP1B1 genotype unknown, *SLCO1B1 521T*, *SLCO1B1 521C*, *SLCO1B1 -11187G* and *SLCO1B1 -11187A* alleles; [d], repaglinide hepatic uptake unbound affinity constant; [e] tab: tablet dissolution profile from literature [69], weibull: weibull function with dissolution time 53.65 minutes (50% dissolved) and dissolution shape 0.66 used for 5 studies; CYP, cytochrome P450; GFR, glomerular filtration rate; n.a., not available; OATP, organic-anion-transporting polypeptide; perm, permeability; SLCO, solute carrier organic anion transporter family member.

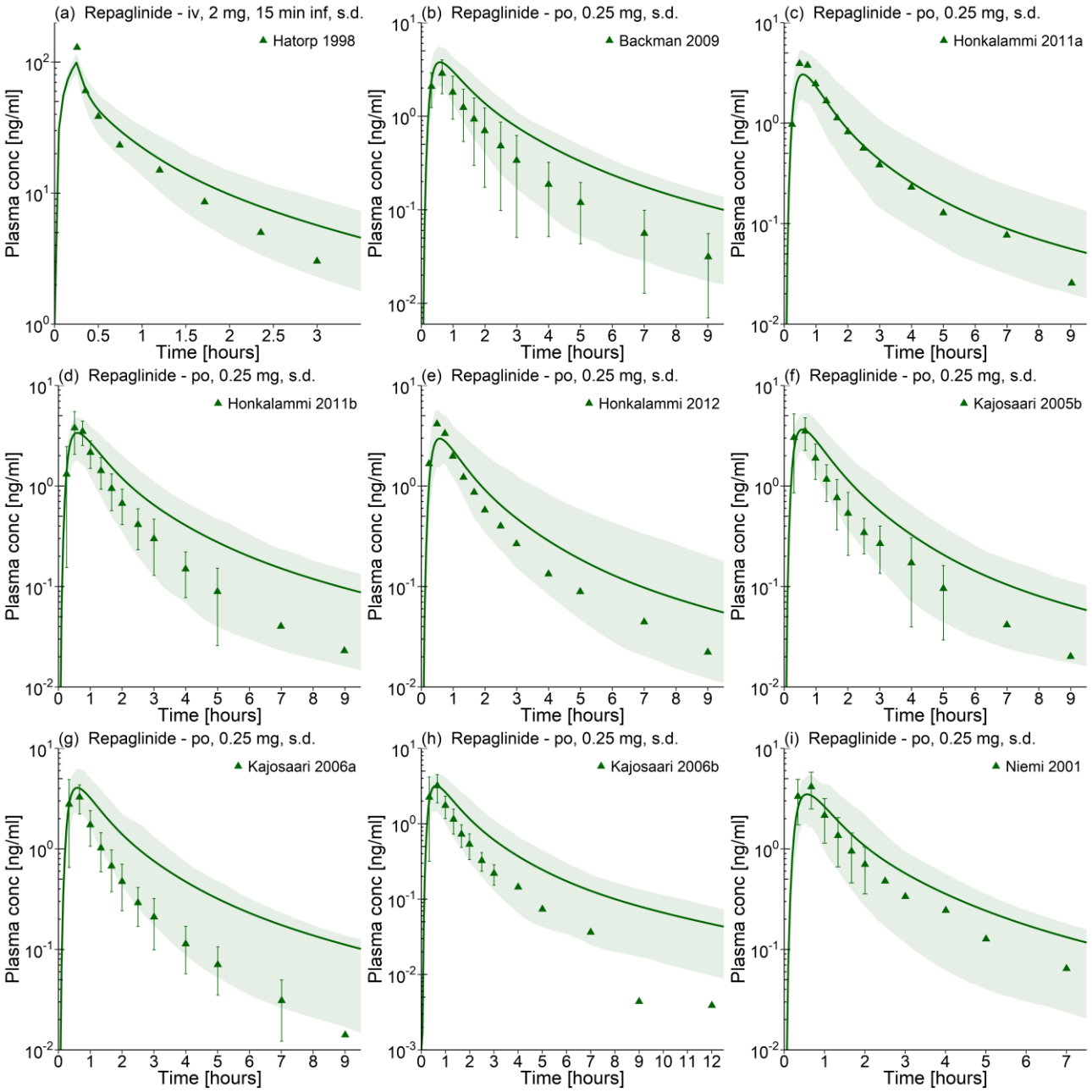
(a) Repaglinide - iv, 2 mg, 15 min inf, s.d.
Hatorp 1998
(b) Repaglinide - po, 0.25 mg, s.d.
Backman 2009
(c) Repaglinide - po, 0.25 mg, s.d.
Honkalammi 2011a
(d) Repaglinide - po, 0.25 mg, s.d.
Honkalammi 2011b
(e) Repaglinide - po, 0.25 mg, s.d.
Honkalammi 2012
(f) Repaglinide - po, 0.25 mg, s.d.
Kajosaari 2005b
(g) Repaglinide - po, 0.25 mg, s.d.
Kajosaari 2006a
(h) Repaglinide - po, 0.25 mg, s.d.
Kajosaari 2006b
(i) Repaglinide - po, 0.25 mg, s.d.
Niemi 2001
Plasma conc [ng/ml]
Time [hours]

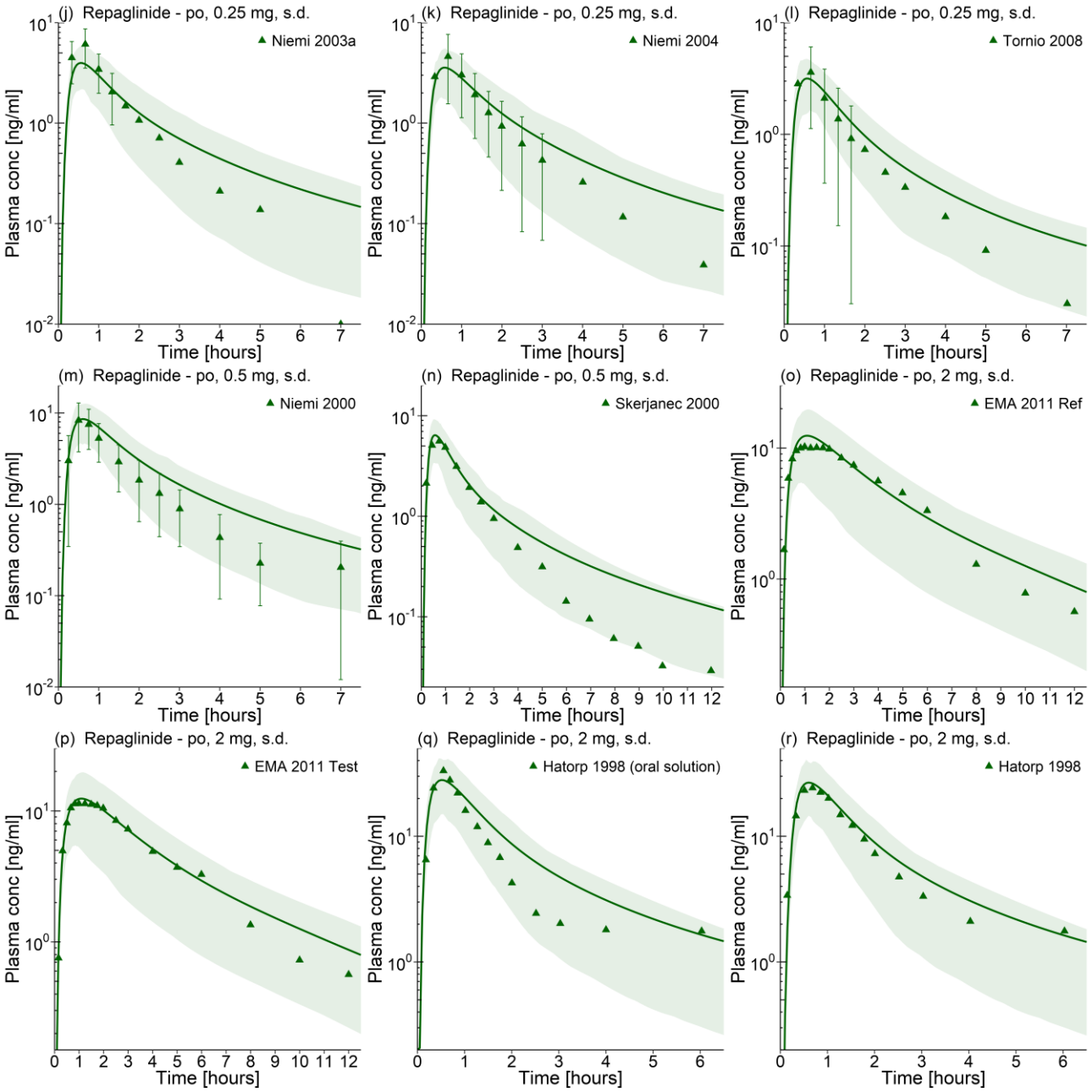
(j) Repaglinide - po, 0.25 mg, s.d.
Niemi 2003a
(k) Repaglinide - po, 0.25 mg, s.d.
Niemi 2004
(l) Repaglinide - po, 0.25 mg, s.d.
Tornio 2008
(m) Repaglinide - po, 0.5 mg, s.d.
Niemi 2000
(n) Repaglinide - po, 0.5 mg, s.d.
Skerjanec 2000
(o) Repaglinide - po, 2 mg, s.d.
EMA 2011 Ref
(p) Repaglinide - po, 2 mg, s.d.
EMA 2011 Test
(q) Repaglinide - po, 2 mg, s.d.
Hatorp 1998 (oral solution)
(r) Repaglinide - po, 2 mg, s.d.
Hatorp 1998
Plasma conc [ng/ml]
Time [hours]

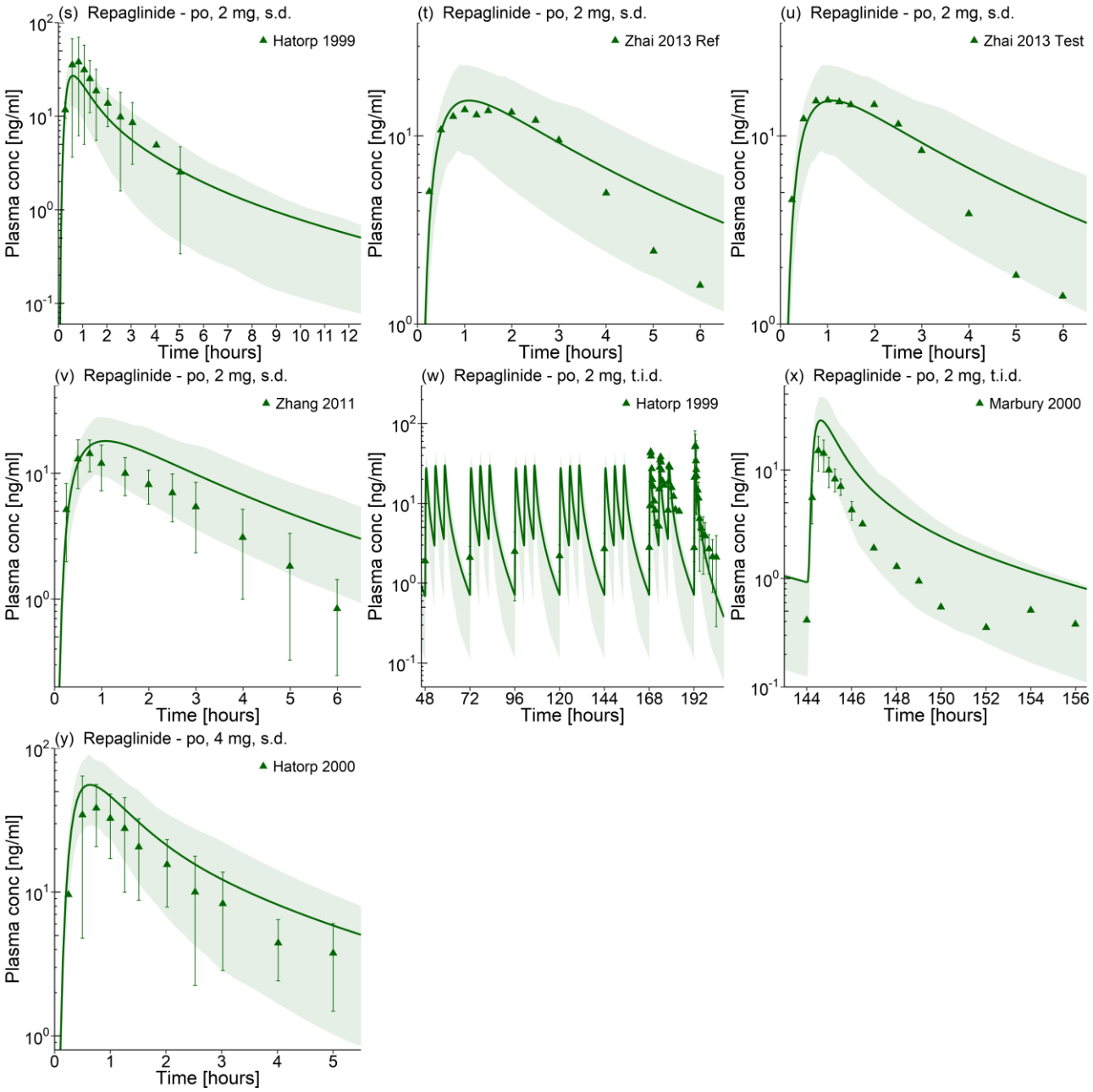

Fig. S3.4.1. Repaglinide plasma concentration-time profiles (semilogarithmic). Observed data are shown as triangles ± SD. Population simulation arithmetic means or geometric means (c, e) are shown as green lines; the shaded areas represent the 68% population prediction intervals. Detailed information about dosing regimens and study populations is given in Table S3.4.1. Predicted and observed AUC and C_{max} values are compared in Table S3.4.4.

conc, concentation; inf, infusion; s.d., single dose; t.i.d., three times daily.

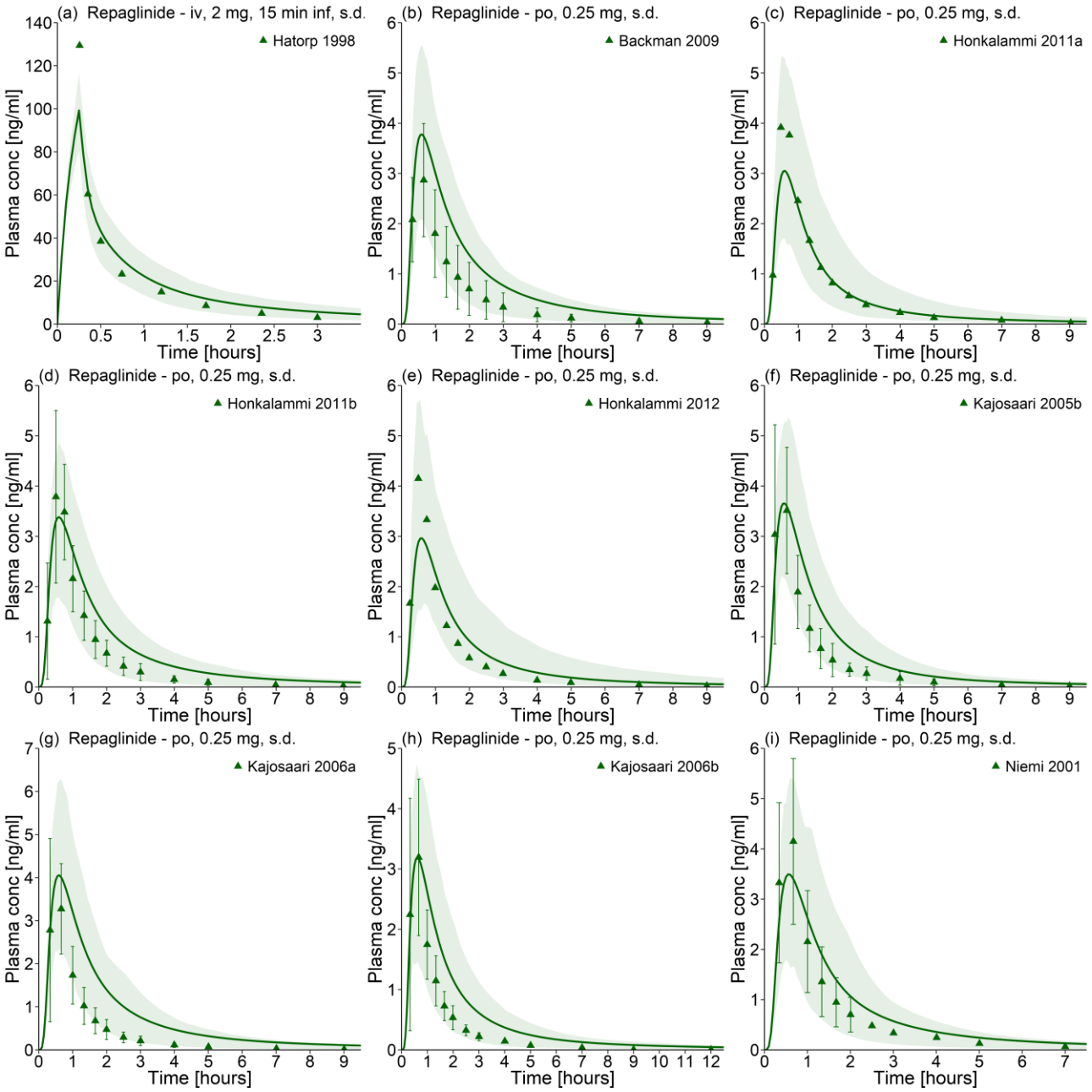
(a) Repaglinide - iv, 2 mg, 15 min inf, s.d.
Hatorp 1998
(b) Repaglinide - po, 0.25 mg, s.d.
Backman 2009
(c) Repaglinide - po, 0.25 mg, s.d.
Honkalammi 2011a
(d) Repaglinide - po, 0.25 mg, s.d.
Honkalammi 2011b
(e) Repaglinide - po, 0.25 mg, s.d.
Honkalammi 2012
(f) Repaglinide - po, 0.25 mg, s.d.
Kajosaari 2005b
(g) Repaglinide - po, 0.25 mg, s.d.
Kajosaari 2006a
(h) Repaglinide - po, 0.25 mg, s.d.
Kajosaari 2006b
(i) Repaglinide - po, 0.25 mg, s.d.
Niemi 2001
Plasma conc [ng/ml]
Time [hours]

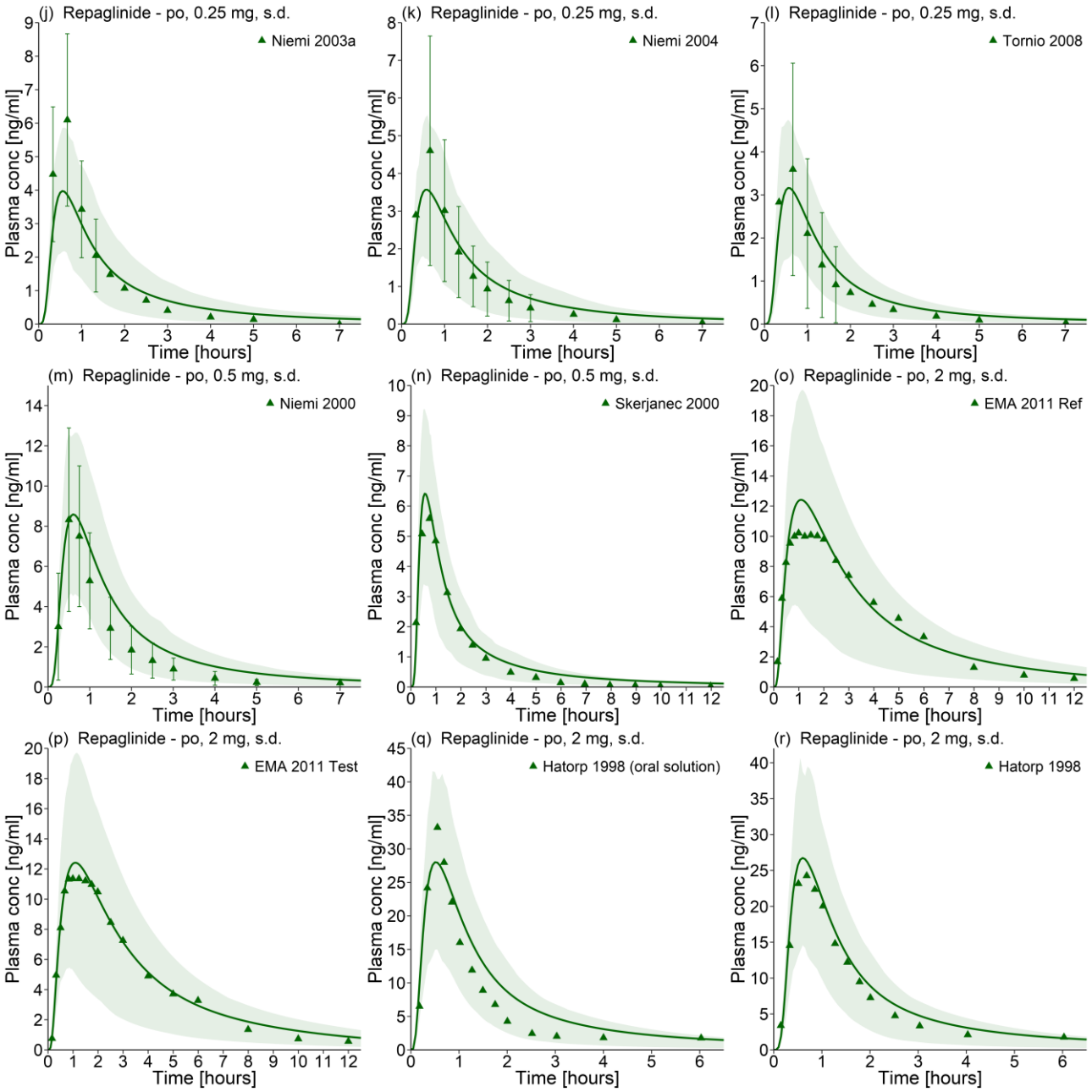
(j) Repaglinide - po, 0.25 mg, s.d.
Niemi 2003a
(k) Repaglinide - po, 0.25 mg, s.d.
Niemi 2004
(l) Repaglinide - po, 0.25 mg, s.d.
Tornio 2008
(m) Repaglinide - po, 0.5 mg, s.d.
Niemi 2000
(n) Repaglinide - po, 0.5 mg, s.d.
Skerjanec 2000
(o) Repaglinide - po, 2 mg, s.d.
EMA 2011 Ref
(p) Repaglinide - po, 2 mg, s.d.
EMA 2011 Test
(q) Repaglinide - po, 2 mg, s.d.
Hatorp 1998 (oral solution)
(r) Repaglinide - po, 2 mg, s.d.
Hatorp 1998
Plasma conc [ng/ml]
Time [hours]

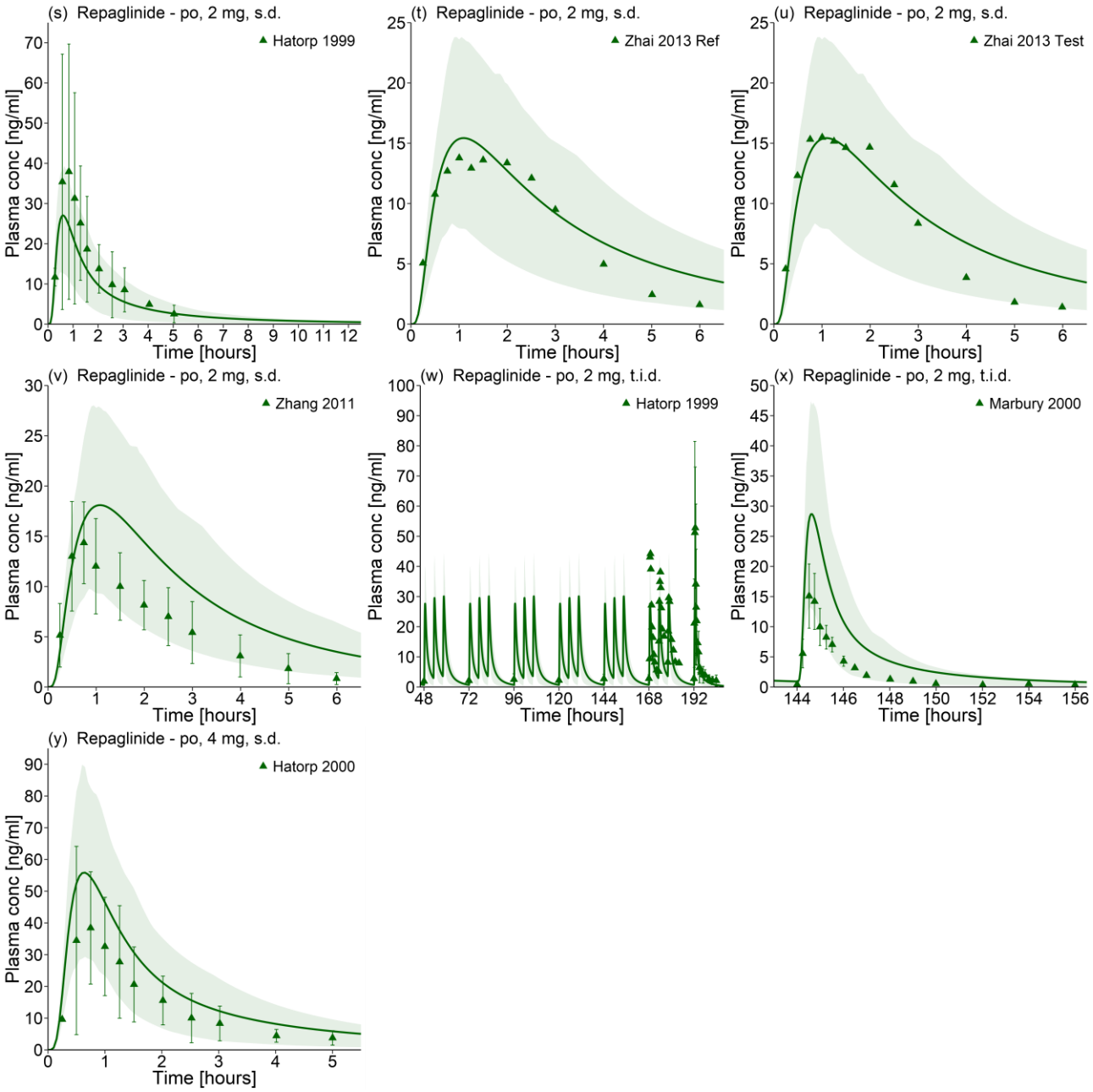

Fig. S3.4.2. Repaglinide plasma concentration-time profiles (linear). Observed data are shown as triangles ± SD. Population simulation arithmetic means or geometric means (c, e) are shown as green lines; the shaded areas represent the 68% population prediction intervals. Detailed information about dosing regimens and study populations is given in Table S3.4.1. Predicted and observed AUC and C_{max} values are compared in Table S3.4.4.

conc, concentration; inf, infusion; s.d., single dose; t.i.d., three times daily.

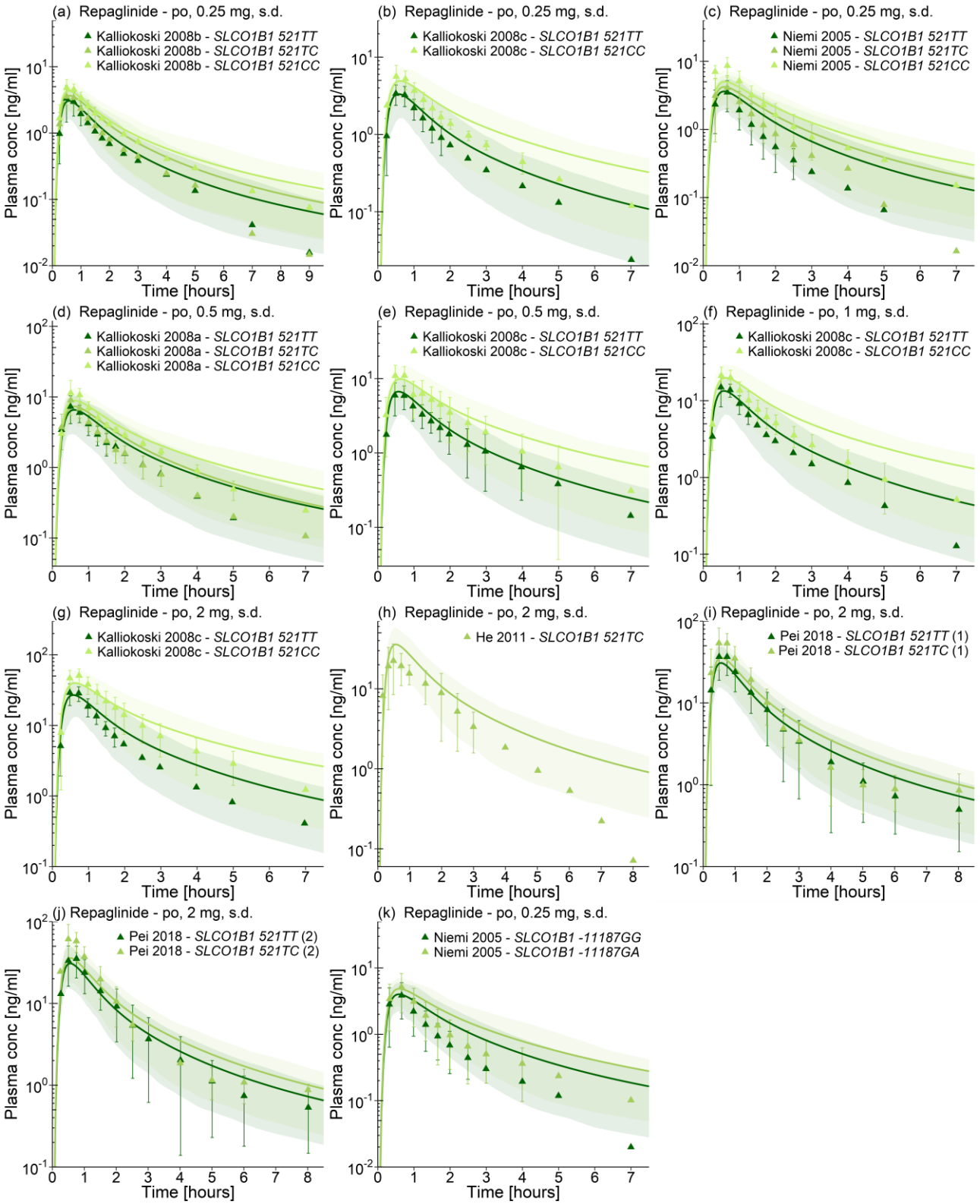
(a) Repaglinide - po, 0.25 mg, s.d.
Kalliokoski 2008b - SLCO1B1 521TT
Kalliokoski 2008b - SLCO1B1 521TC
Kalliokoski 2008b - SLCO1B1 521CC
(b) Repaglinide - po, 0.25 mg, s.d.
Kalliokoski 2008c - SLCO1B1 521TT
Kalliokoski 2008c - SLCO1B1 521CC
(c) Repaglinide - po, 0.25 mg, s.d.
Niemi 2005 - SLCO1B1 521TT
Niemi 2005 - SLCO1B1 521TC
Niemi 2005 - SLCO1B1 521CC
(d) Repaglinide - po, 0.5 mg, s.d.
Kalliokoski 2008a - SLCO1B1 521TT
Kalliokoski 2008a - SLCO1B1 521TC
Kalliokoski 2008a - SLCO1B1 521CC
(e) Repaglinide - po, 0.5 mg, s.d.
Kalliokoski 2008c - SLCO1B1 521TT
Kalliokoski 2008c - SLCO1B1 521CC
(f) Repaglinide - po, 1 mg, s.d.
Kalliokoski 2008c - SLCO1B1 521TT
Kalliokoski 2008c - SLCO1B1 521CC
(g) Repaglinide - po, 2 mg, s.d.
Kalliokoski 2008c - SLCO1B1 521TT
Kalliokoski 2008c - SLCO1B1 521CC
(h) Repaglinide - po, 2 mg, s.d.
He 2011 - SLCO1B1 521TC
(i) Repaglinide - po, 2 mg, s.d.
Pei 2018 - SLCO1B1 521TT (1)
Pei 2018 - SLCO1B1 521TC (1)
(j) Repaglinide - po, 2 mg, s.d.
Pei 2018 - SLCO1B1 521TT (2)
Pei 2018 - SLCO1B1 521TC (2)
(k) Repaglinide - po, 0.25 mg, s.d.
Niemi 2005 - SLCO1B1 -11187GG
Niemi 2005 - SLCO1B1 -11187GA
Plasma conc [ng/ml]
Time [hours]

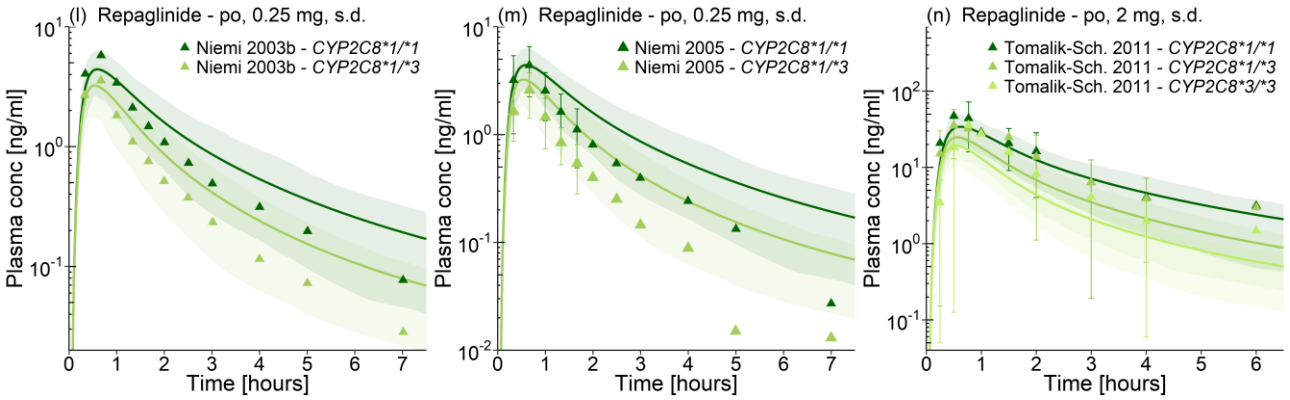

Fig. S3.4.3. Repaglinide plasma concentration-time profiles (semilogarithmic, polymorphism). Observed data are shown as triangles ± SD. Population simulation arithmetic means are shown as lines; the shaded areas represent the 68% population prediction intervals. Detailed information about dosing regimens and study populations is given in Table S3.4.1. Predicted and observed AUC and C_{max} values are compared in Table S3.4.4.

conc, concentration; s.d., single dose.

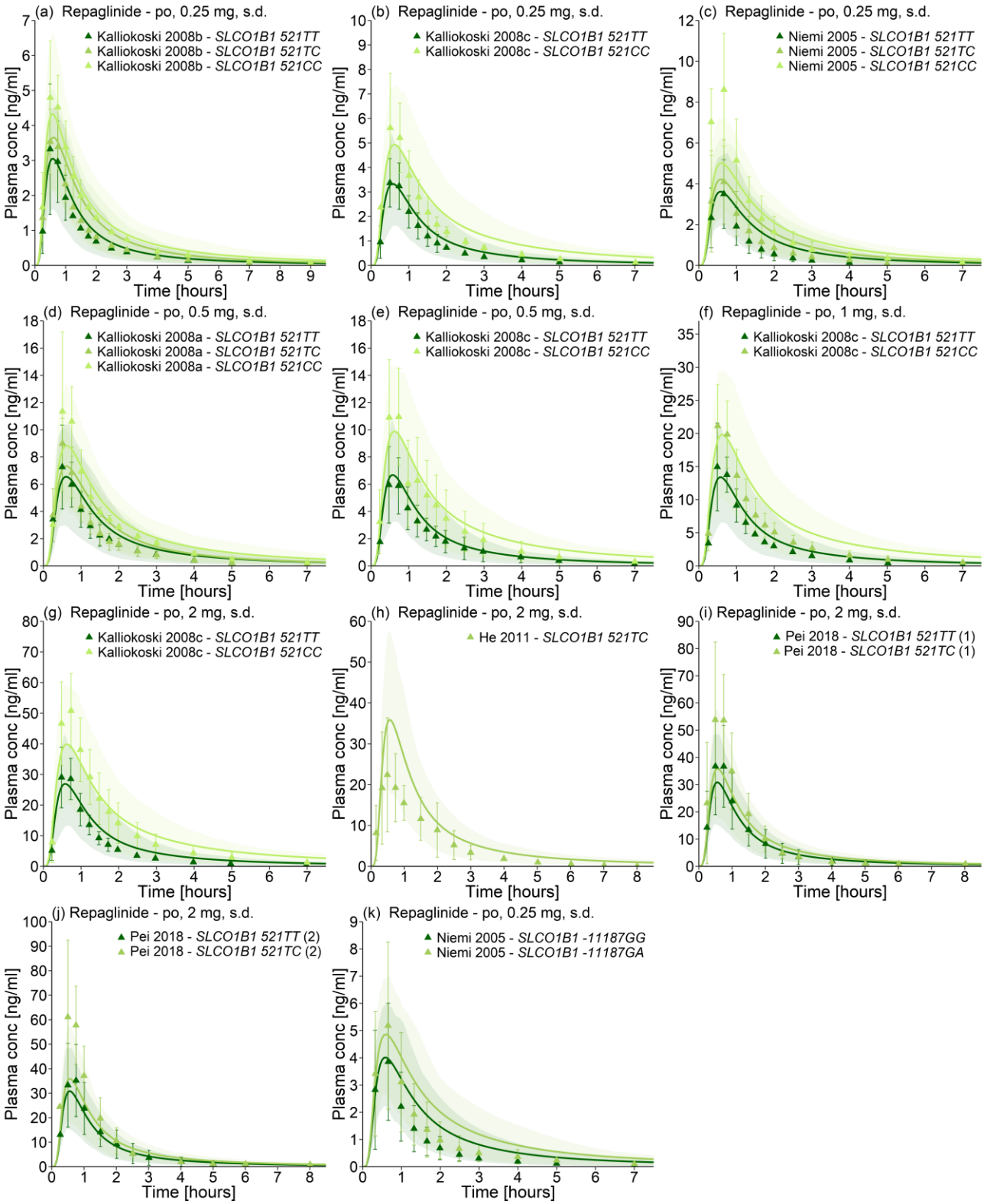
(a) Repaglinide - po, 0.25 mg, s.d.
Kalliokoski 2008b - SLCO1B1 521TT
Kalliokoski 2008b - SLCO1B1 521TC
Kalliokoski 2008b - SLCO1B1 521CC
(b) Repaglinide - po, 0.25 mg, s.d.
Kalliokoski 2008c - SLCO1B1 521TT
Kalliokoski 2008c - SLCO1B1 521CC
(c) Repaglinide - po, 0.25 mg, s.d.
Niemi 2005 - SLCO1B1 521TT
Niemi 2005 - SLCO1B1 521TC
Niemi 2005 - SLCO1B1 521CC
(d) Repaglinide - po, 0.5 mg, s.d.
Kalliokoski 2008a - SLCO1B1 521TT
Kalliokoski 2008a - SLCO1B1 521TC
Kalliokoski 2008a - SLCO1B1 521CC
(e) Repaglinide - po, 0.5 mg, s.d.
Kalliokoski 2008c - SLCO1B1 521TT
Kalliokoski 2008c - SLCO1B1 521CC
(f) Repaglinide - po, 1 mg, s.d.
Kalliokoski 2008c - SLCO1B1 521TT
Kalliokoski 2008c - SLCO1B1 521CC
(g) Repaglinide - po, 2 mg, s.d.
Kalliokoski 2008c - SLCO1B1 521TT
Kalliokoski 2008c - SLCO1B1 521CC
(h) Repaglinide - po, 2 mg, s.d.
He 2011 - SLCO1B1 521TC
(i) Repaglinide - po, 2 mg, s.d.
Pei 2018 - SLCO1B1 521TT (1)
Pei 2018 - SLCO1B1 521TC (1)
(j) Repaglinide - po, 2 mg, s.d.
Pei 2018 - SLCO1B1 521TT (2)
Pei 2018 - SLCO1B1 521TC (2)
(k) Repaglinide - po, 0.25 mg, s.d.
Niemi 2005 - SLCO1B1 -11187GG
Niemi 2005 - SLCO1B1 -11187GA
Plasma conc [ng/ml]
Time [hours]

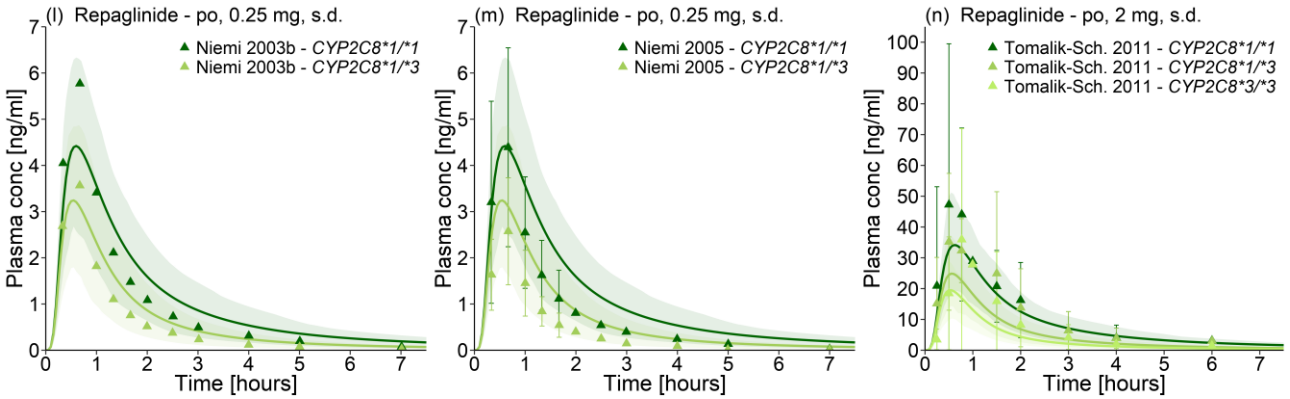

Fig. S3.4.4. Repaglinide plasma concentration-time profiles (linear, polymorphism). Observed data are shown as triangles ± SD. Population simulation arithmetic means are shown as lines; the shaded areas represent the 68% population prediction intervals. Detailed information about dosing regimens and study populations is given in Table S3.4.1. Predicted and observed AUC and C_{max} values are compared in Table S3.4.4.

conc, concentration; s.d., single dose.

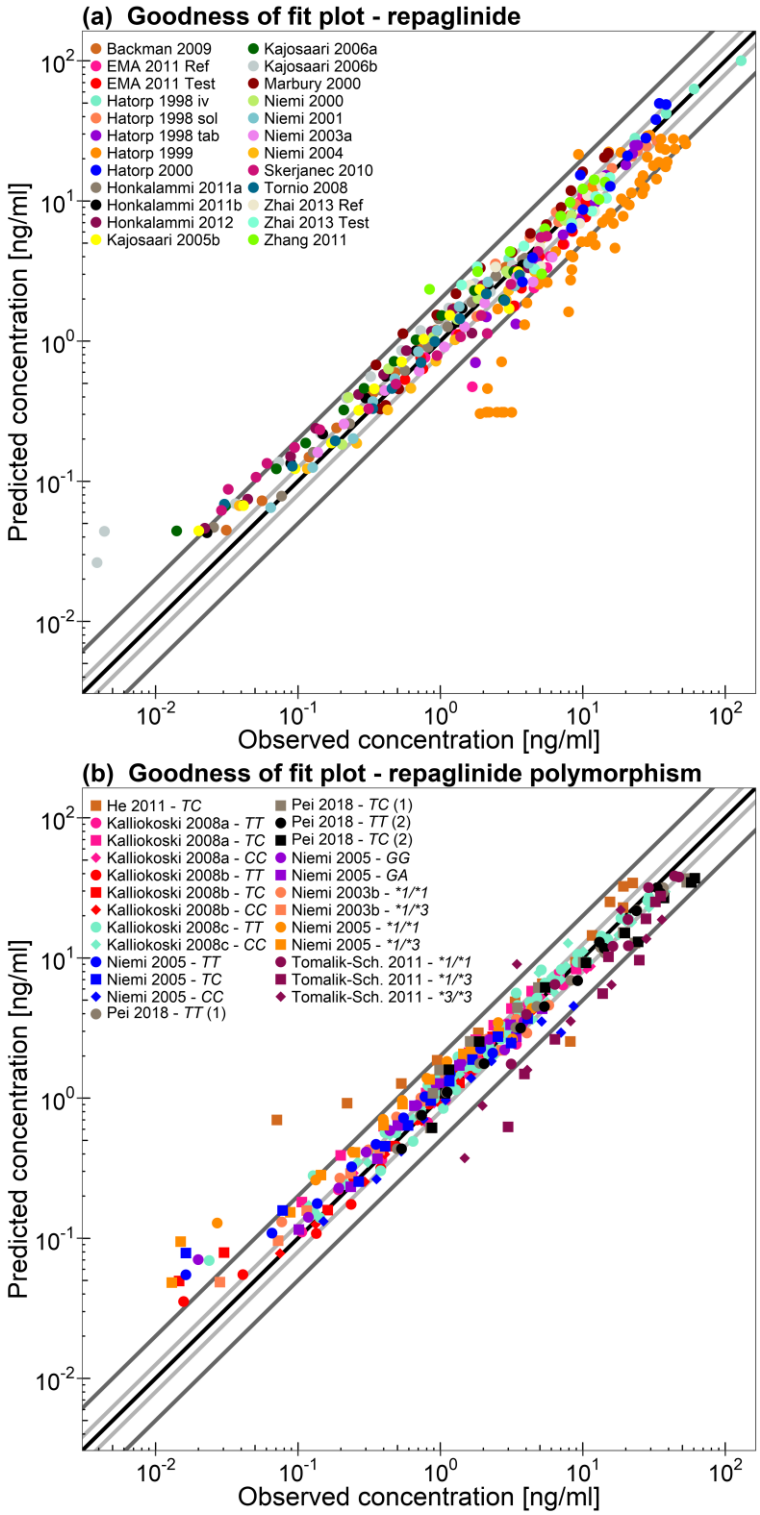

Fig. S3.4.5. Goodness of fit plot. Comparison of predicted versus observed repaglinide plasma concentration values of all studies of subjects with unknown genotypes (a) and of subjects with *CYP2C8* or *SLCO1B1* polymorphisms (b). The black line marks the line of identity. Light grey lines indicate 0.8- to 1.25-fold; dark grey lines indicate 0.5- to 2-fold prediction acceptance limits. Detailed information about dosing regimens and study populations is given in Table S3.4.1.
**1/*1*, *CYP2C8*1/*1*; **1/*3*, *CYP2C8*1/*3*; **3/*3*, *CYP2C8*3/*3*; *CC*, *SLCO1B1 521CC*; *GA*, *SLCO1B1 -11187GA*; *GG*, *SLCO1B1 521GG*; *TC*, *SLCO1B1 521TC*; *TT*, *SLCO1B1 521TT*.

Table S3.4.3. Mean relative deviation values of repaglinide plasma concentration predictions.

Route	Dose [mg]	*CYP2C8* genotype	*SLCO1B1* genotype	MRD	References
Repaglinide					
iv, (15 min, s.d.)	2	-	-	1.17	Hatorp 1998 [45]
po (tab, s.d.)	0.25	-	-	1.29	Backman 2009 [30]
po (tab, s.d.)	0.25	-	-	1.26	Honkalammi 2011a [27]
po (tab, s.d.)	0.25	-	-	1.37	Honkalammi 2011b [18]
po (tab, s.d.)	0.25	-	-	1.53	Honkalammi 2012 [19]
po (tab, s.d.)	0.25	-	-	1.45	Kajosaari 2005b [46]
po (tab, s.d.)	0.25	-	-	1.72	Kajosaari 2006a [47]
po (tab, s.d.)	0.25	-	-	2.55	Kajosaari 2006b [48]
po (tab, s.d.)	0.25	-	*521TT*	1.31	Kalliokoski 2008b [49]
po (tab, s.d.)	0.25	-	*521TC*	1.54	Kalliokoski 2008b [49]
po (tab, s.d.)	0.25	-	*521CC*	1.07	Kalliokoski 2008b [49]
po (tab, s.d.)	0.25	-	*521TT*	1.38	Kalliokoski 2008c [50]
po (tab, s.d.)	0.25	-	*521CC*	1.19	Kalliokoski 2008c [50]
po (tab, s.d.)	0.25	-	-	1.20	Niemi 2001 [51]
po (tab, s.d.)	0.25	-	-	1.29	Niemi 2003a [52]
po (tab, s.d.)	0.25	**1/*1*	-	1.37	Niemi 2003b [3]
po (tab, s.d.)	0.25	**1/*3*	-	1.31	Niemi 2003b [3]
po (tab, s.d.)	0.25	-	-	1.37	Niemi 2004 [53]
po (tab, s.d.)	0.25	-	*521TT*	1.57	Niemi 2005 [4]
po (tab, s.d.)	0.25	-	*521TC*	1.70	Niemi 2005 [4]
po (tab, s.d.)	0.25	-	*521CC*	1.47	Niemi 2005 [4]
po (tab, s.d.)	0.25	-	*-11187GG*	1.55	Niemi 2005 [4]
po (tab, s.d.)	0.25	-	*-11187GA*	1.21	Niemi 2005 [4]
po (tab, s.d.)	0.25	**1/*1*	-	1.92	Niemi 2005 [4]
po (tab, s.d.)	0.25	**1/*3*	-	2.22	Niemi 2005 [4]
po (tab, s.d.)	0.25	-	-	1.35	Tornio 2008 [31]
po (tab, s.d.)	0.5	-	*521TT*	1.15	Kalliokoski 2008a [54]
po (tab, s.d.)	0.5	-	*521TC*	1.43	Kalliokoski 2008a [54]
po (tab, s.d.)	0.5	-	*521CC*	1.14	Kalliokoski 2008a [54]
po (tab, s.d.)	0.5	-	*521TT*	1.17	Kalliokoski 2008c [50]
po (tab, s.d.)	0.5	-	*521CC*	1.14	Kalliokoski 2008c [50]
po (tab, s.d.)	0.5	-	-	1.25	Niemi 2000 [55]
po (-, s.d.)	0.5	-	-	1.65	Skerjanec 2010 [56]
po (tab, s.d.)	1	-	*521TT*	1.33	Kalliokoski 2008c [50]
po (tab, s.d.)	1	-	*521CC*	1.28	Kalliokoski 2008c [50]
po (tab, s.d.)	2	-	*521TT*	1.30	Kalliokoski 2008c [50]
po (tab, s.d.)	2	-	*521CC*	1.24	Kalliokoski 2008c [50]
po (tab, s.d.)	2	-	-	1.53	EMA 2011 Ref [57]
po (tab, s.d.)	2	-	-	1.30	EMA 2011 Test [57]
po (sol, s.d.)	2	-	-	1.35	Hatorp 1998 [45]
po (tab, s.d.),	2	-	-	1.48	Hatorp 1998 [45]
po (-, s.d.)	2	-	-	1.74	Hatorp 1999 [58]
po (tab, s.d.)	2	-	*521TC*	2.43	He 2011 [59]
po (tab, s.d.)	2	-	*521TT*	1.15	Pei 2018 (1) [60]
po (tab, s.d.)	2	-	*521TC*	1.43	Pei 2018 (1) [60]
po (tab, s.d.)	2	-	*521TT*	1.17	Pei 2018 (2) [60]
po (tab, s.d.)	2	-	*521TC*	1.43	Pei 2018 (2) [60]

continued…

continued…

Route	Dose [mg]	*CYP2C8* genotype	*SLCO1B1* genotype	MRD	References
Repaglinide					
po (tab, s.d.)	2	**1/*1*	-	1.35	Tomalik-Sch. 2011 [5]
po (tab, s.d.)	2	**1/*3*	-	2.31	Tomalik-Sch. 2011 [5]
po (tab, s.d.)	2	**3/*3*	-	2.39	Tomalik-Sch. 2011 [5]
po (tab, s.d.)	2	-	-	1.29	Zhai 2013 Ref [61]
po (tab, s.d.)	2	-	-	1.37	Zhai 2013 Test [61]
po (tab, s.d.)	2	-	-	1.52	Zhang 2011 [62]
po (-, t.i.d.)	2	-	-	3.02	Hatorp 1999 [58]
po (-, t.i.d.)	2	-	-	1.52	Marbury 2000 [63]
po (tab, s.d.)	4	-	-	1.29	Hatorp 2000 [64]
			MRD (mean)	**1.49**	
			MRD ≤ 2	**50/56**	

-, not given; CYP, cytochrome P450; iv, intravenous; MRD, mean relative deviation; po, oral; s.d., single dose; sol, solution; tab, tablet; SLCO, solute carrier organic anion transporter family member t.i.d., three times daily.

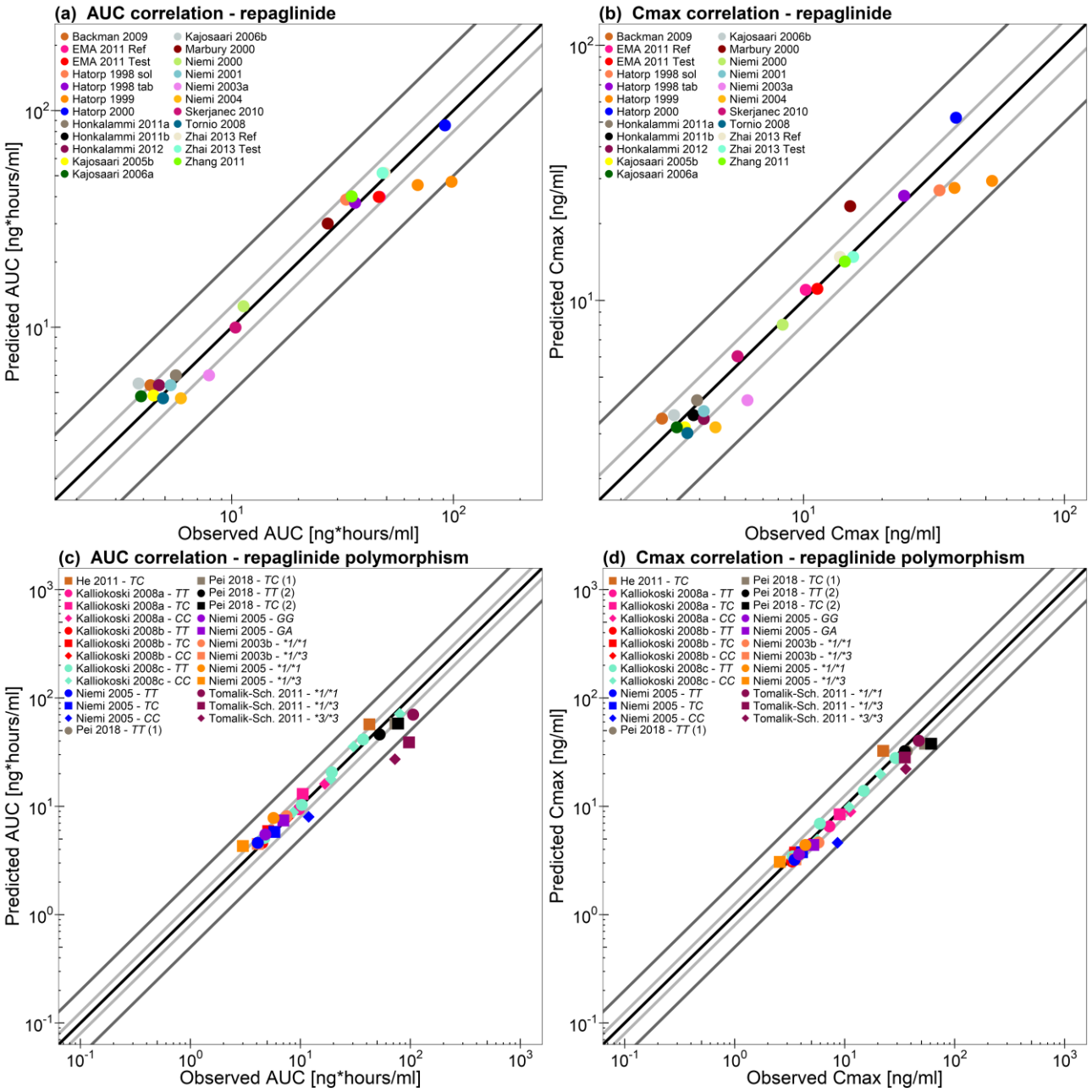

Fig. S3.4.6. Correlation of predicted and observed repaglinide AUC and C_{max} values of all studies. The black line marks the line of identity. Light grey lines indicate 0.8- to 1.25-fold; dark grey lines indicate 0.5- to 2-fold prediction acceptance limits. Detailed information about dosing regimens and study populations is given in Table S3.4.1. The plotted AUC and C_{max} values are listed in Table S3.4.4. **1/*1*, *CYP2C8*1/*1*; **1/*3*, *CYP2C8*1/*3*; **3/*3*, *CYP2C8*3/*3*; *CC*, *SLCO1B1 521CC*; *GA*, *SLCO1B1 -11187GA*; *GG*, *SLCO1B1 521GG*; *TC*, *SLCO1B1 521TC*; *TT*, *SLCO1B1 521TT*.

Table S3.4.4. Predicted and observed AUC and C_{max} values of repaglinide.

Route	Dose [mg]	*CYP2C8* genotype	*SLCO1B1* genotype	AUC [ng*hours/ml]		Pred/Obs AUC	C_{max} [ng/ml]		Pred/Obs C_{max}	References
Repaglinide				*pred*	*obs*		*pred*	*obs*		
iv, (15 min, s.d.)	2	-	-	-	-	-	-	-	-	Hatorp 1998 [45]
po (tab, s.d.)	0.25	-	-	5.4	4.3	1.26	3.44	2.87	1.20	Backman 2009 [30]
po (tab, s.d.)	0.25	-	-	6.0	5.6	1.15	4.06	3.91	1.04	Honkalammi 2011a [27]
po (tab, s.d.)	0.25	-	-	5.4	4.7	1.07	3.55	3.79	0.94	Honkalammi 2011b [18]
po (tab, s.d.)	0.25	-	-	5.4	4.7	1.15	3.43	4.15	0.83	Honkalammi 2012 [19]
po (tab, s.d.)	0.25	-	-	4.84	4.44	1.09	3.18	3.51	0.90	Kajosaari 2005b [46]
po (tab, s.d.)	0.25	-	-	4.8	3.9	1.23	3.18	3.27	0.97	Kajosaari 2006a [47]
po (tab, s.d.)	0.25	-	-	5.5	3.8	1.45	3.55	3.19	1.11	Kajosaari 2006b [48]
po (tab, s.d.)	0.25	-	*521TT*	4.6	4.5	1.02	3.10	3.32	0.93	Kalliokoski 2008b [49]
po (tab, s.d.)	0.25	-	*521TC*	5.9	5.1	1.16	3.74	3.54	1.06	Kalliokoski 2008b [49]
po (tab, s.d.)	0.25	-	*521CC*	7.9	7.8	1.01	4.53	4.79	0.94	Kalliokoski 2008b [49]
po (tab, s.d.)	0.25	-	*521TT*	5.1	4.7	1.09	3.45	3.37	1.03	Kalliokoski 2008c [50]
po (tab, s.d.)	0.25	-	*521CC*	8.8	8.6	1.02	4.92	5.62	0.88	Kalliokoski 2008c [50]
po (tab, s.d.)	0.25	-	-	5.4	5.3	1.02	3.68	4.15	0.89	Niemi 2001 [51]
po (tab, s.d.)	0.25	-	-	6.0	7.9	0.76	4.06	6.10	0.67	Niemi 2003a [52]
po (tab, s.d.)	0.25	**1/*1*	-	8.1	7.5	1.08	4.63	5.77	0.80	Niemi 2003b [3]
po (tab, s.d.)	0.25	**1/*3*	-	4.5	4.1	1.10	3.24	3.56	0.91	Niemi 2003b [3]
po (tab, s.d.)	0.25	-	-	4.7	5.9	0.80	3.18	4.60	0.69	Niemi 2004 [53]
po (tab, s.d.)	0.25	-	*521TT*	4.6	4.1	1.12	3.21	3.50	0.92	Niemi 2005 [4]
po (tab, s.d.)	0.25	-	*521TC*	5.8	5.8	1.00	3.77	4.09	0.92	Niemi 2005 [4]
po (tab, s.d.)	0.25	-	*521CC*	7.99	11.9	0.67	4.61	8.61	0.54	Niemi 2005 [4]
po (tab, s.d.)	0.25	-	*-11187GG*	5.5	4.8	1.15	3.60	3.85	0.93	Niemi 2005 [4]
po (tab, s.d.)	0.25	-	*-11187GA*	7.4	7.0	1.06	4.40	5.18	0.85	Niemi 2005 [4]
po (tab, s.d.)	0.25	**1/*1*	-	7.8	5.7	1.37	4.40	4.39	1.00	Niemi 2005 [4]
po (tab, s.d.)	0.25	**1/*3*	-	4.3	3.0	1.43	3.07	2.57	1.19	Niemi 2005 [4]

continued…

continued…

Route	Dose [mg]	*CYP2C8* genotype	*SLCO1B1* genotype	AUC [ng*hours/ml]		Pred/Obs AUC	C_{max} [ng/ml]		Pred/Obs C_{max}	References
Repaglinide				*pred*	*obs*		*pred*	*obs*		
po (tab, s.d.)	0.25	-	-	4.7	4.9	0.96	3.02	3.59	0.84	Tornio 2008 [31]
po (tab, s.d.)	0.5	-	*521TT*	9.4	9.7	0.97	6.53	7.26	0.90	Kalliokoski 2008a [54]
po (tab, s.d.)	0.5	-	*521TC*	13.0	10.5	1.24	8.43	8.99	0.94	Kalliokoski 2008a [54]
po (tab, s.d.)	0.5	-	*521CC*	16.1	16.7	0.96	8.92	11.3	0.79	Kalliokoski 2008a [54]
po (tab, s.d.)	0.5	-	*521TT*	10.3	10.3	1.00	6.92	5.95	1.16	Kalliokoski 2008c [50]
po (tab, s.d.)	0.5	-	*521CC*	17.8	18.9	0.94	9.85	11.0	0.90	Kalliokoski 2008c [50]
po (tab, s.d.)	0.5	-	-	12.5	11.3	1.11	8.03	8.32	0.96	Niemi 2000 [55]
po (-, s.d.)	0.5	-	-	9.97	10.4 [a]	0.96	6.04	5.59	1.08	Skerjanec 2010 [56]
po (tab, s.d.)	1	-	*521TT*	20.6	19.3	1.07	13.9	14.9	0.93	Kalliokoski 2008c [50]
po (tab, s.d.)	1	-	*521CC*	35.6	30.4	1.17	19.8	21.1	0.94	Kalliokoski 2008c [50]
po (tab, s.d.)	2	-	*521TT*	41.4	37.2	1.11	27.9	29.0	0.96	Kalliokoski 2008c [50]
po (tab, s.d.)	2	-	*521CC*	71.4	80.1	0.89	39.7	50.8	0.78	Kalliokoski 2008c [50]
po (tab, s.d.)	2	-	-	39.932	46.501	0.86	11.1	10.2	1.08	EMA 2011 Ref [57]
po (tab, s.d.)	2	-	-	39.932	46.087	0.87	11.1	11.3	0.98	EMA 2011 Test [57]
po (sol, s.d.)	2	-		38.8	32.8	1.18	27.0	33.2	0.81	Hatorp 1998 [45]
po (tab, s.d.),	2	-		37.5	36.0	1.04	25.7	24.3	1.06	Hatorp 1998 [45]
po (-, s.d.)	2	-	-	45.3	69.0 [a]	0.66	27.6	37.9	0.73	Hatorp 1999 [58]
po (tab, s.d.)	2	-	*521TC*	57.1	42.4	1.35	35.2	22.4	1.57	He 2011 [59]
po (tab, s.d.)	2	-	*521TT*	46.07	52.56	0.88	32.3	36.7	0.88	Pei 2018 (1) [60]
po (tab, s.d.)	2	-	*521TC*	58.06	73.08	0.79	37.8	53.8	0.70	Pei 2018 (1) [60]
po (tab, s.d.)	2	-	*521TT*	46.07	52.46	0.88	32.3	35.2	0.92	Pei 2018 (2) [60]
po (tab, s.d.)	2	-	*521TC*	58.06	77.31	0.75	37.8	61.1	0.62	Pei 2018 (2) [60]
po (tab, s.d.)	2	**1/*1*	-	70.13	105.9	0.66	40.3	47.2	0.85	Tomalik-Sch. 2011 [5]
po (tab, s.d.)	2	**1/*3*	-	38.9	97.2	0.40	28.2	35.2	0.80	Tomalik-Sch. 2011 [5]
po (tab, s.d.)	2	**3/*3*	-	27.2	72.4	0.38	22.1	35.9	0.62	Tomalik-Sch. 2011 [5]

continued…

continued…

Route	Dose [mg]	*CYP2C8* genotype	*SLCO1B1* genotype	AUC [ng*hours/ml]		Pred/Obs AUC	C_{max} [ng/ml]		Pred/Obs C_{max}	References
Repaglinide				*pred*	*obs*		*pred*	*obs*		
po (tab, s.d.)	2	-	-	51.5	49.0	1.05	14.8	13.8	1.07	Zhai 2013 Ref [61]
po (tab, s.d.)	2	-	-	51.5	47.9	1.08	14.8	15.5	0.95	Zhai 2013 Test [61]
po (tab, s.d.)	2	-	-	40.16	34.77 [c]	1.16	14.2	14.4	0.99	Zhang 2011 [62]
po (-, t.i.d.)	2	-	-	46.9	98.1[a]	0.48	29.4	52.8	0.56	Hatorp 1999 [58]
po (-, t.i.d.)	2	-	-	38.1	27.1 [b]	1.41	23.4	15.1	1.55	Marbury 2000 [63]
po (tab, s.d.)	4	-	-	85.4	91.6 [b]	0.93	52.0	38.4	1.35	Hatorp 2000 [64]
					GMFE (range)	**1.21 (1.00-2.66)**			**1.19 (1.00-1.87)**	
					Pred/Obs within 2-fold	**52/55**			**55/55**	

[a], AUC_{0-12}, [b], AUC_{0-48}; [c], AUC_{0-6}; AUC values are AUC_{inf}, if not specified differently; -, not given; AUC, area under the concentration-time curve; C_{max}, maximum plasma concentration; CYP, cytochrome P450; GMFE, geometric mean fold error; iv, intravenous; obs, observed;; po, oral; pred, predicted; s.d., single dose; SLCO, solute carrier organic anion transporter family member ; sol, solution; tab, tablet; t.i.d., three times daily.

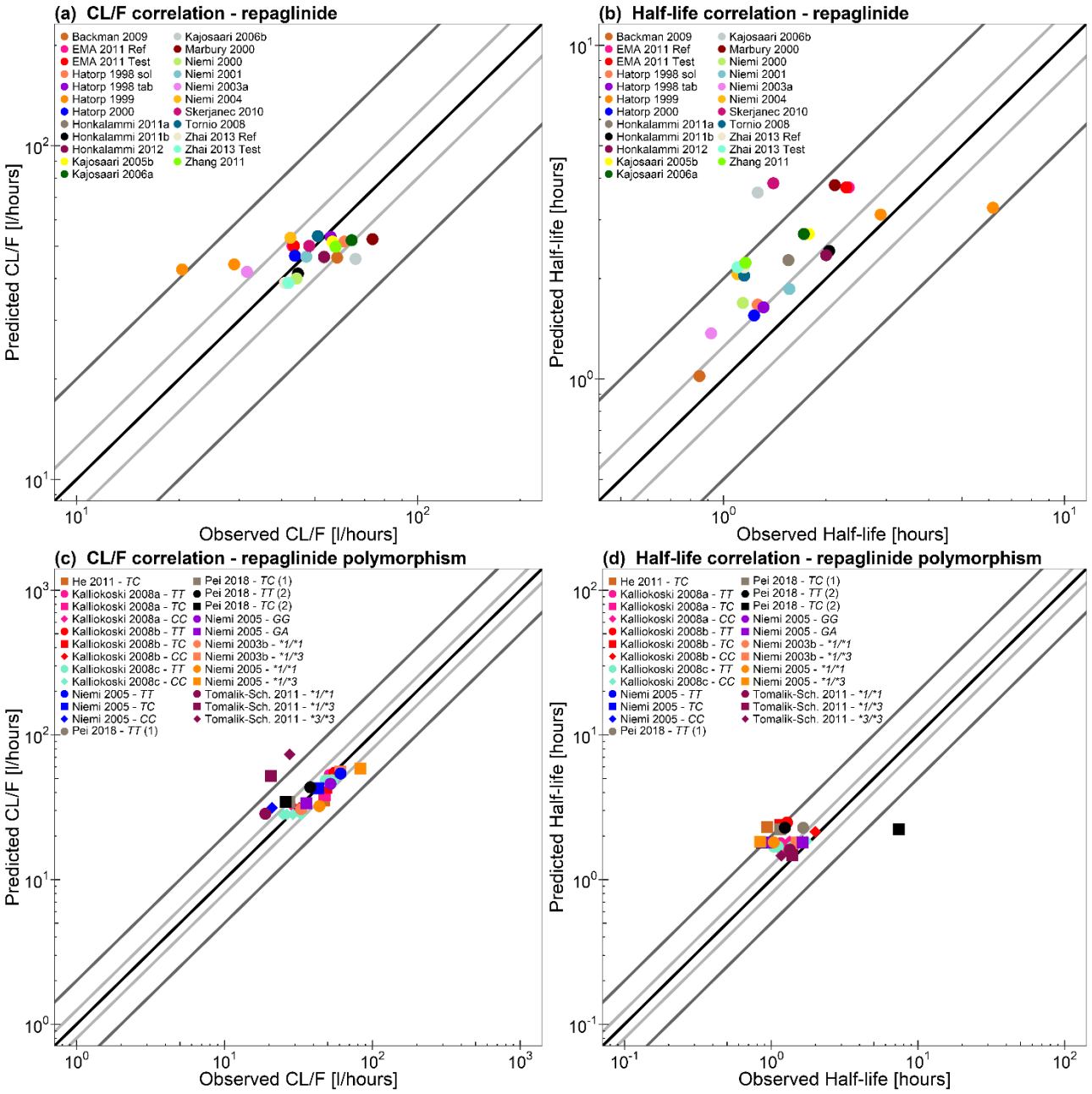

Fig. S3.4.7. Correlation of predicted and observed repaglinide CL/F (a, c) and half-life values (b, d) of all studies. The black line marks the line of identity. Light grey lines indicate 0.8- to 1.25-fold; dark grey lines indicate 0.5- to 2-fold prediction acceptance limits. Detailed information about dosing regimens and study populations is given in Table S3.4.1. The plotted values for CL/F and half-life values are listed in Table S3.4.5.

Table S3.4.5. Predicted and observed CL/F and half-life of repaglinide.

Route	Dose [mg]	*CYP2C8* genotype	*SLCO1B1* genotype	CL/F [a] [l/hours]		Pred/Obs CL/F	Half-life [b] [hours]		Pred/Obs Half-life	References
Repaglinide				*pred*	*obs*		*pred*	*obs*		
iv, (15 min, s.d.)	2	-	-	-	-	-	1.02	0.85	1.19	Hatorp 1998 [45]
po (tab, s.d.)	0.25	-	-	46.2	58.1	0.79	2.32	1.95	1.19	Backman 2009 [30]
po (tab, s.d.)	0.25	-	-	46.3	53.2	0.87	2.27	1.55	1.46	Honkalammi 2011a [27]
po (tab, s.d.)	0.25	-	-	41.4	44.6	0.93	2.42	2.04	1.19	Honkalammi 2011b [18]
po (tab, s.d.)	0.25	-	-	46.5	53.2	0.87	2.35	2.00	1.17	Honkalammi 2012 [19]
po (tab, s.d.)	0.25	-	-	51.6	56.3	0.92	2.72	1.78	1.53	Kajosaari 2005b [46]
po (tab, s.d.)	0.25	-	-	52.1	64.1	0.81	2.72	1.72	1.58	Kajosaari 2006a [47]
po (tab, s.d.)	0.25	-	-	45.8	65.8	0.70	3.62	1.26	2.88	Kajosaari 2006b [48]
po (tab, s.d.)	0.25	-	*521TT*	54.8	55.6	0.99	2.48	1.28	1.93	Kalliokoski 2008b [49]
po (tab, s.d.)	0.25	-	*521TC*	42.3	49.0	0.86	2.38	1.15	2.07	Kalliokoski 2008b [49]
po (tab, s.d.)	0.25	-	*521CC*	31.4	32.1	0.98	2.14	2.00	1.07	Kalliokoski 2008b [49]
po (tab, s.d.)	0.25	-	*521TT*	48.7	53.2	0.92	1.69	1.04	1.63	Kalliokoski 2008c [50]
po (tab, s.d.)	0.25	-	*521CC*	28.2	29.1	0.97	1.84	1.49	1.23	Kalliokoski 2008c [50]
po (tab, s.d.)	0.25	-	-	46.5	47.2	0.98	1.86	1.56	1.19	Niemi 2001 [51]
po (tab, s.d.)	0.25	-	-	41.9	31.6	1.32	1.37	0.92	1.48	Niemi 2003a [52]
po (tab, s.d.)	0.25	**1/*1*	-	30.7	33.0	0.92	1.78	1.49	1.19	Niemi 2003b [3]
po (tab, s.d.)	0.25	**1/*3*	-	55.9	61.0	0.92	1.81	1.49	1.22	Niemi 2003b [3]
po (tab, s.d.)	0.25	-	-	53.0	42.4	1.25	2.06	1.10	1.87	Niemi 2004 [53]
po (tab, s.d.)	0.25	-	*521TT*	54.1	61.0	0.89	1.81	0.98	1.84	Niemi 2005 [4]
po (tab, s.d.)	0.25	-	*521TC*	42.8	43.1	0.99	1.80	0.86	2.10	Niemi 2005 [4]
po (tab, s.d.)	0.25	-	*521CC*	31.3	21.0	1.49	1.83	1.64	1.11	Niemi 2005 [4]
po (tab, s.d.)	0.25	-	*-11187GG*	45.9	52.1	0.88	1.80	0.99	1.81	Niemi 2005 [4]
po (tab, s.d.)	0.25	-	*-11187GA*	33.8	35.7	0.95	1.81	1.64	1.10	Niemi 2005 [4]
po (tab, s.d.)	0.25	**1/*1*	-	32.2	43.9	0.73	1.81	1.04	1.73	Niemi 2005 [4]
po (tab, s.d.)	0.25	**1/*3*	-	58.6	83.3	0.70	1.83	0.84	2.18	Niemi 2005 [4]

continued…

continued…

Route	Dose [mg]	*CYP2C8* genotype	*SLCO1B1* genotype	CL/F [l/hours]		Pred/Obs CL/F	Half-life [hours]		Pred/Obs Half-life	References
Repaglinide				*pred*	*obs*		*pred*	*obs*		
po (tab, s.d.)	0.25	-	-	53.6	51.0	1.05	2.04	1.15	1.78	Tornio 2008 [31]
po (tab, s.d.)	0.5	-	*521TT*	52.9	51.5	1.03	1.78	1.16	1.54	Kalliokoski 2008a [54]
po (tab, s.d.)	0.5	-	*521TC*	38.4	47.6	0.81	1.68	1.20	1.41	Kalliokoski 2008a [54]
po (tab, s.d.)	0.5	-	*521CC*	31.1	29.9	1.04	1.84	1.33	1.38	Kalliokoski 2008a [54]
po (tab, s.d.)	0.5	-	*521TT*	48.6	48.5	1.00	1.68	1.39	1.21	Kalliokoski 2008c [50]
po (tab, s.d.)	0.5	-	*521CC*	28.2	26.5	1.06	1.84	1.74	1.06	Kalliokoski 2008c [50]
po (tab, s.d.)	0.5	-	-	40.0	44.2	0.90	1.69	1.14	1.48	Niemi 2000 [55]
po (-, s.d.)	0.5	-	-	50.1	48.1	1.04	3.86	1.40	2.76	Skerjanec 2010 [56]
po (tab, s.d.)	1	-	*521TT*	48.5	51.8	0.94	1.69	1.11	1.52	Kalliokoski 2008c [50]
po (tab, s.d.)	1	-	*521CC*	28.1	32.9	0.85	1.84	1.61	1.15	Kalliokoski 2008c [50]
po (tab, s.d.)	2	-	*521TT*	48.3	53.8	0.90	1.68	1.79	0.94	Kalliokoski 2008c [50]
po (tab, s.d.)	2	-	*521CC*	28.0	25.0	1.12	1.84	1.67	1.10	Kalliokoski 2008c [50]
po (tab, s.d.)	2	-	-	50.1	43.0	1.16	3.75	2.33	1.61	EMA 2011 Ref [57]
po (tab, s.d.)	2	-	-	50.1	43.4	1.15	3.75	2.29	1.64	EMA 2011 Test [57]
po (sol, s.d.)	2	-		51.6	61.0	0.85	1.67	1.26	1.33	Hatorp 1998 [45]
po (tab, s.d.),	2	-		53.3	55.6	0.96	1.64	1.31	1.25	Hatorp 1998 [45]
po (-, s.d.)	2	-	-	44.1	29.0	1.52	3.11	2.89	1.07	Hatorp 1999 [58]
po (tab, s.d.)	2	-	*521TC*	35.0	47.2	0.74	2.30	0.94	1.25	He 2011 [59]
po (tab, s.d.)	2	-	*521TT*	43.4	38.1	1.14	2.28	1.65	1.38	Pei 2018 (1) [60]
po (tab, s.d.)	2	-	*521TC*	34.4	27.4	1.26	2.22	1.15	1.93	Pei 2018 (1) [60]
po (tab, s.d.)	2	-	*521TT*	43.4	38.1	1.14	2.28	1.24	1.84	Pei 2018 (2) [60]
po (tab, s.d.)	2	-	*521TC*	34.4	25.9	1.33	2.22	7.43	0.30	Pei 2018 (2) [60]
po (tab, s.d.)	2	**1/*1*	-	28.5	18.9	1.51	1.61	1.34	1.19	Tomalik-Sch. 2011 [5]
po (tab, s.d.)	2	**1/*3*	-	52.2	20.6	2.54	1.47	1.39	1.06	Tomalik-Sch. 2011 [5]
po (tab, s.d.)	2	**3/*3*	-	73.4	27.6	2.66	1.46	1.17	1.24	Tomalik-Sch. 2011 [5]

continued…

continued…

Route	Dose [mg]	*CYP2C8* genotype	*SLCO1B1* genotype	CL/F [l/hours]		Pred/Obs CL/F	Half-life [hours]		Pred/Obs Half-life	References
Repaglinide				*pred*	*obs*		*pred*	*obs*		
po (tab, s.d.)	2	-	-	38.8	40.8	0.95	2.16	1.15	1.87	Zhai 2013 Ref [61]
po (tab, s.d.)	2	-	-	38.8	41.8	0.93	2.16	1.10	1.97	Zhai 2013 Test [61]
po (tab, s.d.)	2	-	-	49.8	57.5	0.87	2.23	1.16	1.92	Zhang 2011 [62]
po (-, t.i.d.)	2	-	-	42.6	20.4	2.09	3.26	6.17	0.53	Hatorp 1999 [58]
po (-, t.i.d.)	2	-	-	52.5	73.8	0.71	3.81	2.12	1.80	Marbury 2000 [63]
po (tab, s.d.)	4	-	-	46.8	43.7	1.07	1.55	1.23	1.26	Hatorp 2000 [64]
					GMFE (range)	**1.21 (1.00-2.66)**			**1.52 (1.06-3.35)**	
					Pred/Obs within 2-fold	**52/55**			**49/56**	

[a], calculated from dose/AUC; [b], calculated for observed and predicted concentration-time profiles (same time points for observed and predicted values); -, not given; AUC, area under the concentration-time curve; CL/F, oral clearance; C_{max}, maximum plasma concentration; CYP, cytochrome P450; GMFE, geometric mean fold error; iv, intravenous; obs, observed;; po, oral; pred, predicted; s.d., single dose; SLCO, solute carrier organic anion transporter family member ; sol, solution; tab, tablet; t.i.d., three times daily.

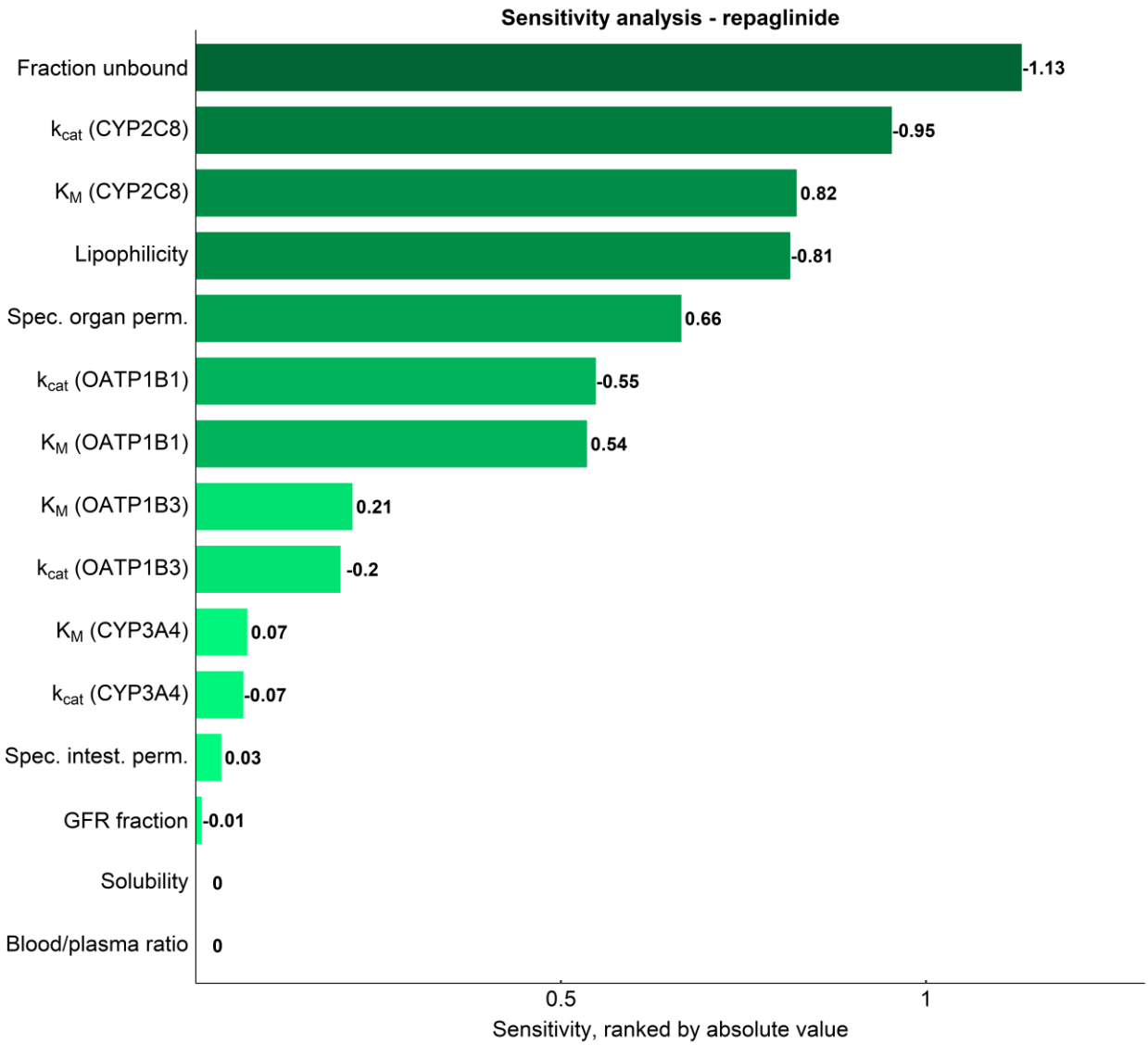

Fig. S3.4.8. Sensitivity analysis of the repaglinide model. Sensitivity of the model to single parameters, determined as change of the simulated AUC from time of the last dose extrapolated to infinity of an oral 4 mg four times daily administration of repaglinide. A sensitivity value of -0.5 indicates a 50% decrease of the simulated AUC for the examined parameter increase of 100%.
CYP, cytochrome P450; GFR, glomerular filtration rate; intest., intestinal; k_{cat}, catalytic rate constant; K_M, Michaelis-Menten constant; OATP, organic-anion-transporting polypeptide; perm., permeability; spec., specific.

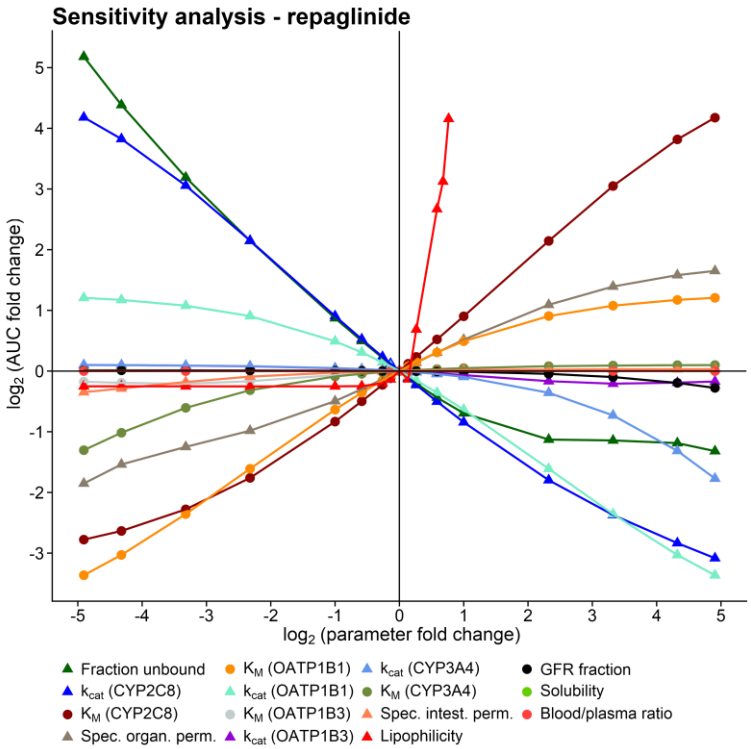

Fig. S3.4.9. Sensitivity analysis spider plot of the repaglinide model. The fold change of AUC is shown as a function of the fold change of the parameter values within a 0.03-fold to 30-fold range. A $\log_2$(fold change) = 1 equals a parameter perturbation of 100% as shown in the sensitivity analysis bar plot. Literature value parameters are shown as circles, optimized parameters are shown as triangles. Lipophilicity was changed only to a maximum absolute value of 10.

3.5 Pioglitazone model development

Pioglitazone is an insulin sensitizer applied in the treatment of type 2 diabetes mellitus. It is a moderate sensitive CYP2C8 substrate [71].

The pioglitazone model was developed using plasma concentration-time profiles of 13 different studies of oral single dose administration of 15 – 30 mg pioglitazone and of oral administration of 30 – 45 mg once daily, as well as the pioglitazone fraction excreted unchanged to urine reported in one study (Table S3.5.1).

The model applies metabolism by CYP2C8 (fraction metabolized of 70-75% [72]), an unspecific hepatic clearance process (first order kinetics) and glomerular filtration. To describe the pioglitazone plasma concentration-time profiles of *CYP2C8*3* allele carriers, CYP2C8 was implemented as described for the repaglinide model (Section 3.4). For pioglitazone, different K_M values were used for *CYP2C8*1* (wild type) and *CYP2C8*3* (high activity of CYP2C8) as reported in the literature [8] and the k_{cat} values for both genotypes were optimized. To incorporate the polymorphic CYP2C8, the parameters of a previously developed model without polymorphism were fixed, *CYP2C8*1* and *CYP2C8*3* were integrated and their k_{cat} values were optimized using studies of pioglitazone in volunteers with different CYP2C8 genotypes. The parameters of the final pioglitazone model are given in Table S3.5.2.

The good descriptive (internal data set) and predictive (external data set) performance of the pioglitazone model is demonstrated in a semilogarithmic (Fig. S3.5.1) as well as a linear plot (Fig. S3.5.2) of population predicted compared to observed plasma concentration-time profiles of all clinical studies. Furthermore, goodness of fit plots comparing predicted versus observed plasma concentrations for pioglitazone are presented (Fig. S3.5.3) and MRD values for each study are given in Table S3.5.3. Correlation of predicted and observed AUC, C_{max}, CL/F and half-life values is presented in Figs. S3.5.4 and S3.5.5, and the corresponding values are given in Tables S3.5.4 and S3.5.5, including calculated model GMFE values.

Sensitivity analysis of a simulation of oral 45 mg pioglitazone twice daily with a parameter perturbation of 100% and a sensitivity threshold value of 0.5 reveals that the pioglitazone model is sensitive to the fraction unbound in plasma (optimized), the pioglitazone lipophilicity (optimized), the CYP2C8 catalytic rate constant (optimized) and the CYP2C8 Michaelis-Menten constant (literature value) (Fig. S3.5.6). A sensitivity analysis spider plot showing the change of AUC over a parameter variation range of 0.03-fold up to 30-fold is presented in Fig. S3.5.7.

Table S3.5.1. Clinical study data of pioglitazone used for PBPK model development.

Route	Dose [mg]	*n*	Females [%]	Age [years]	Weight [kg]	*CYP2C8* genotype	Data set	References
Pioglitazone								
po (-, s.d.)	15	15	73	(35)	(74.5)	**1/*1*	e	Aquilante 2013 [6]
po (-, s.d.)	15	15	67	(37)	(71.0)	**3* [a]	e	Aquilante 2013 [6]
po (tab, s.d.)	15	10	40	20-35	-	-	e	Itkonen 2016 [72]
po (-, s.d.)	15	12	25	20-27	55-85	-	i	Jaakkola 2005 [73]
po (-, s.d.)	15	12	33	21-28	56-90	-	e	Jaakkola 2006b [74]
po (tab, s.d.)	15	8	50	19-25 (21) [b]	56-93 (70)	**1/*1*	i	Tornio 2007 [7]
po (tab, s.d.)	15	5	40	19-25 (21) [b]	60-83 (67)	**1/*3*	e	Tornio 2007 [7]
po (tab, s.d.)	15	3	67	19-25 (21) [b]	44-79 (64)	**3/*3*	i	Tornio 2007 [7]
po (tab, s.d.)	15	26	0	-	-	-	i	Xue 2003 [75]
po (tab, s.d.)	30	24	0	20-36	54-74	-	i	Alim2011 [76] [c]
po (tab, s.d.)	30	10	0	22-23	54-80	-	e	Deng 2005 [77]
po (tab, s.d.)	30	10	30	21-24	57-79	-	e	Jaakkola 2006a [78]
po, (tab, q.d.)	30	62	53	18-44 (29.3)	49-89 (67.1)	-	i	Manitpisitkul 2014 [79]
po (-, q.d.)	45	6	50	(35.7)	(72.8)	-	e	Budde 2003 [80]

[a], *CYP2C8*1/*3*: *n*=14, *CYP2C8*3/*3*: *n*=1; [b], assumed; [c], fraction excreted unchanged to urine only; values for age and weight are given as range (mean); -, not given; CYP, cytochrome P450; e, external data set (model evaluation); i, internal data set (model building); *n*, number of individuals studied; po, oral; q.d., once daily; s.d., single dose; tab, tablet;

Table S3.5.2. Drug-dependent parameters of the final pioglitazone model.

Parameter	Unit	Pioglitazone model	Pioglitazone literature	Description
Pioglitazone				
MW	g/mol	356.40	356.40	Molecular weight
pKa		5.80 (basic), 6.40 (acidic)	[81]	Acid dissociation constant
Solubility (pH)	mg/l	16.8 (6.5)	[82]	Solubility
logP		2.81	3.31 [83]	Lipophilicity
fu		2.07E-03	< 0.01 [81]	Fraction unbound plasma
CYP2C8 K_M [a]	µmol/l	21.0	[8]	CYP2C8 Michaelis-Menten constant
CYP2C8 k_{cat}	1/min	68.09	n.a.	CYP2C8 catalytic rate constant
CYP2C8 (*CYP2C8*1*) k_{cat}	1/min	84.79	n.a.	CYP2C8 catalytic rate constant
CYP2C8 (*CYP2C8*3*) K_M	µmol/l	10.0	[8]	CYP2C8 Michaelis-Menten constant
CYP2C8 (*CYP2C8*3*) k_{cat}	1/min	104.82	n.a.	CYP2C8 catalytic rate constant
Liver plasma clearance (specific clearance)	1/min	2.14	n.a.	Elimination from plasma (first order process in the liver)
GFR fraction		1		Fraction of GFR used for passive elimination by the kidney
Formulation		tab	[84]	Formulation used in predictions
Cell permeabilities		calculated	PK-Sim Standard [42]	Permeation across cell membranes
Partition coefficients		calculated	Berezhkovskiy [43]	Organ-plasma partition coefficients
Specific intestinal perm.	cm/min	4.38E-5	n.a.	Normalized to surface area
Specific organ perm.	cm/min	9.10E-3	calculated	Normalized to surface area

[a], same CYP2C8 Michaelis-Menten constant assumed for CYP2C8 genotype unknown and *CYP2C8*1*; CYP, cytochrome P450; GFR, glomerular filtration rate; n.a., not available; perm, permeability; tab, tablet dissolution profile from literature [84].

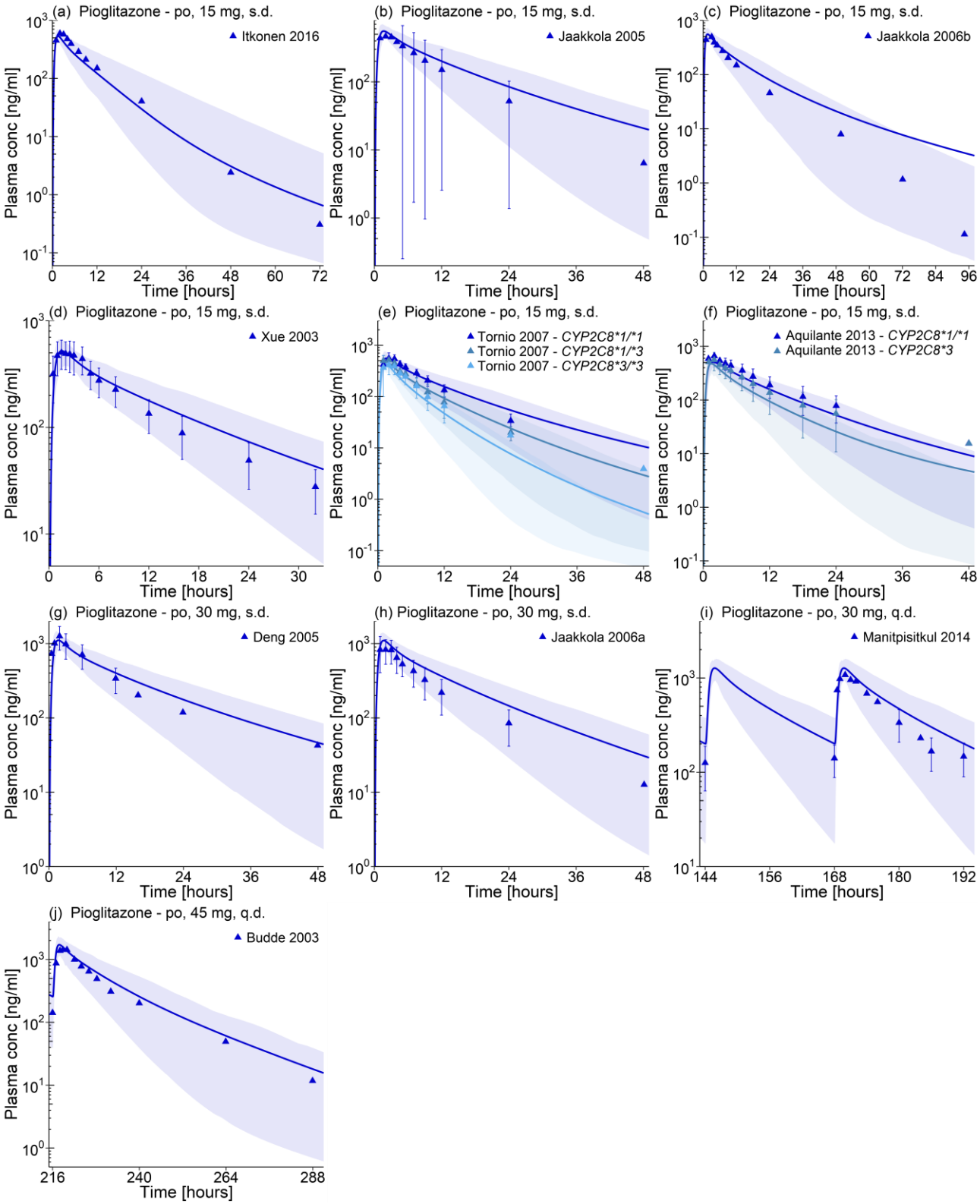

Fig. S3.5.1. Pioglitazone plasma concentration-time profiles (semilogarithmic). Observed data are shown as triangles ± SD. Population simulation arithmetic means or geometric means (a) are shown as blue lines; the shaded areas represent the 68% population prediction intervals. Detailed information about dosing regimens and study populations is given in Table S3.5.1. Predicted and observed AUC and C_{max} values are compared in Table S3.5.4.

conc, concentration; q.d., once daily; s.d., single dose.

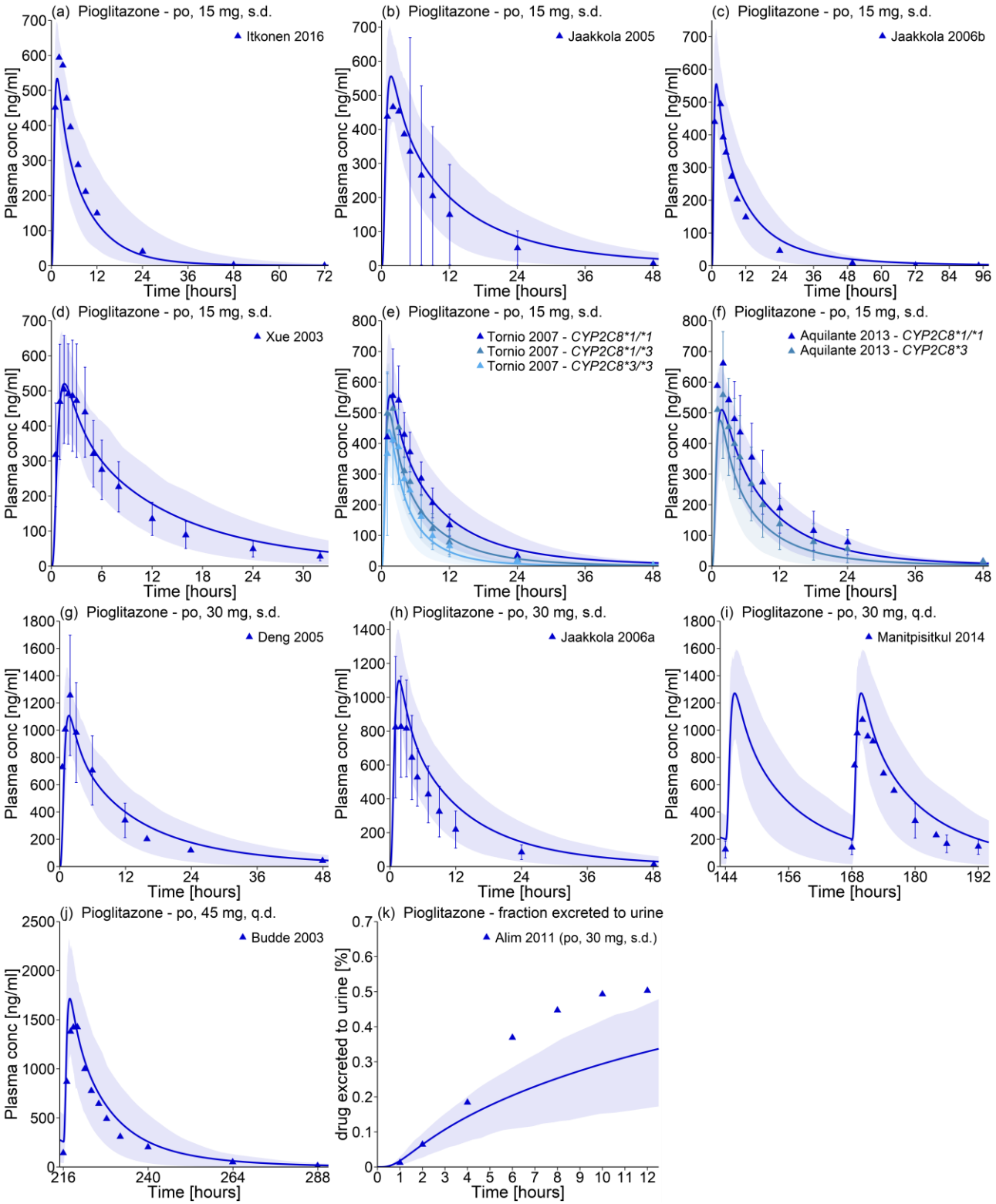

Fig. S3.5.2. Pioglitazone plasma concentration-time profiles (linear) and fraction of pioglitazone excreted to urine (k). Observed data are shown as triangles ± SD. Population simulation arithmetic means or geometric means (a) are shown as blue lines; the shaded areas represent the 68% population prediction intervals. Detailed information about dosing regimens and study populations is given in Table S3.5.1. Predicted and observed AUC and C_{max} values are given in Table S3.5.4.
conc, concentration; q.d., once daily; s.d., single dose.

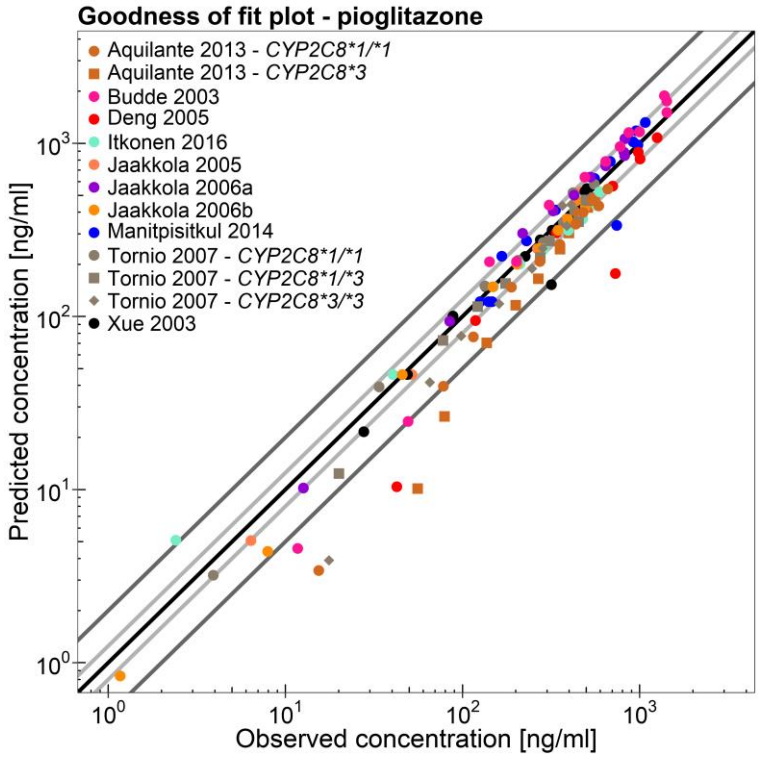

Fig. S3.5.3. Goodness of fit plot. Comparison of predicted versus observed pioglitazone plasma concentration values of all studies. The black line marks the line of identity. Light grey lines indicate 0.8- to 1.25-fold; dark grey lines indicate 0.5- to 2-fold prediction acceptance limits. Detailed information about dosing regimens and study populations is given in Table S3.5.1.

Table S3.5.3. Mean relative deviation values of repaglinide plasma concentration predictions.

Route	Dose [mg]	*CYP2C8* genotype	MRD	References
Pioglitazone				
po (-, s.d.)	15	**1/*1*	1.74	Aquilante 2013 [6]
po (-, s.d.)	15	**3* [a]	3.58	Aquilante 2013 [6]
po (tab, s.d.)	15	-	1.51	Itkonen 2016 [72]
po (-, s.d.)	15	-	1.11	Jaakkola 2005 [73]
po (-, s.d.)	15	-	1.38	Jaakkola 2006b [74]
po (tab, s.d.)	15	**1/*1*	1.13	Tornio 2007 [7]
po (tab, s.d.)	15	**1/*3*	1.87	Tornio 2007 [7]
po (tab, s.d.)	15	**3/*3*	3.08	Tornio 2007 [7]
po (tab, s.d.)	15	-	1.25	Xue 2003 [75]
po (tab, s.d.)	30	-	1.98	Deng 2005 [77]
po (tab, s.d.)	30	-	1.21	Jaakkola 2006a [78]
po, (tab, q.d.)	30	-	1.31	Manitpisitkul 2014 [79]
po (-, q.d.)	45	-	1.48	Budde 2003 [80]
		MRD (mean)	**1.74**	
		MRD ≤ 2	**11/13**	

[a], *CYP2C8*1/*3*: *n*=14, *CYP2C8*3/*3*: *n*=1; -, not given; CYP, cytochrome P450; MRD, mean relative deviation; po, oral; q.d., once daily; s.d., single dose; tab, tablet.

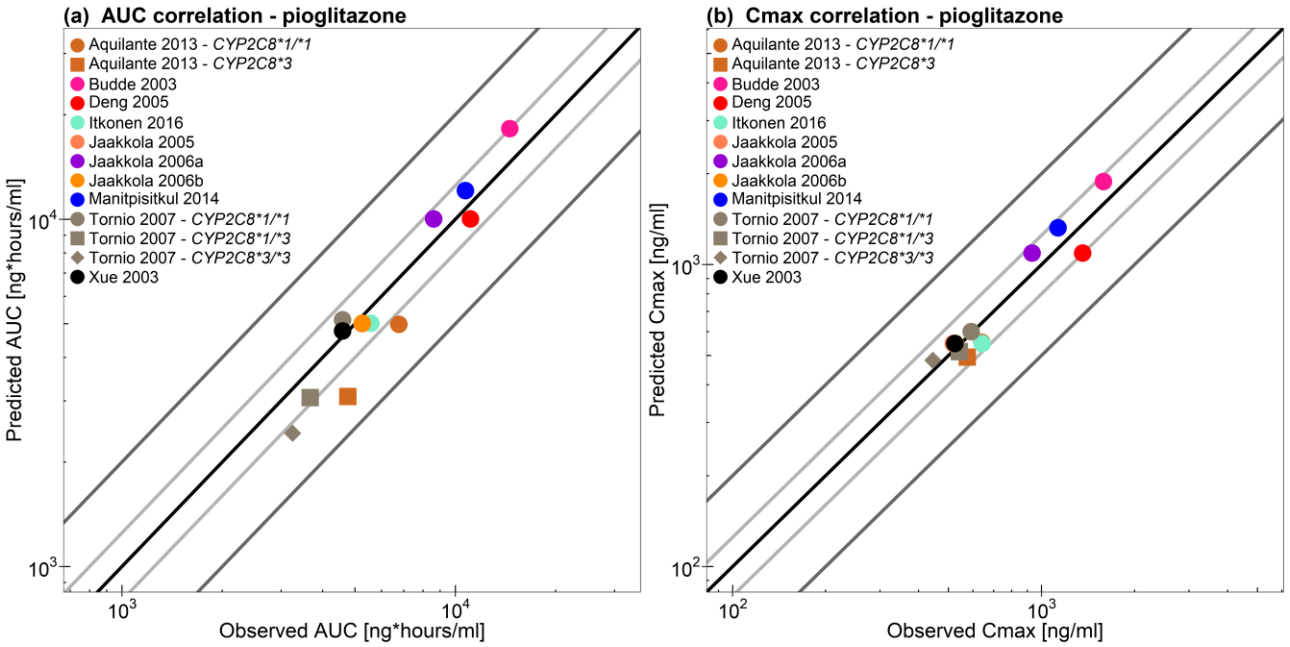

Fig. S3.5.4. Correlation of predicted and observed pioglitazone AUC and C_{max} values of all studies. The black line marks the line of identity. Light grey lines indicate 0.8- to 1.25-fold; dark grey lines indicate 0.5- to 2-fold prediction acceptance limits. Detailed information about dosing regimens and study populations is given in Table S3.5.1. The plotted AUC and C_{max} values are listed in Table S3.5.4.

Table S3.5.4. Predicted and observed AUC and C_{max} values of pioglitazone.

Route	Dose [mg]	*CYP2C8* genotype	AUC [µg*hours/ml]		Pred/Obs AUC	C_{max} [µg/ml]		Pred/Obs C_{max}	References
Pioglitazone			*pred*	*obs*		*pred*	*obs*		
po (-, s.d.)	15	**1/*1*	4983	6770	0.74	553	641	0.86	Aquilante 2013 [6]
po (-, s.d.)	15	**3* [a]	3089	4760	0.65	494	575	0.86	Aquilante 2013 [6]
po (tab, s.d.)	15	-	5017	5580	0.90	548	642	0.85	Itkonen 2016 [72]
po (-, s.d.)	15	-	5006	5250	0.95	548	518	1.06	Jaakkola 2005 [73]
po (-, s.d.)	15	-	5019	5260	0.95	548	526	1.04	Jaakkola 2006b [74]
po (tab, s.d.)	15	**1/*1*	5135	4950 [b]	1.04	600	592 [b]	1.01	Tornio 2007 [7]
po (tab, s.d.)	15	**1/*3*	3066	3670 [b]	0.84	515	542 [b]	0.95	Tornio 2007 [7]
po (tab, s.d.)	15	**3/*3*	2420	3250 [b]	0.74	482	445 [b]	1.08	Tornio 2007 [7]
po (tab, s.d.)	15	-	4769	4590 [c]	1.04	548	524	1.05	Xue 2003 [75]
po (tab, s.d.)	30	-	10021	11100	0.90	1092	1359	0.80	Deng 2005 [77]
po (tab, s.d.)	30	-	10020	8610	1.16	1092	932	1.17	Jaakkola 2006a [78]
po, (tab, q.d.)	30	-	12091	10721 [d]	1.13	1324	1131	1.17	Manitpisitkul 2014 [79]
po (-, q.d.)	45	-	18236	14565 [d]	1.25	1884	1587	1.19	Budde 2003 [80]
				GMFE (range)	**1.17 (1.04-1.54)**			**1.12 (1.01-1.24)**	
				Pred/Obs within 2-fold	**13/13**			**13/13**	

[a], *CYP2C8*1/*3*: *n*=14, *CYP2C8*3/*3*: *n*=1; [b], adjusted for 70kg body weight; [c], $AUC_{0\text{-}32}$; [d], $AUC_{0\text{-}24}$; AUC values are AUC_{inf}, if not specified differently; -, not given; AUC, area under the concentration-time curve; C_{max}, maximum plasma concentration; CYP, cytochrome P450; GMFE, geometric mean fold error; po, oral; pred, predicted; q.d., once daily; s.d., single dose; tab, tablet.

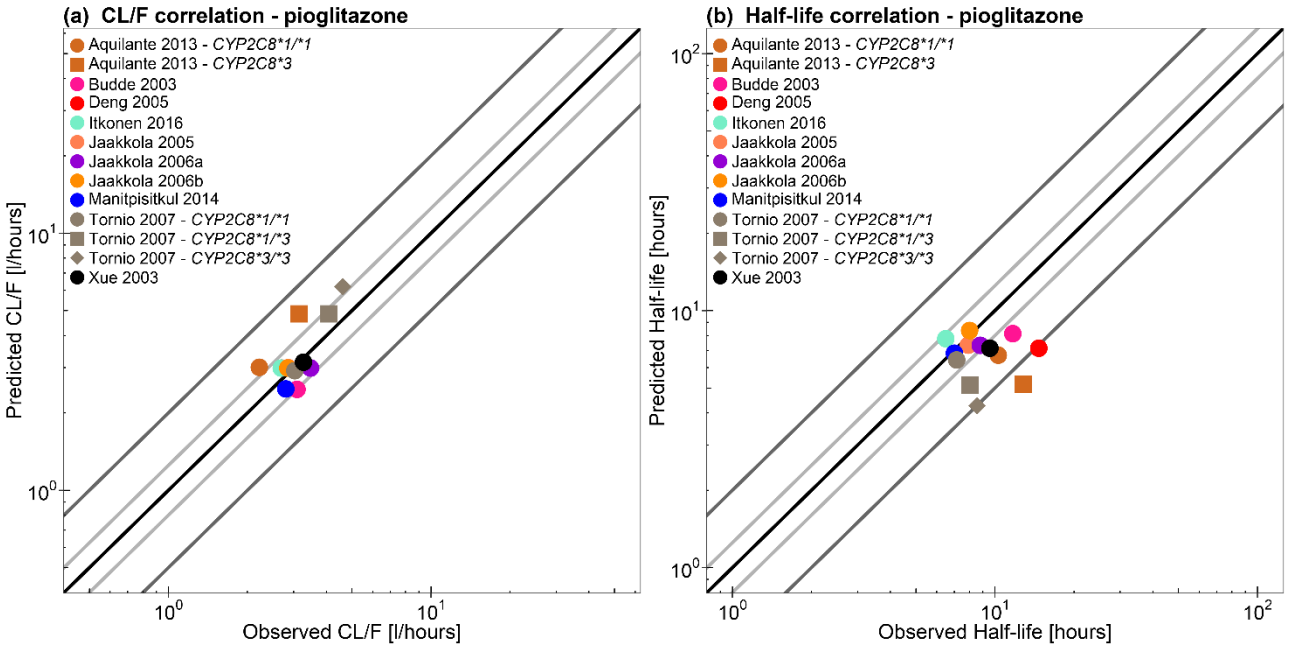

Fig. S3.5.5. Correlation of predicted and observed CL/F and half-life values of all studies. The black line marks the line of identity. Light grey lines indicate 0.8- to 1.25-fold; dark grey lines indicate 0.5- to 2-fold prediction acceptance limits. Detailed information about dosing regimens and study populations is given in Table S3.5.1. The plotted values for CL/F and half-life values are listed in Table S3.5.5.

Table S3.5.5. Predicted and observed CL/F and half-life of pioglitazone.

Route	Dose [mg]	*CYP2C8* genotype	CL/F [a] [l/hours]		Pred/Obs CL/F	Half-life [b] [hours]		Pred/Obs Half-life	References
Pioglitazone			*pred*	*obs*		*pred*	*obs*		
po (-, s.d.)	15	**1/*1*	3.01	2.22	1.36	6.71	10.3	0.65	Aquilante 2013 [6]
po (-, s.d.)	15	**3* [a]	4.86	3.15	1.54	5.17	12.8	0.40	Aquilante 2013 [6]
po (tab, s.d.)	15	-	2.99	2.69	1.11	7.78	6.50	1.20	Itkonen 2016 [72]
po (-, s.d.)	15	-	3.00	2.86	1.05	7.34	7.92	0.93	Jaakkola 2005 [73]
po (-, s.d.)	15	-	2.99	2.85	1.05	8.37	8.01	1.04	Jaakkola 2006b [74]
po (tab, s.d.)	15	**1/*1*	2.92	3.03	0.96	6.43	7.15	0.90	Tornio 2007 [7]
po (tab, s.d.)	15	**1/*3*	4.89	4.09	1.20	5.13	8.04	0.64	Tornio 2007 [7]
po (tab, s.d.)	15	**3/*3*	6.20	4.62	1.34	4.26	8.55	0.50	Tornio 2007 [7]
po (tab, s.d.)	15	-	3.15	3.27	0.96	7.14	9.57	0.75	Xue 2003 [75]
po (tab, s.d.)	30	-	2.99	2.70	1.11	7.41	14.7	0.50	Deng 2005 [77]
po (tab, s.d.)	30	-	2.99	3.48	0.86	7.33	8.79	0.83	Jaakkola 2006a [78]
po, (tab, q.d.)	30	-	2.48	2.80	0.89	6.83	7.01	0.97	Manitpisitkul 2014 [79]
po (-, q.d.)	45	-	2.47	3.09	0.80	8.14	11.7	0.70	Budde 2003 [80]
				GMFE (range)	**1.17 (1.04-1.54)**			**1.41 (1.03-2.48)**	
				Pred/Obs within 2-fold	**13/13**			**11/13**	

[a], calculated from dose/AUC; [b], calculated for observed and predicted concentration-time profiles (same time points for observed and predicted values); -, not given; AUC, area under the concentration-time curve; CL/F, oral clearance; C_{max}, maximum plasma concentration; CYP, cytochrome P450; GMFE, geometric mean fold error; po, oral; pred, predicted; q.d., once daily; s.d., single dose; tab, tablet.

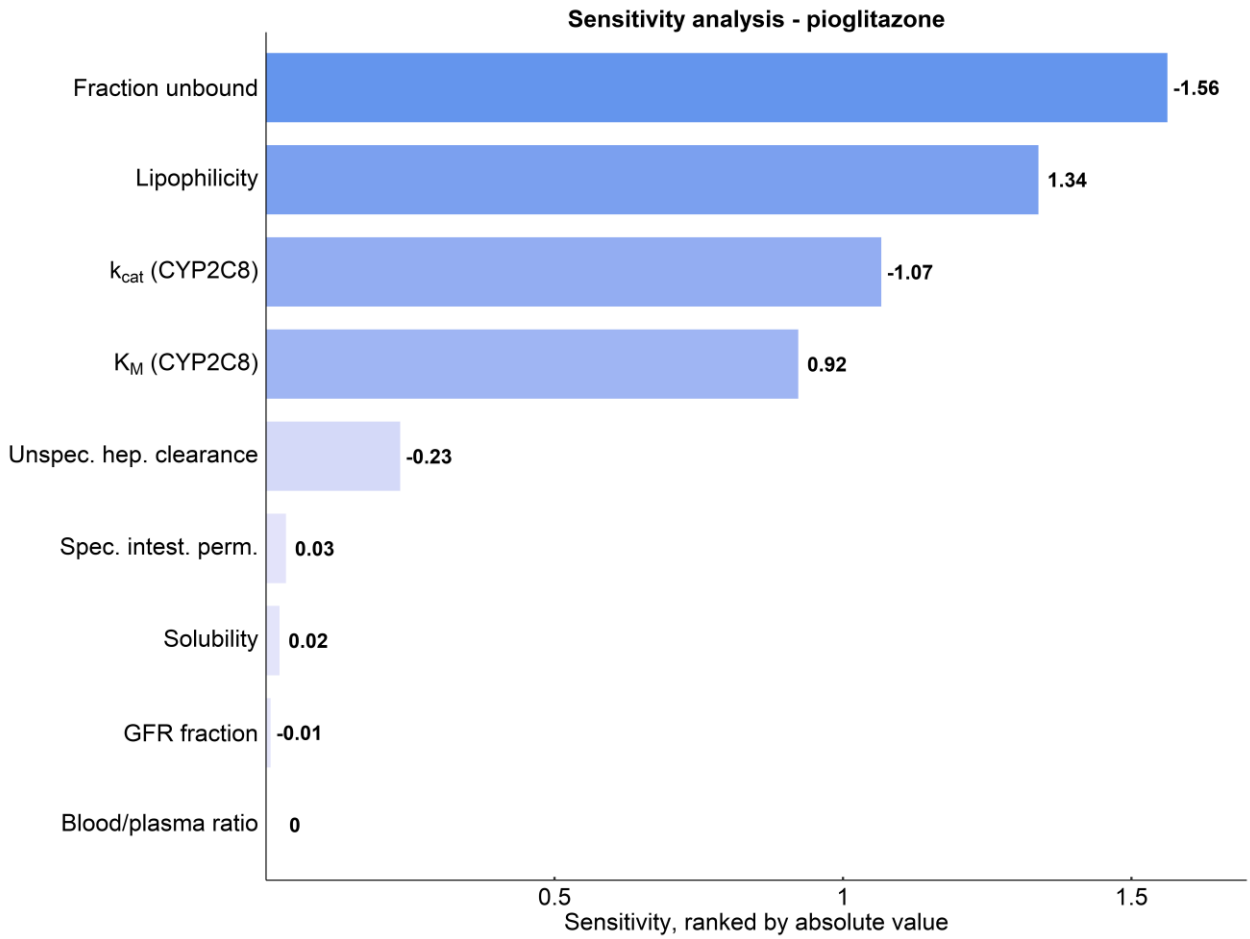

Fig. S3.5.6. Sensitivity analysis of the pioglitazone model. Sensitivity of the model to single parameters, determined as change of the simulated AUC from time of the last dose extrapolated to infinity of an oral 45 mg once daily administration of pioglitazone. A sensitivity value of -0.5 indicates a 50% decrease of the simulated AUC for the examined parameter incraease of 100%.

CYP, cytochrome P450; GFR, glomerular filtration rate; hep., hepatic; intest., intestinal; k_{cat}, catalytic rate constant; K_M, Michaelis-Menten constant; perm, permeability; spec., specific; unspec, unspecific.

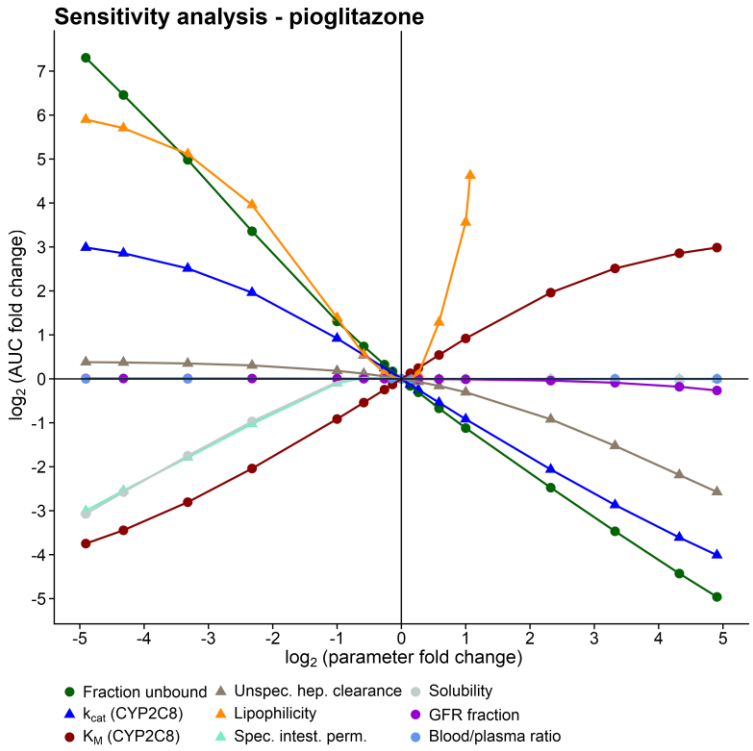

Fig. S3.5.7. Sensitivity analysis spider plot of the pioglitazone model. The fold change of AUC is shown as a function of the fold change of the parameter values within a 0.03-fold to 30-fold range. A $\log_2$(fold change) = 1 equals a parameter perturbation of 100% as shown in the sensitivity analysis bar plot. Literature value parameters are shown as circles, optimized parameters are shown as triangles. Lipophilicity was changed only to a maximum absolute value of 10.

3.6 Itraconazole model extension

The antifungal drug itraconazole is a substrate and a strong inhibitor of CYP3A4 [14]. A previously developed itraconazole parent-metabolite PBPK model [12] was extended and applied in this study. Itraconazole is a poorly soluble compound, leading to variable absorption and, therefore, to large interindividual differences in itraconazole plasma concentration-time profiles and AUC values [85]. In a study of gemfibrozil plus itraconazole co-administration, lower itraconazole and hydroxy-itraconazole plasma concentrations were reported compared to administration of itraconazole alone [73].

To explain this observation, a physicochemical interaction during gemfibrozil-itraconazole co-administration was postulated, leading to reduced itraconazole solubility and absorption. To describe the itraconazole and hydroxy-itraconazole plasma concentrations of this study, the solubility of the existing itraconazole model was adjusted to 14.5 mg/l at pH 6.5 for a capsule formulation in the fasted state during itraconazole monotherapy and to 0.69 mg/l at pH 6.5 during gemfibrozil co-administration. Jaakkola *et al.* [73] and Niemi *et al.* [52] propose an effect of gemfibrozil on itraconazole bioavailability (as implemented in the modeled change of solubility) or the replacement of itraconazole from plasma proteins by gemfibrozil as possible explanations for the lower itraconazole plasma concentrations during gemfibrozil co-administration.

In addition to the study-adjusted itraconazole solubility, K_i values to model the competitive inhibition of OATP1B1 and OATP1B3 by itraconazole were added to the model and optimized with a plasma concentration-time curve of repaglinide during the itraconazole-repaglinide DDI (see Section 4.4). The parameters of the extended itraconazole model are given in Table S3.6.1.

The good descriptive performance of the parent-metabolite model is demonstrated in semilogarithmic as well as linear plots (Figs. S3.6.1 and S3.6.2) of population redicted compared to observed plasma concentration-time profiles of the clinical study.

Table S3.6.1. Drug-dependent parameters of the final itraconazole model.

Parameter	Unit	Itraconazole model	Itraconazole literature	OH-itraconazole model	OH-itraconazole literature	Description
Itraconazole						
MW	g/mol	705.633		721.633		Molecular weight
pKa		3.7 (basic)	[86]	3.7 (basic)	assumed	Acid dissociation constant
Solubility [pH]	mg/l	8.0 (FaSSIF) [a]	[87]			Solubility
logP		4.62	5.66 [86]	3.72	4.5 [88]	Lipophilicity
fu		0.006	0.002, 0.016, 0.036 [86,89–91]	0.017	[89]	Fraction unbound plasma
CYP3A4 K_M	nmol/l	2.07	3.9 [92]	4.17	27.0 [92]	CYP3A4 Michaelis-Menten constant
CYP3A4 k_{cat}	1/min	0.040	predicted [12]	0.020	predicted [12]	CYP3A4 catalytic rate constant
GFR fraction		1		1		Fraction of GFR used for passive elimination by the kidney
K_i CYP3A4	nmol/l	1.3	[92]	14.4	[92]	Inhibitory constant
K_i P-gp	nmol/l	8.0	[93]	-	-	Inhibitory constant
K_i OATP1B1	nmol/l	-	-	18	230 [94] [c]	Inhibitory constant
K_i OATP1B3	nmol/l	-	-	11	100 [94] [c]	Inhibitory constant
Formulation		solution/capsule [b]				Formulation used in predictions
Cell permeabilities		calculated	PK-Sim Standard [42]	calculated	PK-Sim Standard [42]	Permeation across cell membranes
Partition coefficients		calculated	Rodgers and Rowland [95,96]	calculated	Rodgers and Rowland [95,96]	Organ-plasma partition coefficients
Specific intestinal perm.	cm/min	5.33E-06	predicted [12]	1.52E-07	calculated	Normalized to surface area
Specific organ perm.	cm/min	1.44E-04	calculated	1.55E-05	calculated	Normalized to surface area

continued…

continued…

Parameter	Unit	Keto-itraconazole model	Keto-itraconazole literature	ND-itraconazole model	ND-itraconazole literature	Description
MW	g/mol	719.617		649.527		Molecular weight
pKa		3.7 (basic)	assumed	3.7 (base)	assumed	Acid dissociation constant
logP		4.21	4.50 [97]	5.18	4.20 [98]	Lipophilicity
fu		0.010	[89]	0.011	[89]	Fraction unbound plasma
CYP3A4 K_M	nmol/l	2.22	1.4 [92]	0.63	predicted [12]	CYP3A4 Michaelis-Menten constant
CYP3A4 k_{cat}	1/min	0.393	predicted [12]	0.061	predicted [12]	CYP3A4 catalytic rate constant
GFR fraction		1		1		Fraction of GFR used for passive elimination by the kidney
K_i CYP3A4	nmol/l	5.12 [d]	[92]	0.32 [d]	[92]	Inhibitory constant
Cell permeabilities		calculated	PK-Sim Standard [42]	calculated	PK-Sim Standard [42]	Permeation across cell membranes
Partition coefficients		calculated	Rodgers and Rowland [95,96]	calculated	Rodgers and Rowland [95,96]	Organ-plasma partition coefficients
Specific intestinal perm.	cm/min	4.79E-07	calculated	7.37E-06	calculated	Normalized to surface area
Specific organ perm.	cm/min	4.92E-05	calculated	8.91E-04	calculated	Normalized to surface area

[a], solution fasted: 8.0 mg/l (literature value), solution fed: 1.58 mg/l (optimized), capsule fasted: 14.5 mg/l (optimized, itraconazole alone), capsule fasted: 0.69 mg/l (optimized, gemfibrozil co-administration), capsule fed: 0.70 mg/l (optimized); [b], capsule fasted: weibull function with 407 minutes dissolution time (50% dissolved) and dissolution shape 1.1 (both optimized), capsule fed: weibull function with 139 minutes dissolution time (50% dissolved) and dissolution shape 0.82 (both optimized); [c], half maximum inhibitory concentration (IC_{50}) values given in literature but expected to be similar to inhibitory constant (K_i) values; [d], calculated from IC_{50} values via the Cheng-Prusoff equation [99]; -, process not implemented in the model; CYP, cytochrome P450; FaSSIF, fasted state simulated intestinal fluid; GFR, glomerular filtration rate; ND-itraconazole, N-desalkyl-itraconazole; OATP, organic-anion-transporting polypeptide; OH-itraconazole, hydroxy-itraconazole; perm., permeability; P-gp, P-glycoprotein.

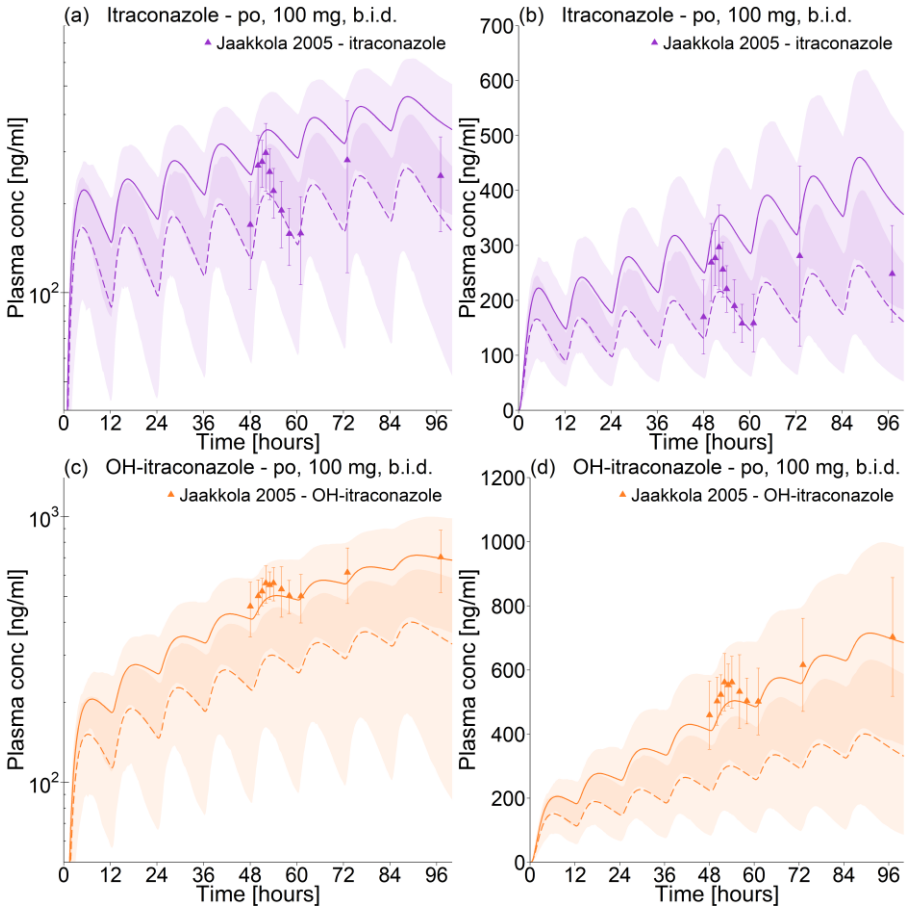

Fig. S3.6.1. Itraconazole and hydroxy-itraconazole (OH-itraconazole) plasma concentration-time profiles in semilogarithmic (left panel) and linear (right panel) plots following administration of itraconazole. Observed data are shown as triangles ± SD. Population simulation arithmetic means are shown as purple (itraconazole) and orange (hydroxy-itraconazole) lines. Dashed lines show predictions of itraconazole and hydroxy-itraconazole before, lines after solubility adjustment. The shaded areas represent the 68% population prediction intervals. Detailed information about dosing regimens and study population is given in Table S4.5.1.

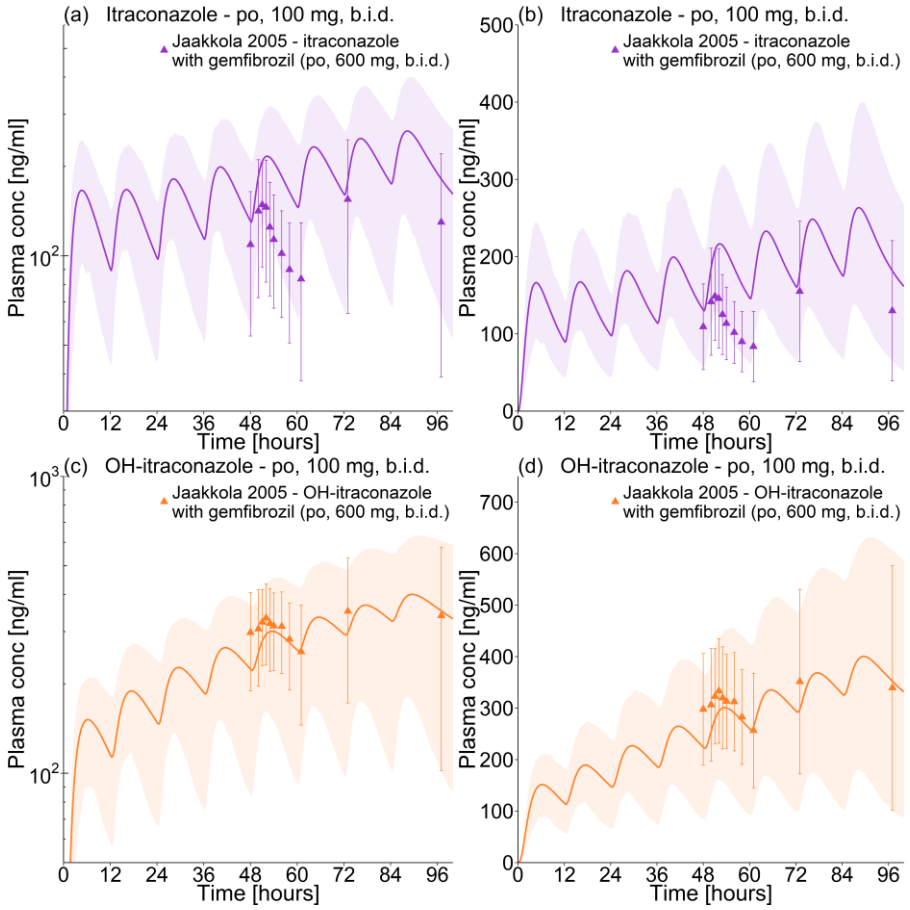

Fig. S3.6.2. Itraconazole and hydroxy-itraconazole (OH-itraconazole) plasma concentration-time profiles in semilogarithmic (left panel) and linear (right panel) plots following administration of itraconazole during co-administration of gemfibrozil. Observed data are shown as triangles ± SD. Population simulation arithmetic means are shown as purple (itraconazole) and orange (hydroxy-itraconazole) lines; the shaded areas represent the 68% population prediction intervals. Detailed information about dosing regimens and study population is given in Table S4.7.1.

3.7 Rifampicin model extension

The antibiotic rifampicin is a strong inducer of different CYP enzymes (including CYP2C8 and CYP3A4) and transporters (including OATP) [14]. A previously developed rifampicin PBPK model [12] was extended by interaction constants describing the induction of CYP2C8 and OATP1B3 as well as the competitive inhibition of CYP2C8, OATP1B1 and OATP1B3 by rifampicin (Section 4.8). The parameters of the extended rifampicin model are given in Table S3.7.1.

Table S3.7.1. Drug-dependent parameters of the final rifampicin model.

Parameter	Unit	Rifampicin model	Rifampicin literature	Description
Rifampicin				
MW	g/mol	822.94		Molecular weight
pKa		1.7 (acidic), 7.9 (basic)	[100]	Acid dissociation constant
Solubility (pH)	mg/l	2800 (7.5)	1100 (6.5), 1400 (6.8), 2540 (6.8), 2800 (7.5), 3350 (7.4) [101–104]	Solubility
logP		2.50	1.30, 2.70 [36,101] [a]	Lipophilicity
fu		0.17	0.11, 0.16, 0.17, 0.175 [101,104–106]	Fraction unbound plasma
B/P ratio		0.89 calculated	0.9 [b] [107]	Blood/plasma ratio
OATP1B1 K_M	µmol/l	1.5	[108]	OATP1B1 Michaelis-Menten constant
OATP1B1 k_{cat}	1/min	7.80	predicted [12]	OATP1B1 catalytic rate constant
AADAC K_M	µmol/l	195.1	[109]	AADAC Michaelis-Menten constant
AADAC k_{cat}	1/min	9.87	predicted [12]	AADAC catalytic rate constant
P-gp K_M	µmol/l	55.0	[110]	P-gp Michaelis-Menten constant
P-gp k_{cat}	1/min	0.61	predicted [12]	P-gp catalytic rate constant
GFR fraction		1		Fraction of GFR used for passive elimination by the kidney
Induction EC_{50}	µmol/l	0.34	[105,106]	Concentration for half-maximal induction
E_{max} OATP1B1		0.38	predicted [12]	Maximum in vivo induction effect
E_{max} OATP1B3		0.38	assumed	Maximum in vivo induction effect
E_{max} AADAC		0.99	predicted [12]	Maximum in vivo induction effect
E_{max} P-gp		2.5	[111]	Maximum in vivo induction effect
E_{max} CYP3A4		9.0	[105]	Maximum in vivo induction effect
E_{max} CYP2C8		3.2	[112]	Maximum in vivo induction effect
K_i OATP1B1	µmol/l	0.477	[17]	Inhibitory constant
K_i OATP1B3	µmol/l	0.90	[113]	Inhibitory constant
K_i P-gp	µmol/l	169.0	[114]	Inhibitory constant
K_i CYP3A4	µmol/l	18.5	[16]	Inhibitory constant
K_i CYP2C8	µmol/l	30.2	[16]	Inhibitory constant

continued…

continued…

Parameter	Unit	Rifampicin model	Rifampicin literature	Description
Formulation		solution		Formulation used in predictions
Cell permeabilities		calculated	PK-Sim Standard [42]	Permeation across cell membranes
Partition coefficients		calculated	Rodgers and Rowland [95,96]	Organ-plasma partition coefficients
Specific intestinal perm.	cm/min	1.24E-07	predicted [12]	Normalized to surface area
Specific organ perm.	cm/min	2.93E-07	calculated	Normalized to surface area

[a], DrugBank entry for rifampicin. https://www.drugbank.ca/drugs/DB01045. Accessed 30 Oct 2018; [b], Blood/serum concentration ratio; AADAC, arylacetamide deacetylase; conc, concentration; CYP, cytochrome P450; GFR, glomerular filtration rate; OATP, organic-anion-transporting polypeptide; perm, permeability; P-gp, P-glycoprotein.

3.8 Clarithromycin model extension

The antibiotic clarithromycin is a strong inhibitor of CYP3A4 and P-glycoprotein [14] as well as an inhibitor of OATP1B1 and OATP1B3 [71]. A previously developed clarithromycin PBPK model [12] was extended by K_i values to model the competitive inhibition of OATP1B1 and OATP1B3 by clarithromycin (Section 4.10). The parameters of the extended clarithromycin model are given in Table S3.8.1.

Table S3.8.1. Drug-dependent parameters of the final clarithromycin model.

Parameter	Unit	Clarithromycin model	Clarithromycin literature	Description
Clarithromycin				
MW	g/mol	747.95		Molecular weight
pKa		8.99 (basic)	[115]	Acid dissociation constant
Solubility (pH)	mg/l	12170 (2.4)	[116]	Solubility
logP		2.3	[117]	Lipophilicity
fu		0.30	0.28, 0.30, 0.40 [118–120]	Fraction unbound plasma
CYP3A4 K_M	µmol/l	48.7	[121]	CYP3A4 Michaelis-Menten constant
CYP3A4 k_{cat}	1/min	76.5	predicted [12]	CYP3A4 catalytic rate constant
CL_{Ren}	ml/min	100	111 - 213 [122]	Renal plasma clearance
K_I CYP3A4	µmol/l	6.04	2.25, 4.12, 5.49, 29.5, 39.2 [123–126]	Concentration for half-maximal inactivation (MBI)
k_{inact} CYP3A4	1/min	0.04	0.04, 0.04, 0.05, 0.07, 0.23 [123–126]	Maximum inactivation rate constant (MBI)
K_i P-gp	µmol/l	4.1	[127]	Inhibitory constant
K_i OATP1B1	µmol/l	5.3	[94] [b]	Inhibitory constant
K_i OATP1B3	µmol/l	14	[94] [b]	Inhibitory constant
Formulation		Weibull [a]		Formulation used in predictions
Cell permeabilities		calculated	PK-Sim Standard [42]	Permeation across cell membranes
Partition coefficients		calculated	Rodgers and Rowland [95,96]	Organ-plasma partition coefficients
Specific inteststinal perm.	cm/min	1.23E-07	predicted [12]	Normalized to surface area
Specific organ perm.	cm/min	3.28E-07	calculated	Normalized to surface area
Perm. into blood cells	cm/min	3.62E-06	predicted [12]	Plasma to blood cells permeability
Perm. out of blood cells	cm/min	1.04E-07	predicted [12]	Blood cells to plasma permeability

[a], Weibull function with 5.0 min dissolution time (50% dissolved) and dissolution shape 2.9 [128]; [b], half maximum inhibitory concentration (IC_{50}) values given in literature but expected to be similar to inhibitory constant (K_i) values; CL, clearance; CYP, cytochrome P450; perm., permeability; P-gp, P-glycoprotein.

3.9 System-dependent parameters and virtual populations

System-dependent parameters, such as reference concentrations and tissue expression profiles of metabolizing enzymes and transporters, are listed in Table S3.9.1. Enterohepatic circulation was enabled by setting the EHC continuous fraction to 1 in all subjects.

To cover the variability of simulated plasma concentration-time profiles in a population, virtual populations containing 100 individuals with demographic properties (% females, age range, weight range, height range, race) adapted to each respective study were created. If no information on the gender of the volunteers was available, a 100% male population was assumed. To model studies that did not report the age range of their individuals, a population between 20 and 50 years of age was created. The reference concentrations of the implemented CYP and UGT enzymes were distributed according to the variabilities provided in the PK-Sim database. If no information was available in the modeling platform, they were set to be log-normally distributed according to literature reports or otherwise with a moderate geometric standard deviation of 1.4 (35% CV), see Table S3.9.1.

As the observed data were mostly reported in terms of arithmetic means and standard deviations, simulated 68% population prediction intervals were plotted that correspond to the range span of ± 1 standard deviation around the mean assuming normal distribution.

Table S3.9.1. System-dependent parameters and expression of relevant enzymes, transporters and other ADME processes.

Enzyme / Transporter / Process	Mean reference concentration [µmol/l] [a]	Geometric standard deviation of the reference concentration	Relative expression in the different organs [b]	Half-life liver [hours]	Half-life intestine [hours]
Enzymes					
AADAC	1.0 [129] [d]	1.40 [e]	RT-PCR [130]	36	23
CYP2C8 (genotype unknown)	2.56 [131]	2.05 [132]	RT-PCR [133]	23	23
CYP2C8 (*CYP2C8*1*)	1.28 [c]	2.05 (assumed) [132]	RT-PCR [133]	23	23
CYP2C8 (*CYP2C8*3*)	1.28 [c]	2.05 (assumed) [132]	RT-PCR [133]	23	23
CYP3A4	4.32 [131]	1.18 liver, 1.46 intestine [132]	RT-PCR [133]	36 [134]	23 [135]
UGT2B7	1.00 [129] [d]	1.60 [132]	EST [136]	36	23
Transporters					
MRP2	1.00 [129] [d]	1.49 [137]	Array [138]	36	23
OATP1B1 (genotype unknown)	1.00 [129] [d]	1.54 [139]	RT-PCR [140]	36	23
OATP1B1 (*SLCO1B1 521T*)	0.5 [f]	1.54 (assumed) [139]	RT-PCR [140]	36	23
OATP1B1 (*SLCO1B1 521C*)	0.5 [f]	1.54 (assumed) [139]	RT-PCR [140]	36	23
OATP1B1 (*SLCO1B1 -11187G*)	0.5 [f]	1.54 (assumed) [139]	RT-PCR [140]	36	23
OATP1B1 (*SLCO1B1 -11187A*)	0.5 [f]	1.54 (assumed) [139]	RT-PCR [140]	36	23
OATP1B3	1.00 [129] [d]	1.54 (assumed) [139]	Array [138]	36	23
P-gp (efflux)	1.41 [12]	1.60 [139]	RT-PCR [140], with the relative expression in intestinal mucosa increased by factor 3.57 [12]	36	23
Processes					
Unspecific hepatic clearance (pioglitazone)	-	1.40 [e]	-	-	-
Active hepatocyte uptake (gemfibrozil)	1.00 [129]	1.40 [e]	Liver only	36	23

[a], [µmol protein/l in the tissue of the highest expression]; [b], PK-Sim® expression database profile; [c], mean reference concentration of CYP2C8 devided by two; [d], If no information on reference concentration was available it was set to 1.0 µmol/l and the catalytic rate constant (k_{cat}) was optimized according to [129]; [e], 35% CV assumed; [f], mean reference concentration of OATP1B1 devided by two; AADAC, arylacetamide deacetylase; CYP, cytochrome P450; ADME, absorption, distribution, metabolism and elimination; Array, ArrayExpress; EST, expressed sequence tags, MRP, multidrug resistance-associated protein; OATP, organic-anion-transporting polypeptide; P-gp, P-glycoprotein; RT-PCR, reverse transcription polymerase chain reaction; SLCO, solute carrier organic anion transporter family member; UGT, UDP-glucuronosyltransferase.

4 DDI modeling

4.1 DDI modeling - general

The correct prediction of the impact of a perpetrator drug on the PK of a victim drug indicates (i) that the perpetrator model adequately describes the drug concentrations at the site(s) of interaction and (ii) that the victim drug model simulates the right amound of drug eliminated via the affected pathway. Therefore, DDI prediction is considered a valuable means of evaluation of both models (provided that the clinical DDI data was not used during model optimization). The simulations of the gemfibrozil-repaglinide, gemfibrozil-pioglitazone, gemfibrozil-itraconazole-repaglinide, rifampicin-repaglinide, rifampicin-pioglitazone and clarithromycin-repaglinide DDIs in this study are predictions, as the interaction constants were taken from literature or optimized using other DDI combinations.

Details on the clinical studies describing the **gemfibrozil-repaglinide**, **gemfibrozil-pioglitazone**, **itraconazole-repaglinide**, **itraconazole-pioglitazone**, **gemfibrozil-itraconazole-repaglinide**, **gemfibrozil-itraconazole-pioglitazone**, **rifampicin-repaglinide**, **rifampicin-pioglitazone** and **clarithromycin-repaglinide** interactions are given in Tables S4.2.1, S4.3.1, S4.4.1, S4.5.1, S4.6.1, S4.7.1, S4.8.1, S4.9.1 and S4.10.1. All perpetrator and victim drugs were administered orally. Plots of population predicted plasma concentration-time profiles of the victim drugs alone and during co-administration, compared to observed data, are given in Figs. S4.2.1, S4.2.2, S4.2.3, S4.2.4, S4.2.5, S4.2.6, S4.3.1, S4.3.2, S4.4.1, S4.5.1, S4.6.1, S4.7.1, S4.8.1, S4.9.1 and S4.10.1 (semilogarithmic and linear plots). Graphical comparisons of predicted to observed DDI AUC ratios (AUC_{last} victim drug during perpetrator co-administration/AUC_{last} victim drug control) and DDI C_{max} ratios (C_{max} victim drug during perpetrator co-administration/C_{max} victim drug control) are shown in Figs. S4.2.7, S4.3.3, S4.4.2, S4.5.2, S4.6.2, S4.7.2, S4.8.2, S4.9.2 and S4.10.2. The corresponding values are listed in Tables S4.2.2, S4.3.2, S4.4.2, S4.5.2, S4.6.2, S4.7.2, S4.8.2, S4.9.2 and S4.10.2, summarizing predicted and observed DDI AUC ratios, DDI C_{max} ratios and model GMFE values. All AUC values used for DDI performance evaluation were calculated from time 0 to the time of the last concentration measurement (AUC_{last}).

4.2 Gemfibrozil-repaglinide DDI

The gemfibrozil-repaglinide DDI was predicted using literature values for all interaction constants without further optimization. To describe the MBI of CYP2C8 by gemfibrozil 1-O-β-glucuronide, values for K_I = 20 µmol/l and k_{inact} = 0.21 min^{-1} were applied, measured with human liver microsomes [15]. The K_I was not corrected for fu_{inc}, according to [141]. The competitive inhibition of CYP2C8 by gemfibrozil was modeled with K_i = 30.4 µmol/l, determined using human liver microsomes [16], with no correction for fu_{inc}, as the gemfibrozil fraction unbound with human liver microsomes was reported to be approximately 1.0 [142]. The competitive inhibition of OATP1B1 by gemfibrozil and gemfibrozil 1-O-β-glucuronide was modeled as described in Section 3.3.

Details on the 23 modeled clinical studies investigating the gemfibrozil-repaglinide DDI are given in Table S4.2.1. The population predictions of repaglinide plasma concentration-time profiles with and without gemfibrozil co-administration, compared to observed data, are shown in Figs. S4.2.1, S4.2.2, S4.2.3, S4.2.4, S4.2.5 and S4.2.6. The correlation of predicted and observed DDI AUC ratios and DDI C_{max} ratios is shown in Fig. S4.2.7. Table S4.2.2 lists the corresponding predicted and observed DDI AUC ratios, DDI C_{max} ratios as well as GMFE values.

Table S4.2.1. Clinical study data of the gemfibrozil-repaglinide DDI.

Perpetrator drug administration	Victim drug administration	Interval [hours] [a]	*n*	Females [%]	Age [years]	Weight [kg]	*SLCO1B1* genotype	Data set	References
Gemfibrozil	*Repaglinide*								
30 mg, s.d.	0.25 mg, s.d.	1	10	10	20-26 (23)	60-88 (73)	-	e	Honkalammi 2011b [18]
100 mg, s.d.	0.25 mg, s.d.	1	10	10	20-26 (23)	60-88 (73)	-	e	Honkalammi 2011b [18]
300 mg, s.d.	0.25 mg, s.d.	1	10	10	20-26 (23)	60-88 (73)	-	e	Honkalammi 2011b [18]
600 mg, s.d.	0.25 mg, s.d.	0	10	50	31-34	-	-	e	Honkalammi 2011a [27]
600 mg, s.d.	0.25 mg, s.d.	1	10	50	31-34	-	-	e	Honkalammi 2011a [27]
600 mg, s.d.	0.25 mg, s.d.	3	10	50	31-34	-	-	e	Honkalammi 2011a [27]
600 mg, s.d.	0.25 mg, s.d.	6	10	50	31-34	-	-	e	Honkalammi 2011a [27]
900 mg, s.d.	0.25 mg, s.d.	1	10	10	20-26 (23)	60-88 (73)	-	e	Honkalammi 2011b [18]
30 mg, b.i.d.	0.25 mg, s.d.	1	10	40	21-30 (24)	66-88 (75)	-	e	Honkalammi 2012 [19]
100 mg, b.i.d.	0.25 mg, s.d.	1	10	40	21-30 (24)	66-88 (75)	-	e	Honkalammi 2012 [19]
600 mg, b.i.d.	0.25 mg, s.d.	1	9	22	19-25	64-87	-	e	Backman 2009 [30]
600 mg, b.i.d.	0.25 mg, s.d.	24	9	22	19-25	64-87	-	e	Backman 2009 [30]
600 mg, b.i.d.	0.25 mg, s.d.	48	9	22	19-25	64-87	-	e	Backman 2009 [30]
600 mg, b.i.d.	0.25 mg, s.d.	96	9	22	19-25	64-87	-	e	Backman 2009 [30]
600 mg, b.i.d.	0.25 mg, s.d.	1	10	40	21-30 (24)	66-88 (75)	-	e	Honkalammi 2012 [19]
600 mg, b.i.d.	0.25 mg, s.d.	1	12	25	(24)	(75)	*521TT*	e	Kalliokoski 2008b [49]
600 mg, b.i.d.	0.25 mg, s.d.	1	6	17	(23)	(74)	*521TC*	e	Kalliokoski 2008b [49]
600 mg, b.i.d.	0.25 mg, s.d.	1	6	17	(23)	(75)	*521CC*	e	Kalliokoski 2008b [49]
600 mg, b.i.d.	0.25 mg, s.d.	1	12	67	20-24	46-84	-	e	Niemi 2003a [52]
600 mg, b.i.d.	0.25 mg, s.d.	0	10	10	-	58-98 (79)	-	e	Tornio 2008 [31]
600 mg, b.i.d.	0.25 mg, s.d.	3	10	10	-	58-98 (79)	-	e	Tornio 2008 [31]
600 mg, b.i.d.	0.25 mg, s.d.	6	10	10	-	58-98 (79)	-	e	Tornio 2008 [31]
600 mg, b.i.d.	0.25 mg, s.d.	12	10	10	-	58-98 (79)	-	e	Tornio 2008 [31]

[a], time intervals between (last) perpetrator and victim drug administration; values for age and weight are given as range (mean); -, not given; b.i.d., twice daily; DDI, drug-drug interaction; e, external data set (model evaluation); *n*, number of individuals studied; s.d., single dose; SLCO, solute carrier organic anion transporter family member.

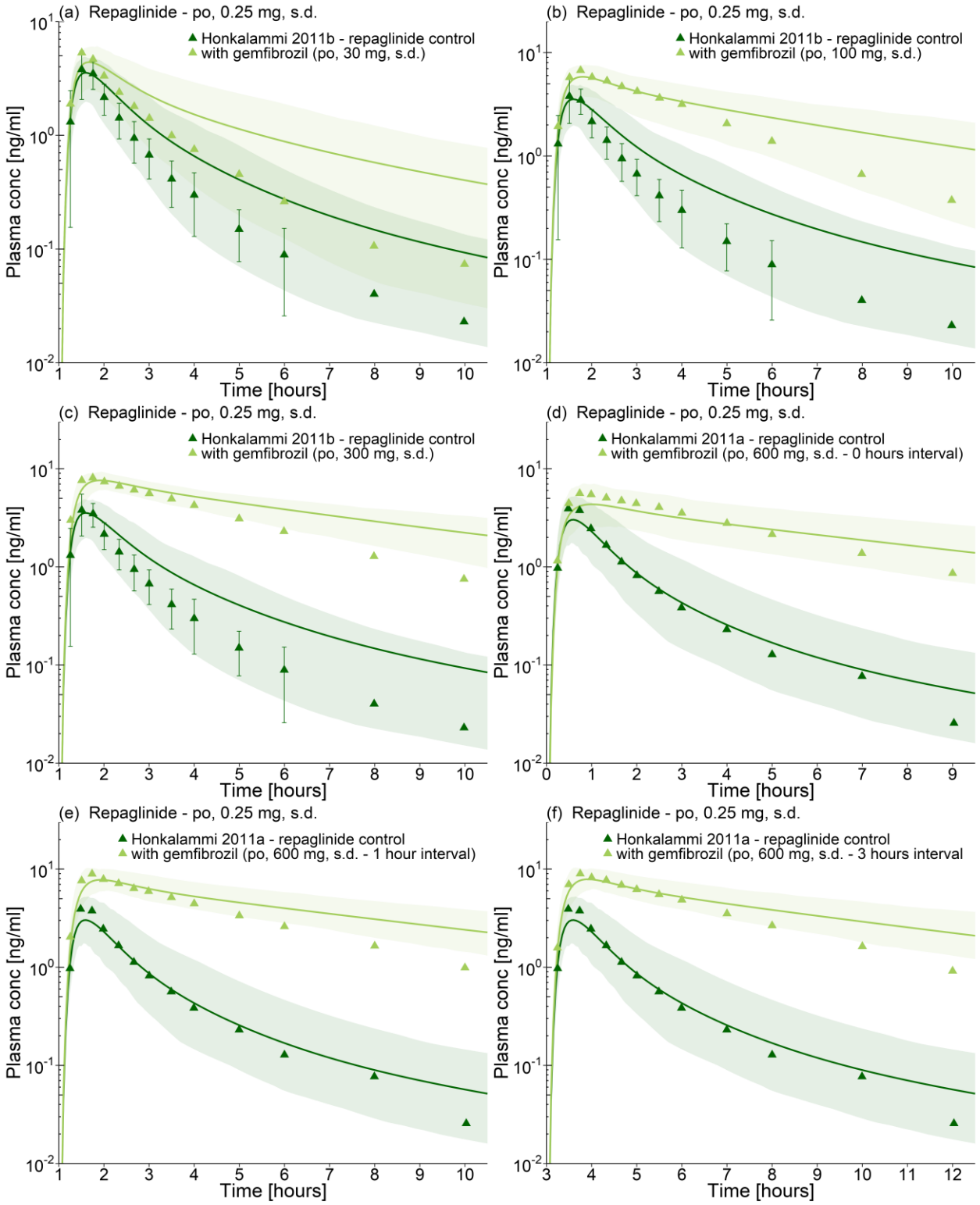
(a) Repaglinide - po, 0.25 mg, s.d.
Honkalammi 2011b - repaglinide control
with gemfibrozil (po, 30 mg, s.d.)
(b) Repaglinide - po, 0.25 mg, s.d.
Honkalammi 2011b - repaglinide control
with gemfibrozil (po, 100 mg, s.d.)
(c) Repaglinide - po, 0.25 mg, s.d.
Honkalammi 2011b - repaglinide control
with gemfibrozil (po, 300 mg, s.d.)
(d) Repaglinide - po, 0.25 mg, s.d.
Honkalammi 2011a - repaglinide control
with gemfibrozil (po, 600 mg, s.d. - 0 hours interval)
(e) Repaglinide - po, 0.25 mg, s.d.
Honkalammi 2011a - repaglinide control
with gemfibrozil (po, 600 mg, s.d. - 1 hour interval)
(f) Repaglinide - po, 0.25 mg, s.d.
Honkalammi 2011a - repaglinide control
with gemfibrozil (po, 600 mg, s.d. - 3 hours interval
Plasma conc [ng/ml]
Time [hours]

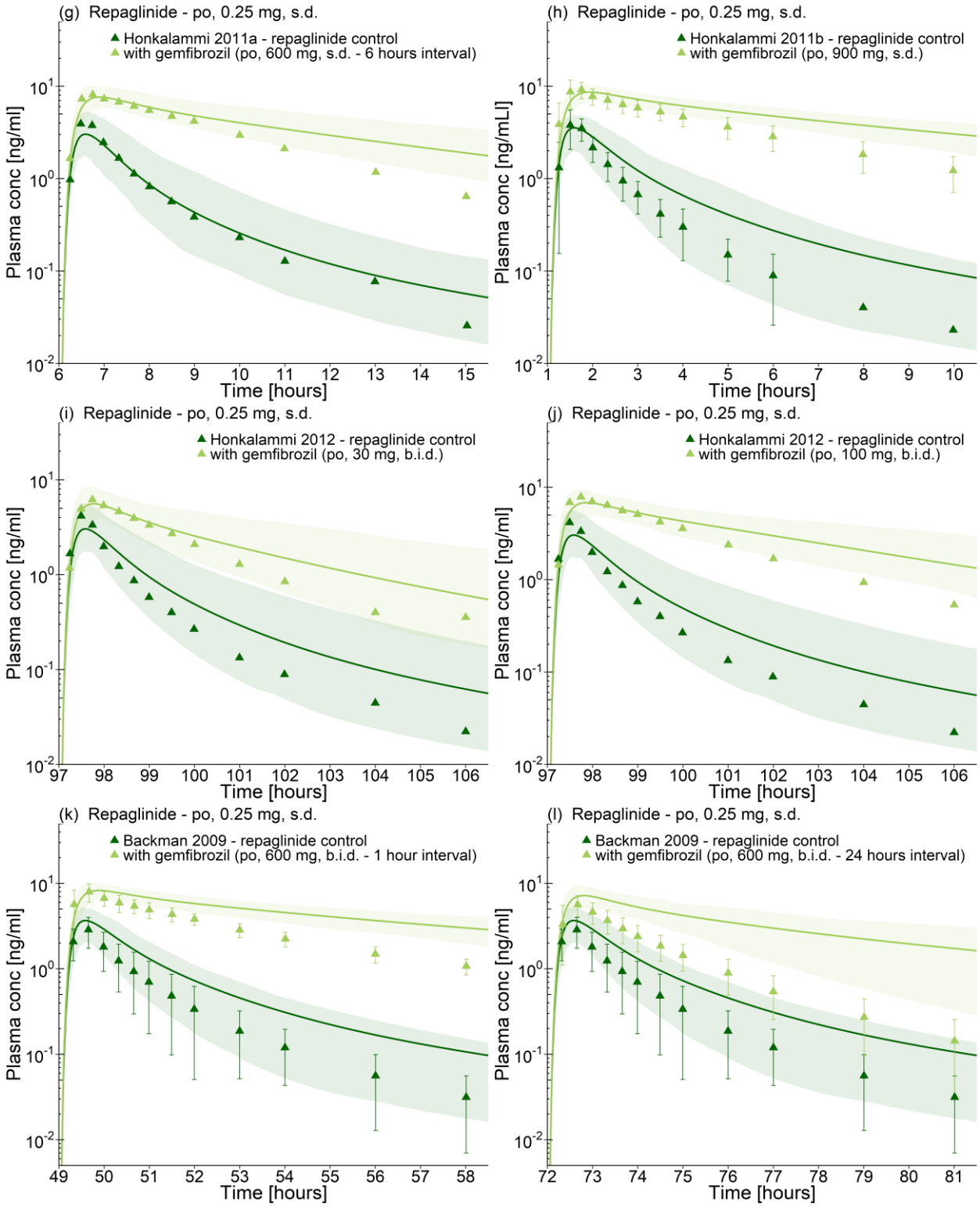
(g) Repaglinide - po, 0.25 mg, s.d.
Honkalammi 2011a - repaglinide control
with gemfibrozil (po, 600 mg, s.d. - 6 hours interval)
Plasma conc [ng/ml]
Time [hours]
(h) Repaglinide - po, 0.25 mg, s.d.
Honkalammi 2011b - repaglinide control
with gemfibrozil (po, 900 mg, s.d.)
Plasma conc [ng/mL]
Time [hours]
(i) Repaglinide - po, 0.25 mg, s.d.
Honkalammi 2012 - repaglinide control
with gemfibrozil (po, 30 mg, b.i.d.)
Plasma conc [ng/ml]
Time [hours]
(j) Repaglinide - po, 0.25 mg, s.d.
Honkalammi 2012 - repaglinide control
with gemfibrozil (po, 100 mg, b.i.d.)
Plasma conc [ng/ml]
Time [hours]
(k) Repaglinide - po, 0.25 mg, s.d.
Backman 2009 - repaglinide control
with gemfibrozil (po, 600 mg, b.i.d. - 1 hour interval)
Plasma conc [ng/ml]
Time [hours]
(l) Repaglinide - po, 0.25 mg, s.d.
Backman 2009 - repaglinide control
with gemfibrozil (po, 600 mg, b.i.d. - 24 hours interval)
Plasma conc [ng/ml]
Time [hours]

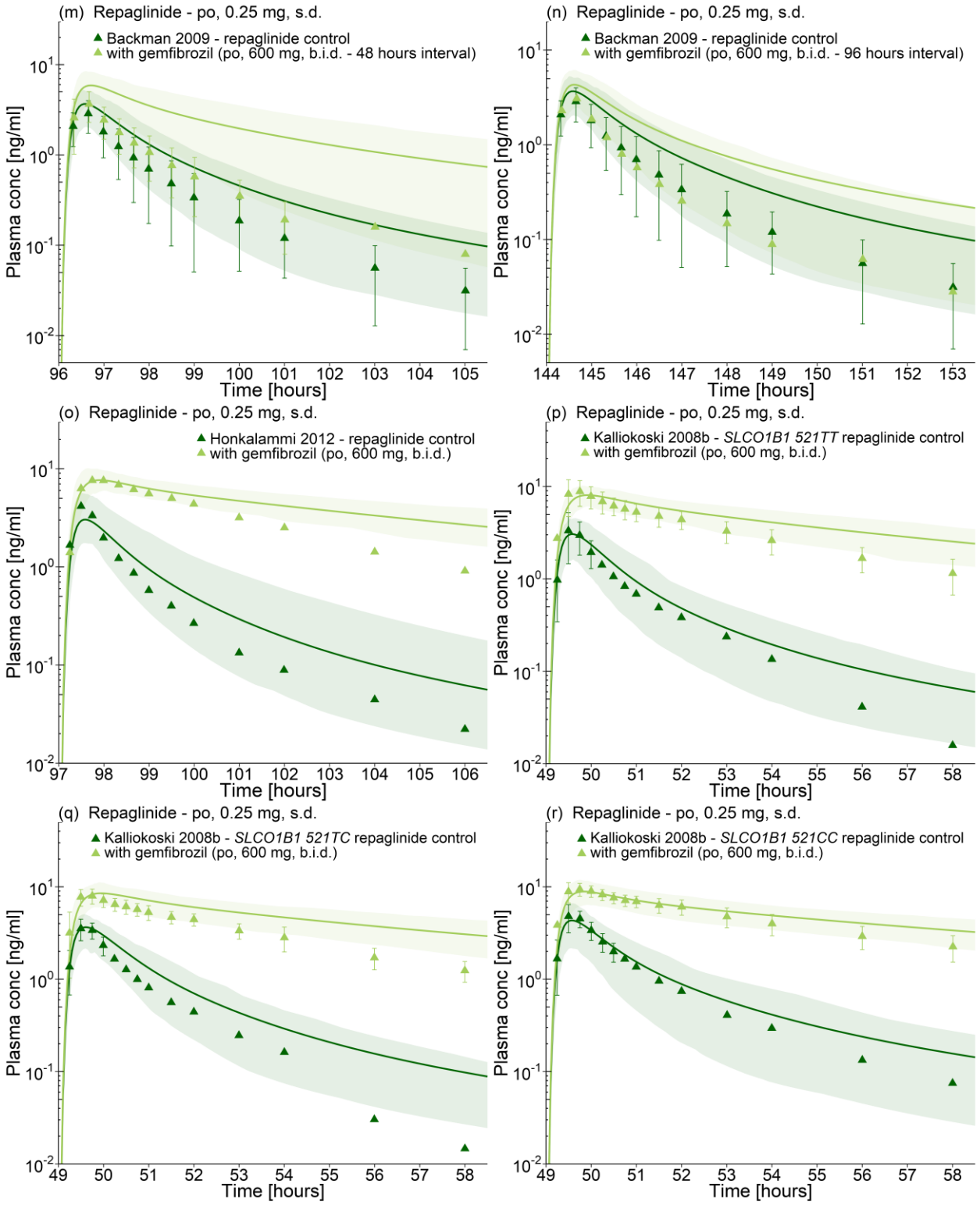
(m) Repaglinide - po, 0.25 mg, s.d.
Backman 2009 - repaglinide control
with gemfibrozil (po, 600 mg, b.i.d. - 48 hours interval)
Plasma conc [ng/ml]
Time [hours]
(n) Repaglinide - po, 0.25 mg, s.d.
Backman 2009 - repaglinide control
with gemfibrozil (po, 600 mg, b.i.d. - 96 hours interval)
Plasma conc [ng/ml]
Time [hours]
(o) Repaglinide - po, 0.25 mg, s.d.
Honkalammi 2012 - repaglinide control
with gemfibrozil (po, 600 mg, b.i.d.)
Plasma conc [ng/ml]
Time [hours]
(p) Repaglinide - po, 0.25 mg, s.d.
Kalliokoski 2008b - SLCO1B1 521TT repaglinide control
with gemfibrozil (po, 600 mg, b.i.d.)
Plasma conc [ng/ml]
Time [hours]
(q) Repaglinide - po, 0.25 mg, s.d.
Kalliokoski 2008b - SLCO1B1 521TC repaglinide control
with gemfibrozil (po, 600 mg, b.i.d.)
Plasma conc [ng/ml]
Time [hours]
(r) Repaglinide - po, 0.25 mg, s.d.
Kalliokoski 2008b - SLCO1B1 521CC repaglinide control
with gemfibrozil (po, 600 mg, b.i.d.)
Plasma conc [ng/ml]
Time [hours]

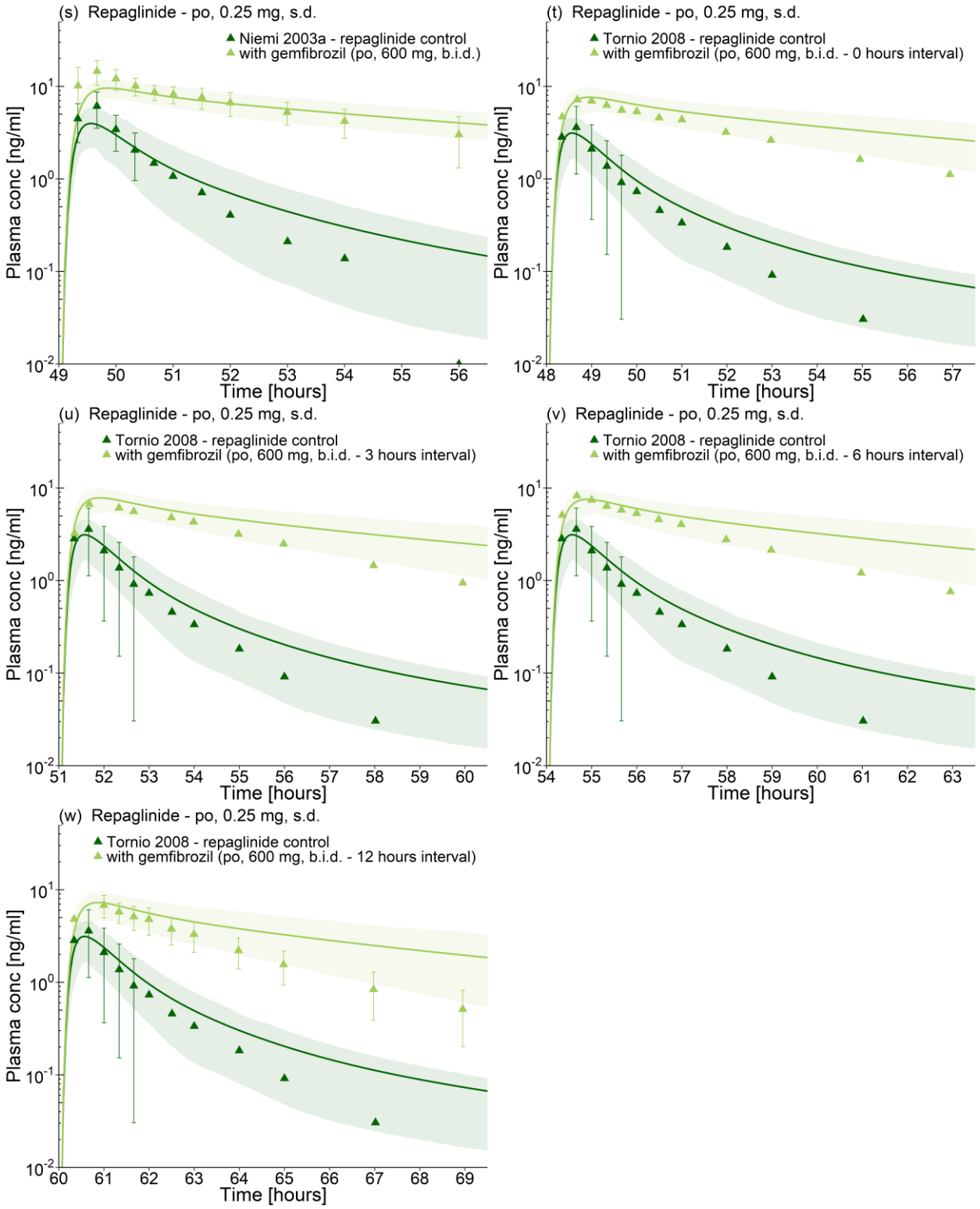

Fig. S4.2.1. Repaglinide plasma concentration-time profiles during the gemfibrozil-repaglinide DDI (semilogarithmic). Observed data are shown as triangles ± SD (dark green: control, light green: with gemfibrozil). Repaglinide population simulation arithmetic means or geometric means (d, e, f, g, i, j and o) are shown as lines (dark green: control, light green: with gemfibrozil). The shaded areas represent the 68% population prediction intervals. Detailed information about dosing regimens and study populations is given in Table S4.2.1. Predicted and observed DDI AUC ratios and DDI C_{max} ratios are compared in Table S4.2.2.

b.i.d., twice daily; conc, concentration; s.d., single dose.

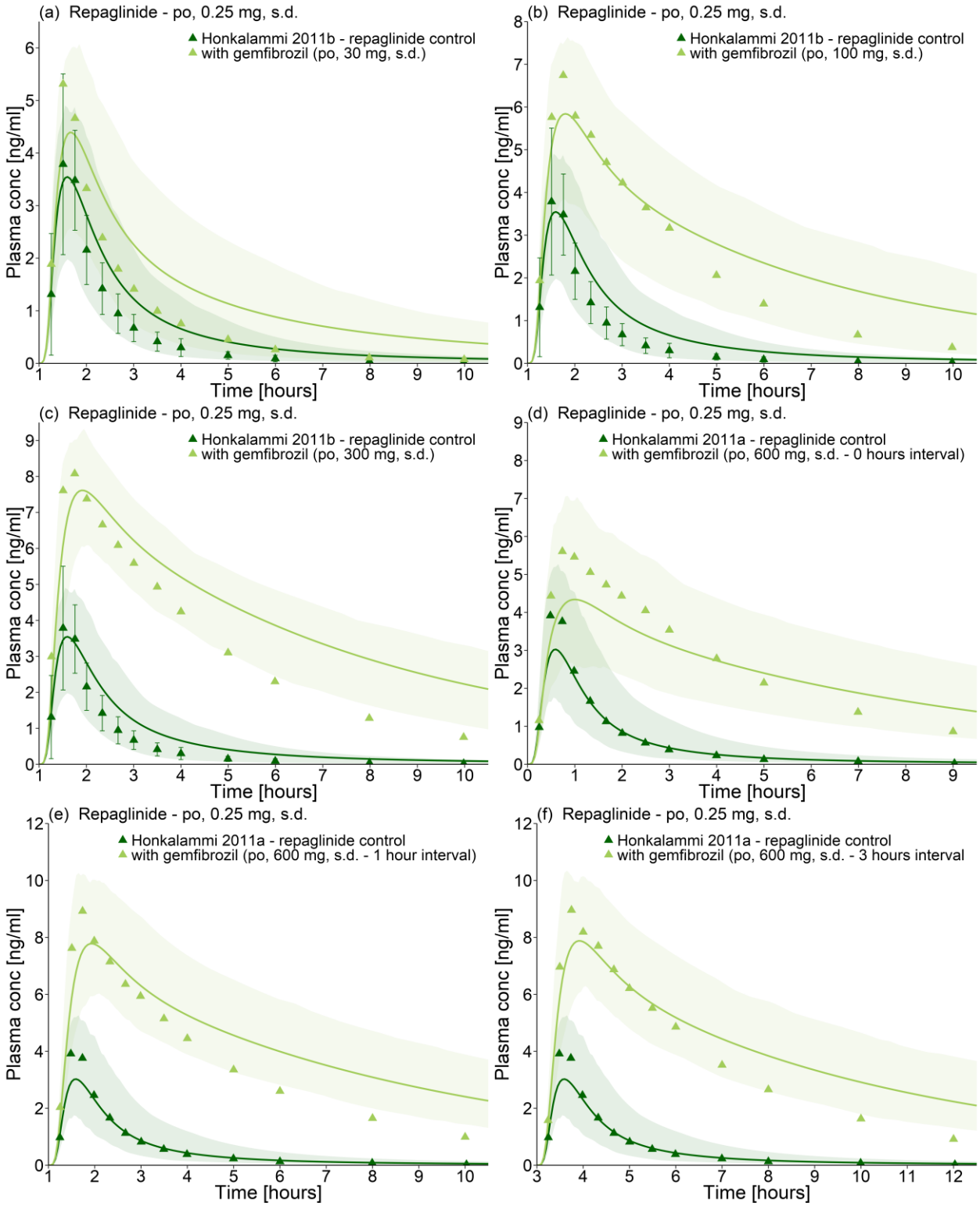
(a) Repaglinide - po, 0.25 mg, s.d.
Honkalammi 2011b - repaglinide control
with gemfibrozil (po, 30 mg, s.d.)
Plasma conc [ng/ml]
Time [hours]
(b) Repaglinide - po, 0.25 mg, s.d.
Honkalammi 2011b - repaglinide control
with gemfibrozil (po, 100 mg, s.d.)
Plasma conc [ng/ml]
Time [hours]
(c) Repaglinide - po, 0.25 mg, s.d.
Honkalammi 2011b - repaglinide control
with gemfibrozil (po, 300 mg, s.d.)
Plasma conc [ng/ml]
Time [hours]
(d) Repaglinide - po, 0.25 mg, s.d.
Honkalammi 2011a - repaglinide control
with gemfibrozil (po, 600 mg, s.d. - 0 hours interval)
Plasma conc [ng/ml]
Time [hours]
(e) Repaglinide - po, 0.25 mg, s.d.
Honkalammi 2011a - repaglinide control
with gemfibrozil (po, 600 mg, s.d. - 1 hour interval)
Plasma conc [ng/ml]
Time [hours]
(f) Repaglinide - po, 0.25 mg, s.d.
Honkalammi 2011a - repaglinide control
with gemfibrozil (po, 600 mg, s.d. - 3 hours interval
Plasma conc [ng/ml]
Time [hours]

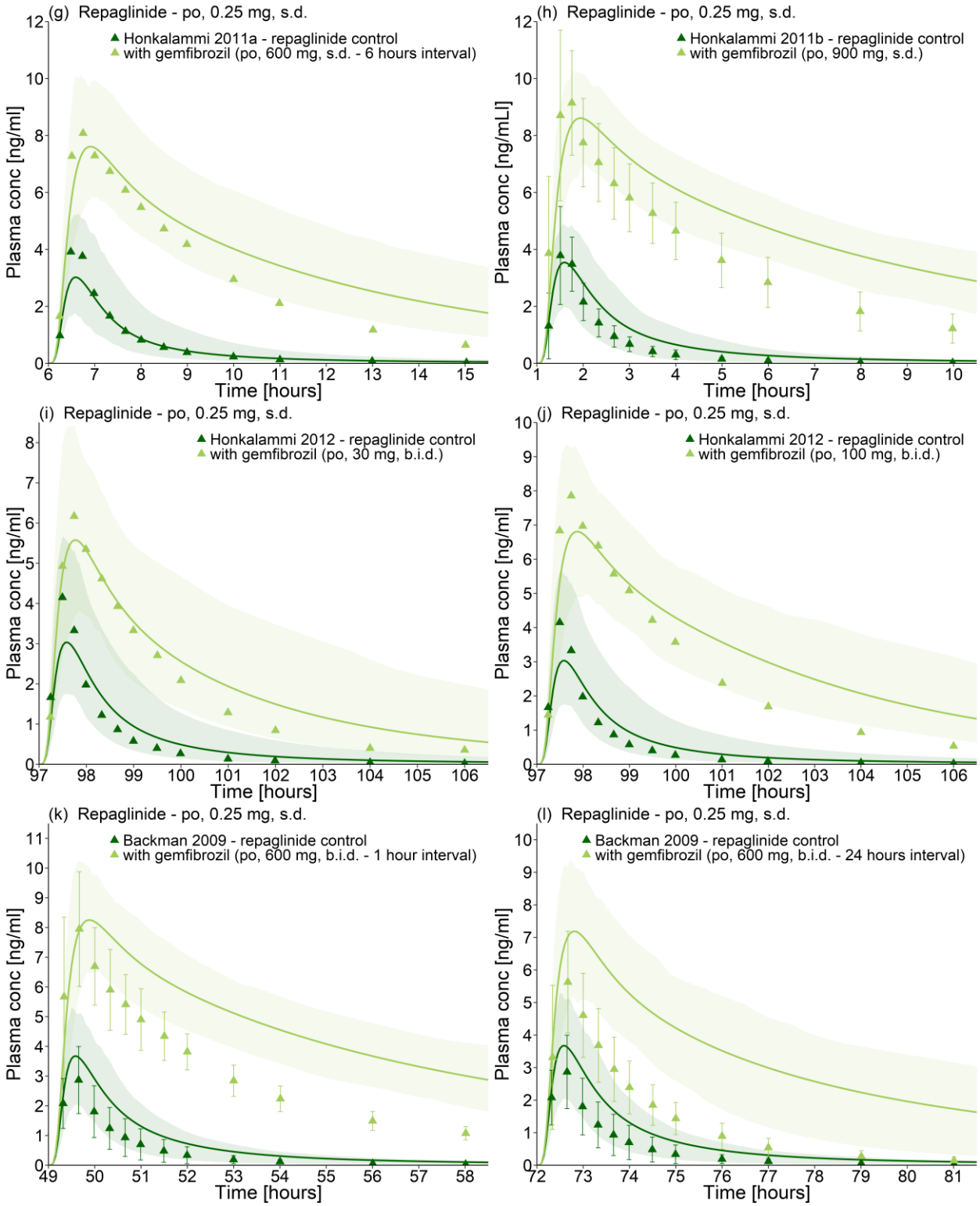
(g) Repaglinide - po, 0.25 mg, s.d.
Honkalammi 2011a - repaglinide control
with gemfibrozil (po, 600 mg, s.d. - 6 hours interval)
Plasma conc [ng/ml]
Time [hours]
(h) Repaglinide - po, 0.25 mg, s.d.
Honkalammi 2011b - repaglinide control
with gemfibrozil (po, 900 mg, s.d.)
Plasma conc [ng/mLl]
Time [hours]
(i) Repaglinide - po, 0.25 mg, s.d.
Honkalammi 2012 - repaglinide control
with gemfibrozil (po, 30 mg, b.i.d.)
Plasma conc [ng/ml]
Time [hours]
(j) Repaglinide - po, 0.25 mg, s.d.
Honkalammi 2012 - repaglinide control
with gemfibrozil (po, 100 mg, b.i.d.)
Plasma conc [ng/ml]
Time [hours]
(k) Repaglinide - po, 0.25 mg, s.d.
Backman 2009 - repaglinide control
with gemfibrozil (po, 600 mg, b.i.d. - 1 hour interval)
Plasma conc [ng/ml]
Time [hours]
(l) Repaglinide - po, 0.25 mg, s.d.
Backman 2009 - repaglinide control
with gemfibrozil (po, 600 mg, b.i.d. - 24 hours interval)
Plasma conc [ng/ml]
Time [hours]

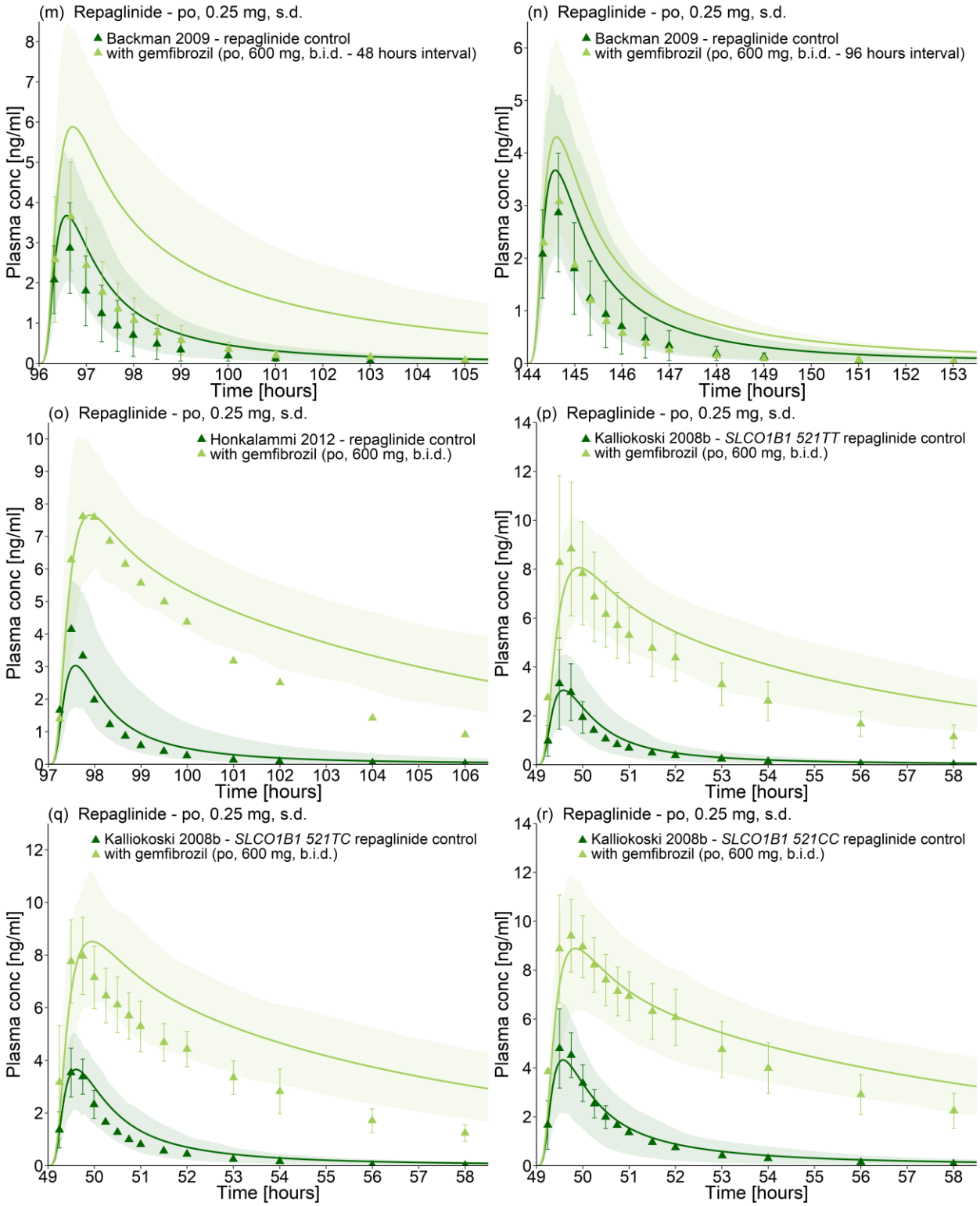
(m) Repaglinide - po, 0.25 mg, s.d.
Backman 2009 - repaglinide control
with gemfibrozil (po, 600 mg, b.i.d. - 48 hours interval)
Plasma conc [ng/ml]
Time [hours]
(n) Repaglinide - po, 0.25 mg, s.d.
Backman 2009 - repaglinide control
with gemfibrozil (po, 600 mg, b.i.d. - 96 hours interval)
Plasma conc [ng/ml]
Time [hours]
(o) Repaglinide - po, 0.25 mg, s.d.
Honkalammi 2012 - repaglinide control
with gemfibrozil (po, 600 mg, b.i.d.)
Plasma conc [ng/ml]
Time [hours]
(p) Repaglinide - po, 0.25 mg, s.d.
Kalliokoski 2008b - SLCO1B1 521TT repaglinide control
with gemfibrozil (po, 600 mg, b.i.d.)
Plasma conc [ng/ml]
Time [hours]
(q) Repaglinide - po, 0.25 mg, s.d.
Kalliokoski 2008b - SLCO1B1 521TC repaglinide control
with gemfibrozil (po, 600 mg, b.i.d.)
Plasma conc [ng/ml]
Time [hours]
(r) Repaglinide - po, 0.25 mg, s.d.
Kalliokoski 2008b - SLCO1B1 521CC repaglinide control
with gemfibrozil (po, 600 mg, b.i.d.)
Plasma conc [ng/ml]
Time [hours]

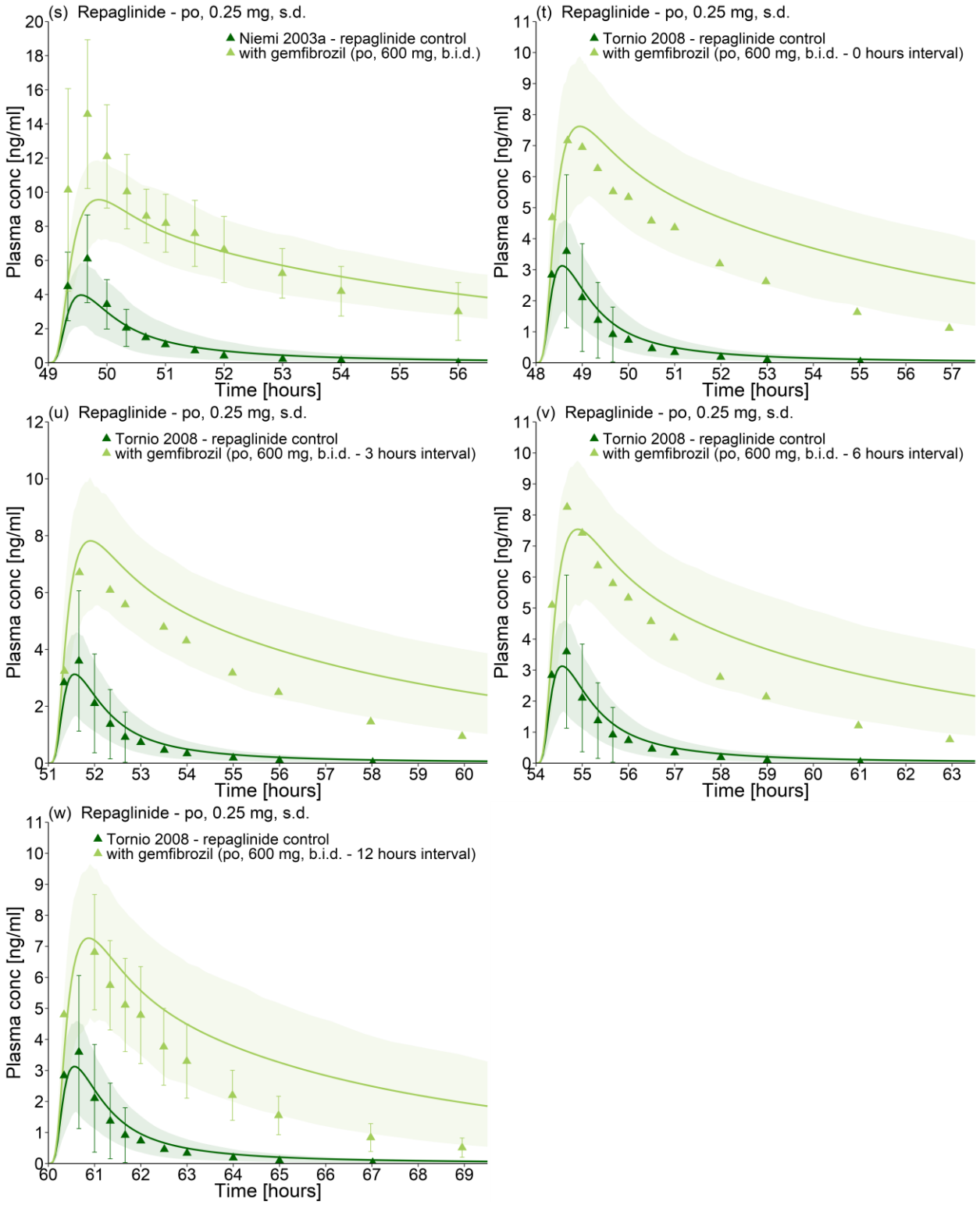

Fig. S4.2.2. Repaglinide plasma concentration-time profiles during the gemfibrozil-repaglinide DDI (linear). Observed data are shown as triangles ± SD (dark green: control, light green: with gemfibrozil). Repaglinide population simulation arithmetic means or geometric means (d, e, f, g, i, j and o) are shown as lines (dark green: control, light green: with gemfibrozil). The shaded areas represent the 68% population prediction intervals. Detailed information about dosing regimens and study populations is given in Table S4.2.1. Predicted and observed DDI AUC ratios and DDI C_{max} ratios are compared in Table S4.2.2.

b.i.d., twice daily; conc, concentration; s.d., single dose.

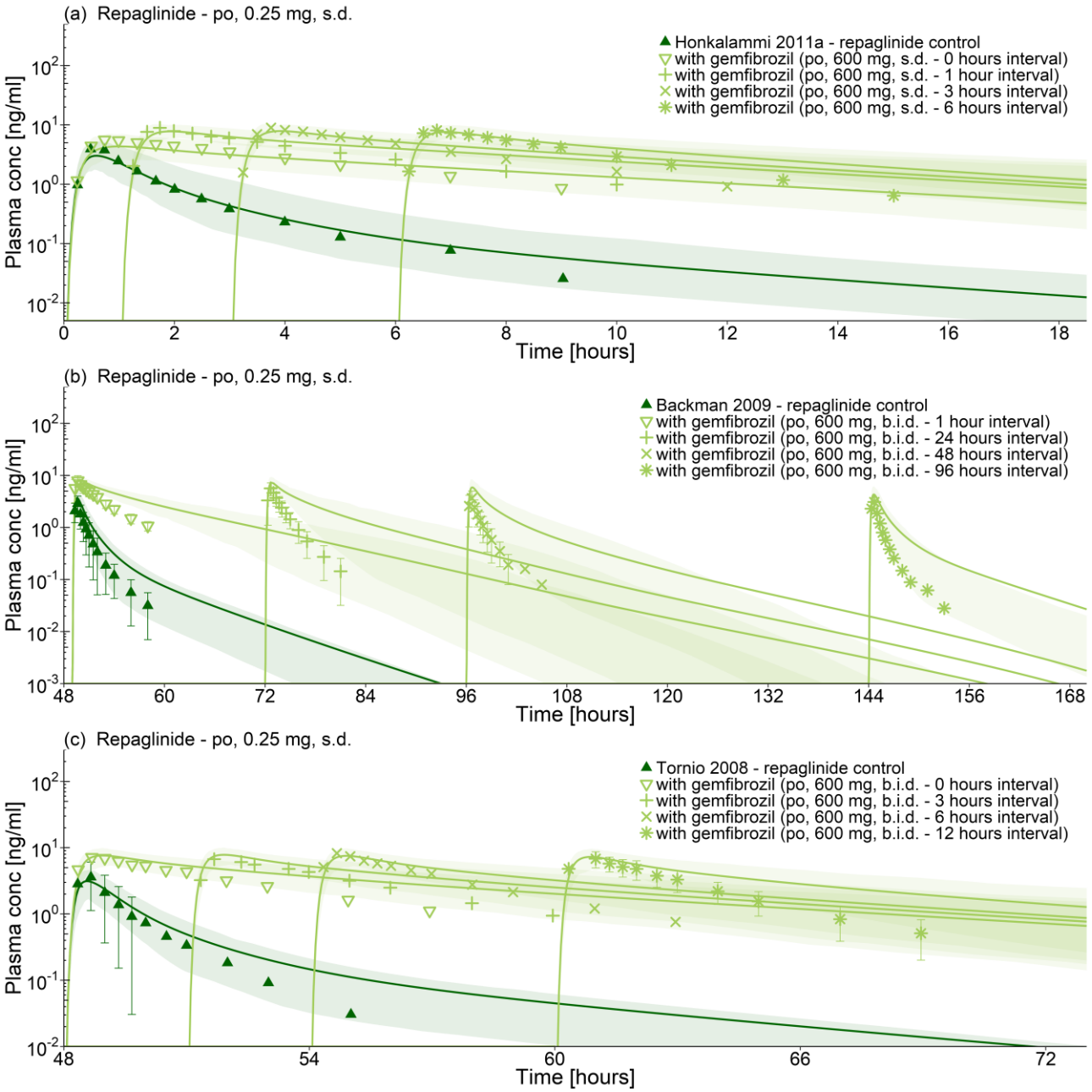

Fig. S4.2.3. Repaglinide plasma concentration-time profiles during the gemfibrozil-repaglinide DDI (time-dependency, semilogarithmic). Observed data are shown as triangles, crosses or stars ± SD (dark green: control, light green: with gemfibrozil). Repaglinide population simulation arithmetic means or geometric means (a) are shown as lines (dark green: control, light green: with gemfibrozil). The shaded areas represent the 68% population prediction intervals. Detailed information about dosing regimens and study populations is given in Table S4.2.1. Predicted and observed DDI AUC ratios and DDI C_{max} ratios are compared in Table S4.2.2.

b.i.d., twice daily; conc, concentration; s.d., single dose.

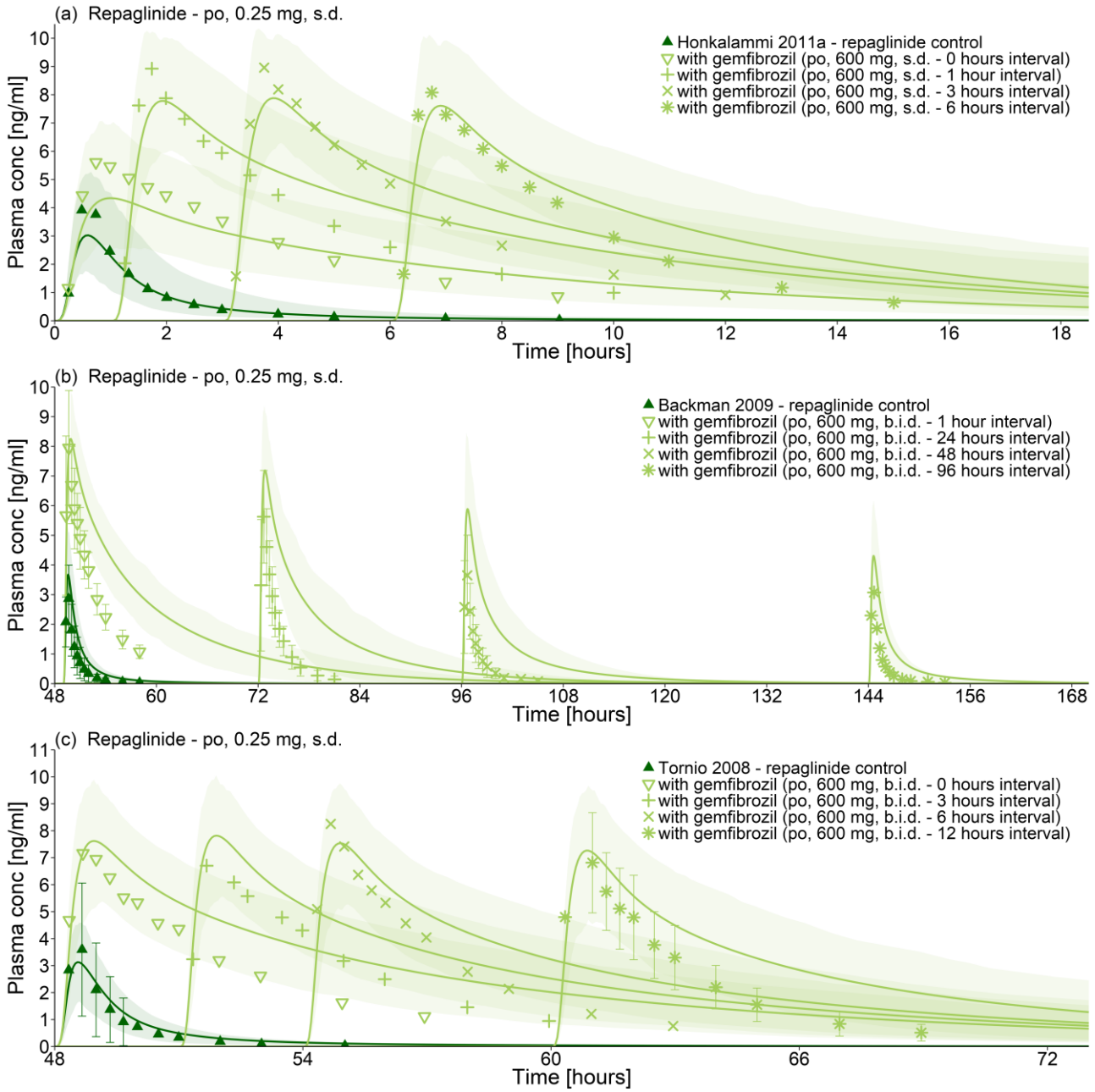

Fig. S4.2.4. Repaglinide plasma concentration-time profiles during the gemfibrozil-repaglinide DDI (time-dependency, linear). Observed data are shown as triangles, crosses or stars ± SD (dark green: control, light green: with gemfibrozil). Repaglinide population simulation arithmetic means or geometric means (a) are shown as lines (dark green: control, light green: with gemfibrozil). The shaded areas represent the 68% population prediction intervals. Detailed information about dosing regimens and study populations is given in Table S4.2.1. Predicted and observed DDI AUC ratios and DDI C_{max} ratios are compared in Table S4.2.2.

b.i.d., twice daily; conc, concentration; s.d., single dose.

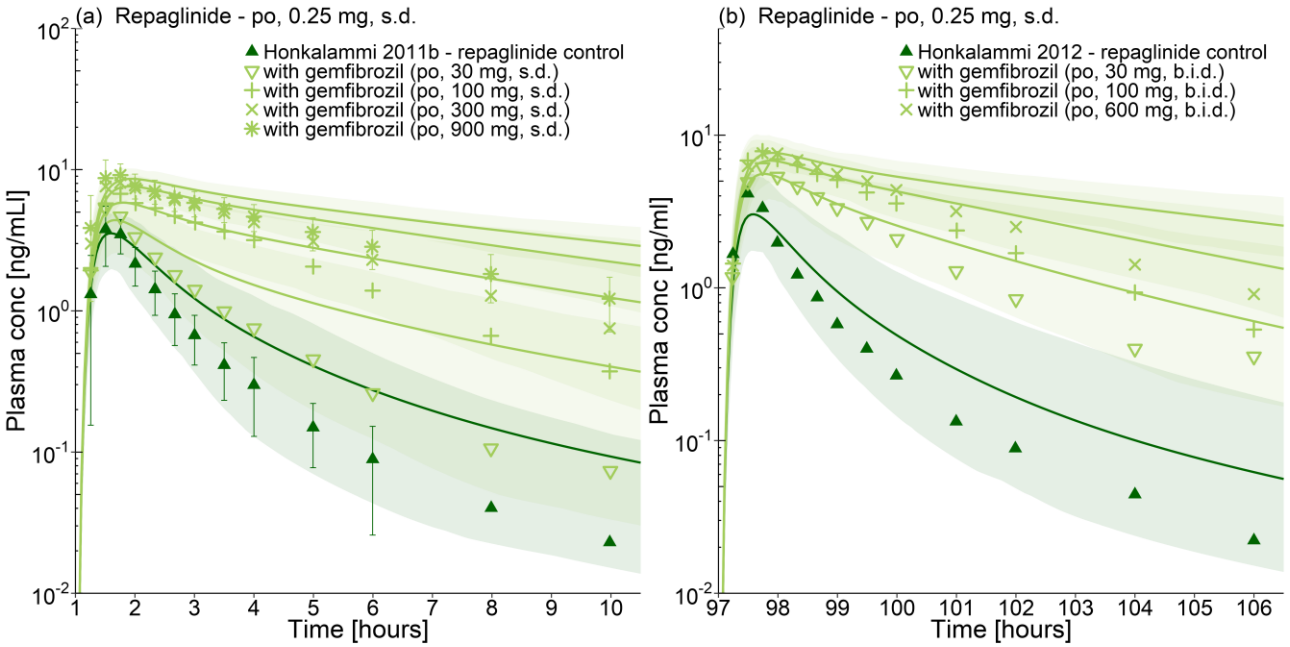

Fig. S4.2.5. Repaglinide plasma concentration-time profiles during the gemfibrozil-repaglinide DDI (dose-dependency, semilogarithmic). Observed data are shown as triangles, crosses or stars ± SD (dark green: control, light green: with gemfibrozil). Repaglinide population simulation arithmetic means or geometric means (a) are shown as lines (dark green: control, light green: with gemfibrozil). The shaded areas represent the 68% population prediction intervals. Detailed information about dosing regimens and study populations is given in Table S4.2.1. Predicted and observed DDI AUC ratios and DDI C_{max} ratios are compared in Table S4.2.2.

b.i.d., twice daily; conc, concentration; s.d., single dose.

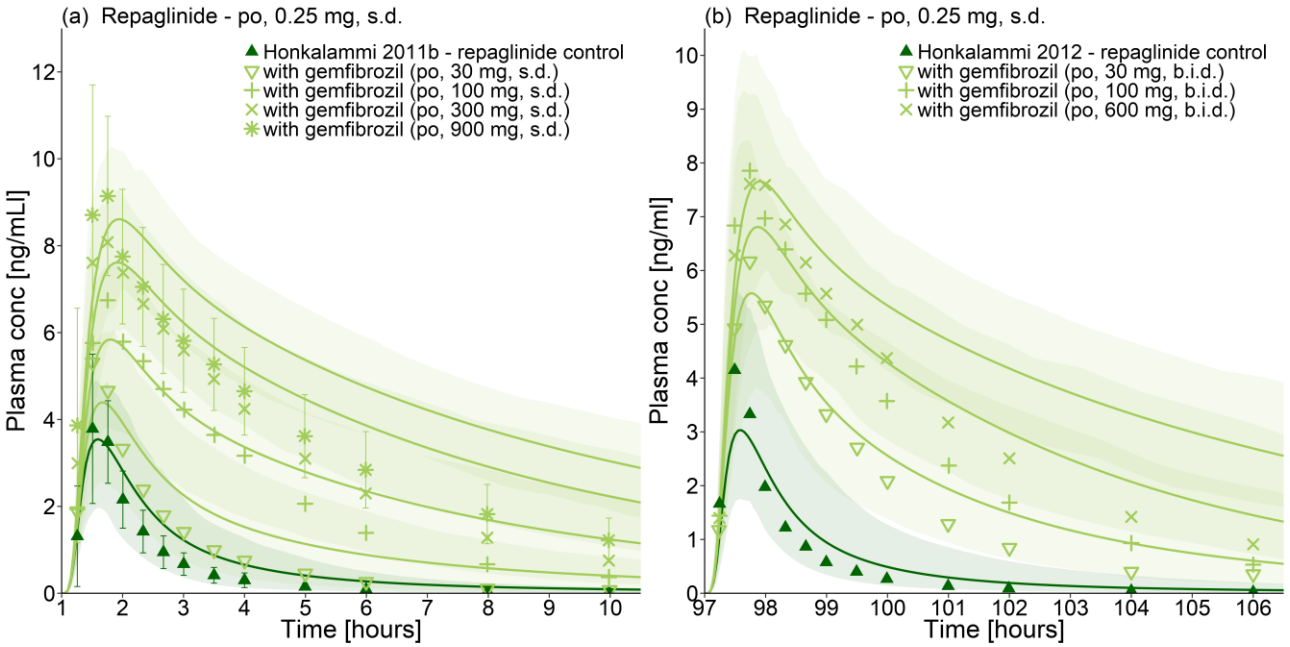

Fig. S4.2.6. Repaglinide plasma concentration-time profiles during the gemfibrozil-repaglinide DDI (dose-dependency, linear). Observed data are shown as triangles, crosses or stars ± SD (dark green: control, light green: with gemfibrozil). Repaglinide population simulation arithmetic means or geometric means (a) are shown as lines (dark green: control, light green: with gemfibrozil). The shaded areas represent the 68% population prediction intervals. Detailed information about dosing regimens and study populations is given in Table S4.2.1. Predicted and observed DDI AUC ratios and DDI C_{max} ratios are compared in Table S4.2.2.

b.i.d., twice daily; conc, concentration; s.d., single dose.

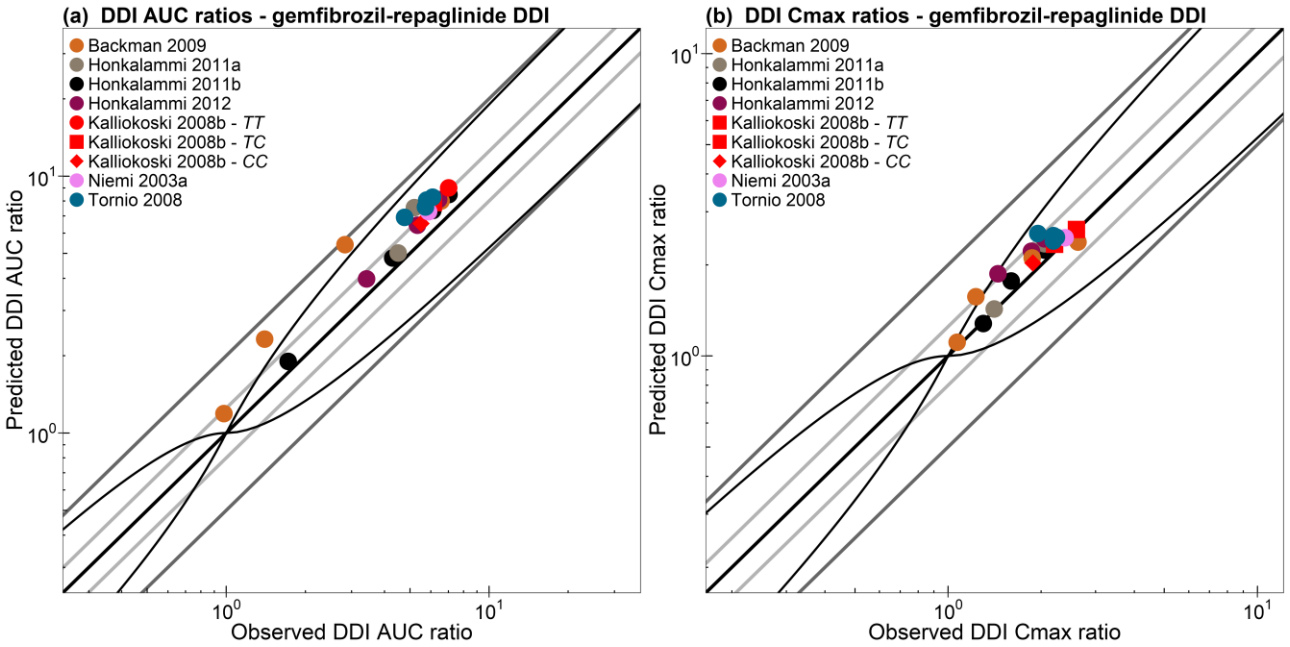

Fig. S4.2.7. Correlation of predicted and observed gemfibrozil-repaglinide DDI AUC ratios and DDI C_{max} ratios of all studies. The straight black line marks the line of identity. Light grey lines indicate 0.8- to 1.25-fold; dark grey lines indicate 0.5- to 2-fold prediction acceptance limits. The curved black lines show the prediction success limits suggested by Guest *et al.* [143]. Detailed information about dosing regimens and study populations is given in Table S4.2.1. The plotted DDI AUC ratios and DDI C_{max} ratios are listed in Table S4.2.2.

CC, *SLCO1B1 521CC*; *TC*, *SLCO1B1 521TC*; *TT*, *SLCO1B1 521TT*.

Table S4.2.2. Predicted and observed DDI AUC ratios and DDI C_{max} ratios of the gemfibrozil-repaglinide DDI.

Perpetrator drug administration	Victim drug administration	Interval [hours] [a]	*SLCO1B1* genotype	t_{last} [hours]	DDI AUC ratio		Pred/Obs DDI AUC ratio	DDI C_{max} ratio		Pred/Obs DDI C_{max} ratio	References
Gemfibrozil	*Repaglinide*				*pred*	*obs*		*pred*	*obs*		
30 mg, s.d.	0.25 mg, s.d.	1	-	9	1.90	1.72	1.10	1.28	1.30	0.98	Honkalammi 2011b [18]
100 mg, s.d.	0.25 mg, s.d.	1	-	9	4.80	4.30	1.12	1.77	1.60	1.10	Honkalammi 2011b [18]
300 mg, s.d.	0.25 mg, s.d.	1	-	9	7.35	6.11	1.20	2.24	2.05	1.10	Honkalammi 2011b [18]
600 mg, s.d.	0.25 mg, s.d.	0	-	9	5.02	4.51 [b]	1.10	1.43	1.41	1.01	Honkalammi 2011a [27]
600 mg, s.d.	0.25 mg, s.d.	1	-	9	8.12	5.93 [b]	1.37	2.41	2.09	1.15	Honkalammi 2011a [27]
600 mg, s.d.	0.25 mg, s.d.	3	-	9	7.93	6.11 [b]	1.30	2.41	2.07	1.16	Honkalammi 2011a [27]
600 mg, s.d.	0.25 mg, s.d.	6	-	9	7.54	5.20 [b]	1.45	2.35	2.05	1.15	Honkalammi 2011a [27]
900 mg, s.d.	0.25 mg, s.d.	1	-	9	8.48	7.04	1.20	2.45	2.23	1.10	Honkalammi 2011b [18]
30 mg, b.i.d.	0.25 mg, s.d.	1	-	9	3.98	3.42 [b]	1.17	1.87	1.45	1.28	Honkalammi 2012 [19]
100 mg, b.i.d.	0.25 mg, s.d.	1	-	9	6.44	5.34 [b]	1.21	2.22	1.86	1.19	Honkalammi 2012 [19]
600 mg, b.i.d.	0.25 mg, s.d.	1	-	9	8.00	6.57	1.22	2.38	2.63	0.90	Backman 2009 [30]
600 mg, b.i.d.	0.25 mg, s.d.	24	-	9	5.41	2.83	1.91	2.11	1.87	1.13	Backman 2009 [30]
600 mg, b.i.d.	0.25 mg, s.d.	48	-	9	2.32	1.40	1.65	1.57	1.23	1.27	Backman 2009 [30]
600 mg, b.i.d.	0.25 mg, s.d.	96	-	9	1.19	0.98	1.22	1.11	1.07	1.04	Backman 2009 [30]
600 mg, b.i.d.	0.25 mg, s.d.	1	-	9	8.11	6.43 [b]	1.26	2.44	2.05	1.19	Honkalammi 2012 [19]
600 mg, b.i.d.	0.25 mg, s.d.	1	*521TT*	9	9.00	7.02	1.28	2.62	2.60	1.01	Kalliokoski 2008b [49]
600 mg, b.i.d.	0.25 mg, s.d.	1	*521TC*	9	7.89	6.14	1.28	2.34	2.21	1.06	Kalliokoski 2008b [49]
600 mg, b.i.d.	0.25 mg, s.d.	1	*521CC*	9	6.54	5.51	1.19	2.03	1.88	1.08	Kalliokoski 2008b [49]
600 mg, b.i.d.	0.25 mg, s.d.	1	-	7	7.27	5.89	1.23	2.46	2.39	1.03	Niemi 2003a [52]
600 mg, b.i.d.	0.25 mg, s.d.	0	-	9	8.28	6.10	1.36	2.50	2.19	1.14	Tornio 2008 [31]
600 mg, b.i.d.	0.25 mg, s.d.	3	-	9	8.07	5.79	1.39	2.54	1.95	1.30	Tornio 2008 [31]
600 mg, b.i.d.	0.25 mg, s.d.	6	-	9	7.58	5.73	1.32	2.47	2.24	1.10	Tornio 2008 [31]
600 mg, b.i.d.	0.25 mg, s.d.	12	-	9	6.91	4.77	1.45	2.40	2.19	1.10	Tornio 2008 [31]
						GMFE	**1.29 (1.10-1.91)**			**1.12 (1.01-1.30)**	
					Pred/obs within 2-fold		**23/23**			**23/23**	

[a], time intervals between (last) perpetrator and victim drug administration; [b], calculated from observed plasma concentration-time profiles; -, not given; AUC, area under the concentration-time curve; b.i.d., twice daily; C_{max}, maximum plasma concentration; DDI, drug-drug interaction; GMFE, geometric mean fold error; obs, observed; pred, predicted, s.d., single dose; SLCO, solute carrier organic anion transporter family member; t_{last}, time of the last concentration measurement.

4.3 Gemfibrozil-pioglitazone DDI

The gemfibrozil-pioglitazone DDI was predicted using the inhibition parameters of gemfibrozil and gemfibrozil 1-O-β-glucuronide as described in Section 4.2.

Details on the 4 modeled clinical studies investigating the gemfibrozil-pioglitazone DDI are given in Table S4.3.1. The population predictions of pioglitazone plasma concentration-time profiles with and without gemfibrozil co-administration, compared to observed data, are shown in Figs. S4.3.1 and S4.3.2. The correlation of predicted and observed DDI AUC ratios and DDI C_{max} ratios is shown in Fig. S4.3.3. Table S4.3.2 lists the corresponding predicted and observed DDI AUC ratios, DDI C_{max} ratios as well as GMFE values.

Table S4.3.1. Clinical study data of the gemfibrozil-pioglitazone DDI.

Perpetrator drug administration	Victim drug administration	Interval [hours] [a]	*n*	Females [%]	Age [years]	Weight [kg]	*CYP2C8* genotype	Data set	References
Gemfibrozil	*Pioglitazone*								
600 mg, b.i.d.	15 mg, s.d.	1	15	73	(35)	(74.5)	**1/*1*	e	Aquilante 2013 [6]
600 mg, b.i.d.	15 mg, s.d.	1	15	67	(37)	(71.0)	**3* [b]	e	Aquilante 2013 [6]
600 mg, b.i.d.	15 mg, s.d.	1	12	25	20-27	55-85	-	e	Jaakkola 2005 [73]
600 mg, b.i.d.	30 mg, s.d.	1	10	0	22-23	54-80	-	e	Deng 2005 [77]

[a], time intervals between (last) perpetrator and victim drug administration; [b], *CYP2C8*1/*3*: n=14, *CYP2C8*3/*3*: n=1; values for age and weight are given as range (mean); -, not given; b.i.d., twice daily; CYP, cytochrome P450; DDI, drug-drug interaction; e, external data set (model evaluation); *n*, number of individuals studied; s.d., single dose.

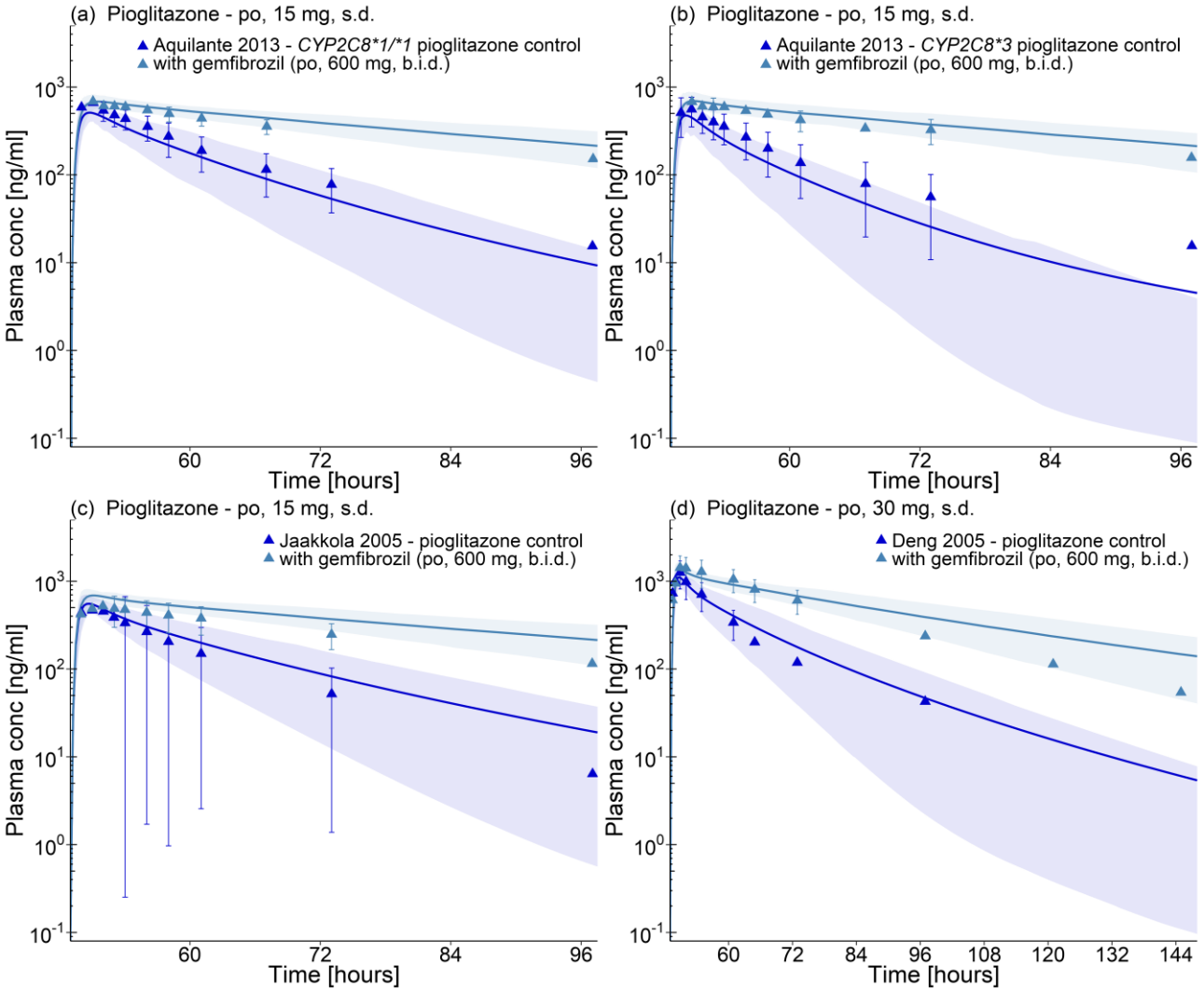

Fig. S4.3.1. Pioglitazone plasma concentration-time profiles during the gemfibrozil-pioglitazone DDI (semilogarithmic). Observed data are shown as triangles ± SD (dark blue: control, light blue: with gemfibrozil). Pioglitazone population simulation arithmetic means are shown as lines (dark blue: control, light blue: with gemfibrozil). The shaded areas represent the 68% population prediction intervals. Detailed information about dosing regimens and study populations is given in Table S4.3.1. DDI AUC ratios and DDI C_{max} ratios are compared in Table S4.3.2.
b.i.d., twice daily; conc, concentration; s.d., single dose.

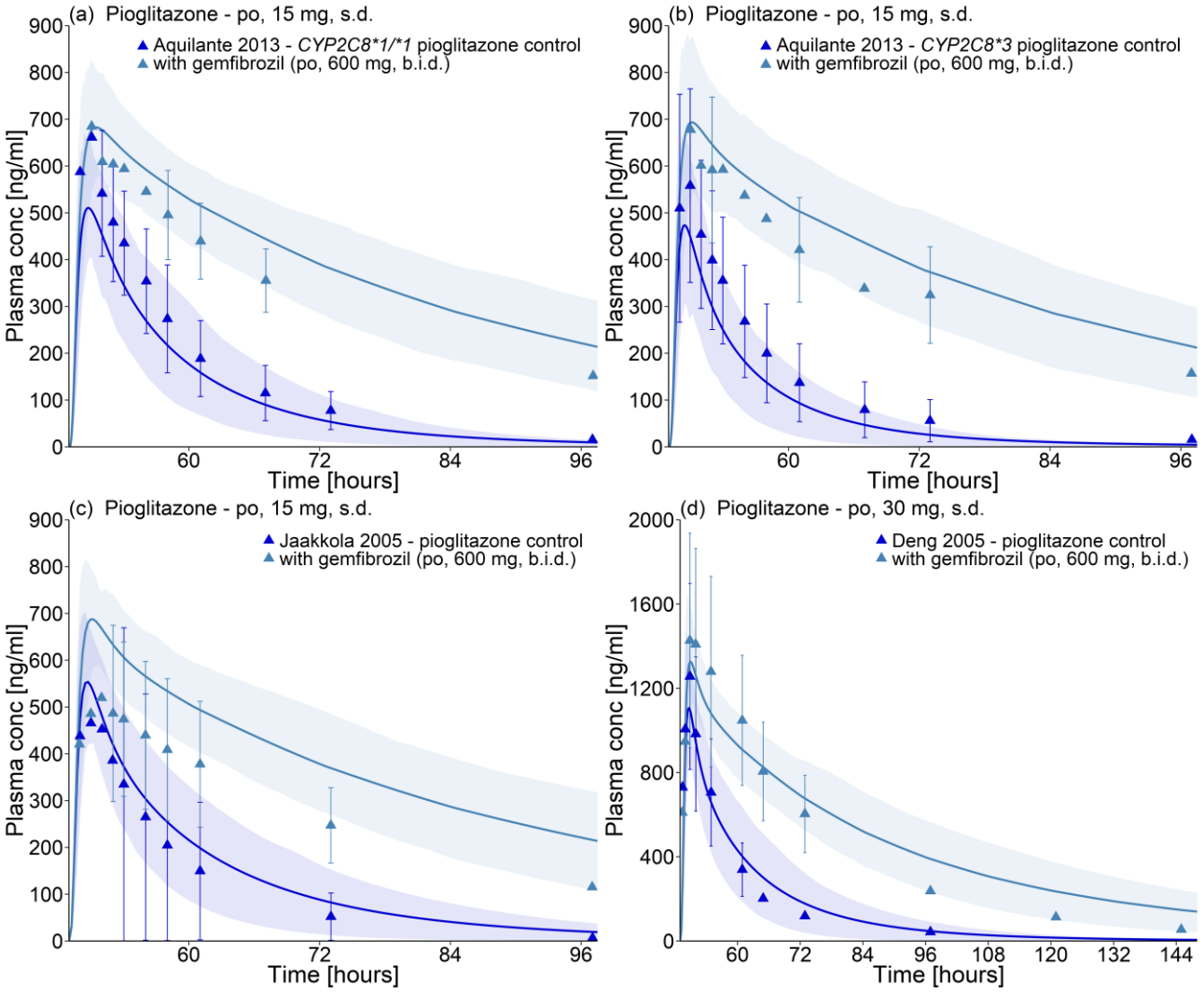

Fig. S4.3.2. Pioglitazone plasma concentration-time profiles during the gemfibrozil-pioglitazone DDI (linear). Observed data are shown as triangles ± SD (dark blue: control, light blue: with gemfibrozil). Pioglitazone population simulation arithmetic means are shown as lines (dark blue: control, light blue: with gemfibrozil). The shaded areas represent the 68% population prediction intervals. Detailed information about dosing regimens and study populations is given in Table S4.3.1. Predicted and observed DDI AUC ratios and DDI C_{max} ratios are compared in Table S4.3.2.
b.i.d., twice daily; conc, concentration; s.d., single dose.

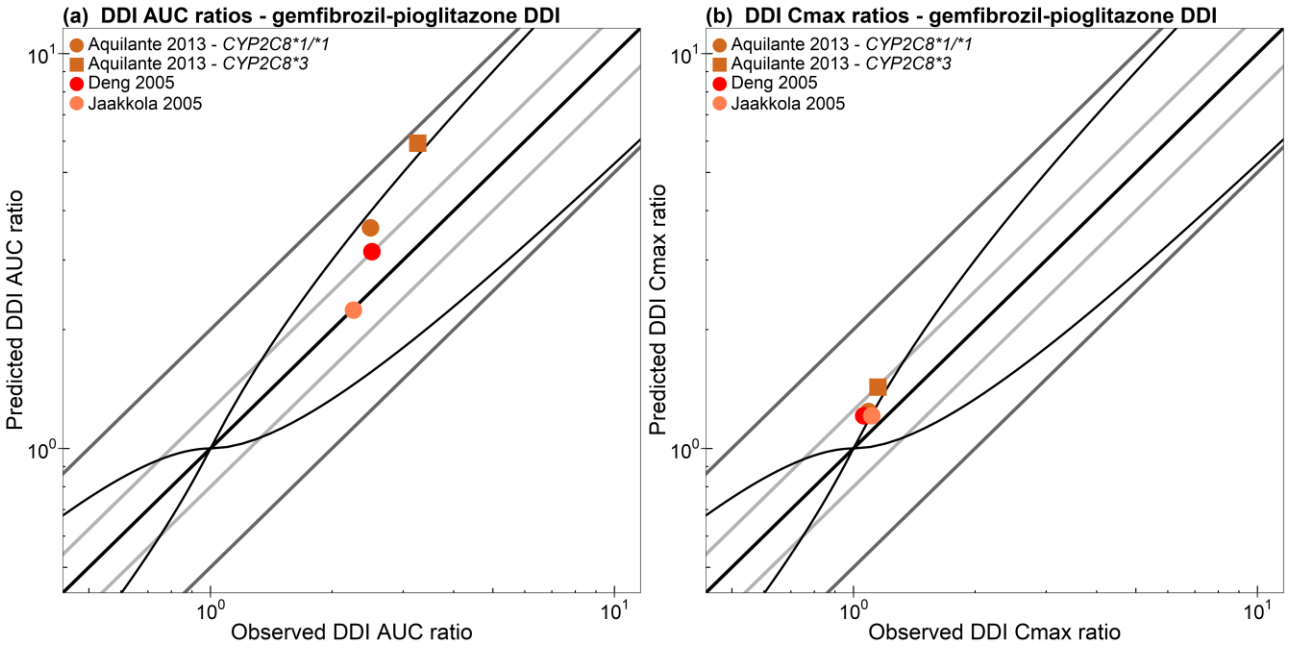

Fig. S4.3.3. Correlation of predicted and observed gemfibrozil-pioglitazone DDI AUC ratios and DDI C_{max} ratios of all studies. The straight black line marks the line of identity. Light grey lines indicate 0.8- to 1.25-fold; dark grey lines indicate 0.5- to 2-fold prediction acceptance limits. The curved black lines show the prediction success limits suggested by Guest *et al.* [143]. Detailed information about dosing regimens and study populations is given in Table S4.3.1. The plotted DDI AUC ratios and DDI C_{max} ratios are listed in Table S4.3.2.

Table S4.3.2. Predicted compared to observed DDI AUC ratios and DDI C_{max} ratios of the gemfibrozil-pioglitazone DDI.

Perpetrator drug administration	Victim drug administration	Interval [hours] [a]	*CYP2C8* genotype	t_{last} [hours]	DDI AUC ratio		Pred/Obs DDI AUC ratio	DDI C_{max} ratio		Pred/Obs DDI C_{max} ratio	References
Gemfibrozil	*Pioglitazone*				*pred*	*obs*		*pred*	*obs*		
600 mg, b.i.d.	15 mg, s.d.	1	**1/*1*	48	3.62	2.49	1.45	1.24	1.09	1.14	Aquilante 2013 [6]
600 mg, b.i.d.	15 mg, s.d.	1	**3* [b]	48	5.93	3.26	1.82	1.43	1.15	1.25	Aquilante 2013 [6]
600 mg, b.i.d.	15 mg, s.d.	1	-	48	3.15	2.51	1.26	1.21	1.06	1.14	Jaakkola 2005 [73]
600 mg, b.i.d.	30 mg, s.d.	1	-	24	2.24	2.26	0.99	1.21	1.11	1.09	Deng 2005 [77]
						GMFE	**1.35 (1.01-1.82)**			**1.16 (1.09-1.25)**	
					Pred/obs within 2-fold		**4/4**			**4/4**	

[a], time intervals between (last) perpetrator and victim drug administration; [b], *CYP2C8*1/*3*: n=14, *CYP2C8*3/*3*: n=1; -, not given; AUC, area under the concentration-time curve; b.i.d., twice daily; C_{max}, maximum plasma concentration; CYP, cytochrome P450; DDI, drug-drug interaction; GMFE, geometric mean fold error; obs, observed; pred, predicted, s.d., single dose; t_{last}, time of the last concentration measurement.

4.4 Itraconazole-repaglinide DDI

The itraconazole-repaglinide DDI was simulated using literature values to model the competitive inhibition of CYP3A4 by itraconazole, hydroxy-itraconazole, keto-itraconazole and N-desalkyl-itraconazole [92], as described previously [12]. The inhibition of OATP1B1 and OATP1B3 following itraconazole administration is most likely caused by hydroxy-itraconazole [94]. Therefore, K_i values for the inhibition of OATP1B1 and OATP1B3 by hydroxy-itraconazole were optimized (OATP1B1 K_i = 18 nmol/l and OATP1B3 K_i = 11 nmol/l) to describe the repaglinide plasma concentration-time profiles during itraconazole co-administration. Itraconazole was modeled using formulation properties (capsule fasted assumed) described previously [12] together with the optimized solubility value of 14.5 mg/l at pH 6.5, as specified in Section 3.6.

Details on the modeled clinical study investigating the itraconazole-repaglinide DDI are given in Table S4.4.1. The population predictions of repaglinide plasma concentration-time profiles with and without itraconazole co-administration, compared to observed data, are shown in Fig. S4.4.1. The correlation of predicted and observed DDI AUC ratios and DDI C_{max} ratios is shown in Fig. S4.4.2. Table S4.4.2 lists the corresponding predicted and observed DDI AUC ratios, DDI C_{max} ratios as well as GMFE values.

Table S4.4.1. Clinical study data of the itraconazole-repaglinide DDI.

Perpetrator drug administration	Victim drug administration	Interval [hours] [a]	*n*	Females [%]	Age [years]	Weight [kg]	Data set	References
Itraconazole	*Repaglinide*							
100 mg [b], b.i.d.	0.25 mg, s.d.	1	12	67	20-24	46-84	i	Niemi 2003a [52]

[a], time intervals between (last) perpetrator and victim drug administration; [b], first itraconazole dose 200 mg; values for age and weight are given as range; b.i.d., twice daily; DDI, drug-drug interaction; i, internal data set (model building); *n*, number of individuals studied; s.d., single dose.

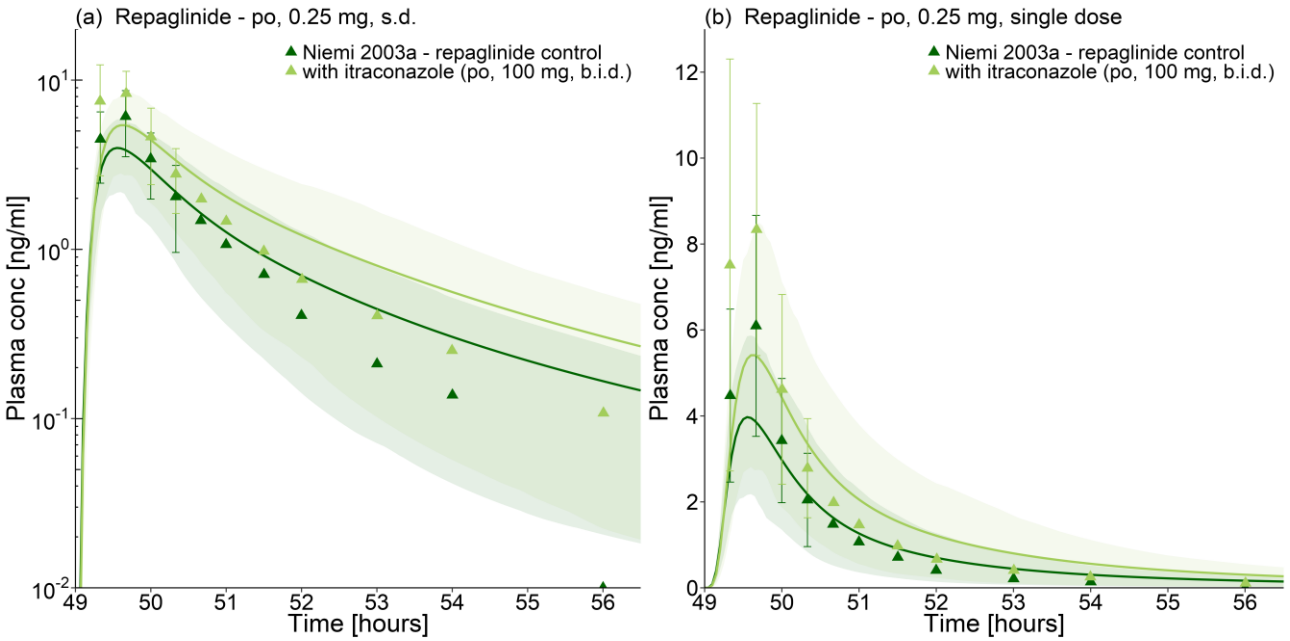

Fig. S4.4.1. Repaglinide plasma concentration-time profiles during the itraconazole-repaglinide DDI (semilogarithmic and linear). Observed data are shown as triangles ± SD (dark green: control, light green: with itraconazole). Repaglinide population simulation arithmetic means are shown as lines (dark green: control, light green: with itraconazole). The shaded areas represent the 68% population prediction intervals. Detailed information about dosing regimens and study population is given in Table S4.4.1. Predicted and observed DDI AUC ratios and DDI C_{max} ratios are compared in Table S4.4.2.

b.i.d., twice daily; conc, concentration; s.d., single dose.

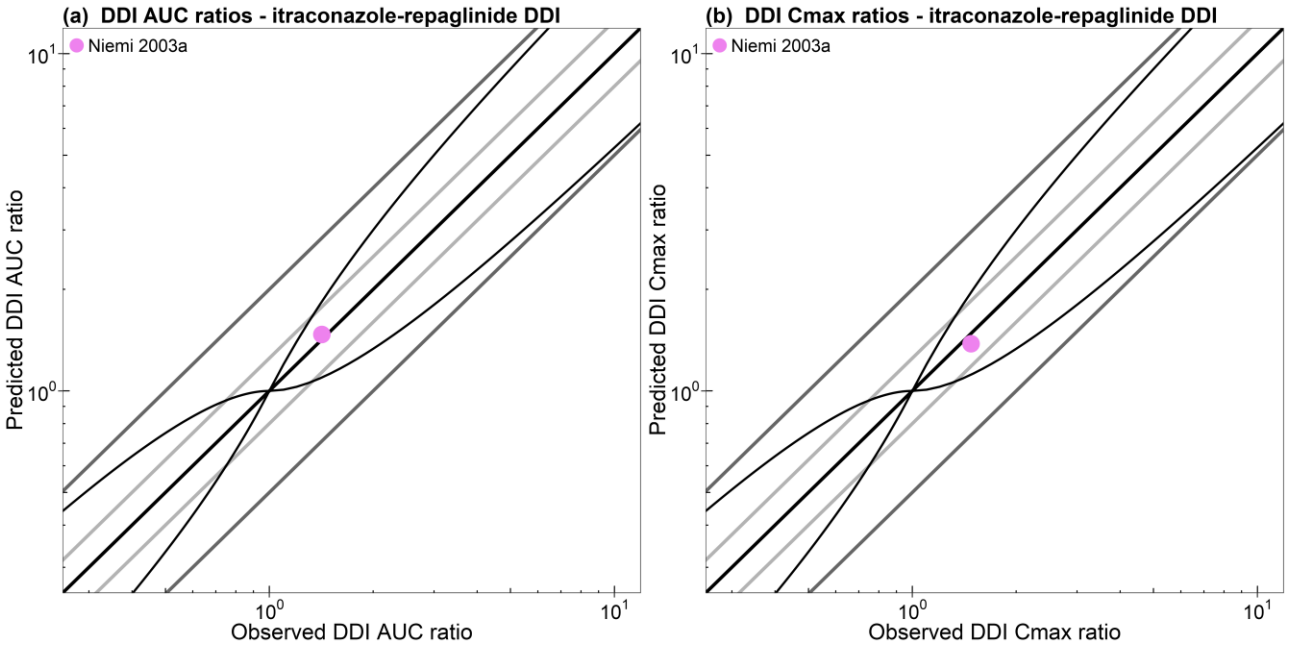

Fig. S4.4.2. Correlation of predicted and observed itraconazole-repaglinide DDI AUC ratios and DDI C_{max} ratios. The straight black line marks the line of identity. Light grey lines indicate 0.8- to 1.25-fold; dark grey lines indicate 0.5- to 2-fold prediction acceptance limits. The curved black lines show the prediction success limits suggested by Guest *et al.* [143]. Detailed information about dosing regimens and study population is given in Table S4.4.1. The plotted DDI AUC ratios and DDI C_{max} ratios are listed in Table S4.4.2.

Table S4.4.2. Predicted compared to observed DDI AUC ratios and DDI C_{max} ratios of the itraconazole-repaglinide DDI.

Perpetrator drug administration	Victim drug administration	Interval [hours] [a]	t_{last} [hours]	DDI AUCratio		Pred/Obs DDI AUC ratio	DDI C_{max} ratio		Pred/Obs DDI C_{max} ratio	References
Itraconazole	*Repaglinide*			*pred*	*obs*		*pred*	*obs*		
100 mg [b], b.i.d.	0.25 mg, s.d.	1	7	1.47	1.42	1.03	1.38	1.48	0.94	Niemi 2003a [52]
					GMFE	**1.03**			**1.07**	
					Pred/obs within 2-fold	**1/1**			**1/1**	

[a], time intervals between (last) perpetrator and victim drug administration; [b], first itraconazole dose 200 mg; AUC, area under the concentration-time curve; b.i.d., twice daily; C_{max}, maximum plasma concentration; DDI, drug-drug interaction; GMFE, geometric mean fold error; obs, observed; pred, predicted, s.d., single dose; t_{last}, time of the last concentration measurement.

4.5 Itraconazole-pioglitazone DDI

The itraconazole-pioglitazone DDI was modeled using the inhibition and solubility parameters of itraconazole as described in Section 4.4.

Details on the modeled clinical study investigating the itraconazole-pioglitazone DDI are given in Table S4.5.1. The population predictions of pioglitazone plasma concentration-time profiles with and without itraconazole co-administration, compared to observed data, are shown in Fig. S4.5.1. The correlation of predicted and observed DDI AUC ratios and DDI C_{max} ratios is shown in Fig. S4.5.2. Table S4.5.2 lists the corresponding predicted and observed DDI AUC ratios, DDI C_{max} ratios as well as GMFE values.

Table S4.5.1. Clinical study data of the itraconazole-pioglitazone DDI.

Perpetrator drug administration	Victim drug administration	Interval [hours] [a]	*n*	Females [%]	Age [years]	Weight [kg]	Data set	References
Itraconazole	*Pioglitazone*							
100 mg [b], b.i.d.	15 mg, s.d.	1	12	25	20-27	55-85	e	Jaakkola 2005 [73]

[a], time intervals between (last) perpetrator and victim drug administration; [b], first itraconazole dose 200 mg; values for age and weight are given as range; b.i.d., twice daily; DDI, drug-drug interaction; e, external data set (model evaluation); *n*, number of individuals studied; s.d., single dose.

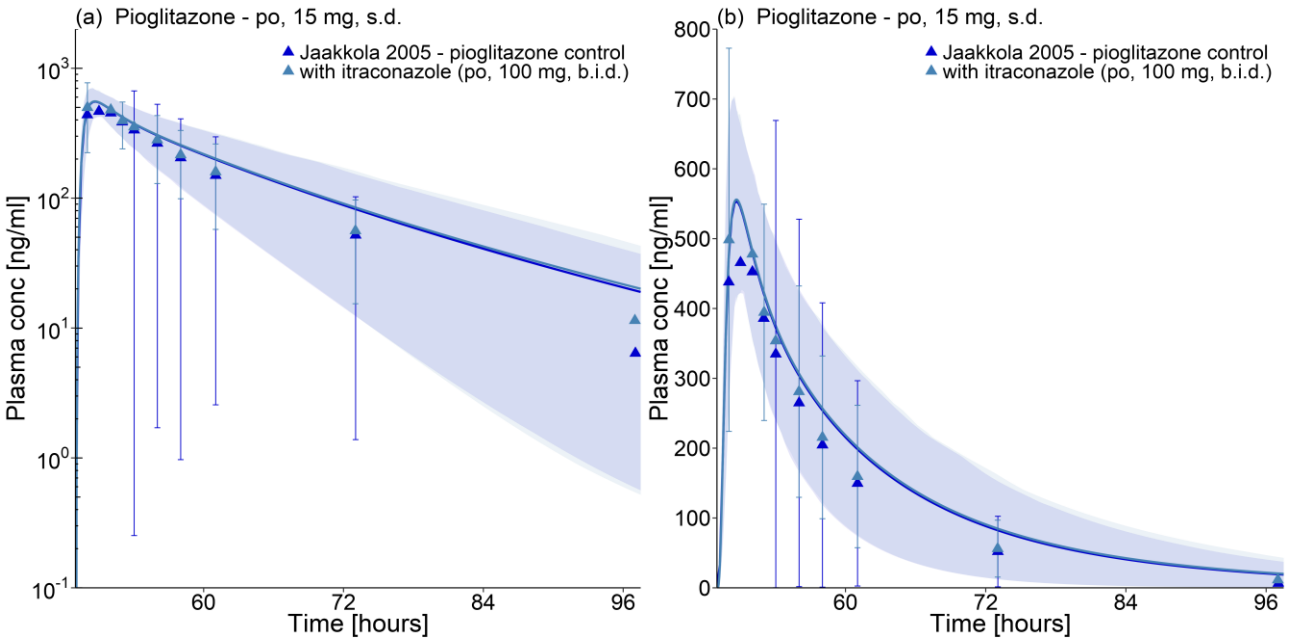

Fig. S4.5.1. Pioglitazone plasma concentration-time profiles during the itraconazole-pioglitazone DDI (semilogarithmic and linear). Observed data are shown as triangles ± SD (dark blue: control, light blue: with itraconazole). Pioglitazone population simulation arithmetic means are shown as lines (dark blue: control, light blue: with itraconazole). The shaded areas represent the 68% population prediction intervals. Detailed information about dosing regimens and study population is given in Table S4.5.1. Predicted and observed DDI AUC ratios and DDI C_{max} ratios are compared in Table S4.5.2.

b.i.d., twice daily; conc, concentration; s.d., single dose.

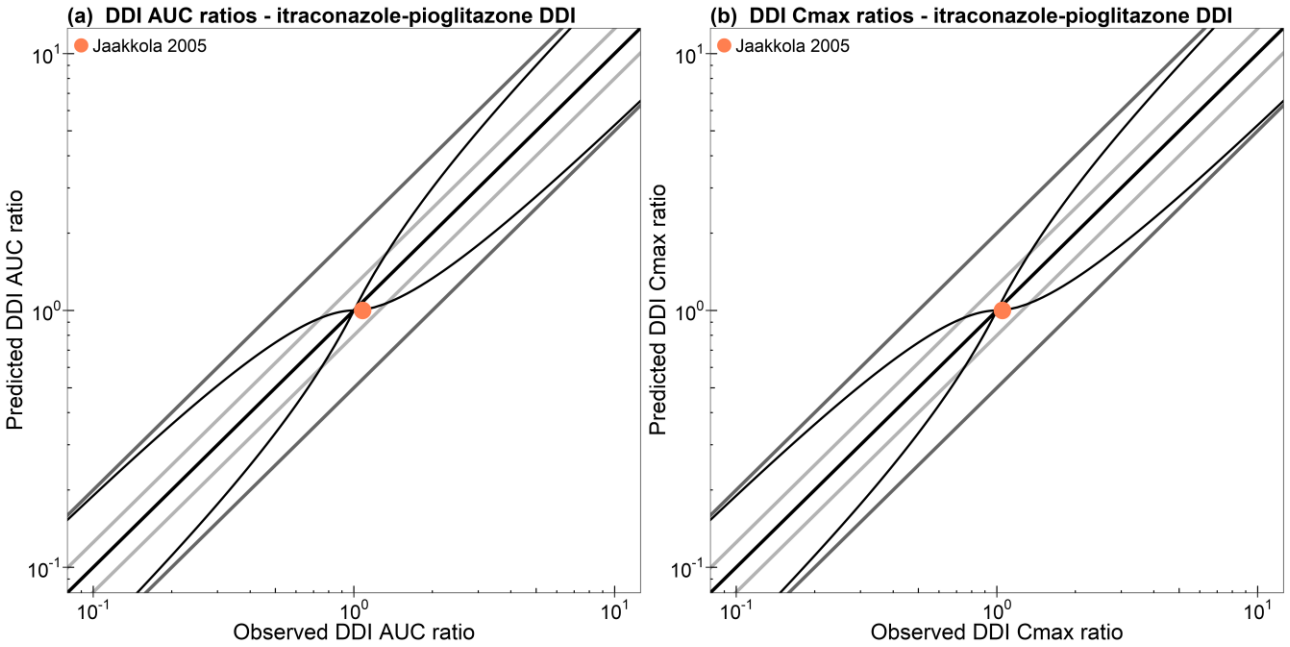

Fig. S4.5.2. Correlation of predicted and observed itraconazole-pioglitazone DDI AUC ratios and DDI C_{max} ratios. The straight black line marks the line of identity. Light grey lines indicate 0.8- to 1.25-fold; dark grey lines indicate 0.5- to 2-fold prediction acceptance limits. The curved black lines show the prediction success limits suggested by Guest *et al.* [143]. Detailed information about dosing regimens and study population is given in Table S4.5.1. The plotted DDI AUC ratios and DDI C_{max} ratios are listed in Table S4.5.2.

Table S4.5.2. Predicted compared to observed DDI AUC ratios and DDI C_{max} ratios of the itraconazole-pioglitazone DDI.

Perpetrator drug administration	Victim drug administration	Interval [hours] [a]	t_{last} [hours]	DDI AUC ratio		Pred/Obs DDI AUC ratio	DDI C_{max} ratio		Pred/Obs DDI C_{max} ratio	References
Itraconazole	*Pioglitazone*			*pred*	*obs*		*pred*	*obs*		
100 mg [b], b.i.d.	15 mg, s.d.	1	48	1.00	1.08	0.92	1.00	1.05	0.95	Jaakkola 2005 [73]
					GMFE	**1.08**			**1.05**	
					Pred/obs within 2-fold	**1/1**			**1/1**	

[a], time intervals between (last) perpetrator and victim drug administration; [b], first itraconazole dose 200 mg; AUC, area under the concentration-time curve; b.i.d., twice daily; C_{max}, maximum plasma concentration; DDI, drug-drug interaction; GMFE, geometric mean fold error; obs, observed; pred, predicted; s.d., single dose; t_{last}, time of the last concentration measurement.

4.6 Gemfibrozil-itraconazole-repaglinide DDI

The gemfibrozil-itraconazole-repaglinide DDI was predicted using inhibition parameters of gemfibrozil, gemfibrozil 1-O-β-glucuronide and itraconazole as described in Sections 4.2 and 4.4. Itraconazole was modeled using formulation properties (capsule fasted assumed) described previously [12] together with the optimized solubility value in the presence of gemfibrozil (0.69 mg/l at pH 6.5), as specified in Section 3.6.

Details on the modeled clinical study investigating the gemfibrozil-itraconazole-repaglinide DDI are given in Table S4.6.1. The population predictions of repaglinide plasma concentration-time profiles with and without gemfibrozil plus itraconazole co-administration, compared to observed data, are shown in Fig. S4.6.1. The correlation of predicted and observed DDI AUC ratios and DDI C_{max} ratios is shown in Fig. S4.6.2. Table S4.6.2 lists the corresponding predicted and observed DDI AUC ratios, DDI C_{max} ratios as well as GMFE values.

Table S4.6.1. Clinical study data of the gemfibrozil-itracaonazole-repaglinide DDI.

Perpetrator drug administration	Victim drug administration	Interval [hours] [a]	*n*	Females [%]	Age [years]	Weight [kg]	Data set	References
Gemfibrozil + Itraconazole	*Repaglinide*							
G: 600 mg, b.i.d.+	0.25 mg, s.d.	1	12	67	20-24	46-84	e	Niemi 2003a [52]
I: 100 mg [b], b.i.d.								

[a], time intervals between (last) perpetrator and victim drug administration; [b], first itraconazole dose 200 mg; values for age and weight are given as range; b.i.d., twice daily; DDI, drug-drug interaction; e, external data set (model evaluation); *n*, number of individuals studied; s.d., single dose.

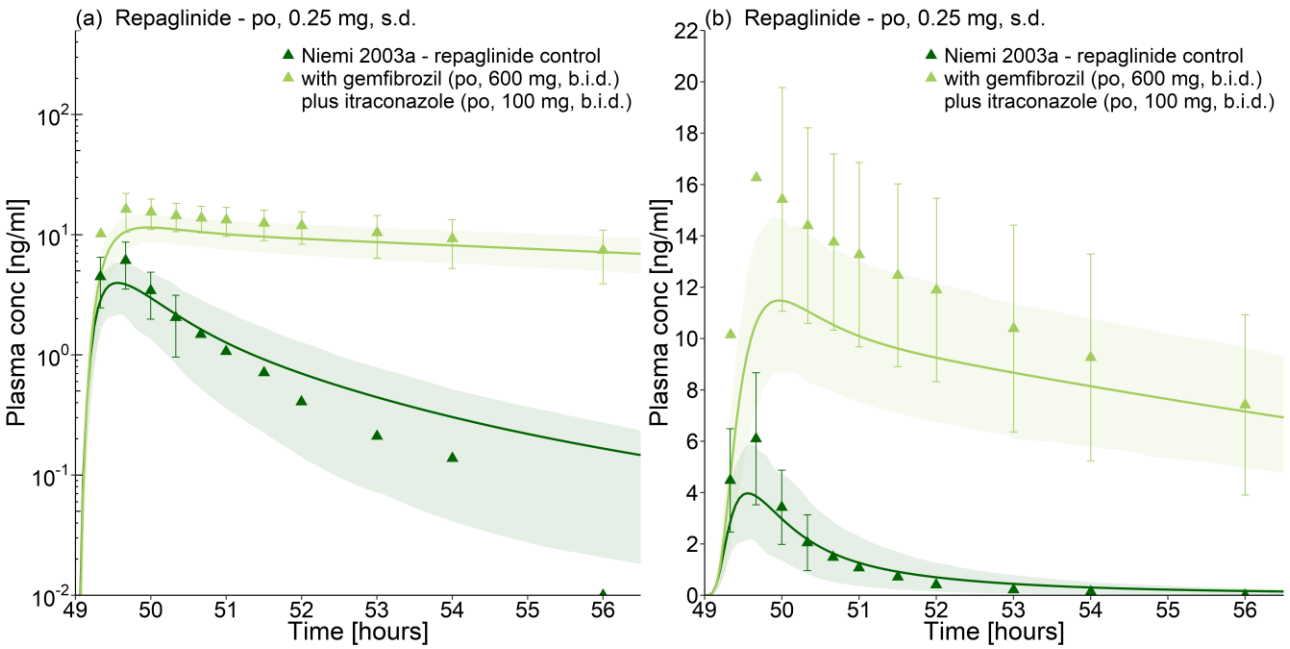

Fig. S4.6.1. Repaglinide plasma concentration-time profiles during the gemfibrozil-itraconazole-repaglinide DDI (semilogarithmic and linear). Observed data are shown as triangles ± SD (dark green: control, light green: with gemfibrozil plus itraconazole). Repaglinide population simulation arithmetic means are shown as lines (dark green: control, light green: with gemfibrozil plus itraconazole). The shaded areas represent the 68% population prediction intervals. Detailed information about dosing regimens and study population is given in Table S4.6.1. Predicted and observed DDI AUC ratios and DDI C_{max} ratios are compared in Table S4.6.2.

b.i.d., twice daily; conc, concentration; s.d., single dose.

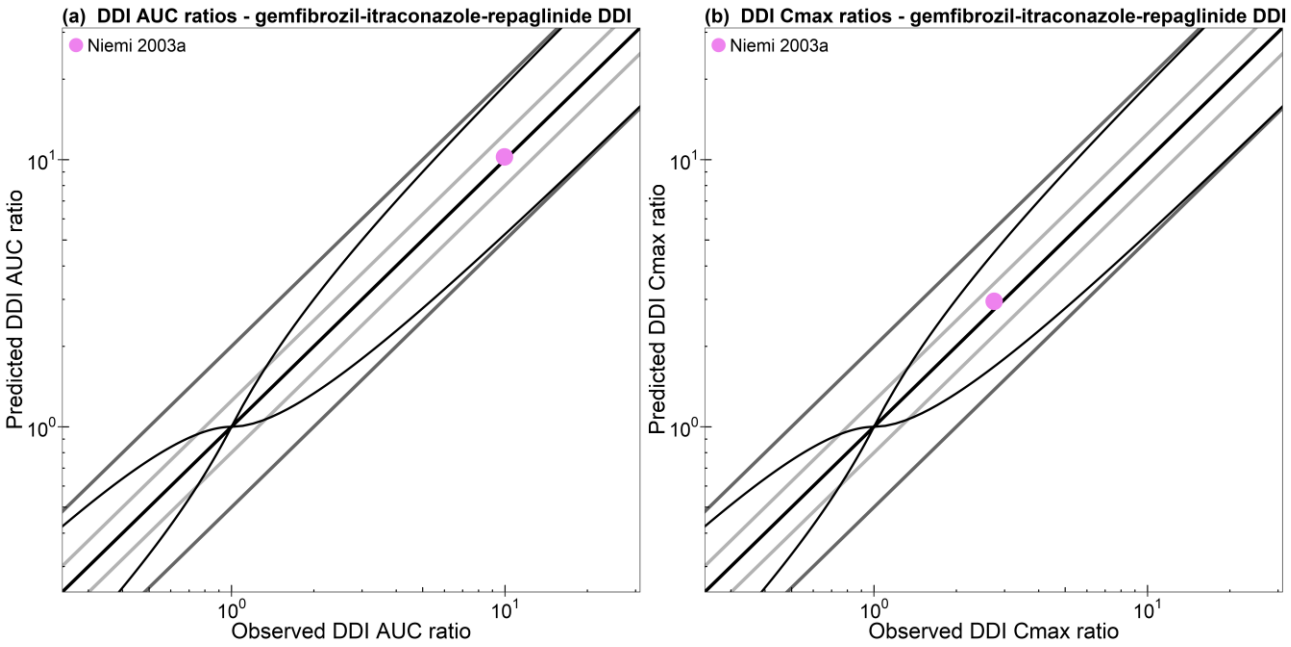

Fig. S4.6.2. Correlation of predicted and observed gemfibrozil-itraconazole-repaglinide DDI AUC ratios and DDI C_{max} ratios. The straight black line marks the line of identity. Light grey lines indicate 0.8- to 1.25-fold; dark grey lines indicate 0.5- to 2-fold prediction acceptance limits. The curved black lines show the prediction success limits suggested by Guest *et al.* [143]. Detailed information about dosing regimens and study population is given in Table S4.6.1. The plotted DDI AUC ratios and DDI C_{max} ratios are listed in Table S4.6.2.

Table S4.6.2. Predicted compared to observed DDI AUC ratios and DDI C_{max} ratios of the gemfibrozil-itraconazole-repaglinide DDI.

Perpetrator drug administration	Victim drug administration	Interval [hours] [a]	t_{last} [hours]	DDI AUCratio		Pred/Obs DDI AUC ratio	DDI C_{max} ratio		Pred/Obs DDI C_{max} ratio	References
Gemfibrozil + Itraconazole	*Repaglinide*			*pred*	*obs*		*pred*	*obs*		
G: 600 mg, b.i.d.+	0.25 mg, s.d.	1	7	10.24	9.95	1.03	2.95	2.75	1.07	Niemi 2003a [52]
I: 100 mg [b], b.i.d.										
					GMFE	**1.03**			**1.07**	
					Pred/obs within 2-fold	**1/1**			**1/1**	

[a], time intervals between (last) perpetrator and victim drug administration; [b], first itraconazole dose 200 mg; AUC, area under the concentration-time curve; b.i.d., twice daily; C_{max}, maximum plasma concentration; DDI, drug-drug interaction; GMFE, geometric mean fold error; obs, observed; pred, predicted, s.d., single dose; t_{last}, time of the last concentration measurement.

4.7 Gemfibrozil-itraconazole-pioglitazone DDI

The gemfibrozil-itraconazole-pioglitazone DDI was modeled using the inhibition parameters of gemfibrozil, gemfibrozil 1-O-β-glucuronide and itraconazole as described in Sections 4.2 and 4.4.

The gemfibrozil-itraconazole-pioglitazone interaction study was utilized to optimize the itraconazole solubility values in the absence (14.5 mg/l at pH 6.5) and presence of gemfibrozil (0.69 mg/l at pH 6.5), as in this study, itraconazole concentration-time profiles before and during gemfibrozil co-administration are reported, in addition to the DDI victim drug concentrations [73]. The gemfibrozil-itraconazole-pioglitazone DDI was modeled using the optimized solubility value in the presence of gemfibrozil (0.69 mg/l at pH 6.5), as specified in Section 3.6.

Furthermore, to describe the plasma concentrations of pioglitazone during gemfibrozil plus itraconazole co-administration, a second physicochemical interaction impacting pioglitazone solubility was assumed. Gemfibrozil-pioglitazone co-administration leads to observed DDI ratios of 2.51 for AUC and of 1.06 for C_{max} [73]. Itraconazole-pioglitazone co-administration leads to observed DDI ratios of 1.08 for AUC and of 1.05 for C_{max} [73] (no interaction assumed). The co-administration of both perpetrator drugs together with pioglitazone leads to observed DDI ratios of 2.15 for AUC and of 0.75 for C_{max} [73], which is much less than during the gemfibrozil-pioglitazone DDI. Like itraconazole, pioglitazone is poorly soluble with a reported solubility of 16.8 mg/l at pH 6.5 [82]. To describe the pioglitazone plasma concentrations during the gemfibrozil-itraconazole-pioglitazone DDI, pioglitazone solubility was optimized to 1.59 mg/l at pH 6.5.

Details on the modeled clinical study investigating the gemfibrozil-itraconazole-pioglitazone DDI are given in Table S4.7.1. The population predictions of pioglitazone plasma concentration-time profiles with and without gemfibrozil plus itraconazole co-administration, compared to observed data, are shown in Fig. S4.7.1. The correlation of predicted and observed DDI AUC ratios and DDI C_{max} ratios is shown in Fig. S4.7.2. Table S4.7.2 lists the corresponding predicted and observed DDI AUC ratios, DDI C_{max} ratios as well as GMFE values.

Table S4.7.1. Clinical study data of the gemfibrozil-itraconazole-pioglitazone DDI.

Perpetrator drug administration	Victim drug administration	Interval [hours] [a]	*n*	Females [%]	Age [years]	Weight [kg]	Data set	References
Gemfibrozil + Itraconazole	*Pioglitazone*							
G: 600 mg, b.i.d. + I: 100 mg [b], b.i.d.	15 mg, s.d.	1	12	25	20-27	55-85	e	Jaakkola 2005 [73]

[a], time intervals between (last) perpetrator and victim drug administration; [b], first itraconazole dose 200 mg; values for age and weight are given as range; b.i.d., twice daily; DDI, drug-drug interaction; e, external data set (model evaluation); *n*, number of individuals studied; s.d., single dose.

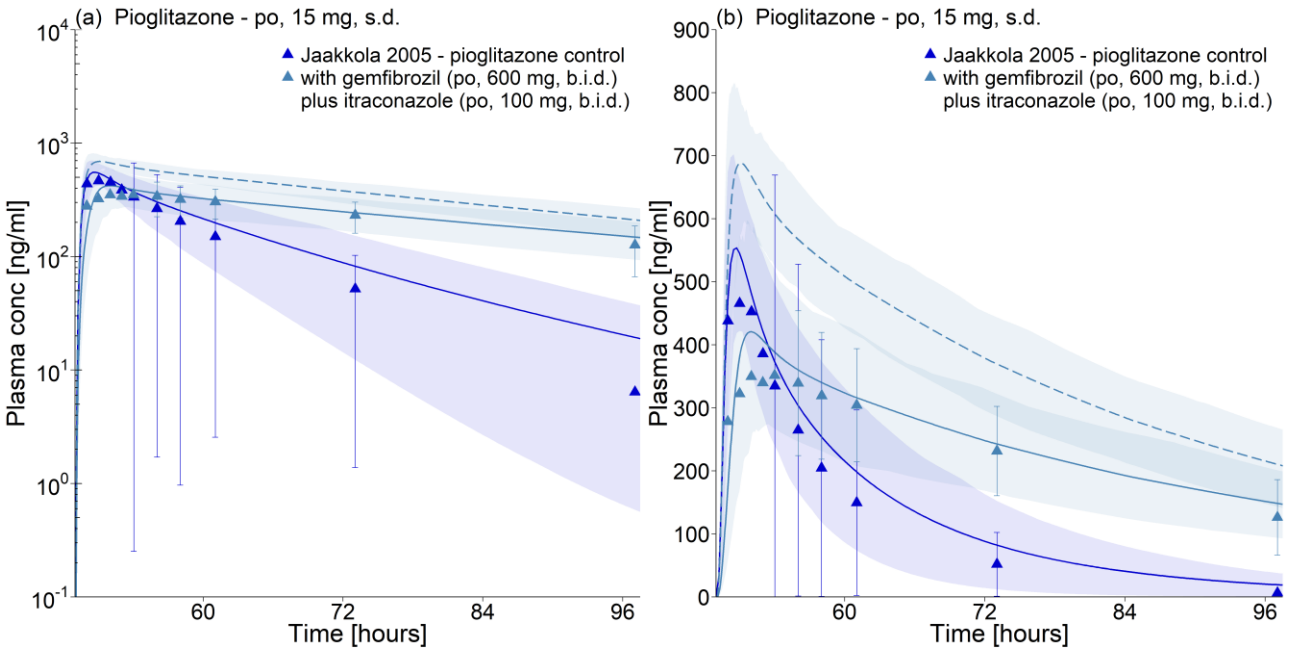

Fig. S4.7.1. Pioglitazone plasma concentration-time profiles during the gemfibrozil-itraconazole-pioglitazone DDI (semilogarithmic and linear). Observed data are shown as triangles ± SD (dark blue: control, light blue: with gemfibrozil plus itraconazole). Pioglitazone population simulation arithmetic means are shown as solid lines (dark blue: control, light blue: with gemfibrozil plus itraconazole), dashed lines illustrate the prediction of the gemfibrozil-itraconazole-pioglitazone DDI without pioglitazone solubility adjustment. The shaded areas represent the 68% population prediction intervals. Detailed information about dosing regimens and study population is given in Table S4.7.1. Predicted and observed DDI AUC ratios and DDI C_{max} ratios are compared in Table S4.7.2.

b.i.d., twice daily; conc, concentration; s.d., single dose.

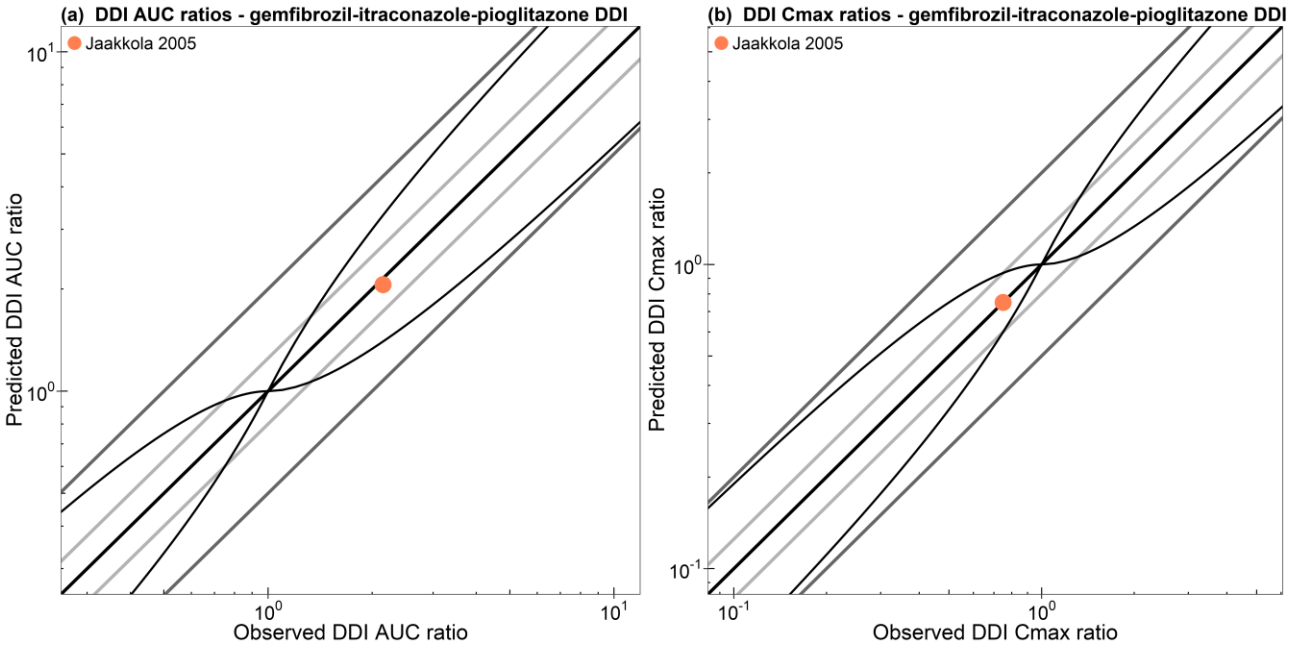

Fig. S4.7.2. Correlation of predicted and observed gemfibrozil-itraconazole-pioglitazone DDI AUC ratios and DDI C_{max} ratios. The straight black line marks the line of identity. Light grey lines indicate 0.8- to 1.25-fold; dark grey lines indicate 0.5- to 2-fold prediction acceptance limits. The curved black lines show the prediction success limits suggested by Guest *et al.* [143]. Detailed information about dosing regimens and study population is given in Table S4.7.1. The plotted DDI AUC ratios and DDI C_{max} ratios are listed in Table S4.7.2.

Table S4.7.2. Predicted compared to observed DDI AUC ratios and DDI C_{max} ratios of the gemfibrozil-itraconazole-pioglitazone DDI.

Perpetrator drug administration	Victim drug administration	Interval [hours] [a]	t_{last} [hours]	DDI AUC ratio		Pred/Obs DDI AUC ratio	DDI C_{max} ratio		Pred/Obs DDI C_{max} ratio	References
Gemfibrozil + Itraconazole	*Pioglitazone*			*pred*	*obs*		*pred*	*obs*		
G: 600 mg, b.i.d. + I: 100 mg [b], b.i.d.	15 mg, s.d.	1	48	2.06	2.15	0.96	0.75	0.75	0.99	Jaakkola 2005 [73]
					GMFE	**1.05**			**1.01**	
					Pred/obs within 2-fold	**1/1**			**1/1**	

[a], time intervals between (last) perpetrator and victim drug administration; [b], first itraconazole dose 200 mg; AUC, area under the concentration-time curve; b.i.d., twice daily; C_{max}, maximum plasma concentration; DDI, drug-drug interaction; GMFE, geometric mean fold error; obs, observed; pred, predicted; s.d., single dose; t_{last}, time of the last concentration measurement.

4.8 Rifampicin-repaglinide DDI

The rifampicin-repaglinide DDI was predicted using interaction parameters for the induction of CYP3A4 and OATP1B1 and for the competitive inhibition of CYP3A4, that have been established during the rifampicin model development [12]. To model the induction of CYP2C8 by rifampicin, the same mechanism of transcriptional activation via PXR [144] and therefore, the same EC_{50} value was assumed as for the rifampicin CYP3A4 induction (EC_{50} = 0.34 µmol/l) [105,106]; E_{max} = 3.2 was taken from literature, measured in human hepatocytes [112]. The competitive inhibition of CYP2C8 by rifampicin was modeled with K_i = 30.2 µmol/l, determined with human liver microsomes [16]. According to [141], the fu_{inc} of rifampicin in this microsomal assay is assumed to be very close to 1.0. To describe the competitive inhibition of OATP1B1 by rifampicin, K_i = 0.477 µmol/l was applied, measured with OATP1B1-expressing HEK-293 cells [17]. For lack of information on binding of rifampicin in this assay, fu_{inc} was assumed to be 1.0. To model the induction of OATP1B3 by rifampicin, the same EC_{50} = 0.34 µmol/l and E_{max} = 0.38 were applied as for the induction of OATP1B1 [12]. The competitive inhibition of OATP1B3 by rifampicin was described with K_i = 0.90 µmol/l, determined in OATP1B3-transfected CHO cells [113]. As no information on binding of rifampicin in this uptake assay was available, fu_{inc} was assumed to be 1.0. Details on the modeled clinical study investigating the rifampicin-repaglinide DDI are given in Table S4.8.1. The population predictions of repaglinide plasma concentration-time profiles with and without rifampicin co-administration, compared to observed data, are shown in Fig. S4.8.1. The correlation of predicted and observed DDI AUC ratios and DDI C_{max} ratios is shown in Fig. S4.8.2. Table S4.8.2 lists the corresponding predicted and observed DDI AUC ratios, DDI C_{max} ratios as well as GMFE values.

Table S4.8.1. Clinical study data of the rifampicin-repaglinide DDI.

Perpetrator drug administration	Victim drug administration	Interval [hours] [a]	*n*	Females [%]	Age [years]	Weight [kg]	Data set	References
Rifampicin	*Repaglinide*							
600 mg, q.d.	0.25 mg, s.d.	12.5	9	56	19-25	48-80	e	Niemi 2000 [55]

[a], time intervals between (last) perpetrator and victim drug administration; values for age and weight are given as range; DDI, drug-drug interaction; e, external data set (model evaluation); *n*, number of individuals studied; q.d., once daily; s.d., single dose.

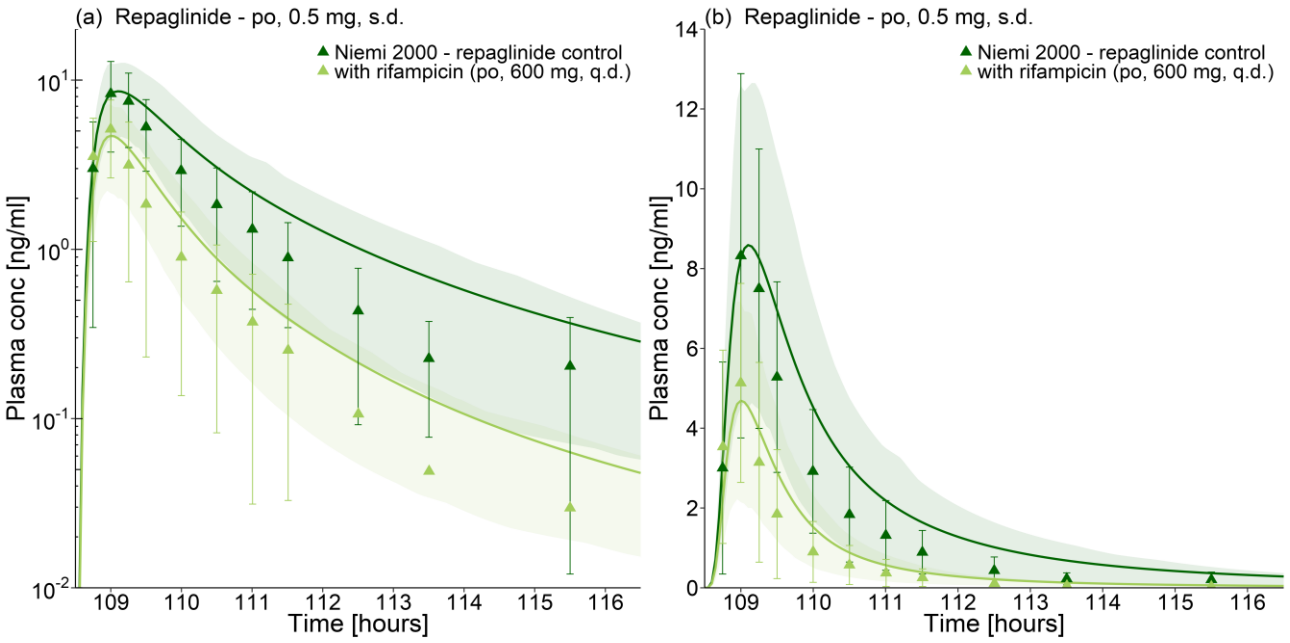

Fig. S4.8.1. Repaglinide plasma concentration-time profiles during the rifampicin-repaglinide DDI (semilogarithmic and linear). Observed data are shown as triangles ± SD (dark green: control, light green: with rifampicin). Repaglinide population simulation arithmetic means are shown as lines (dark green: control, light green: with rifampicin). The shaded areas represent the 68% population prediction intervals. Detailed information about dosing regimens and study population is given in Table S4.8.1. Predicted and observed DDI AUC ratios and DDI C_{max} ratios are compared in Table S4.8.2.

conc, concentration; q.d. once daily; s.d., single dose.

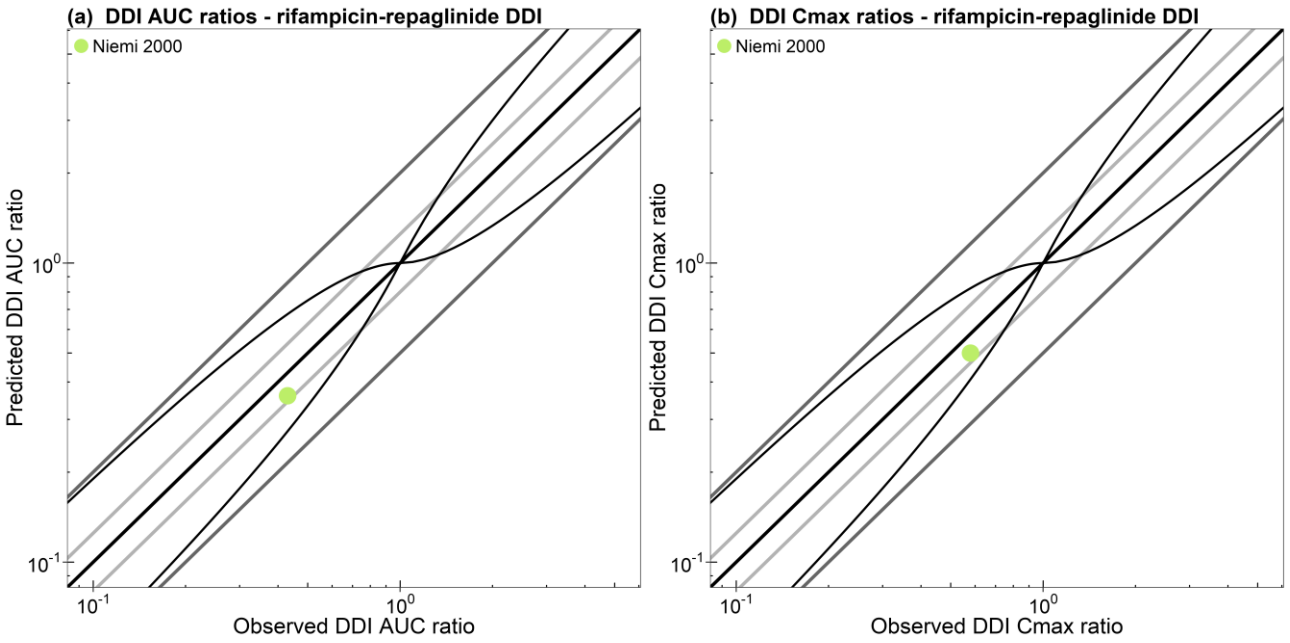

Fig. S4.8.2. Correlation of predicted and observed rifampicin-repaglinide DDI AUC ratios and DDI C_{max} ratios. The straight black line marks the line of identity. Light grey lines indicate 0.8- to 1.25-fold; dark grey lines indicate 0.5- to 2-fold prediction acceptance limits. The curved black lines show the prediction success limits suggested by Guest *et al.* [143]. Detailed information about dosing regimens and study population is given in Table S4.8.1. The plotted DDI AUC ratios and DDI C_{max} ratios are listed in Table S4.8.2.

Table S4.8.2. Predicted compared to observed DDI AUC ratios and DDI C_{max} ratios of the rifampicin-repaglinide DDI.

Perpetrator drug administration	Victim drug administration	Interval [hours] [a]	t_{last} [hours]	DDI AUCratio		Pred/Obs DDI AUC ratio	DDI C_{max} ratio		Pred/Obs DDI C_{max} ratio	References
Rifampicin	*Repaglinide*			*pred*	*obs*		*pred*	*obs*		
600 mg, q.d.	0.25 mg, s.d.	12.5	7	0.36	0.43	0.83	0.50	0.58	0.85	Niemi 2000 [55]
					GMFE	**1.20**			**1.17**	
					Pred/obs within 2-fold	**1/1**			**1/1**	

[a], time intervals between (last) perpetrator and victim drug administration; AUC, area under the concentration-time curve; C_{max}, maximum plasma concentration; DDI, drug-drug interaction; GMFE, geometric mean fold error; obs, observed; pred, predicted, q.d., once daily; s.d., single dose; t_{last}, time of the last concentration measurement.

4.9 Rifampicin-pioglitazone DDI

The rifampicin-pioglitazone DDI was predicted using the interaction parameters of rifampicin as described in Section 4.8.

Details on the modeled clinical study investigating the rifampicin-pioglitazone DDI are given in Table S4.9.1. The population predictions of pioglitazone plasma concentration-time profiles with and without rifampicin co-administration, compared to observed data, are shown in Fig. S4.9.1. The correlation of predicted and observed DDI AUC ratios and DDI C_{max} ratios is shown in Fig. S4.9.2. Table S4.9.2 lists the corresponding predicted and observed DDI AUC ratios, DDI C_{max} ratios as well as GMFE values.

Table S4.9.1. Clinical study data of the rifampicin-pioglitazone DDI.

Perpetrator drug administration	Victim drug administration	Interval [hours] [a]	*n*	Females [%]	Age [years]	Weight [kg]	Data set	References
Rifampicin	*Pioglitazone*							
600 mg, q.d.	30 mg, s.d.	13	10	30	21-24	57-79	e	Jaakkola 2006a [78]

[a], time intervals between (last) perpetrator and victim drug administration; values age and weight given as range; DDI, drug-drug interaction; e, external data set (model evaluation); *n*, number of individuals studied; q.d., once daily; s.d., single dose.

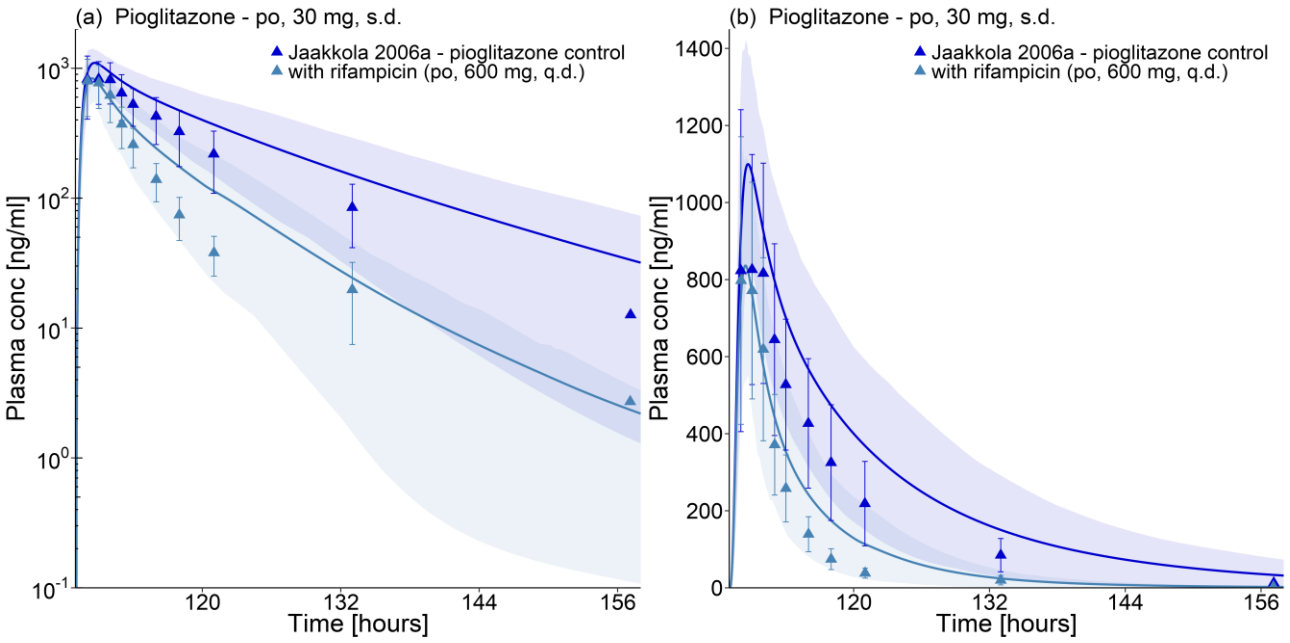

Fig. S4.9.1 Pioglitazone plasma concentration-time profiles during the rifampicin-pioglitazone DDI (semilogarithmic and linear). Observed data are shown as triangles ± SD (dark blue: control, light blue: with rifampicin). Pioglitazone population simulation arithmetic means are shown as lines (dark blue: control, light blue: with rifampicin). The shaded areas represent the 68% population prediction intervals. Detailed information about dosing regimens and study population is given in Table S4.9.1. Predicted and observed DDI AUC ratios and DDI C_{max} ratios are compared in Table S4.9.2.
conc, concentration; q.d., once daily; s.d., single dose.

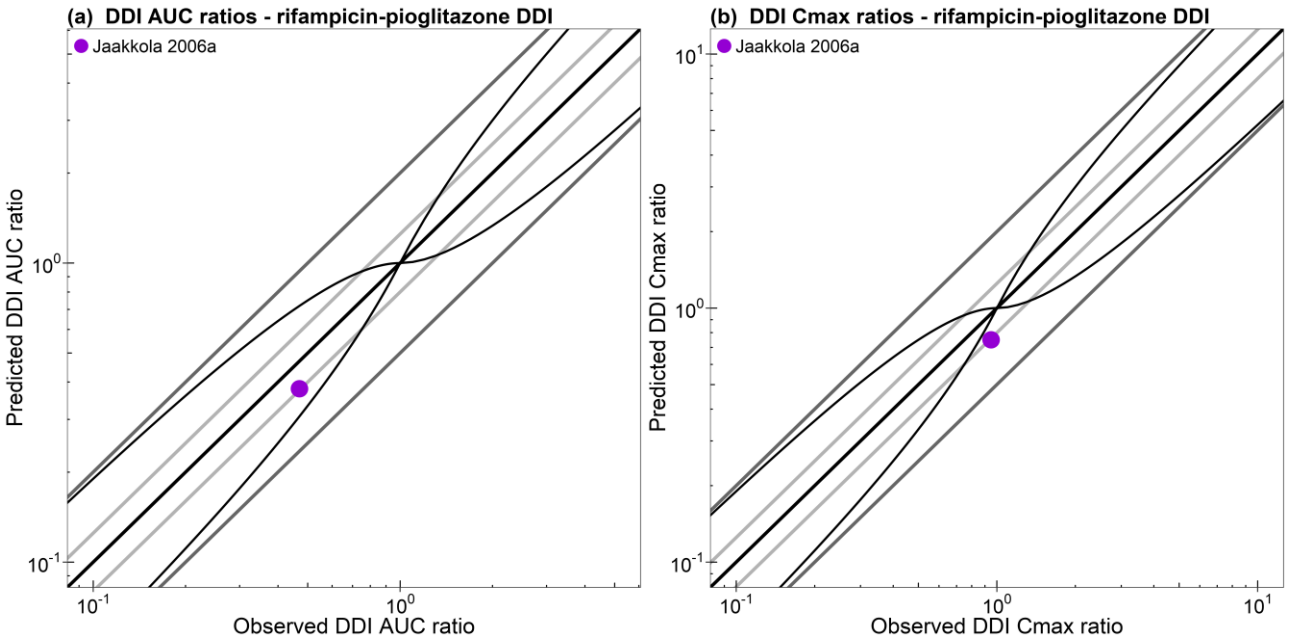

Fig. S4.9.2. Correlation of predicted and observed rifampicin-pioglitazone DDI AUC ratios and DDI C_{max} ratios. The straight black line marks the line of identity. Light grey lines indicate 0.8- to 1.25-fold; dark grey lines indicate 0.5- to 2-fold prediction acceptance limits. The curved black lines show the prediction success limits suggested by Guest *et al.*[143]. Detailed information about dosing regimens and study population is given in Table S4.9.1. The plotted DDI AUC ratios and DDI C_{max} ratios are listed in Table S4.9.2.

Table S4.9.2. Predicted compared to observed DDI AUC ratios and DDI C_{max} ratios of the rifampicin-pioglitazone DDI.

Perpetrator drug administration	Victim drug administration	Interval [hours] [a]	t_{last} [hours]	DDI AUC ratio		Pred/Obs DDI AUC ratio	DDI C_{max} ratio		Pred/Obs DDI C_{max} ratio	References
Rifampicin	*Pioglitazone*			*pred*	*obs*		*pred*	*obs*		
600 mg, q.d.	30 mg, s.d.	13	48	0.38	0.47	0.82	0.75	0.95	0.79	Jaakkola 2006a [78]
					GMFE	**1.21**			**1.27**	
					Pred/obs within 2-fold	**1/1**			**1/1**	

[a], time intervals between (last) perpetrator and victim drug administration; AUC, area under the concentration-time curve; C_{max}, maximum plasma concentration; DDI, drug-drug interaction; GMFE, geometric mean fold error; obs, observed; pred, predicted, q.d., once daily; s.d., single dose; t_{last}, time of the last concentration measurement.

4.10 Clarithromycin-repaglinide DDI

The clarithromycin-repaglinide DDI was predicted using interaction parameters for the MBI of CYP3A4 by clarithromycin that have been established during the clarithromycin model development [12]. The competitive inhibition of OATP1B1 and OATP1B3 by clarithromycin was modeled with K_i = 5.3 µmol/l for OATP1B1 and K_i = 14.0 µmol/l for OATP1B3, measured in OATP1B1 and OATP1B3 overexpressing HEK-293 cells [94]. No correction of these in vitro values to account for fu_{inc} was applied, as no information on clarithromycin binding in this uptake assay could be found.

Details on the modeled clinical study investigating the clarithromycin-repaglinide DDI are given in Table S4.10.1. The population predictions of repaglinide plasma concentration-time profiles with and without clarithromycin co-administration, compared to observed data, are shown in Fig. S4.10.1. The correlation of predicted and observed DDI AUC ratios and DDI C_{max} ratios is shown in Fig. S4.10.2. Table S4.10.2 lists the corresponding predicted and observed DDI AUC ratios, DDI C_{max} ratios as well as GMFE values.

Table S4.10.1. Clinical study data of the clarithromycin-repaglinide DDI.

Perpetrator drug administration	Victim drug administration	Interval [hours] [a]	*n*	Females [%]	Age [years]	Weight [kg]	Data set	References
Clarithromycin	*Repaglinide*							
250 mg, b.i.d.	0.25 mg, s.d.	1	9	44	22-27 (24.0)	52-83 (67.4)	e	Niemi 2001 [51]

[a], time intervals between (last) perpetrator and victim drug administration; values for age and weight are given as range (mean); b.i.d., twice daily; DDI, drug-drug interaction; e, external data set (model evaluation); *n*, number of individuals studied; s.d., single dose.

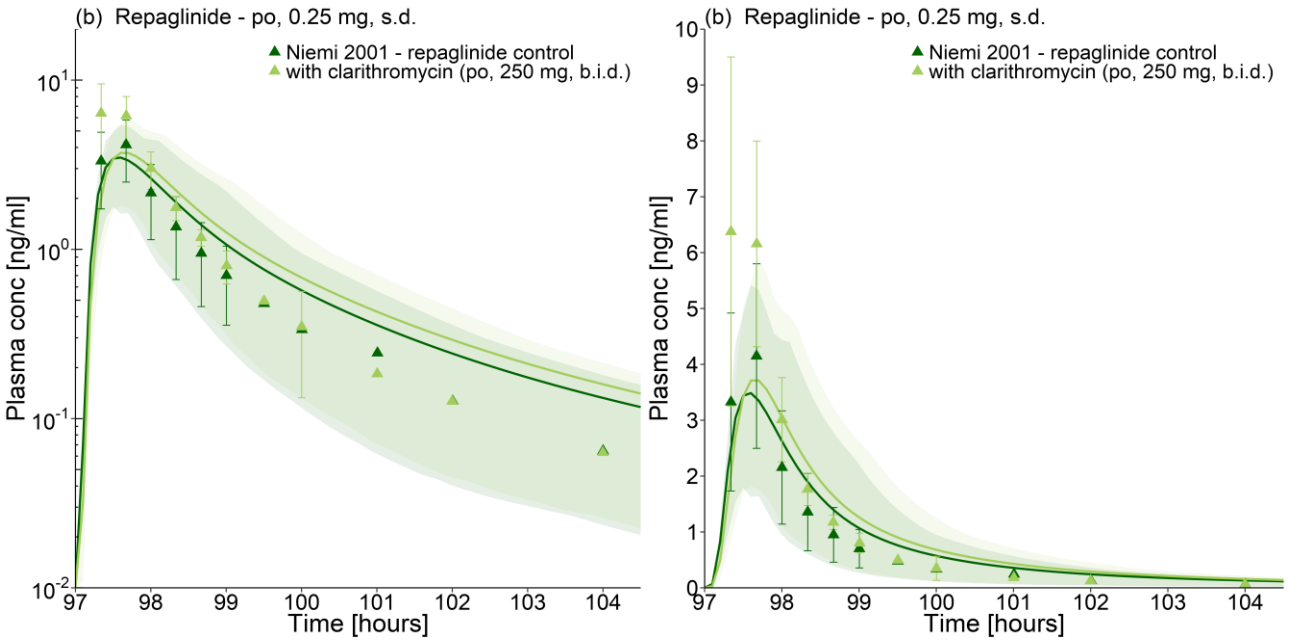

Fig. S4.10.1. Repaglinide plasma concentration-time profiles during the clarithromycin-repaglinide DDI (semilogarithmic and linear). Observed data are shown as triangles ± SD (dark green: control, light green: with clarithromycin). Repaglinide population simulation arithmetic means are shown as lines (dark green: control, light green: with clarithromycin). The shaded areas represent the 68% population prediction intervals. Detailed information about dosing regimens and study population is given in Table S4.10.1. Predicted and observed DDI AUC ratios and DDI C_{max} ratios are compared in Table S4.10.2. b.i.d., twice daily; s.d., single dose.

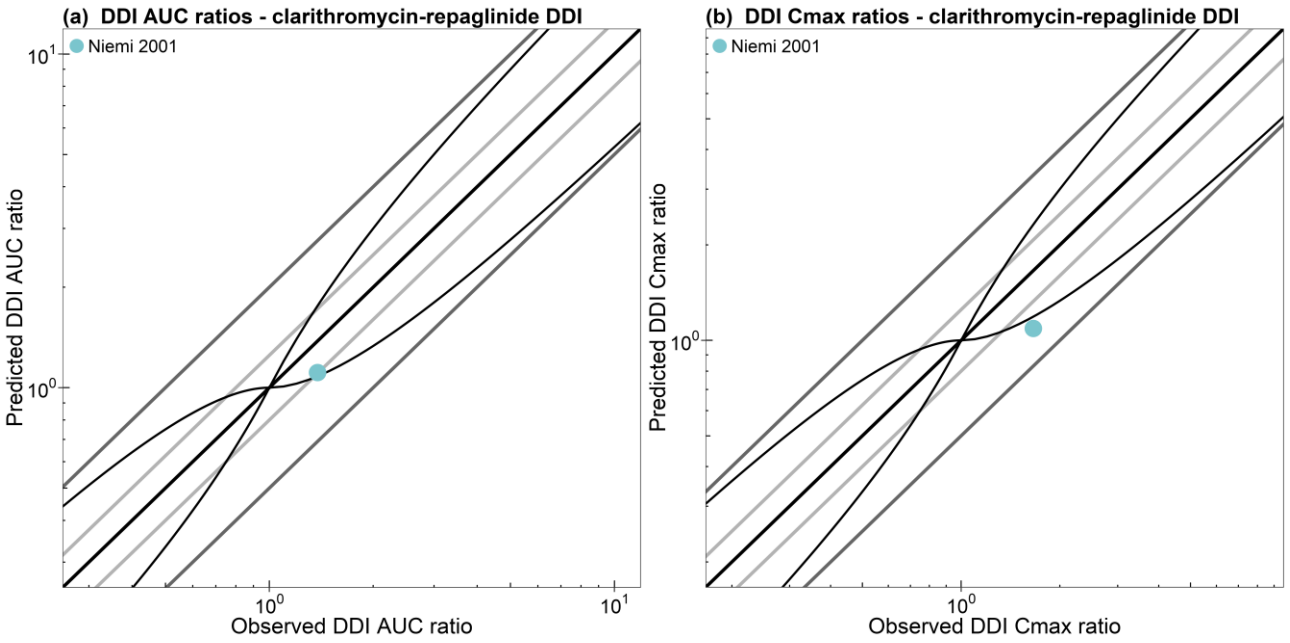

Fig. S4.10.2. Correlation of predicted and observed clarithromycin-repaglinide DDI AUC ratios and DDI C_{max} ratios. The straight black line marks the line of identity. Light grey lines indicate 0.8- to 1.25-fold; dark grey lines indicate 0.5- to 2-fold prediction acceptance limits. The curved black lines show the prediction success limits suggested by Guest *et al.* [143]. Detailed information about dosing regimens and study population is given in Table S4.10.1. The plotted DDI AUC ratios and DDI C_{max} ratios are listed in Table S4.10.2.

Table S4.10.2. Predicted compared to observed DDI AUC ratios and DDI C_{max} ratios of the clarithromycin-repaglinide DDI.

Perpetrator drug administration	Victim drug administration	Interval [hours] [a]	t_{last} [hours]	DDI AUC ratio		Pred/Obs DDI AUC ratio	DDI C_{max} ratio		Pred/Obs DDI C_{max} ratio	References
Clarithromycin	*Repaglinide*			*pred*	*obs*		*pred*	*obs*		
250 mg, b.i.d.	0.25 mg, s.d.	1	7	1.11	1.38	0.80	1.09	1.66	0.66	Niemi 2001 [51]
					GMFE	**1.25**			**1.52**	
					Pred/obs within 2-fold	**1/1**			**1/1**	

[a], time intervals between (last) perpetrator and victim drug administration; AUC, area under the concentration-time curve; b.i.d., twice daily, C_{max}, maximum plasma concentration; DDI, drug-drug interaction; GMFE, geometric mean fold error; obs, observed; pred, predicted, s.d., single dose; t_{last}, time of the last concentration measurement.

5 References

1. Dai D, Zeldin DC, Blaisdell JA, Chanas B, Coulter SJ, Ghanayem BI, et al. Polymorphisms in human CYP2C8 decrease metabolism of the anticancer drug paclitaxel and arachidonic acid. Pharmacogenetics. 2001;11:597–607.

2. Totah RA, Rettie AE. Cytochrome P450 2C8: substrates, inhibitors, pharmacogenetics, and clinical relevance. Clin Pharmacol Ther. 2005;77:341–52.

3. Niemi M, Leathart JB, Neuvonen M, Backman JT, Daly AK, Neuvonen PJ. Polymorphism in CYP2C8 is associated with reduced plasma concentrations of repaglinide. Clin Pharmacol Ther. 2003;74:380–7.

4. Niemi M, Backman JT, Kajosaari LI, Leathart JB, Neuvonen M, Daly AK, et al. Polymorphic organic anion transporting polypeptide 1B1 is a major determinant of repaglinide pharmacokinetics. Clin Pharmacol Ther. 2005;77:468–78.

5. Tomalik-Scharte D, Fuhr U, Hellmich M, Frank D, Doroshyenko O, Jetter A, et al. Effect of the CYP2C8 genotype on the pharmacokinetics and pharmacodynamics of repaglinide. Drug Metab Dispos. 2011;39:927–32.

6. Aquilante CL, Kosmiski LA, Bourne DWA, Bushman LR, Daily EB, Hammond KP, et al. Impact of the CYP2C8 *3 polymorphism on the drug-drug interaction between gemfibrozil and pioglitazone. Br J Clin Pharmacol. 2013;75:217–26.

7. Tornio A, Niemi M, Neuvonen PJ, Backman JT. Trimethoprim and the CYP2C8*3 allele have opposite effects on the pharmacokinetics of pioglitazone. Drug Metab Dispos. 2007;36:73–80.

8. Muschler E, Lal J, Jetter A, Rattay A, Zanger U, Zadoyan G, et al. The role of human CYP2C8 and CYP2C9 variants in pioglitazone metabolism in vitro. Basic Clin Pharmacol Toxicol. 2009;105:374–9.

9. Pasanen MK, Backman JT, Neuvonen PJ, Niemi M. Frequencies of single nucleotide polymorphisms and haplotypes of organic anion transporting polypeptide 1B1 SLCO1B1 gene in a Finnish population. Eur J Clin Pharmacol. 2006;62:409–15.

10. Ramsey LB, Johnson SG, Caudle KE, Haidar CE, Voora D, Wilke RA, et al. The Clinical Pharmacogenetics Implementation Consortium guideline for SLCO1B1 and simvastatin-induced myopathy: 2014 update. Clin Pharmacol Ther. 2014;96:423–8.

11. Kalliokoski A, Niemi M. Impact of OATP transporters on pharmacokinetics. Br J Pharmacol. 2009;158:693–705.

12. Hanke N, Frechen S, Moj D, Britz H, Eissing T, Wendl T, et al. PBPK models for CYP3A4 and P-gp DDI prediction: a modeling network of rifampicin, itraconazole, clarithromycin, midazolam,

alfentanil, and digoxin. CPT pharmacometrics Syst Pharmacol. 2018;7:647–59.
13. Edginton AN, Schmitt W, Willmann S. Development and evaluation of a generic physiologically based pharmacokinetic model for children. Clin Pharmacokinet. 2006;45:1013–34.
14. U.S. Food and Drug Administration. Clinical drug interaction Studies - Study Design, Data Analysis, and Clinical Implications. Draft Guidance for Industry. 2017.
15. Ogilvie BW, Zhang D, Li W, Rodrigues AD, Gipson AE, Holsapple J, et al. Glucuronidation converts gemfibrozil to a potent, metabolism-dependent inhibitor of CYP2C8: implications for drug-drug interactions. Drug Metab Dispos. 2006;34:191–7.
16. Kajosaari LI, Laitila J, Neuvonen PJ, Backman JT. Metabolism of repaglinide by CYP2C8 and CYP3A4 in vitro: effect of fibrates and rifampicin. Basic Clin Pharmacol Toxicol. 2005;97:249–56.
17. Hirano M, Maeda K, Shitara Y, Sugiyama Y. Drug-drug interaction between pitavastatin and various drugs via OATP1B1. Drug Metab Dispos. 2006;34:1229–36.
18. Honkalammi J, Niemi M, Neuvonen PJ, Backman JT. Dose-dependent interaction between gemfibrozil and repaglinide in humans: strong inhibition of CYP2C8 with subtherapeutic gemfibrozil doses. Drug Metab Dispos. 2011;39:1977–86.
19. Honkalammi J, Niemi M, Neuvonen PJ, Backman JT. Gemfibrozil is a strong inactivator of CYP2C8 in very small multiple doses. Clin Pharmacol Ther. Nature Publishing Group; 2012;91:846–55.
20. Randinitis EJ, Kinkel AW, Nelson C, Parker TD. Gas chromatographic determination of gemfibrozil and its metabolites in plasma and urine. J Chromatogr. 1984;307:210–5.
21. Randinitis EJ, Parker TD, Kinkel AW. Liquid chromatographic determination of gemfibrozil and its metabolite in plasma. J Chromatogr. 1986;383:444–8.
22. Rouini MR, Baluchestani M, Hakemi L. Study of dose-linearity of gemfibrozil pharmacokinetics in human. Int J Pharmacol. 2006;2:75–8.
23. Nakagawa A, Shigeta A, Iwabuchi H, Horiguchi M, Nakamura K, Takahagi H. Simultaneous determination of gemfibrozil and its metabolites in plasma and urine by a fully automated high performance liquid chromatographic system. Biomed Chromatogr. 1991;5:68–73.
24. Apotex Corp. Gemfibrozil Tablets USP 600 mg, comparative bioavailability study. 1998.
25. Busse KH, Hadigan C, Chairez C, Alfaro RM, Formentini E, Kovacs JA, et al. Gemfibrozil concentrations are significantly decreased in the presence of lopinavir/ritonavir. J Acquir Immune Defic Syndr. 2009;52:235–9.
26. González-Peñas E, Agarraberes S, López-Ocariz A, García-Quetglas E, Campanero MA, Carballal JJ, et al. A sensitive method for the determination of gemfibrozil in human plasma samples by RP-LC. J Pharm Biomed Anal. 2001;26:7–14.

27. Honkalammi J, Niemi M, Neuvonen PJ, Backman JT. Mechanism-based inactivation of CYP2C8 by gemfibrozil occurs rapidly in humans. Clin Pharmacol Ther. 2011;89:579–86.
28. Rouini MR, Ardakani YH, Mirfazaelian A, Hakemi L, Baluchestani M. Investigation on different levels of in vitro-in vivo correlation: gemfibrozil immediate release capsule. Biopharm Drug Dispos. 2008;29:349–55.
29. Su L, Guo J, Xia H, Liu G, Chen J, Jiang X. LC determination and pharmacokinetic study of gemfibrozil in human plasma. Chromatographia. 2010;71:833–8.
30. Backman JT, Honkalammi J, Neuvonen M, Kurkinen KJ, Tornio A, Niemi M, et al. CYP2C8 activity recovers within 96 hours after gemfibrozil dosing: estimation of CYP2C8 half-life using repaglinide as an in vivo probe. Drug Metab Dispos. 2009;37:2359–66.
31. Tornio A, Niemi M, Neuvonen M, Laitila J, Kalliokoski A, Neuvonen PJ, et al. The effect of gemfibrozil on repaglinide pharmacokinetics persists for at least 12 h after the dose: evidence for mechanism-based inhibition of CYP2C8 in vivo. Clin Pharmacol Ther. 2008;84:403–11.
32. Knauf H, Kölle EU, Mutschler E. Gemfibrozil absorption and elimination in kidney and liver disease. Klin Wochenschr. 1990;68:692–8.
33. Fernández L, Machín R, Zornoza A, Vélaz I, Martín C, Martínez-Ohárriz MC. Mechanism of sorption and release of a weak acid from β-cyclodextrin polymers. J Incl Phenom Macrocycl Chem. 2011;69:411–5.
34. Varma MVS, Lai Y, Kimoto E, Goosen TC, El-Kattan AF, Kumar V. Mechanistic modeling to predict the transporter- and enzyme-mediated drug-drug interactions of repaglinide. Pharm Res. 2013;30:1188–99.
35. Luner PE, Babu SR, Radebaugh GW. The effects of bile salts and lipids on the physicochemical behavior of gemfibrozil. Pharm Res. 1994;11:1755–60.
36. Wishart DS, Knox C, Guo AC, Shrivastava S, Hassanali M, Stothard P, et al. DrugBank: a comprehensive resource for in silico drug discovery and exploration. Nucleic Acids Res. 2006;34:D668-72.
37. Westerhoff P, Yoon Y, Snyder S, Wert E. Fate of endocrine-disruptor, pharmaceutical, and personal care product chemicals during simulated drinking water treatment processes. Environ Sci Technol. 2005;39:6649–63.
38. Shitara Y, Hirano M, Sato H, Sugiyama Y. Gemfibrozil and its glucuronide inhibit the organic anion transporting polypeptide 2 (OATP2/OATP1B1:SLC21A6)-mediated hepatic uptake and CYP2C8-mediated metabolism of cerivastatin: analysis of the mechanism of the clinically relevant drug-drug interaction between cerivastatin and gemfibrozil. J Pharmacol Exp Ther. 2004;311:228–36.

39. Sabordo L, Sallustio BC, Evans AM, Nation RL. Hepatic disposition of the acyl glucuronide 1-O-gemfibrozil-β-D-glucuronide: effects of clofibric acid, acetaminophen, and acetaminophen glucuronide. J Pharmacol Exp Ther. 2000;295:44–50.

40. Mano Y, Usui T, Kamimura H. The UDP-glucuronosyltransferase 2B7 isozyme is responsible for gemfibrozil glucuronidation in the human liver. Drug Metab Dispos. 2007;35:2040–4.

41. Open Systems Pharmacology Suite Community. Open Systems Pharmacology Suite Manual, Version 7.0.0. 2017.

42. Kawai R, Lemaire M, Steimer JL, Bruelisauer A, Niederberger W, Rowland M. Physiologically based pharmacokinetic study on a cyclosporin derivative, SDZ IMM 125. J Pharmacokinet Biopharm. 1994;22:327–65.

43. Berezhkovskiy LM. Volume of distribution at steady state for a linear pharmacokinetic system with peripheral elimination. J Pharm Sci. 2004;93:1628–40.

44. Ménochet K, Kenworthy KE, Houston JB, Galetin A. Use of mechanistic modeling to assess interindividual variability and interspecies differences in active uptake in human and rat hepatocytes. Drug Metab Dispos. 2012;40:1744–56.

45. Hatorp V, Oliver S, Su CA. Bioavailability of repaglinide, a novel antidiabetic agent, administered orally in tablet or solution form or intravenously in healthy male volunteers. Int J Clin Pharmacol Ther. 1998;36:636–41.

46. Kajosaari LI, Niemi M, Neuvonen M, Laitila J, Neuvonen PJ, Backman JT. Cyclosporine markedly raises the plasma concentrations of repaglinide. Clin Pharmacol Ther. 2005;78:388–99.

47. Kajosaari LI, Niemi M, Backman JT, Neuvonen PJ. Telithromycin, but not montelukast, increases the plasma concentrations and effects of the cytochrome P450 3A4 and 2C8 substrate repaglinide. Clin Pharmacol Ther. 2006;79:231–42.

48. Kajosaari LI, Jaakkola T, Neuvonen PJ, Backman JT. Pioglitazone, an in vitro inhibitor of CYP2C8 and CYP3A4, does not increase the plasma concentrations of the CYP2C8 and CYP3A4 substrate repaglinide. Eur J Clin Pharmacol. 2006;62:217–23.

49. Kalliokoski A, Backman JT, Kurkinen KJ, Neuvonen PJ, Niemi M. Effects of gemfibrozil and atorvastatin on the pharmacokinetics of repaglinide in relation to SLCO1B1 polymorphism. Clin Pharmacol Ther. 2008;84:488–96.

50. Kalliokoski A, Neuvonen M, Neuvonen PJ, Niemi M. The effect of SLCO1B1 polymorphism on repaglinide pharmacokinetics persists over a wide dose range. Br J Clin Pharmacol. 2008;66:818–25.

51. Niemi M, Neuvonen PJ, Kivistö KT. The cytochrome P4503A4 inhibitor clarithromycin increases the plasma concentrations and effects of repaglinide. Clin Pharmacol Ther. 2001;70:58–65.

52. Niemi M, Backman JT, Neuvonen M, Neuvonen PJ. Effects of gemfibrozil, itraconazole, and their combination on the pharmacokinetics and pharmacodynamics of repaglinide: potentially hazardous interaction between gemfibrozil and repaglinide. Diabetologia. 2003;46:347–51.

53. Niemi M, Kajosaari LI, Neuvonen M, Backman JT, Neuvonen PJ. The CYP2C8 inhibitor trimethoprim increases the plasma concentrations of repaglinide in healthy subjects. Br J Clin Pharmacol. 2004;57:441–7.

54. Kalliokoski A, Neuvonen M, Neuvonen PJ, Niemi M. Different effects of SLCO1B1 polymorphism on the pharmacokinetics and pharmacodynamics of repaglinide and nateglinide. J Clin Pharmacol. 2008;48:311–21.

55. Niemi M, Backman JT, Neuvonen M, Neuvonen PJ, Kivistö KT. Rifampin decreases the plasma concentrations and effects of repaglinide. Clin Pharmacol Ther. 2000;68:495–500.

56. Skerjanec A, Wang J, Maren K, Rojkjaer L. Investigation of the pharmacokinetic interactions of deferasirox, a once-daily oral iron chelator, with midazolam, rifampin, and repaglinide in healthy volunteers. J Clin Pharmacol. 2010;50:205–13.

57. European Medicines Agency, Committee for medicinal products for human use (CHMP). Assessment report Repaglinide Accord. 2011.

58. Hatorp V, Huang WC, Strange P. Repaglinide pharmacokinetics in healthy young adult and elderly subjects. Clin Ther. 1999;21:702–10.

59. He J, Qiu Z, Li N, Yu Y, Lu Y, Han D, et al. Effects of SLCO1B1 polymorphisms on the pharmacokinetics and pharmacodynamics of repaglinide in healthy Chinese volunteers. Eur J Clin Pharmacol. 2011;67:701–7.

60. Pei Q, Liu JY, Yin JY, Yang GP, Liu SK, Zheng Y, et al. Repaglinide-irbesartan drug interaction: effects of SLCO1B1 polymorphism on repaglinide pharmacokinetics and pharmacodynamics in Chinese population. Eur J Clin Pharmacol. 2018;74:1021–8.

61. Zhai XJ, Hu K, Chen F, Lu YN. Comparative bioavailability and tolerability of a single 2-mg dose of 2 repaglinide tablet formulations in fasting, healthy Chinese male volunteers: an open-label, randomized-sequence, 2-period crossover study. Curr Ther Res Clin Exp. 2013;75:48–52.

62. Zhang J, Gao F, Guan X, Sun YT, Gu JK, Fawcett JP. Determination of repaglinide in human plasma by high-performance liquid chromatography–tandem mass spectrometry. Acta Pharm Sin B. 2011;1:40–5.

63. Marbury TC, Ruckle JL, Hatorp V, Andersen MP, Nielsen KK, Huang WC, et al. Pharmacokinetics of repaglinide in subjects with renal impairment. Clin Pharmacol Ther. 2000;67:7–15.

64. Hatorp V, Walther KH, Christensen MS, Haug-Pihale G. Single-dose pharmacokinetics of

repaglinide in subjects with chronic liver disease. J Clin Pharmacol. 2000;40:142–52.

65. Mandić Z, Gabelica V. Ionization, lipophilicity and solubility properties of repaglinide. J Pharm Biomed Anal. 2006;41:866–71.

66. Seedher N, Kanojia M. Co-solvent solubilization of some poorly-soluble antidiabetic drugs. Pharm Dev Technol. 2009;14:185–92.

67. Sieger P, Cui Y, Scheuerer S. pH-dependent solubility and permeability profiles: A useful tool for prediction of oral bioavailability. Eur J Pharm Sci. 2017;105:82–90.

68. Plum A, Müller LK, Jansen JA. The effects of selected drugs on the in vitro protein binding of repaglinide in human plasma. Methods Find Exp Clin Pharmacol. 2000;22:139–43.

69. Zhu Z, Yang T, Zhao Y, Gao N, Leng D, Ding P. A simple method to improve the dissolution of repaglinide and exploration of its mechanism. Asian J Pharm Sci. 2014;9:218–25.

70. Schmitt W. General approach for the calculation of tissue to plasma partition coefficients. Toxicol In Vitro. 2008;22:457–67.

71. U.S. Food and Drug Administration. Drug development and drug interactions: table of substrates, inhibitors and inducers. 2017. https://www.fda.gov/Drugs/DevelopmentApprovalProcess/DevelopmentResources/DrugInteractionsLabeling/ucm093664.htm. Accessed 19 Oct 2018.

72. Itkonen MK, Tornio A, Neuvonen M, Neuvonen PJ, Niemi M, Backman JT. Clopidogrel markedly increases plasma concentrations of CYP2C8 substrate pioglitazone. Drug Metab Dispos. 2016;44:1364–71.

73. Jaakkola T, Backman JT, Neuvonen M, Neuvonen PJ. Effects of gemfibrozil, itraconazole, and their combination on the pharmacokinetics of pioglitazone. Clin Pharmacol Ther. 2005;77:404–14.

74. Jaakkola T, Backman JT, Neuvonen M, Niemi M, Neuvonen PJ. Montelukast and zafirlukast do not affect the pharmacokinetics of the CYP2C8 substrate pioglitazone. Eur J Clin Pharmacol. 2006;62:503–9.

75. Xue YJ, Turner KC, Meeker JB, Pursley J, Arnold M, Unger S. Quantitative determination of pioglitazone in human serum by direct-injection high-performance liquid chromatography mass spectrometry and its application to a bioequivalence study. J Chromatogr B. 2003;795:215–26.

76. Alim M, Nawaz R, Asi MR, Shahid M, Iqbql SZ, Abbas M. Study of urinary excretion and renal clearance of pioglitazone in male volunteers. Asian J Chem. 2011;23:63–6.

77. Deng LJ, Wang F, Li H De. Effect of gemfibrozil on the pharmacokinetics of pioglitazone. Eur J Clin Pharmacol. 2005;61:831–6.

78. Jaakkola T, Backman JT, Neuvonen M, Laitila J, Neuvonen PJ. Effect of rifampicin on the

pharmacokinetics of pioglitazone. Br J Clin Pharmacol. 2006;61:70–8.
79. Manitpisitkul P, Curtin CR, Shalayda K, Wang SS, Ford L, Heald D. Pharmacokinetic interactions between topiramate and pioglitazone and metformin. Epilepsy Res. 2014;108:1519–32.
80. Budde K, Neumayer HH, Fritsche L, Sulowicz W, Stompôr T, Eckland D. The pharmacokinetics of pioglitazone in patients with impaired renal function. Br J Clin Pharmacol. 2003;55:368–74.
81. Takeda Canada Inc. ACTOS® (pioglitazone hydrochloride) 15, 30, 45 mg Tablets USP - Product Monograph. 2018.
82. Tsume Y, Amidon GL, Takeuchi S. Dissolution effect of gastric and intestinal pH fora BCS class II drug, pioglitazone: new in vitro dissolution system to predict in vivo dissolution. J Bioequiv Availab. 2013;5:224–7.
83. Giaginis C, Theocharis S, Tsantili-Kakoulidou A. Investigation of the lipophilic behaviour of some thiazolidinediones. Relationships with PPAR-γ activity. J Chromatogr B. 2007;857:181–7.
84. Saha SK, Chowdhury AKA, Bachar SC, Das SC, Kuddus RH, Uddin MA. Comparative in vitro-in vivo correlation analysis with pioglitazone tablets. Asian Pacific J Trop Dis. 2013;3:487–91.
85. Domínguez-Gil Hurlé A, Sánchez Navarro A, García Sánchez MJ. Therapeutic drug monitoring of itraconazole and the relevance of pharmacokinetic interactions. Clin Microbiol Infect. 2006;12:97–106.
86. Heykants J, Van Peer A, Van de Velde V, Van Rooy P, Meuldermans W, Lavrijsen K, et al. The clinical pharmacokinetics of itraconazole: an overview. Mycoses. 1989;32 Suppl 1:67–87.
87. Taupitz T, Dressman JB, Buchanan CM, Klein S. Cyclodextrin-water soluble polymer ternary complexes enhance the solubility and dissolution behaviour of poorly soluble drugs. Case example: itraconazole. Eur J Pharm Biopharm. 2013;83:378–87.
88. National Center for Biotechnology Information. Hydroxy-itraconazole - PubChem Identifier: CID 108222. PubChem Database. https://pubchem.ncbi.nlm.nih.gov/compound/108222. Accessed 04 Jan 2019.
89. Riccardi K, Cawley S, Yates PD, Chang C, Funk C, Niosi M, et al. Plasma protein binding of challenging compounds. J Pharm Sci. 2015;104:2627–36.
90. Ishigam M, Uchiyama M, Kondo T, Iwabuchi H, Inoue S, Takasaki W, et al. Inhibition of in vitro metabolism of simvastatin by itraconazole in humans and prediction of in vivo drug-drug interactions. Pharm Res. 2001;18:622–31.
91. Templeton IE, Thummel KE, Kharasch ED, Kunze KL, Hoffer C, Nelson WL, et al. Contribution of itraconazole metabolites to inhibition of CYP3A4 in vivo. Clin Pharmacol Ther. 2008;83:77–85.
92. Isoherranen N, Kunze KL, Allen KE, Nelson WL, Thummel KE. Role of itraconazole metabolites in

CYP3A4 inhibition. Drug Metab Dispos. 2004;32:1121–31.
93. Shityakov S, Foerster C. In silico structure-based screening of versatile P-glycoprotein inhibitors using polynomial empirical scoring functions. Adv Appl Bioinforma Chem. 2014;7:1–9.
94. Vermeer LMM, Isringhausen CD, Ogilvie BW, Buckley DB. Evaluation of ketoconazole and its alternative clinical CYP3A4/5 inhibitors as inhibitors of drug transporters: the in vitro effects of ketoconazole, ritonavir, clarithromycin, and itraconazole on 13 clinically-relevant drug transporters. Drug Metab Dispos. 2016;44:453–9.
95. Rodgers T, Leahy D, Rowland M. Physiologically based pharmacokinetic modeling 1: predicting the tissue distribution of moderate-to-strong bases. J Pharm Sci. 2005;94:1259–76.
96. Taylor MJ, Tanna S, Sahota T. In vivo study of a polymeric glucose-sensitive insulin delivery system using a rat model. J Pharm Sci. 2010;99:4215–27.
97. National Center for Biotechnology Information. Keto-itraconazole - PubChem Identifier: CID 45039625. PubChem Database. https://pubchem.ncbi.nlm.nih.gov/compound/45039625. Accessed 04 Jan 2019.
98. National Center for Biotechnology Information. N-Desalkyl-itraconazole - PubChem Identifier: CID 53789808. PubChem Database. https://pubchem.ncbi.nlm.nih.gov/compound/53789808. Accessed 04 Jan 2019.
99. Cheng YC, Prusoff WH. Relationship between the inhibition constant (KI) and the concentration of inhibitor which causes 50 per cent inhibition (I50) of an enzymatic reaction. Biochem Pharmacol. 1973;22:3099–108.
100. The Merck Index 14th edition: Rifampin. Merck Research Laboratories, Whitehouse Station, NJ, USA. 2006;p 8217.
101. Baneyx G, Parrott N, Meille C, Iliadis A, Lavé T. Physiologically based pharmacokinetic modeling of CYP3A4 induction by rifampicin in human: influence of time between substrate and inducer administration. Eur J Pharm Sci. 2014;56:1–15.
102. Panchagnula R, Gulati I, Varma MVS, Ashok Raj Y. Dissolution methodology for evaluation of rifampicin-containing fixed-dose combinations using biopharmaceutic classification system based approach. Clin Res Regul Aff. 2007;24:61–76.
103. Agrawal S, Panchagnula R. Implication of biopharmaceutics and pharmacokinetics of rifampicin in variable bioavailability from solid oral dosage forms. Biopharm Drug Dispos. 2005;26:321–34.
104. Boman G, Ringberger VA. Binding of rifampicin by human plasma proteins. Eur J Clin Pharmacol. 1974;7:369–73.
105. Templeton IE, Houston JB, Galetin A. Predictive utility of in vitro rifampin induction data

generated in fresh and cryopreserved human hepatocytes, Fa2N-4, and HepaRG cells. Drug Metab Dispos. 2011;39:1921–9.
106. Shou M, Hayashi M, Pan Y, Xu Y, Morrissey K, Xu L, et al. Modeling, prediction, and in vitro in vivo correlation of CYP3A4 induction. Drug Metab Dispos. 2008;36:2355–70.
107. Loos U, Musch E, Jensen JC, Mikus G, Schwabe HK, Eichelbaum M. Pharmacokinetics of oral and intravenous rifampicin during chronic administration. Klin Wochenschr. 1985;63:1205–11.
108. Tirona RG, Leake BF, Wolkoff AW, Kim RB. Human organic anion transporting polypeptide-C (SLC21A6) is a major determinant of rifampin-mediated pregnane X receptor activation. J Pharmacol Exp Ther. 2003;304:223–8.
109. Nakajima A, Fukami T, Kobayashi Y, Watanabe A, Nakajima M, Yokoi T. Human arylacetamide deacetylase is responsible for deacetylation of rifamycins: rifampicin, rifabutin, and rifapentine. Biochem Pharmacol. 2011;82:1747–56.
110. Collett A, Tanianis-Hughes J, Hallifax D, Warhurst G. Predicting P-glycoprotein effects on oral absorption: correlation of transport in Caco-2 with drug pharmacokinetics in wild-type and mdr1a(-/-) mice in vivo. Pharm Res. 2004;21:819–26.
111. Greiner B, Eichelbaum M, Fritz P, Kreichgauer HP, von Richter O, Zundler J, et al. The role of intestinal P-glycoprotein in the interaction of digoxin and rifampin. J Clin Invest. 1999;104:147–53.
112. Buckley DB, Wiegand CM, Prentiss PL, Fahmi OA. Time-course of cytochrome P450 (CYP450) induction in cultured human hepatocytes: Evaluation of activity and mRNA expression profiles for six inducible CYP450 enzymes. ISSX. 2013.
113. Annaert P, Ye ZW, Stieger B, Augustijns P. Interaction of HIV protease inhibitors with OATP1B1, 1B3, and 2B1. Xenobiotica. 2010;40:163–76.
114. Reitman ML, Chu X, Cai X, Yabut J, Venkatasubramanian R, Zajic S, et al. Rifampin's acute inhibitory and chronic inductive drug interactions: experimental and model-based approaches to drug-drug interaction trial design. Clin Pharmacol Ther. 2011;89:234–42.
115. McFarland JW, Berger CM, Froshauer SA, Hayashi SF, Hecker SJ, Jaynes BH, et al. Quantitative structure-activity relationships among macrolide antibacterial agents: in vitro and in vivo potency against Pasteurella multocida. J Med Chem. 1997;40:1340–6.
116. Salem II, Düzgünes N. Efficacies of cyclodextrin-complexed and liposome-encapsulated clarithromycin against Mycobacterium avium complex infection in human macrophages. Int J Pharm. 2003;250:403–14.
117. Lappin G, Shishikura Y, Jochemsen R, Weaver RJ, Gesson C, Houston JB, et al. Comparative pharmacokinetics between a microdose and therapeutic dose for clarithromycin, sumatriptan,

propafenone, paracetamol (acetaminophen), and phenobarbital in human volunteers. Eur J Pharm Sci. 2011;43:141–50.
118. Davey PG. The pharmacokinetics of clarithromycin and its 14-OH metabolite. J Hosp Infect. 1991;19:29–37.
119. Chu SY, Granneman GR, Pichotta PJ, Decourt JP, Girault J, Fourtillan JB. Effect of moderate or severe hepatic impairment on clarithromycin pharmacokinetics. J Clin Pharmacol. 1993;33:480–5.
120. Noreddin AM, Roberts D, Nichol K, Wierzbowski A, Hoban DJ, Zhanel GG. Pharmacodynamic modeling of clarithromycin against macrolide-resistant [PCR-positive mef(A) or erm(B)] Streptococcus pneumoniae simulating clinically achievable serum and epithelial lining fluid free-drug concentrations. Antimicrob Agents Chemother. 2002;46:4029–34.
121. Rodrigues AD, Roberts EM, Mulford DJ, Yao Y, Ouellet D. Oxidative metabolism of clarithromycin in the presence of human liver microsomes. Major role for the cytochrome P4503A (CYP3A) subfamily. Drug Metab Dispos. 1997;25:623–30.
122. Rodvold KA. Clinical pharmacokinetics of clarithromycin. Clin Pharmacokinet. 1999;37:385–98.
123. Polasek TM, Miners JO. Quantitative prediction of macrolide drug-drug interaction potential from in vitro studies using testosterone as the human cytochrome P4503A substrate. Eur J Clin Pharmacol. 2006;62:203–8.
124. Jones DR, Ekins S, Li L, Hall SD. Computational approaches that predict metabolic intermediate complex formation with CYP3A4 (+b5). Drug Metab Dispos. 2007;35:1466–75.
125. Mayhew BS, Jones DR, Hall SD. An in vitro model for predicting in vivo inhibition of cytochrome P450 3A4 by metabolic intermediate complex formation. Drug Metab Dispos. 2000;28:1031–7.
126. Ito K, Ogihara K, Kanamitsu SI, Itoh T. Prediction of the in vivo interaction between midazolam and macrolides based on in vitro studies using human liver microsomes. Drug Metab Dispos. 2003;31:945–54.
127. Eberl S, Renner B, Neubert A, Reisig M, Bachmakov I, König J, et al. Role of p-glycoprotein inhibition for drug interactions: evidence from in vitro and pharmacoepidemiological studies. Clin Pharmacokinet. 2007;46:1039–49.
128. Moj D, Hanke N, Britz H, Frechen S, Kanacher T, Wendl T, et al. Clarithromycin, midazolam, and digoxin: application of PBPK modeling to gain new insights into drug-drug interactions and co-medication regimens. AAPS J. 2017;19:298–312.
129. Meyer M, Schneckener S, Ludewig B, Kuepfer L, Lippert J. Using expression data for quantification of active processes in physiologically based pharmacokinetic modeling. Drug Metab Dispos. 2012;40:892–901.

130. Nishimura M, Naito S. Tissue-specific mRNA expression profiles of human phase I metabolizing enzymes except for cytochrome P450 and phase II metabolizing enzymes. Drug Metab Pharmacokinet. 2006;21:357–74.

131. Rodrigues AD. Integrated cytochrome P450 reaction phenotyping: attempting to bridge the gap between cDNA-expressed cytochromes P450 and native human liver microsomes. Biochem Pharmacol. 1999;57:465–80.

132. PK-Sim® Ontogeny Database Documentation, Version 7.3. 2017.

133. Nishimura M, Yaguti H, Yoshitsugu H, Naito S, Satoh T. Tissue distribution of mRNA expression of human cytochrome P450 isoforms assessed by high-sensitivity real-time reverse transcription PCR. Yakugaku Zasshi. 2003;123:369–75.

134. Rowland Yeo K, Walsky RL, Jamei M, Rostami-Hodjegan A, Tucker GT. Prediction of time-dependent CYP3A4 drug-drug interactions by physiologically based pharmacokinetic modelling: impact of inactivation parameters and enzyme turnover. Eur J Pharm Sci. 2011;43:160–73.

135. Greenblatt DJ, von Moltke LL, Harmatz JS, Chen G, Weemhoff JL, Jen C, et al. Time course of recovery of cytochrome p450 3A function after single doses of grapefruit juice. Clin Pharmacol Ther. 2003;74:121–9.

136. Expressed Sequence Tags (EST) from UniGene. National Center for Biotechnology Information (NCBI). https://www.ncbi.nlm.nih.gov/unigene.

137. Deo AK, Prasad B, Balogh L, Lai Y, Unadkat JD. Interindividual variability in hepatic expression of the multidrug resistance-associated protein 2 (MRP2/ABCC2): quantification by liquid chromatography/tandem mass spectrometry. Drug Metab Dispos. 2012;40:852–5.

138. Kolesnikov N, Hastings E, Keays M, Melnichuk O, Tang YA, Williams E, et al. ArrayExpress update-simplifying data submissions. Nucleic Acids Res. 2015;43:D1113–6.

139. Prasad B, Evers R, Gupta A, Hop CECA, Salphati L, Shukla S, et al. Interindividual variability in hepatic organic anion-transporting polypeptides and P-glycoprotein (ABCB1) protein expression: quantification by liquid chromatography tandem mass spectroscopy and influence of genotype, age, and sex. Drug Metab Dispos. 2014;42:78–88.

140. Nishimura M, Naito S. Tissue-specific mRNA expression profiles of human ATP-binding cassette and solute carrier transporter superfamilies. Drug Metab Pharmacokinet. 2005;20:452–77.

141. Austin RP, Barton P, Cockroft SL, Wenlock MC, Riley RJ. The influence of nonspecific microsomal binding on apparent intrinsic clearance, and its prediction from physicochemical properties. Drug Metab Dispos. 2002;30:1497–503.

142. Kilford PJ, Gertz M, Houston JB, Galetin A. Hepatocellular binding of grugs: correction for

unbound fraction in hepatocyte incubations using microsomal binding or drug lipophilicity data. Drug Metab Dispos. 2008;36:1194–7.

143. Guest EJ, Aarons L, Houston JB, Rostami-Hodjegan A, Galetin A. Critique of the two-fold measure of prediction success for ratios: application for the assessment of drug-drug interactions. Drug Metab Dispos. 2011;39:170–3.

144. Pelkonen O, Turpeinen M, Hakkola J, Honkakoski P, Hukkanen J, Raunio H. Inhibition and induction of human cytochrome P450 enzymes: current status. Arch Toxicol. 2008;82:667–715.